Uncoupling force and calcium flux to develop novel therapeutics for

subarachnoid hemorrhage-induced vasospasm

By

Kyle Mitchell Hocking

Dissertation

Submitted to the Faculty of the

Graduate School of Vanderbilt University

In partial fulfillment of the requirements

For the degree of

DOCTOR OF PHILOSOPHY

In

Biomedical Engineering

August, 2014

Nashville, Tennessee

Approved:

Craig L. Duvall, Ph.D.

Colleen M. Brophy, M.D.

Franz J. Baudenbacher, Ph.D.

Hak-Joon Sung, Ph.D.

Susan Gunst, Ph.D.

This work is dedicated to Heather Mayzell, Grant Hocking, and

Elsie Hocking whose support has made this work possible.

ACKNOWLEDGEMENTS

TABLE OF CONTENTS

CHAPTER 1

Introduction and Significance

Subarachnoid hemorrhage (SAH) affects approximately 30,000 people each year and accounts for 1-7% of all strokes. Most cases of SAH are from trauma, but spontaneous SAH is due to the rupture of a cerebral aneurysm 85% of the time. SAH is characterized primarily by loss of cerebral autoregulation, development of cerebral vasospasm and subsequent ischemia. Neurological deficits that are direct sequelae of vasospastic events are the most common cause for morbidity and mortality in patients with SAH [2]. Cerebral vasospasm is initiated as the body's response to preserve blood volume.

Young adults account for a large portion of the patient population that suffer from SAH. Mortality rates for patients who suffer from a subarachnoid hemorrhage are roughly 45% [3]. Patients who survive the event have a 25% chance of having significant lifestyle limitations. These limitations are many, and include frequent headaches, depression, fatigue, poor physical health, post-traumatic stress disorder, anxiety, and cognitive impairment[4], all of which beget difficulty in maintaining employment and independence.

There is still much to be understood about vasospasm that occurs after a subarachnoid hemorrhage and how to properly treat this phenomenon. When a patient is suffering from cerebral vasospasm their cerebral blood flow is decreased from a normal range of 50-70 mL/min per 100mg to a level of less than 20 mL/min per 100mg[5-7]. Current treatment modalities for subarachnoid hemorrhages include "Triple-H therapy", vasoactive pharmaceutical intervention, and balloon angioplasty of the spastic vessels. "Triple-H therapy" refers to the technique of maintaining permissive hypertension, hypervolemia, and hemodilution to optimize cerebral blood flow. Cerebral perfusion pressure (CPP) is a measurement used to guide physicians in

determining cerebral blood flow of a patient[8,9]. CPP is defined as the mean arterial blood pressure (MAP) minus the intracranial pressure (ICP) [9]. Decreased CPP in SAH patients is the primary pathophysiologic mechanism that leads to acute cerebral ischemia [8]. "Triple-H therapy" increases CPP by promoting increased cerebral blood flow, while also ensuring adequate systemic blood pressure (MAP) [9]. The cranium is understood to be a fixed space occupied by the brain, blood, and cerebral spinal fluid, thus by increasing the blood volume of an individual one may increase the amount of blood in the cranium. Unfortunately, there are many complications associated with "Triple-H therapy," including pulmonary edema, dilutional hyponatremia, and infection due to invasive monitoring techniques [2].

Pharmacotherapy for cerebral vasospasm has utilized a variety of mechanisms to improve cerebral blood flow. The most successful therapeutic has been nimodipine, a calcium channel antagonist, that while not shown to be vasodilatory to the constricted arteries, appears to decrease mortality among patients. Another studied therapeutic, papaverine, is a phosphodiesterase inhibitor that has been shown to vasodilate the constricted vessels. Unfortunately it does not consistently improve patient outcome. There are many other pharmacologic agents used to promote cerebral vasodilation, however, they are often contra-indicated due to their ability to critically lower mean arterial pressure. This occurs due to the vasodilation that occurrs throughout the body when they are given.

Angioplasty is the process of mechanically dilating a spastic artery by inflating a balloon of air within the vessel lumen. The objective of this is to increase blood flow through this artery by widening the artery. Unfortunately, when compared to Triple-H therapy, balloon angioplasty does not improve patient outcomes[10]. Thus, there remains a largely unmet need for the treatment of SAH-induced cerebral vasospasm to prevent the development of cerebral ischemia.

Approach

Vasospasm is sustained contraction of blood vessels that may be due to enhanced contraction or impaired relaxation. This proposal will focus on the molecular mechanisms underlying the processes of contraction and relaxation of blood vessels. The two major filaments of smooth muscle, the thick and thin filaments, are the structural components that modulate tone. Thick filaments are composed of myosin. Smooth muscle myosin is also known as myosin II, and has two heavy chains. Myosin also contains two types of light chains, MLC20 and MLC17 with MLC20 being the regulatory chain that is active in contraction. Thin filaments are composed of actin and actin binding proteins (HSP20, VASP, cofilin, and paxillin). Actin can be present in either filamentous or globular form. Filamentous actin is the polymerized form of actin that enables myosin to attach to its filaments in order to initiate contraction. Globular actin is the monomeric building block that forms filamentous actin.

Increases in intracellular calcium concentrations ($[Ca^{2+}]_i$) lead to the activation of myosin light chain kinase (MLCK) and promotion of myosin light chain phosphorylation (p-MLC). These modifications lead to cross-bridge cycling and initiation of smooth muscle contraction. Thus, intracellular calcium is essential for the initiation of actomyosin interactions. Cross bridges constitute interaction of the globular heads of the myosin filaments (thick filaments) with actin and actin binding proteins (thin filaments). On the other hand, increases in intracellular cyclic nucleotide content (cAMP and cGMP) lead to activation of cyclic nucleotide-dependent protein kinases (PKA and PKG) resulting in relaxation of either agonist pre-contracted smooth muscle, or inhibition of agonist-induced contraction. Downstream from the activation of PKA and PKG is a protein associated with the disruption of actin polymerization, heat shock protein 20 (HSP20). HSP20 can be phosphorylated by either cGMP or cAMP, and its phosphorylation

3

has been associated with smooth muscle relaxation in various tissues from multiple species. While HSP20 is also downstream of PKG, there are other downstream proteins including phospholamban and the IP_3 receptor that too modulate $[Ca^{2+}]_i$ leading to smooth muscle relaxation

Dogma states that contraction and relaxation are mediated by the thick filaments in vascular smooth muscle[11,12]. Unlike striated and cardiac smooth muscle, non-cardiac smooth muscle does not contain troponin to regulate the binding actin to myosin. Instead, smooth muscle contains the messenger protein calmodulin to bind with calcium and initiate myosin light chain kinase (MLCK) [13]. Another unique property of non-cardiac smooth muscle is its ability to sustain a contraction after the $[Ca^{2+}]_i$ levels have returned to basal or near basal levels. This sustained phase of contraction is also known as the tonic stage of contraction (Figure 2.1). The ability to have a tonic phase of contraction is important in maintenance of force for blood vessels and other smooth muscle tissue. The latch mechanism hypothesis has been developed to explain this phenomenon where intracellular calcium concentrations decrease under circumstances in which vascular tone remains elevated[14]. The latch bridge hypothesis implies that myosin is responsible for contraction and relaxation of vascular tissue, but does not allow a role for actin and actin associated proteins. In smooth muscle, myosin attaches to actin and through a power stroke that creates force. While myosin plays a major role, actin may indeed also have a significant role in contraction and relaxation that has not been extensively considered.

Through activation of the cyclic nucleotide-mediated thin filament pathway, it may be possible to create conditions where contraction is mitigated while cross-bridge cycling is still occurring. Under these conditions force would be inhibited but $[Ca^{2+}]_I$ and myosin light chain phosphorylation would in fact be potentiated suggesting that calcium signaling and force

generation could be "uncoupled." *The overall goal of this project is to develop model systems to uncouple the thin and thick filament pathways to better understand the roles of thick and thin filaments and their associated proteins in the regulation of smooth muscle contraction and relaxation.*

Innovation

The current challenge in treating SAH is that any agent that lowers the tone of the spastic cerebral vessels necessarily promotes systemic vasorelaxation, leading to hypotension, and decreased intracranial perfusion pressure. We hypothesized that uncoupling force and intracellular calcium concentrations might lead to treatment of vasospastic vessels without impacting normal vessels. To determine the physiologic changes that occur to vasculature during cerebral vasospasm, a model was created that mimicked some of the biochemical changes that occur in vasospastic tissue. Using siRNA, and a diblock copolymer to enhance its delivery, HSP20 was knocked down, while physiologic function and calcium measurements were concurrently determined. Cell-permeant peptide sequences were used to produce proteins and peptides that modulated vasomotor tone.

A phosphomimetic peptide of HSP20 was used to cause relaxation of blood vessels by calcium-independent mechanisms that are downstream of PKA. A simple and translational method is demonstrated for formulation of endosomolytic, electrostatically-complexed nanoparticles (i.e. nano-polyplexes, or NPs) that efficiently deliver pHSP20 into vascular tissues, enhancing peptide bioactivity. pHSP20-NPs have potential for clinical translation to ameliorate cerebral vasospasm without causing systemic hypotension. The NP approach also represents a novel pharmaceutical technology poised for generalized use as a delivery vector for bioactive peptides.

5

Specific Aims

The *hypothesis* of this investigation is that inhibition of agonist-induced contraction is not simply due to a reversal of the processes that initiate contraction ($[Ca^{2+}]_i$/p-MLC) but rather involves phosphorylation of specific actin regulatory proteins and hence, is dependent on the thin filament mechanism. The specific aims of this work are the following:

Specific Aim 1: *Develop a model system that inhibits force without inhibiting increases in Ca2+ to uncouple force production from thick filament regulation*. Dogma states that a rise in intracellular calcium leads to the production of force due to cross-bridge cycling. The goal of this aim is to create conditions that completely block force transduction but do not completely block calcium transients using the adenylate cyclase activator forskolin. To ensure that this is not due to a decrease in calcium sensitivity by increased cAMP, myosin light chain phosphorylation will be concurrently measured.

Specific Aim 2: *Use the dose of forskolin identified in Aim 1 to investigate biochemical events including calcium and actin regulatory processes*. Porcine coronary arteries will be used for analysis of biochemical events at basal, contracted, relaxed, and inhibited contraction conditions. Understanding the role of increased cAMP levels with and without contractile agonist histamine pre-treatment was used to determine how contraction is inhibited.

Specific Aim 3: *Demonstrate that PKG activation inhibits force without uncoupling intracellular calcium*. Activation of the PKG pathway should inhibit force production through inhibition of increases in intracellular calcium concentrations in addition to thin filament regulatory processes. Nitric oxide donors and phosphodiesterase inhibitors will be used to activate PKG, and to determine if force can be uncoupled from changes in intracellular calcium and MLC phorphorylation after activation of the PKG pathway.

Specific Aim 4: *Modulate HSP20 to uncouple force and calcium*. Phosphorylation of HSP 20 has been shown to correlate inversely with smooth muscle tissue-generated stress. A HSP20 phospho-peptidomimetic to inhibit force production will be used to uncouple the force transduction from a rise in intracellular calcium.

These studies will aid in discerning the role that thin and thick filaments play in contraction and relaxation in vascular smooth muscle. Besides analyzing traditional myosin and calcium changes that occur during relaxation, actin polymerization will be studied in depth to emphasize thin filament effects. By activating cAMP and cGMP pathways, the role of actin filaments in cyclic nucleotide-induced relaxation of smooth muscle will become better understood. These aims will lead to new approaches to locally treat SAH-induced vasospasm.

CHAPTER 2

Vasodilation for Cerebral Vasospasm
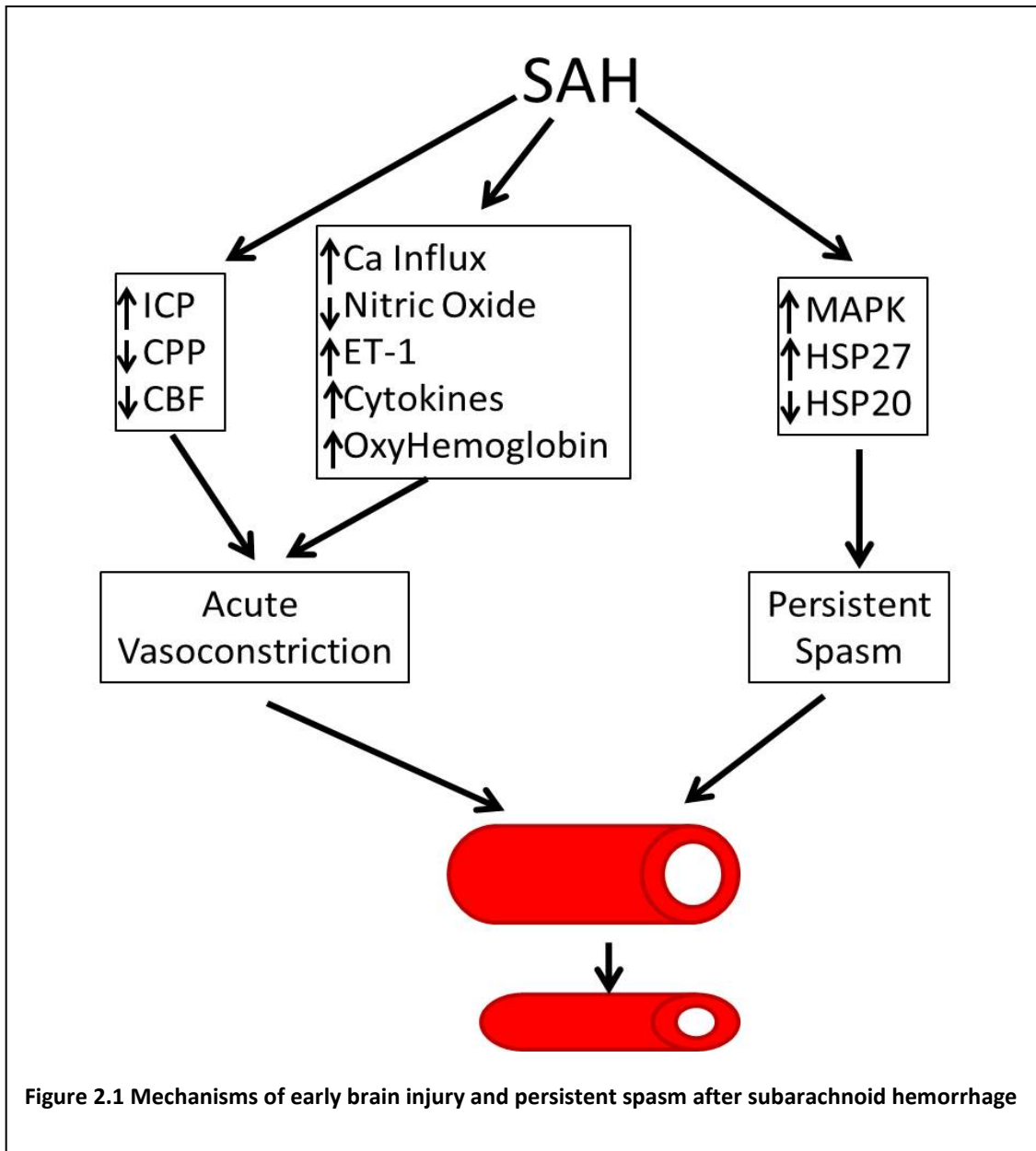
Introduction

Cerebral vasospasm occurs after subarachnoid hemorrhage in patients and is one of the leading causes of death for these patients. Early brain injury that occurs with subarachnoid hemorrhage is associated with the inflammatory pathway, ionic changes, and physiologic changes. These three categories create prolonged vasospasm in patients and propagate the constriction of the tissue. Vasospasm can be detected in patients by angiography, and is present in 40 – 70% of patients following SAH[15]. The prolonged vasospasm often leads to delayed cerebral ischemia occurring 3-4 days after the bleed[16], and 20-30% of these patients will exhibit neurological deficits[17].

Cerebral vasospasm occurs as a result of oxyhemoglobin, Endothelin-1, platelet derived growth factor (PDGF), and inflammatory cytokines that are elevated after blood interacts with the surface of the brain. Pathogenesis of spasm is not clearly defined although contraction, inflammation, and histological changes to the artery have been observed.

Oxyhemoglobin leads to the release of free radicals, lipid peroxidation, metabolism of oxyhemoglobin to bilirubin, release of endothelin, and inhibition of endothelial-dependent relaxation[18]. Oxyhemoglobin autoxidizes into methemoglobin, and releases superoxide into the subarachnoid space[18,19]. Free radicals have been shown to decrease smooth muscle relaxation by depleting nitric oxide stores by converting it to peroxynitrite[18,20]. Metabolism of oxyhemoglobin leads to the production of bilirubin which has been shown to cause spasm in cerebral arteries at concentrations of 10-30 μM[21]. Oxyhemoglobin and other iron based hemoproteins are known to cause the inhibition of endothelial dependent relaxation[22]. Since oxyhemoglobin is able to inhibit

endothelial dependent relaxation, it suggests that the prolonged contraction of the cerebral

vessels may be due to this decrease in the arteries' ability to relax[18]. As well as having

Figure 2.1 Mechanisms of early brain injury and persistent spasm after subarachnoid hemorrhage

vasoconstrictive properties alone, oxyhemoglobin accentuates the contractile effects of hypoxia,

serotonin, potassium, and fibrin degradation products[18]. Taken together, oxyhemoglobin

propagates the constriction of vascular smooth muscle; leading to spasm of the vessel and poor

perfusion of the brain.

Endothelin-1 is a vasoactive peptide that leads to the constriction of vascular tissue. ET-1 receptor activation results in the stimulation of several signaling pathways associated with cellular growth, hypertrophy, and proliferation. These pathways include MAPK, IP3, and protein kinase B. PDGF is a growth factor that is present in blood and is important for normal growth and development, inflammatory reactions, and atherosclerosis[23]. PDGF has direct mitogen activity on smooth muscle cells, and has been shown to induce intimal lesions and vasospastic responses in porcine coronary arteries[24]. Inflammatory cytokines genes have been shown to be upregulated in response to subarachnoid hemorrhage leading to cerebral vasospasm[25]. Inflammation due to the cytokine increase is thought to have a role in the development of cerebral vasospasm; further elucidation of the precise roles of inflammatory events in cerebral vasospasm is needed[26].

Along with these inflammatory changes in the cerebral artery there are ionic changes that are occurring after subarachnoid hemorrhage. Among these are calcium influx, potassium efflux, and low magnesium. The influx of calcium is expected due to the large role calcium plays in the contraction of vascular smooth muscle. Calcium plays an important role in cellular communication and in regulating vascular tone. The initial spike in calcium is potentially toxic to the surrounding tissue leading to cell death and initiating cerebral vasospasm. Potassium efflux occurs during the onset of vasospasm by oxyhemoglobin interfering with the voltage dependent potassium channel current and leads to increased contraction of the vascular tissue. Magnesium is a known vasodilator and has shown to have neuroprotective properties in tissue, but treatment of cerebral vasospasm with magnesium sulfate has not shown promising outcomes[27].

Ischemia often occurs after SAH and is marked by a decrease in the cerebral blood flow, usually measured by Doppler ultrasound. With this onset ischemia HIF-1alpha, VEGF, and p53 are increased in response. HIF-1alpha is a mediator of ischemic response in tissue and interacts with important cellular proteins CREB binding protein and STAT3. HIF-1 alpha has also been shown to increase VEGF and activate p53 as a response to hypoxia[28]. VEGF is elevated after focal cerebral ischemia and is shown to be neuroprotective[29], but has been speculated to contribute to brain injury by increasing the permeability of the blood brain barrier[30]. It is still not understood if elevation of VEGF during ischemia is beneficial to the patient or increases the damage caused by the brain bleed. p53 is potentially involved in the apoptosis of endothelial cells noticed during cerebral vasospasm, and potentially leading to increased intimal thickening and wall stiffness[28].

A decrease in cerebral blood flow occurs after subarachnoid hemorrhage, and if perfusion reduces to below 40% of baseline for 60 minutes 24 hour mortality was predicted to be 100% [31]. During this time intracranial pressure (ICP) becomes elevated and cerebral perfusion pressure drops initially and slowly rises. With the great increase in ICP the perfusion to the cerebral portion of the brain remains low. Constriction of the cerebral vessels may be in response to the decreased CPP in the individual despite having normal mean arterial blood pressure. The perfusion to the cerebral portion of the brain that the patient has correlates with the neurological status of the patient. Patients that have vasospasm generally have worse cerebral blood flow and lowered neurologic status.

Current treatments

Triple H therapy includes the use of hypertension, hypervolemia, and hemodilution to prevent and treat cerebral vasospasm. Cerebral perfusion pressure (CPP) is used to guide

11

physicians in determining cerebral blood flow of a patient [8,9]. CPP is related to the mean arterial

blood pressure minus the intracranial pressure of the patient [9]. Decreased CPP has been observed

from patients who have subarachnoid hemorrhage and leads to acute ischemia of the brain [8].

Triple H therapy is designed to increase CPP by increasing the patient's blood volume so that the

brain remains adequately perfused [9]. The purpose of using hypervolemia instead of vasodilators

is to maintain normotensive systemic blood pressure. Some of the complications associated with

Triple-H therapy are: pulmonary edema, dilutional hyponatremia, and complications due to the

additional invasive monitoring used [2].

Vasoactive pharmaceuticals are not commonly used for treatment of subarachnoid

hemorrhages because of the change in systemic blood pressure that comes along with them.

Antihypertensive medications are avoided when systolic blood pressure is below 140 mmHg and

diastolic blood pressure is below 90 mmHg [2]. Documented use of intra-arterial infusion of

papaverine, a phosphodiesterases inhibitor, improved vessel diameter in a large portion of

patients after treatment [32-34]. Papaverine has shown to be one of the most effective

pharmaceutical interventions of subarachnoid hemorrhage [32]. Although this reversal of

vasospasm seems promising, it did not always correlate with improved clinical outcomes of

patients [34].

The most successful treatment of cerebral vasospasm to date is the use of nimodipine, a

calcium channel antagonist; although it does not show angiographic evidence that vasodilation is

occurring[27]. This could mean that nimodipine is potentially blocking calcium from having

detrimental effects on neurologic tissue and is not affecting the vascular tissue. Also other

calcium channel antagonists have been used without promising results.

Angioplasty of spastic vessels is a technique where a balloon is used to widen the vessel diameter by inflating a balloon. Usually inserted into the femoral artery and threaded up into the site of vasospasm, a flexible guide wire and catheter are used to place the balloon in the correct location. Balloon angioplasty has been shown to offer patients improvement to ischemic deficits after cerebral vasospasm [35]. When compared with traditional Triple-H therapy balloon angioplasty did not show any additional benefit to patient outcome [36]. Balloon angioplasty comes with its own set of morbidity, and patients must be carefully selected based on vital sign status and the vessels response to conventional treatment [37].

The problem with current treatments of subarachnoid hemorrhage is that vasospasm is not successfully reversed or prevented because the cellular mechanisms are not completely understood. The previously described initiators of cerebral vasospasm all have a role in increasing intracellular calcium and phosphorylation of the myosin light chain, but this phosphorylation of the myosin light chain and elevated calcium are transient while constriction of the vessel remains suggesting that other mechanisms are also occuring.

Preventing SAH induced vasospasm would prevent costly and devastating neurologic compromise in young patients. This represents a large unmet need in that there are no current treatment modalities that are proven to be effective at preventing or reversing cerebral vasospasm after SAH. The cyclic nucleotide pathway will be further researched to elucidate force inhibition uncoupled from calcium signaling. This proposal focuses on a new approach to modulate cerebrovascular tone, namely thin filament regulation.

Recent findings have shown that there are biochemical changes in the vascular tissue that undergoes vasospasm. Among them are the down regulation of heat shock protein 20 (HSP20) and increased phosphorylation of heat shock protein 27 (HSP27). There is a marked decrease in

13

HSP20 associated with a decrease in perfusion in a rat model system for cerebral vasospasm [38,39]. It has been shown that restoration of HSP20 can be used to treat and prevent vasospasm from occurring[39]. The evidence suggests that heat shock protein changes are responsible for vasospasm occurring in these vessels. Restoration to physiologic levels of these heat shock proteins could potentially result in normal function of the cerebral vessels.

Mitogen-activated protein kinases are thought to have a causative role in cerebral vasospasm, and may explain increased phosphorylation of HSP27. Phosphorylated HSP27 promotes actin remodeling and competitively inhibits the phosphorylation of HSP20 by PKA and PKG. MAPK may be activated by oxyhemoglobin, ET-1, PDGF, and inflammatory cytokines all leading to sustained calcium independent smooth muscle contraction and vascular remodeling[40].

Cyclic Nucleotide Signaling

Figure 2.2 depicts the relationship between force and calcium over time after agonist induced contraction

Smooth muscle activation of the H1 receptor via histamine is linked to the intracellular G protein (Gαq) and Gαq-coupled receptors that activate phospholipase C (PLC) and RhoA (reviewed in [41]). Activation of PLC induces inositol 1, 4, 5-trisphosphate (IP$_3$) production, causing calcium to be released from the sarcoplasmic reticulum (SR). This increase in intracellular calcium activates calmodulin-dependent myosin light chain kinase (MLCK), leading to increases

in the phosphorylation of 20 KDa myosin light chains (MLC). Crossbridge phosphorylation of

the actomyosin apparatus results in the generation of force in vascular smooth muscle [11,42,43].

While Ca^{2+} and MLC phosphorylation are important for the initiation of contraction, the tonic

phase, or force maintenance, of smooth muscle contraction can occur where $[Ca^{2+}]_i$ levels and

MLC phosphorylation are near basal levels, suggesting other pathways are engaged during force

maintenance in smooth muscle [12,42,44-50]. During the sustained phase of contraction, stiffness and

force are maintained at high levels while intracellular calcium concentrations $[Ca^{2+}]_i$, cross-

bridge phosphorylation, and shortening velocity fall to intermediate values [12,45,51-53] (Figure 1).

Maintenance of force despite intermediate levels of cross-bridge phosphorylation and velocity

has been explained using a model referred to as the latch phenomenon [53,54]. However, reversal of

these three two processes alone does not account for the force inhibition that occurs during

relaxation or inhibition of contraction, implicating that other mechanisms, such as actin

cytoskeletal rearrangement, play a role in the suppression of force.

Vascular smooth muscle relaxation, or inhibition of force, can be mediated by

vasodilators that activate guanylyl cyclase (e.g. nitric oxide) or adenylyl cyclase (e.g.

prostacyclin, β-agonists, and forskolin), leading to increases in cGMP and cAMP, respectively.

The cyclic nucleotides, in turn, activate cGMP-dependent protein kinase (PKG) and cAMP-

dependent protein kinase (PKA) [55,56], leading to several phosphorylation events resulting in

relaxation or inhibition of force. Cyclic nucleotide-induced relaxation or inhibition of force in

smooth muscle involves at least three major pathways: decreases in intracellular free calcium

concentrations, calcium sensitivity and actin cytoskeletal regulation (reviewed in [56-58]). While

the role of a decrease in $[Ca^{2+}]_i$ and Ca^{2+} sensitivity in the regulation of smooth muscle cell

contraction has been established, the role of actin cytoskeleton and actin-associated proteins is

15

still unclear. Although several investigations have suggested the regulation of actin and actin-associated proteins in smooth muscle contraction, (reviewed in[59]) very few reports have addressed the role of second messenger regulation of actin-associated proteins during inhibition of force. Actin-associated proteins that are implicated in the regulation of smooth muscle contraction include the small heat shock-related protein 20 (HSP20), cofilin, and vasodilator-stimulated phosphoprotein (VASP) [60].

HSP20 is a 160 amino acid protein that contains an alpha crystallin domain and two phosphorylation sites[61]. HSP20 is also an actin binding protein that is phosphorylated by PKG and PKA on serine 16, inducing relaxation and inhibition of contraction through the modulation of actin cytoskeletal dynamics[55,62-64].   Activation of cyclic nucleotide-dependent signaling pathways in vascular smooth muscles prevents vein graft spasm and intimal hyperplasia, two processes that lead to short and long term failure of aortocoronary and peripheral vascular reconstructions. It has been demonstrated that the cyclic nucleotide signaling pathways converge at the phosphorylation of a small heat shock-related protein, HSP20 [63]. HSP20 has a prominent amino acid sequence from 111 to 123 that is similar to the inhibitory sequence of troponin I in striated muscle[65], and this region is believed to have part of the vasodilatory effect in smooth muscle[66]. There is also a serine phosphorylation site at 157 that has not been correlated with contraction and relaxation of smooth muscle[61].
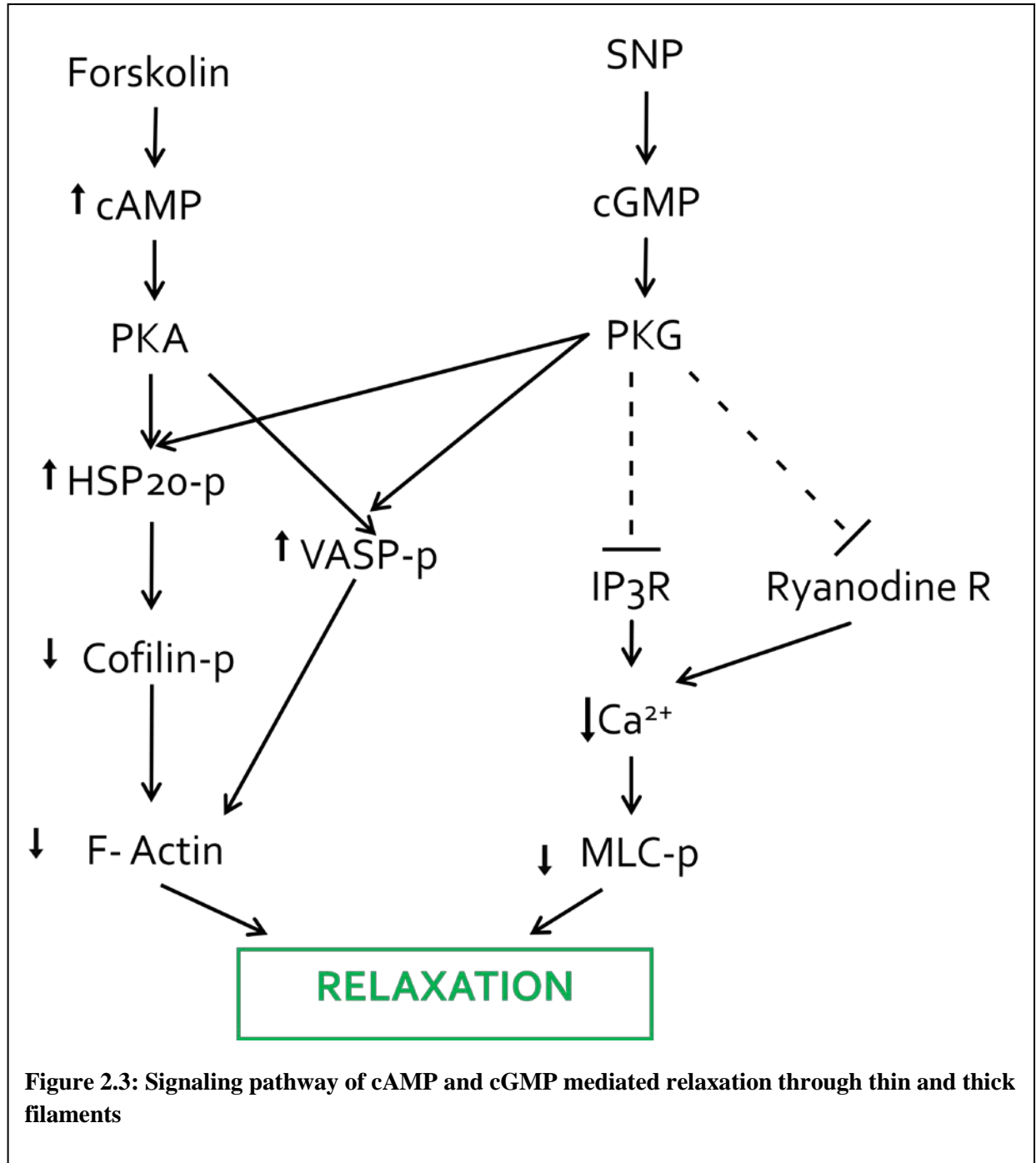
Figure 2.3: Signaling pathway of cAMP and cGMP mediated relaxation through thin and thick filaments

HSP27 is a 205 amino acid long protein which also includes an alpha crystallin domain. HSP27 has direct links to MAPKAP kinase (MK2) through a hydrophobic domain containing a WDPF motif, which is essential for chaperone activity in this heat shock protein[61]. Just as HSP20 phosphorylation is directly linked to cyclic nucleotide signaling so is HSP27

phosphorylation related to MK2 signaling. The phosphorylation of HSP27 inhibits phosphorylation of HSP20 by PKA[67].

Cyclic nucleotide-dependent relaxation is associated with decreases in the phosphorylation of the actin depolymerizing protein cofilin in vascular, as well as, airway smooth muscle cells[64,68]. Cofilin binds to actin filaments and causes depolmerization at the minus end of filaments when dephosphorylated. Cofilin as well as actin depolymerizing factor (ADF) can sever actin filaments, and cofilin shows a pH dependence on actin polymerization. The afiinity to actin when coiflin is phosphorylated decreases 10-20 fold in vitro, thus inactivating the cofilin [69].

VASP is an actin binding protein that is localized to focal adhesions and cell-to-cell contacts [60]. VASP is known to be a PKA and PKG substrate that links cellular signaling to cytoskeletal organization and movement. VASP contains three possible phosphorylation sites: serine 157, serine 239, and threonine 278, all of which may be phosphorylated by either PKA or PKG. Serine 239 is known to be preferentially phosphorylated by PKG while the other two are show no preference. Forskolin treatment leads to phosphorylation of VASP and regulates the actin cytoskeleton in rat aortic smooth muscle cells [70] and[1] human airway smooth muscle cells [68]. Actin filament elongation has been shown to be necessary for contraction in vascular smooth muscle, and VASP phosphorylation is known to inhibit actin polymerization[71]. VASP is known to interact with target proteins such as vinculin, zyxin, and palladin[72] which are responsible for the interactions with actin. Dephosphorylation of VASP allows for actin polymerization at the barbed end of the filament[73]. Vinculin is associated with membrane adhesion junctions in smooth muscle tissue, linking actin filaments to the extracellular matrix allowing contraction to

occur[74]. Zyxin is also involved in the mechano-transduction of smooth muscle as a focal adhesion protein that is associated with the actin cytoskeleton[75].

Measurement of Intracellular Calcium
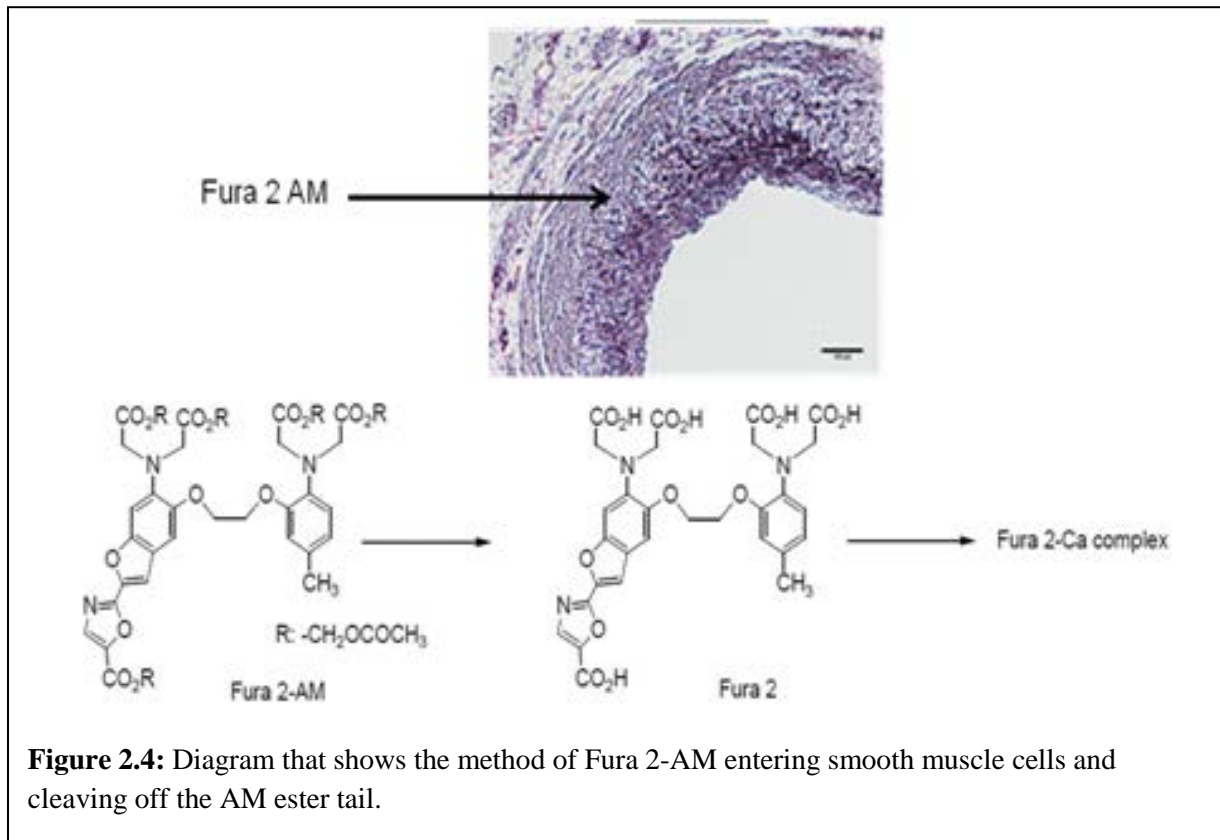
Figure 2.4: Diagram that shows the method of Fura 2-AM entering smooth muscle cells and cleaving off the AM ester tail.

To develop a fully integrated system combining a muscle bath apparatus for force transduction measurements and a fluorescence detection system for Ca^{2+} flux with multiple chambers. A custom designed ADInstruments data acquisition system allowed us to integrate the musclebath apparatus system, which measures force transduction, with a Fluoroplex controller to determine absolute $[Ca^{2+}]_i$ using the ratiometric dye Fura-2.

Fura 2 is a fluorescently labeled dye that permeates the tissue. The AM tail allows the Fura 2 to permeate the cell membrane. Once inside the cell, esterases cleave the AM ester off of the Fura 2 trapping it inside of the cells (Figure 3). Inside the cells intracellular calcium binds to

the Fura 2 compound creating a fura 2-Ca^{2+} complex that emits light at 510 nm light when excited with 340 or 380 nm light. The ratio between the amount of light emitted when excited with either 340 or 380 nm of light gives the 340/380 ratio which is related to the intracellular calcium concentration. When Fura 2 binds with calcium the excitation spectrum for Fura 2 shifts to shorter wavelengths (Figure 4). This shift in spectrum is why a ratiometric calculation is used. The 340 nm excitation light reflects calcium that is bound to the Fura 2 and the 380 excitation light is unbound Fura 2. An increase in this ratio correlates with an increase in bound Fura 2 to calcium.

Figure 2.5: Emission and excitation wavelengths of Fura-2 AM.
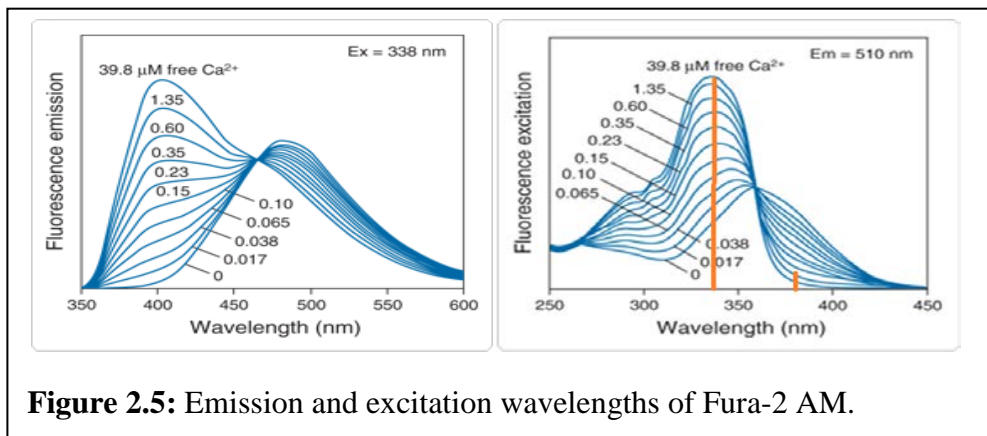
In order to increase the delivery of Fura-2 AM into vascular tissue Pluronic F-127 was used.

Pluroinc F-127 is a nonionic, surfactant polyol used to facilitate the solubilization of water insoluble dyes into physiologic media. The surfactant polyol is in a solution that contains DMSO, a colorless liquid that acts as a polar solvent that is able to create a homogenous solution for dyes such as Fura 2-AM. The final physiologic solution contained 0.01% DMSO in the bicarbonate buffer.

Ratiometric dyes are useful for situations where photobleaching, uneven dye loading, motion artifacts, or variable tissue thickness is present. In the case of rings of vascular tissue where constant 95% O2 and 5% CO2 are being added the necessity for a dye that will

compensate for motion artifacts and variable tissue thickness becomes very important. Although the measurements are not taken over a very long period of time, it is important to always keep in mind that photobleaching of the tissue occurs with Fura 2-AM. The Fluoroplex system uses optical fibers running from the multiplexer to the tissue baths where the tissue is excited with either 340 nm or 380 nm light and then the emission light is passed back to the multiplexer. The use of filters and dichroic mirrors (described further in Chapter 3,Figure5). Fura-2 poses advantages over other calcium indicators, such as aequorin, in that it emits more light, avoiding problems like calcium buffering or the damping of a calcium transient.

Transmembrane Delivery of Small Molecules

siRNA

Small interfering RNA (siRNA) is used for its role in the RNA interference pathway to silence the expression of a specific gene. siRNA's are double stranded RNA molecules that vary in length between 20 and 25 base pairs. siRNA has great clinical potential because of the specificity of a target mRNA that one wishes to silence. One of the major challenges in creating a clinical solution with siRNA is the delivery into the cytoplasm. siRNA alone is not permeable to cell membranes and is quickly degraded by nucleases present in the body

Current delivery strategies to improve the delivery of siRNA involve incorporating a carrier. Typically a carrier for siRNA will be cationic in order to electrostatically complex the negatively charged siRNA. Lipofecatime is an example of a cationic lipid used to deliver siRNA, but in addition to lipids, liposomes, nanoparticles, and polymers may be used. Lipofectamine is a known reagent for transfecting siRNA into cells, but does not yield the same transfection rates in tissue. Delivery of siRNA into tissue poses extra obstacles to traditional cellular transfection.

Transfection into intact tissue requires a more robust approach and polymers and nanoparticles were developed for siRNA delivery. A benefit of using cationic polymers is that they condense the siRNA and protect it against nuclease degradation. To approach the issue of transfecting siRNA in an ex vivo model, an endosomolytic diblock copolymer was used that had been previously developed (Duvall, Stayton et al)[76]. This pH responsive carrier of siRNA was designed to mediate endosomal release of the siRNA, lowering the degradation from nucleases. This diblock copolymer is made of N,N-Dimethylaminoethyl methacrylate (DMAEMA), polypropyl acrylic acid (PAA), and butyl methacrylate, synthesized using a reversible addition fragmentation chain transfer polymerization.

The first block of the materials is DMAEMA, and is used to condense the siRNA at a physiologic pH. The second block of this copolymer is ampholytic and contains DMAEMA, PAA, and BMA which undergoes a conformational change at low pH's. At physiologic pH ranges this block is ampholytic; however once this block reaches a lower pH the PAA carboxylate becomes protonated allowing it to enter the endosome's membrane. This delivery mechanism is based on the change in pH that occurs from outside of the cell to the endosomes which have a pH of 6.2-6.5.

Peptides

The use of peptides as therapeutics is a growing field. Peptides have many advantages over small molecules in terms of specificity and affinity for targets, and have a size advantage over antibodies[77]. A large problem for peptide therapeutics is addressing proteolytic degradation. Methods such as pegylation, antibody attachment, and the binding to serum albumin protect peptides from proteases[77]. In 2012 six peptides received marketing approval in the USA[78], and one of these peptides has been removed for safety reasons. The six peptides

22

approved had different indications such as: RDS, anemia, cushing's disease, multiple myeloma, constipation, short bowel syndrome. Among these peptides four are receptor agonists, one is a surfactant, and the last is a protease inhibitor. Signifor, a peptide therapeutic for Cushing's disease, was voluntarily withdrawn after approval when three deaths occurred although there were no issues in the 2300 person clinical trial. Novartis is an EPO receptor agonist, and it may be brought back to a clinical setting in the future[78].

Figure 2.6 HSP20 phospho peptidomimetic transduction domain and carrier peptide
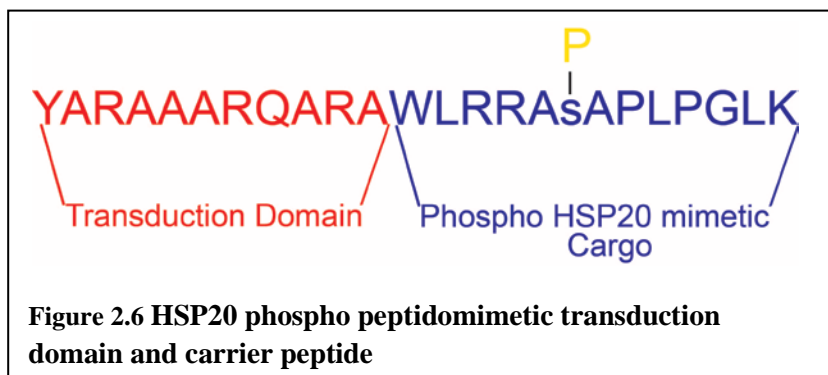
Cell penetrating peptides (CPPs), are generally cationic and interact with the negative charge of cell membranes. They are often conjugated to biologic therapeutics such as peptides, DNA, and siRNA to increase cell uptake of these "cargo" compounds. Thus cell penetrating peptides are composed of two parts, the transduction domain (PTD) and the cargo that is to be delivered. The most famous of transduction domains is a component of HIV-1, TAT. PTD's enter cells in a rapid, receptor-independent fashion[79]. TAT has been optimized to create synthetic PTD's[80]. PTDs were created to attempt at strengthening the existing structure of YGRKKRRQRRR. The peptide, "YARAAARQARA" yielded the highest transduction potential relative to the TAT peptide. This was determined by fluorescent confocal microscopy of treated cells having the PRD within the cytoplasm and nucleus of the cell[80]. This PTD was used to create a cell permeant phosphorylated HSP20 mimetic.

Even with the benefits that PTDs offer in the delivery of the cargo inside of cells, substantial synthetic and functional limitations still exist in terms of multi-functional drug

carriers that simultaneously address the key delivery barriers of stability, cellular uptake, escape from the endo-lysosomal pathway, and an effective means to 'un-package' or release the desired therapeutic into the proper intracellular micro-environment. The CPPs often do not escape the endo-lysosomal trafficking pathway, and to combat this issue, polymers that have conformational changes increasing the unpackaging of the cargo inside of the cell to maximize delivery were created.

Conclusions

SAH induced cerebral vasospasm has shown to create biochemical changes in the tissue with proteins such as HSP20, HSP27, and MAPK. With the aid of tools able to transfect siRNA ex vivo and CPP's capable of penetrating cells, the manipulation of these targets presents itself as a viable option for mimicking the changes that occur in cerebral vasospasm. Creation of this vasospastic model system in intact tissue allows for the testing of treatment options and would allow determining the potential effects on vasospasm.

CHAPTER 3

Calcium Independent Force Inhibition

Aim 1 *Develop a model system that inhibits force without inhibiting increases in Ca2+ to uncouple force production from thick filament regulation*

Aim 2 *Use the dose of forskolin identified in aim 1 to investigate biochemical events including calcium and actin regulatory processes*

Text partially adapted from:

Hocking KM, Baudenbacher FJ, Putumbaka G, Venkatraman S, Cheung-Flynn J, Brophy CM, Komalavilas P. Role of Cyclic Nucleotide-Dependent Actin Cytoskeletal Dynamics: [Ca2+]i and Force Suppression in Forskolin-Pretreated Porcine Coronary Arteries. PLOS One

Introduction

Smooth muscle activation of the H1 receptor via histamine is linked to the intracellular G protein (Gαq) and Gαq-coupled receptors that activate phospholipase C (PLC) and RhoA (reviewed in [41]). Activation of PLC induces inositol 1, 4, 5-trisphosphate (IP$_3$) production, causing calcium to be released from the sarcoplasmic reticulum (SR). This increase in intracellular calcium activates calmodulin-dependent myosin light chain kinase (MLCK), leading to increases in the phosphorylation of 20 KDa myosin light chains (MLC). Crossbridge phosphorylation of the actomyosin apparatus results in the generation of force in vascular smooth muscle [11,42,43]. While Ca^{2+} and MLC phosphorylation are important for the initiation of contraction, the tonic phase, or force maintenance, of smooth muscle contraction can occur where [Ca^{2+}]$_i$ levels and MLC phosphorylation are near basal levels, suggesting other pathways are engaged during force maintenance in smooth muscle [42,44-48]. During the sustained phase of

contraction, stiffness and force are maintained at high levels while Ca^{2+}, crossbridge

phosphorylation, and shortening velocity fall to intermediate values [45,51,52,81]. Maintenance of

high force despite intermediate levels of crossbridge phosphorylation and velocity was explained

to be due to the latch phenomenon [53,54]. Other investigators have suggested that force

maintenance is due to the regulation of ADP association with muscle fibers [82]. More recently,

actin cytoskeletal dynamics have been implicated in the modulation of vascular smooth muscle

tone [59,83]. Similarly, sustained phase of swine carotid artery contraction was associated with

increased paxillin (Y118) phosphorylation and actin polymerization [84].

Vascular smooth muscle relaxation, or inhibition of force, can be mediated by

vasodilators that activate guanylyl cyclase (e.g. nitric oxide) or adenylyl cyclase (e.g.

prostacyclin, β-agonists, and forskolin), leading to increases in cGMP and cAMP, respectively.

The cyclic nucleotides, in turn, activate cGMP-dependent protein kinase (PKG) and cAMP-

dependent protein kinase (PKA) [56], leading to several phosphorylation events resulting in

relaxation or inhibition of force. Cyclic nucleotide-induced relaxation or inhibition of force in

smooth muscle involves at least three major pathways: decreases in intracellular free calcium

concentrations, calcium sensitivity and actin cytoskeletal regulation (reviewed in [56,57]). While

the role of a decrease in $[Ca^{2+}]_i$ and Ca^{2+} sensitivity in the regulation of smooth muscle cell

contraction has been established, the role of actin cytoskeleton and actin-associated proteins is

still unclear. Although several investigations have suggested the regulation of actin and actin-

associated proteins in smooth muscle contraction (reviewed in [59]), very few reports have

addressed the role of second messenger regulation of actin-associated proteins during inhibition

of force. Actin-associated proteins that are implicated in the regulation of smooth muscle

contraction include the small heat shock-related protein 20 (HSP20 or HSPB6), cofilin,

vasodilator-stimulated phosphoprotein (VASP) and paxillin. HSP20 is an actin binding protein that is phosphorylated by PKG and PKA on serine 16, inducing relaxation and inhibition of contraction through the modulation of actin cytoskeletal dynamics [55,62-64]. Cyclic nucleotide-dependent relaxation is associated with decreases in the phosphorylation of the actin depolymerizing protein cofilin in vascular, as well as, airway smooth muscle cells [64,68]. VASP is an actin binding protein that is localized to focal adhesions and cell-to-cell contacts [60]. Forskolin treatment leads to phosphorylation of VASP and regulates the actin cytoskeleton in rat aortic smooth muscle cells [70] and human airway smooth muscle cells [68]. Paxillin is a scaffolding protein that serves as a multi-domain adaptor at the interface between the plasma membrane and the actin cytoskeleton (reviewed in [85]). Paxillin undergoes phosphorylation and activation in response to contractile stimulation in many smooth muscle tissue types and is involved in the regulation of actin polymerization during contraction [84,86].

In this study, we hypothesized that cyclic nucleotide-induced force suppression is dependent upon changes in actin cytoskeletal dynamics. We developed a physiological model in which histamine-induced force was completely suppressed by forskolin pretreatment in PCA smooth muscle. In this novel approach, force and $[Ca^{2+}]_i$ were measured concurrently using a FluoroPlex Tissue Bath Fluorometry System, and polymerization of actin, phosphorylation of actomyosin and actin-associated proteins were determined. Our results indicate that forskolin-induced suppression of force does not completely abolish Ca^{2+} transients or MLC phosphorylation but causes depolymerization of actin dose-dependently, and changes in the phosphorylation of proteins such as HSP20, cofilin, VASP and paxillin that regulate actin polymerization. Since force can be completely suppressed without abolishing $[Ca^{2+}]_i$, this model

system can be employed to elucidate as yet unidentified Ca^{2+}-independent molecular determinants of force inhibition in vascular smooth muscle.

Methods

Materials

All chemicals were purchased from Sigma Chemical Co. (St. Louis, MO) unless specified otherwise. Pre-cast acrylamide gels, Sodium dodecyl sulfate (SDS), Tris-glycine-SDS buffer (TGS), Tris-glycine (TG) and prestained Precision Blue Protein Standards were purchased from Bio-Rad (Hercules, CA). Urea and CHAPS (3-[(3-Cholamidopropyl) dimethylammonio]-1-propanesulfonate) were from Research Organics Inc. (Cleveland, OH). F/G Actin assay kit was from Cytoskeleton Inc., (Denver, CO). Fura 2-AM and Pluronic F-127 was purchased from Invitrogen (Carlsbad, CA).

Procurement of porcine coronary artery smooth muscle tissue and physiologic measurements

Fresh cadaveric hearts were isolated immediately from euthanized, discarded animals from Vanderbilt University Medical Center. All procedures for collection of cadaveric tissue were reviewed and approved by the Vanderbilt University Animal Care and Use Committee. Porcine hearts were also collected from the local slaughter house (C&F Meats, Triune, TN) after obtaining permission from the slaughter house to use the tissue for research. The heart was procured and placed directly in HEPES buffer (140 mM NaCl, 4.7 mM KCl, 1.0 mM $MgSO_4$, 1.0 mM NaH_2PO_4, 1.5 mM $CaCl_2$, 10 mM glucose, and 10 mM HEPES, pH 7.4), and the coronary arteries were dissected and tested immediately or after overnight storage at 4°C in University of Wisconsin solution. Subcutaneous fat and adventitial tissues were removed and the vessel was cut into transverse rings of 3.0 mm in width. To focus on the smooth muscle-

derived changes during inhibition of force, endothelium was denuded by gently rolling the luminal surface of each ring at the tip of a fine forceps. Rings were suspended in a muscle bath containing a bicarbonate buffer (120 mM NaCl, 4.7 mM KCl, 1.0 mM $MgSO_4$, 1.0 mM NaH_2PO_4, 10 mM glucose, 1.5 mM $CaCl_2$, and 25 mM Na_2HCO_3, pH 7.4), equilibrated with 95% O_2 / 5% CO_2, at 37°C. Force measurements were obtained with either a Kent Scientific (Litchfield, CT) force transducer (TRN001) or a Radnoti force transducer (Radnoti Glass Technology Inc., Monrovia, CA) interfaced with Power Lab from AD Instruments (Colorado Springs, CO). Data were recorded with Chart software, version 5.1.1 (AD Instruments). Rings were washed every 15 min with 37°C bicarbonate buffer for 1 hr, and each ring was progressively stretched to its optimal resting tension (approximately 1 g) that would produce a maximal response to contractile agonists as determined previously, then maintained at the resting tension and equilibrated for another hour. Rings were then contracted multiple times with high extracellular potassium (110 mM KCl, with equimolar replacement of NaCl in bicarbonate buffer) and the force generated was measured. Measured force was normalized for ring weight and length and converted to Stress using the formula: Stress [10^5Newtons (N)/m^2] = force (g) x 0.0987 / area, where area is equal to the wet weight [mg / length (mm at maximal length)] divided by 1.055. The maximal tension obtained was taken as 100%. Rings were equilibrated for an additional 30 min and dose response curves for histamine contraction and forskolin relaxation were determined to select the correct dose of agents for the experiment. To determine the inhibition of contraction, rings were either treated with buffer alone (control), histamine (5 µM) for 3 min, forskolin (5 µM) for 10 min, or forskolin (1, 5, or 10 µM) for 10 min followed by histamine (5 µM) for 3 min. At the end of the experiments, all rings were washed and contracted with KCl to ensure continued viability of the tissues. To determine the role of

phosphorylation of proteins during inhibition of force, physiologic experiments were conducted as described above and the tissues were snap frozen under tension using forceps precooled in liquid nitrogen at 3 min and then pulverized. These pulverized tissues were stored at -80°C for later analysis using urea glycerol gel, SDS polyacrylamide gel electrophoresis (PAGE) or isoelectric focusing and western blotting. For actin assay to determine the level of F-actin compared to G-actin, the tissues were used immediately after treatment without freezing.

Cytosolic [Ca^{2+}]$_i$ measurements

Fluroplex

The complete system incorporates a musclebath apparatus that measures the force
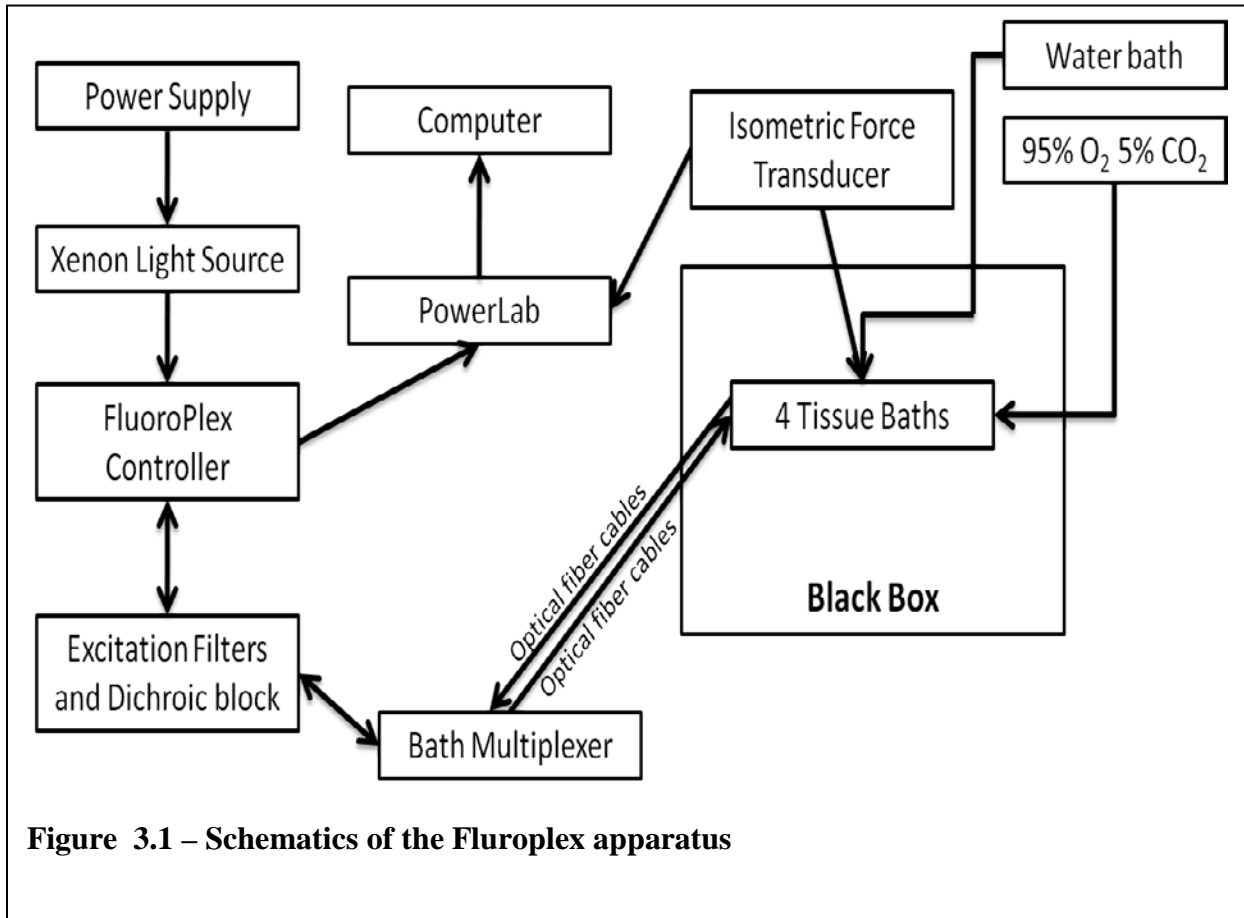
Figure 3.1 – Schematics of the Fluroplex apparatus

generated by the arteries, a xenon arc lamp to create light, power source, fluroplex controller,

bath multiplexer, PowerLab device, optical fibers, water bath for heating, 95% O_2 5% CO_2 tank,

and excitation filters. All of these elements are displayed in Figure 5, and show how the system

is integrated together.

Figure 3.2: Schematics for the light pathway from arc lamp to tissue, through excitation filters and dichroic blocks. [1]
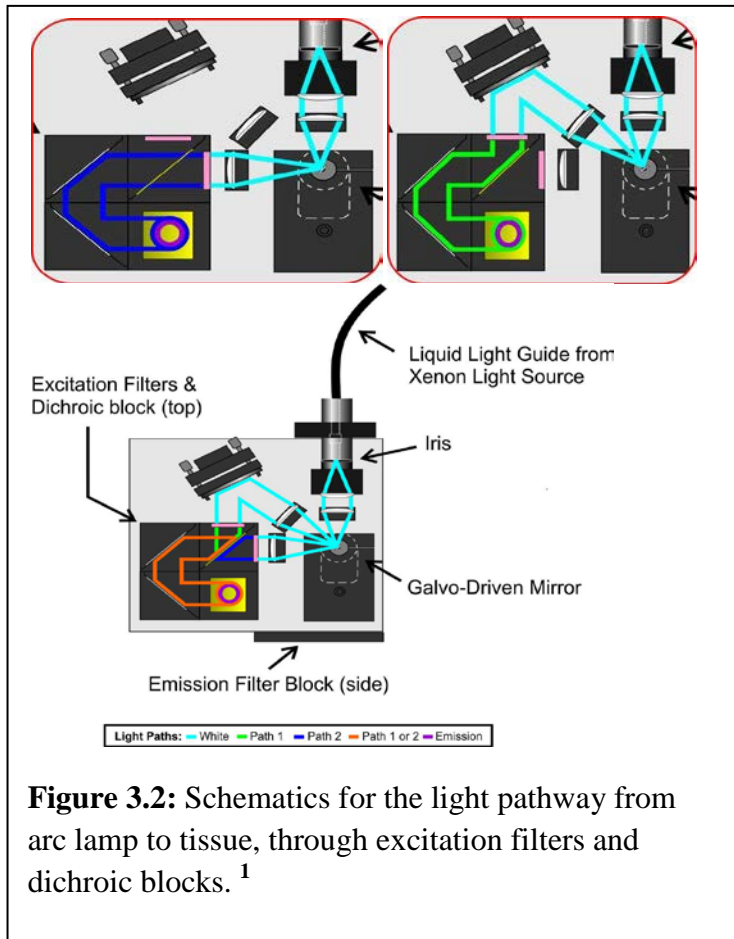
Light from a xenon arc lamp source is filtered with a neutral density filter block and the light is guided to the FluoroPlex multiplexer box where it is collimated, focused, and then filtered (Figure 3.2). Since two excitation wavelengths are needed to determine the intracellular calcium concentration, a galvo driven mirror is used to guide the light down one of two paths. The first path for 340 nm wavelength light is focused onto a lens and then shone upon an excitation filter and then a dichroic mirror that reflects the 340 nm wavelength light down its path filtering out the rest of the light. After this light has passed the galvo-driven mirror focuses the next light wave onto a different lens that filters the light through excitation filters to 380 nm and passed through a dichroic mirror. Both of these light sources are reflected onto the multiplexer that then delivers light to the tissue bath apparatus. The timing of the two different wavelengths of light is how the FluoroPlex determines ratiometric data from emission light.

After the fura 2 has been excited by either 340 or 380 nm light it emits 510 nm light which is passed through the optical fiber and directed by the multiplexer to the emission filter block dichroic mirror which eliminates and auto fluorescent light at a wavelength that is not 510

nm. This light is then passed into a photomultiplier tube which converts the emission light intensity to an electronic signal that is interpreted by the Fluroplex.

In order to concurrently measure force and calcium, loading conditions for Fura 2-AM had to be established for intact tissue rings that were under tension. Fura-2 AM has been used in vascular smooth muscle cells, but rarely loaded into intact vascular tissue segments. In order to load Fura-2 AM many experimental protocols were used and a unique method for loading was developed (Appendix II). The new technique involved the loading of 5µM Fura-2 AM in 0.1% Pluronic F-127 and DMSO. Below describes the optimal loading conditions found for porcine coronary arteries for use in the Fluroplex apparatus.
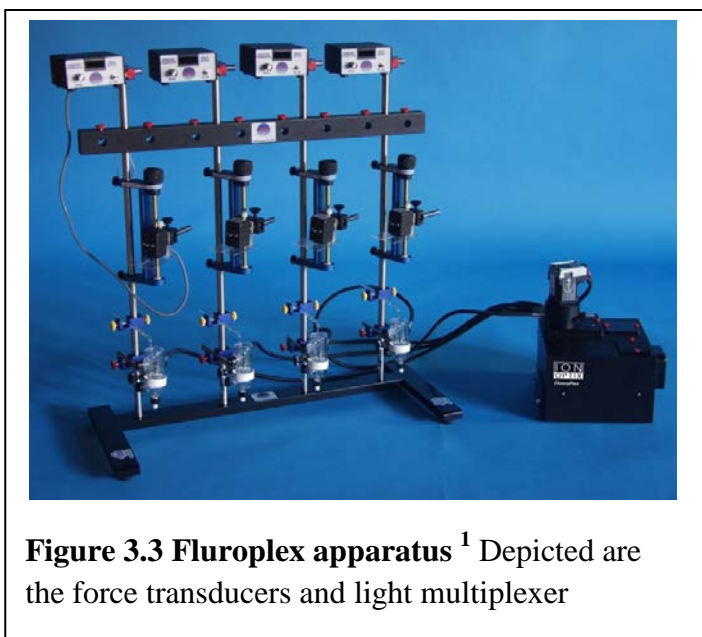
Figure 3.3 Fluroplex apparatus [1] Depicted are the force transducers and light multiplexer

Rings of PCA were suspended on hooks in a Fluroplex (Figure 3.3) (Tissue Bath Fluorometry System, IonOptix LLC, Milton, MA) which enables fluorescence ion recording in parallel with force measurement. Force measurements were obtained with a Radnoti force transducer (Radnoti Glass Technology Inc., Monrovia, CA) interfaced with Power Lab from AD Instruments (Colorado Springs, CO). Rings were loaded at room temperature with 5 µM Fura-2 AM ester in the bicarbonate buffer for 4 hrs. After loading, rings were washed every 10 min with 37°C bicarbonate buffer for 1 hr. Fluorescence was measured at both 380 and 340 nm of wavelength simultaneously. The ratio of the emission of the two wavelengths was used to determine intracellular changes in calcium concentration.

Baseline ratio was set at 1.0 and changes in this ratio in response to stimuli were measured.

Baseline calcium fluorescence was measured and the background was set to zero as an output of

1 volt. To determine the inhibition of contraction, rings were either treated with forskolin (5 µM

for 10 min) followed by histamine (5 µM) or histamine alone. To add forskolin or histamine

while continuously measuring intracellular calcium concentrations, an infusion line filled with

bicarbonate buffer was used to keep the system in a closed light impenetrable state. The amount

of buffer in the infusion line was adjusted to achieve the final concentration of the agonist in the

bath. Force and calcium fluorescence were measured continuously for 15 min after the addition

of histamine.

Determination of VASP, cofilin and paxillin phosphorylation

Proteins from frozen muscle rings were extracted in UDC buffer (8 M urea, 10 mM

dithiothreitol (DTT), 4% CHAPS containing protease inhibitor, Phosphatase I and II inhibitor

cocktail (Sigma, St. Louis, MO). The mixtures were vortexed at room temperature overnight,

and then centrifuged at 14,000 rpm for 15 min at 4°C. Soluble protein concentrations were

determined using the Bradford assay (Pierce Chemical, Rockfort, IL). Equal amounts (20-50 µg)

of proteins were placed in a Laemmli sample buffer (Bio-Rad laboratories, Inc. Hercules, CA),

heated for 5 min at 100°C and separated on SDS polyacrylamide gels. Proteins from the gels

were transferred onto nitrocellulose membranes (Li-COR Biosciences, Lincoln, NE) and blocked

prior to incubation overnight at 4°C with the following primary antibodies: anti-VASP (1:2000,

ECM Biosciences, Versailles, KY); anti-phospho-cofilin 2 (Ser 3) (1:500), and anti-cofilin

(1:500, Cell Signaling Technology, Santa Cruz, CA), anti phospho (Tyr 118)-paxillin (1:250,

Santa Cruz Biotechnology, Inc.) and anti-paxillin (1:250, BD Transduction Laboratories). VASP

phosphorylation by PKA at Ser 157 causes a significant mobility shift on one dimensional SDS-

PAGE gels [87] enabling to separate phospho(p) and non-phospho(np) VASP on the same gel and

was detected by using an antibody that recognizes both phospho and non-phospho forms.

Membranes were washed three times with TBS containing Tween 20 (0.1%) (TBST), and

incubated with appropriate infrared-labeled secondary antibodies (Li-Cor, Lincoln, NE) for 1h at

room temperature. The membranes were subsequently washed with TBST, and protein-antibody

complexes were visualized and quantified using the Odyssey direct infrared fluorescence

imaging system (Li-Cor Biosciences NE). Phosphorylation was calculated as a ratio of the

phosphorylated protein to total protein (p- plus np- protein) and was then normalized to the

unstimulated control with the control value set as 1.0.

Determination of MLC phosphorylation

MLC phosphorylation was determined using a modification of an established urea

glycerol method that separates p- and np- MLC [88,89]. The frozen tissue was pulverized, placed in

a frozen slurry of precipitating solution consisting of 90% acetone, 10% trichloroacetic acid, and

10 mM DTT, and then allowed to melt to room temperature. The precipitating solution was

removed, and the tissues were washed three times with 90% acetone and 10 mM DTT. The

samples were dried, and the pellets were suspended in UDC buffer as described above and

vortexed to solubilize the proteins. Ten micrograms of protein were diluted with 10 μl of urea

sample buffer (6.7 M urea, 18 mM Tris, 20 mM glycine, 9 mM DTT, 4.6% saturated sucrose,

and .004% bromophenol blue) and separated on glycerol-urea mini gels (40% glycerol, 10%

acrylamide, 0.5% bisacrylamide, 20 mM Tris, and 22 mM glycine). Proteins were transferred

onto nitrocellulose membranes in a buffer containing 10 mM Na_2HPO_4 pH 7.6 at 25 V for 1 hr at

20°C. The blot was probed with anti MLC antibody (1: 7000, gift from Dr. James Stull,

University of Texas, Galveston TX), and processed as described above. The p- and np- MLC

bands were quantitated by densitometric analysis. The relative amount of the p-MLC was calculated.

Determination of HSP20 phosphorylation

Phosphorylation of HSP20 in response to forskolin was examined by isoelectric focusing, which separates the p- and np- forms of HSP20 and detected by western blotting. 30 µg of extracted proteins from the treated PCA samples were separated on one-dimensional isoelectric focusing gel (8.3X7.3 cm) with 5% ampholines (4 parts pI 4-7 and 1 part pI 3-10, GE Healthcare Bio-Sciences) using 20 mM sodium hydroxide as a cathode buffer and 10 mM phosphoric acid as an anode buffer. Proteins were focused for 100 V for 1 hr, 250 V for 1 hr and 500 V for 30 min and transferred to nitrocellulose membrane at 25 V in 0.7% acetic acid with the direction of the gel sandwich reversed (acetic acid give proteins a positive charge) for 1 hr at room temperature. The blot was probed with anti-HSP20 antibody (1:3,000 dilution, Advanced Immunochemical Inc., Long Beach, CA); and the p- and np- forms of HSP20 were quantitated by densitometry and the ratio of p-HSP20 to total HSP20 was calculated.

Actin Assay

The amount of F-actin versus G-actin was measured using the G-actin/F-actin *In Vivo* Assay kit (Cytoskeleton, Denver, CO), per manufacturer's protocol. Briefly, treated PCA samples were homogenized in 1 ml of lysis buffer (50 mM PIPES pH 6.9, 50 mM NaCl, 5 mM $MgCl_2$ 5 mM EGTA, 5% (v/v) Glycerol, 0.1 % Nonidet P40, 0.1% Triton X-100, 0.1% Tween 20, 0.1% 2-mercapto-ethanol, 0.001% Antifoam C, 4 µM Tosyl arginine methyl ester, 15 µM Leupeptin, 10 µM Pepstatin A, 10 mM Benzamidine, 1 mM ATP warmed to 37°C) for 1 min with a mortar and pestle that fit into the 1.5 ml microfuge tube. The lysate was centrifuged at 2000 rpm for 5 min at 37°C to pellet unbroken cells. The supernatants were centrifuged at

36

100,000 x g for 1 hr at 37°C. Supernatants (contains the G-actin) were transferred to pre-cooled

tubes and placed on ice. The pellets (contain F-actin) were resuspended in 1 ml of ice-cold 10

µM cytochalasin D in deionized water, and F- actin was depolymerized by incubating for 1 hr on

ice with mixing every 15 min. Equal volume of supernatants and pellets along with actin

standards (2-20 µg) were separated on 12% SDS-polyacrylamide gels and transferred to

nitrocellulose membrane in 1X TG buffer at 100 volts for 1 hr. The membrane was probed with

anti actin antibody and the amount of actin in each fraction was quantified comparing to actin

standards loaded on the same gel.

Statistical analysis

All data are reported as the mean responses $\pm$ standard error of the mean (SEM).

Statistical analysis was performed by unpaired Student's *t* test or one-way *ANOVA,* followed by

Tukey's post test (GraphPad Software, Inc. San Diego, CA). The criterion for significance was p

< 0.05.

Results

*The effect of forskolin on inhibition of contraction, Ca^{2+} transients, and MLC phosphorylation*To

study the role of actin cytoskeletal dynamics during inhibition of contraction we first developed a

physiological model system with conditions in which agonist-induced force was completely

suppressed in the presence of Ca^{2+} transients with no significant change in the MLC

phosphorylation. This allowed the study of putative mechanisms, other than calcium

desensitization, that regulate the suppression of force. Initial experiments were conducted using

rious doses of histamine (0.1 to 10 µM) to contract PCA, and a dose of histamine (5 µM) which

produced greater than 60% of maximal potassium-induced contraction was selected for our

experiment (Figure 3.4 A). Treatment of PCA with histamine (5 µM) alone induced force (62 %

of KCl stress, Figure 3.4 A, E) and increased Ca^{2+} transients (0.35± 0.05 AU, n=9) (Figure 3.4
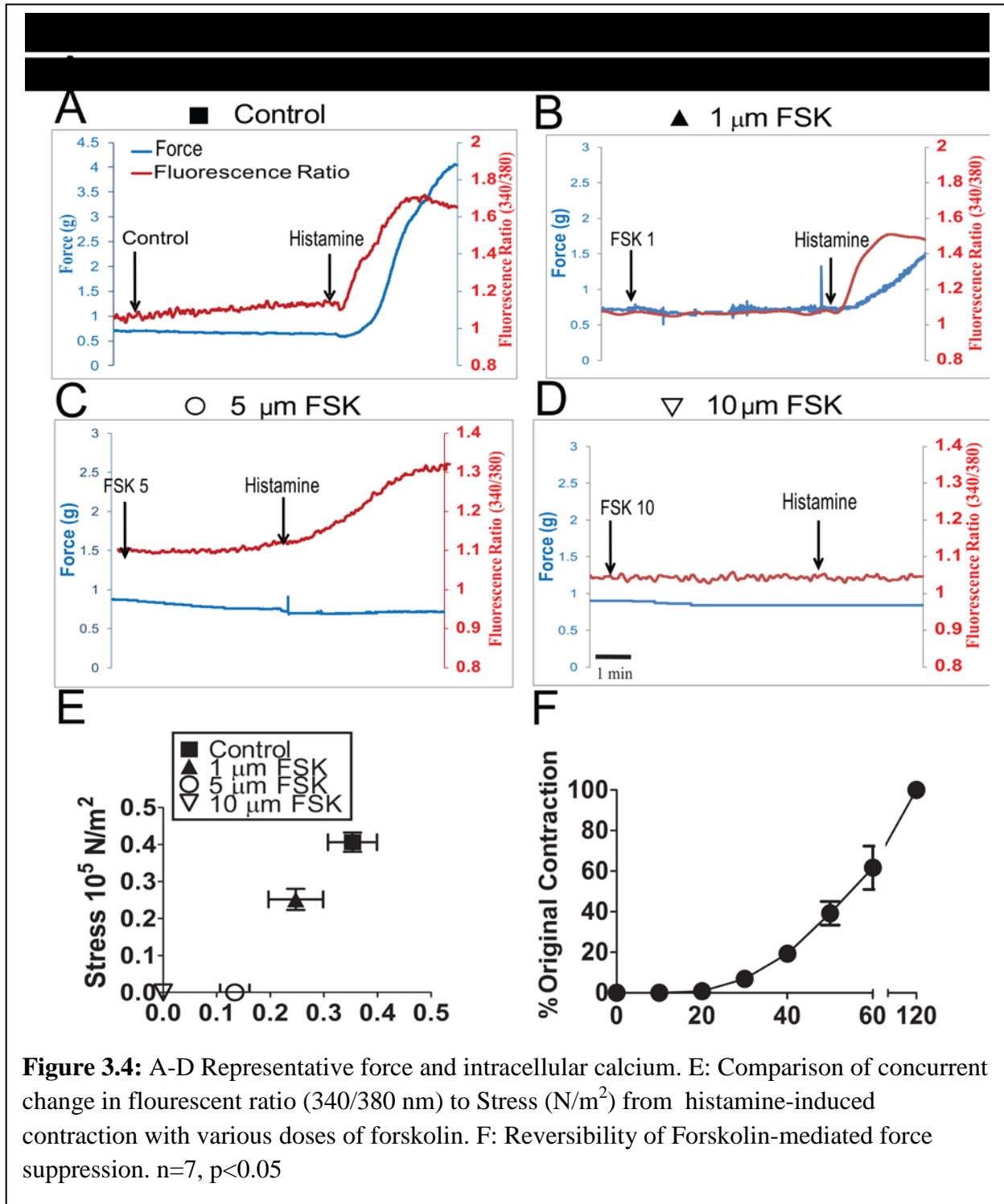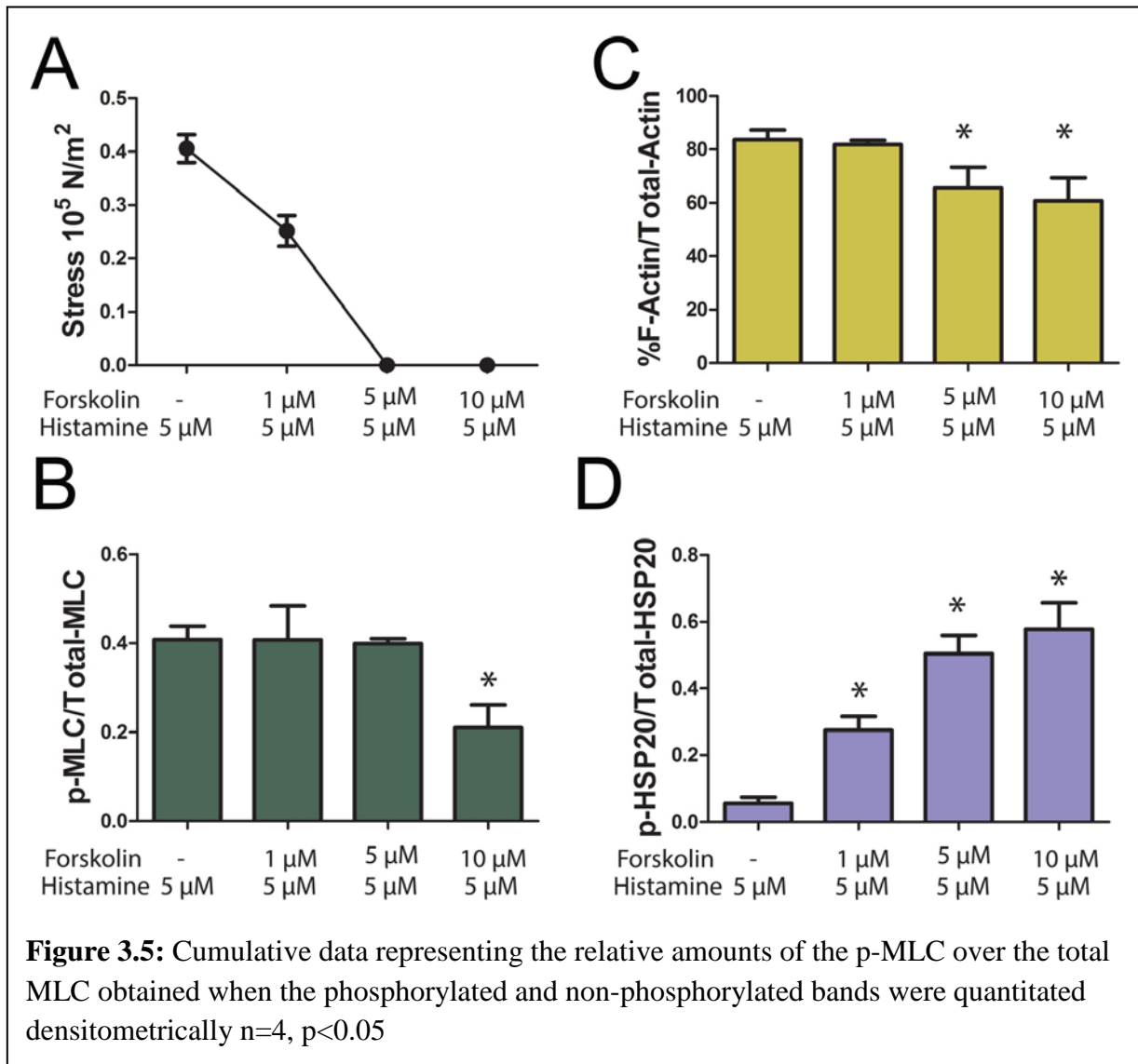

Figure 3.4: A-D Representative force and intracellular calcium. E: Comparison of concurrent change in flourescent ratio (340/380 nm) to Stress (N/m^2) from histamine-induced contraction with various doses of forskolin. F: Reversibility of Forskolin-mediated force suppression. n=7, p<0.05

A, E). Changes in Ca^{2+} transients occurred before the initiation of contraction, and the
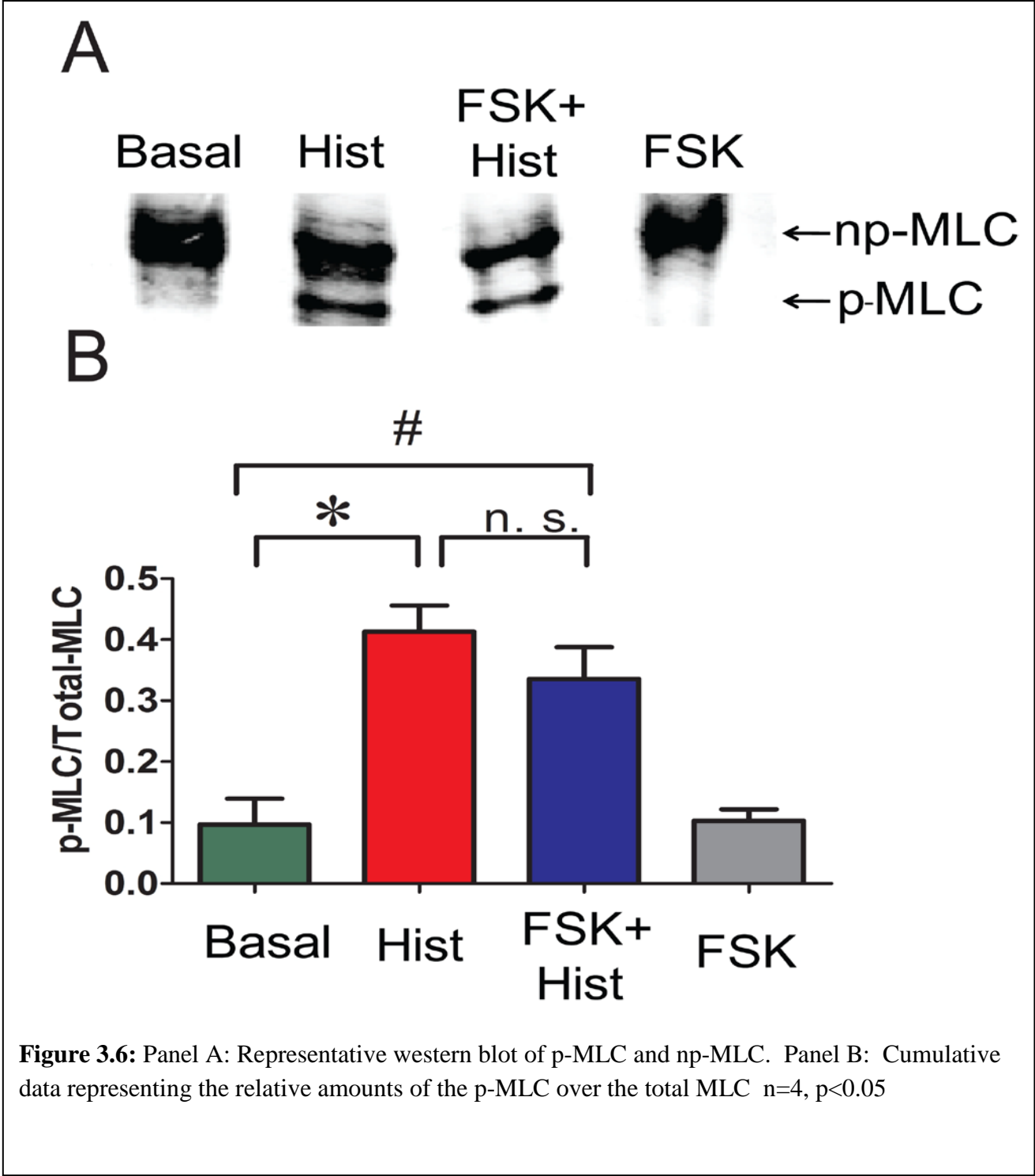
fluorescence ratio reached a maximum value while force was still increasing. The maximum

fluorescence ratio sustained for 45 seconds and dropped prior to any decrease in force. To

develop a physiological model system with force completely suppressed in the presence of Ca^{2+}

transients with no significant change in the MLC phosphorylation, we pretreated PCA with

different doses of forskolin (1, 5, and 10 μM) for 10 min followed by histamine (5 μM) for 3 min

and force, $[Ca^{2+}]_i$, MLC phosphorylation, F-actin levels and HSP20 phosphorylation were

measured. Pretreatment of PCA with forskolin at 1 μM did not abolish histamine-induced force

(38% of KCl stress, Figure 3.4B, E), $[Ca^{2+}]_i$ (0.25 $\pm$ 0.05 AU, n=7)   (Figure 3.4 B, E), MLC

phosphorylation (0.41 $\pm$ .03 and 0.41 $\pm$ 0.08 p-MLC/total MLC for histamine and 1 μM forskolin

plus histamine, respectively, Figure 2B) or significantly change the F-actin concentration (84 $\pm$

4%and 82 $\pm$ 2% for histamine and forskolin plus histamine, respectively, Figure 2C). However,

pretreatment with 1 μM forskolin increased the phosphorylation of HSP20 (0.06 $\pm$ 0.02 and 0.28

$\pm$ 0.04 p-HSP20/total HSP20 for histamine and forskolin plus histamine, respectively, Figure

2D). Forskolin at 5 μM completely suppressed histamine-induced force (0% of KCl stress,

Figure 1B, E, Figure 3.5A) but did not abolish $[Ca^{2+}]_i$ (0.13 $\pm$ 0.03 AU, n=9) (Figure 3.4 C, E).

The magnitude of the change in fluorescence ratio was significantly greater for tissue contracted

with histamine (0.35 $\pm$ 0.05 AU) when compared to tissue treated with 5 μM forskolin followed

by histamine (0.13 $\pm$ 0.03 AU)(n=7, p<0.01, Figure 3.4E). The time it took for the $[Ca^{2+}]_i$ to rise

from 10% to 90% of its maximal was significantly shorter (54.40 $\pm$ 8.23 seconds) for tissue that

was treated with histamine alone compared to forskolin followed by histamine treatment (192.8

$\pm$ 45.63 seconds n=5, p=0.024, data not shown). Forskolin at 5 μM did not significantly change

MLC phosphorylation (0.4.$\pm$ 0.03 and 0.39 $\pm$.01 p-MLC/total MLC for histamine and forskolin

plus histamine, respectively, Figure 2B), however it decreased F-actin levels (84 $\pm$ 4% and 66 $\pm$

8% for histamine and forskolin plus histamine, respectively, Figure 3.5C) and increased the phosphorylation of HSP20 (0.06 ± 0.02 and $0.50 \pm .0.05$ p-HSP20/total HSP20 for histamine and forskolin plus histamine, respectively, Figure 3.5D). Forskolin at 10 µM completely suppressed histamine-induced force (0 % of KCl stress, Figure 3.4 D, E) as well as $[Ca^{2+}]_i$ (0 AU, n=7) (Figure 3.4D, E). Forskolin at 10 µM significantly decreased the MLC phosphorylation ($0.4.\pm 0.03$ and $0.21.\pm 0.05$ p-MLC/total MLC for histamine and forskolin plus histamine, respectively, Figure 2B), and F-actin levels ($84 \pm 4\%$ and $60 \pm 9\%$ for histamine and forskolin plus histamine,


Figure 3.5: Cumulative data representing the relative amounts of the p-MLC over the total MLC obtained when the phosphorylated and non-phosphorylated bands were quantitated densitometrically n=4, p<0.05

respectively, Figure 2C) while it increased the phosphorylation of HSP20 (0.06 ±0.02 and 0.50 ±.0.05 p-HSP20/total HSP20 for histamine and forskolin plus histamine, respectively, Figure 2D). Hence, 5 µM forskolin was chosen for our model system and using these conditions we further performed experiments to characterize the effect of forskolin-induced suppression of force on phosphorylation changes of actin associated proteins and compared to basal levels. Forskolin-induced suppression of force was reversible as washing the rings repeatedly for 50 min allowed the PCA to contract (~40% of original contraction) to 5 µM histamine in a time-dependent manner (Figure 3.4F), and demonstrated that the doses of histamine and forskolin used in this study did not affect the viability of the tissue. Washing the rings for 2 hr allowed the PCA to recover completely and produced 100% of the original contraction to 5 µM histamine.

Histamine treatment significantly increased the phosphorylation of MLC (0.41 ± 0.04 p-MLC/ total MLC) when compared to untreated basal (0.09 ± 0.04 p-MLC/ total MLC) (n=4, p=0.01). Forskolin plus histamine treatment also significantly increased (0.34 ± 0.05 p-MLC/total MLC the phosphorylation of MLC when compared to untreated basal (0.09 ± 0.04 p-MLC/ total MLC, n=4, p=0.02). There was no significant difference in the MLC phosphorylation between histamine and forskolin plus histamine treated tissues (Figure 3.6), which suggests that forskolin treatment did not result in significant dephosphorylation of MLC.

Figure 3.6: Panel A: Representative western blot of p-MLC and np-MLC. Panel B: Cumulative data representing the relative amounts of the p-MLC over the total MLC n=4, p<0.05

Forskolin treatment decreases filamentous actin levels

Several investigators have demonstrated that actin is polymerized during
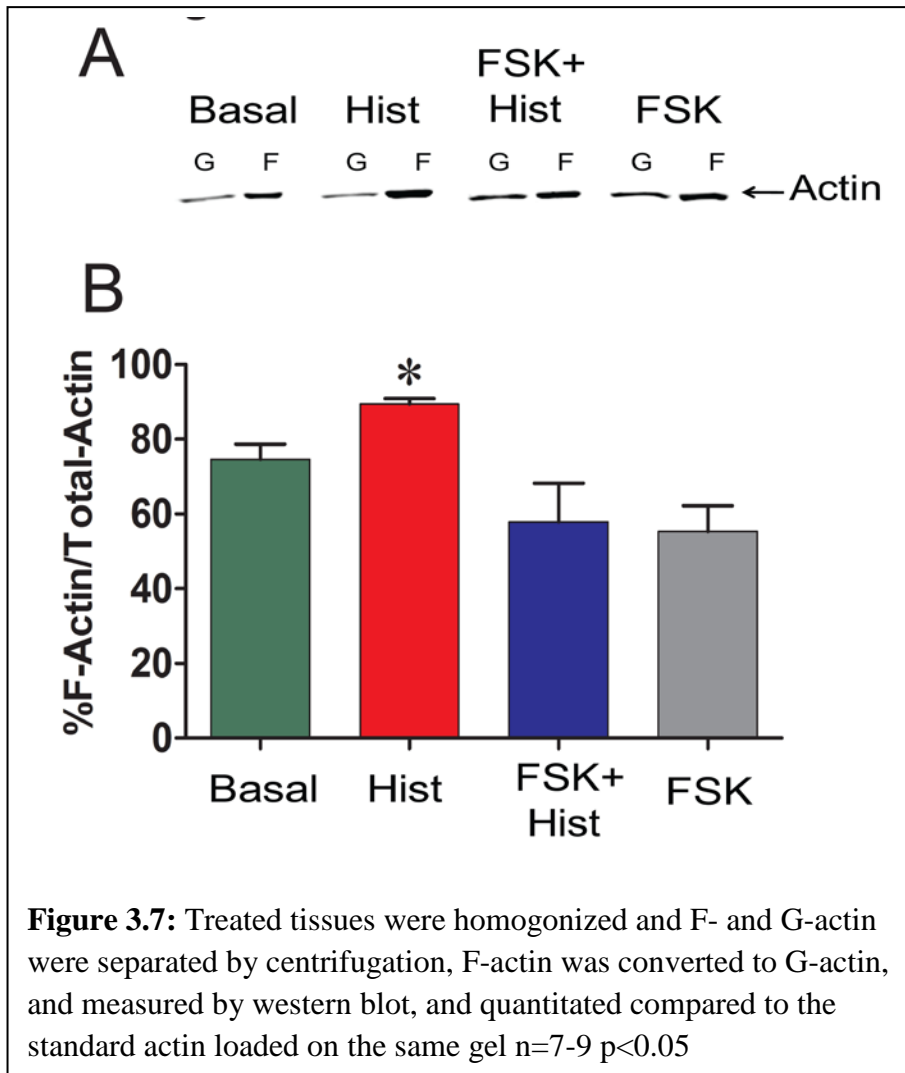
contraction of smooth muscle, and agents that inhibit actin polymerization result in inhibition of contraction (reviewed in [59]). To examine the effect of activation of cyclic nucleotide-dependent pathways by forskolin on actin polymerization, actin polymerization was measured in PCA contracted with histamine with or

Figure 3.7: Treated tissues were homogonized and F- and G-actin were separated by centrifugation, F-actin was converted to G-actin, and measured by western blot, and quantitated compared to the standard actin loaded on the same gel n=7-9 p<0.05

without forskolin pretreatment (Figure 3.7). Treatment with histamine led to increases in F-actin by 14 % (75 ± 4 % to 89 ± 1% for basal and histamine, respectively), while treatment with forskolin reduced F-actin by 10% (75 ± 4 % to 65 ± 6 % for basal and forskolin, respectively). Pretreatment with forskolin before histamine stimulation reduced the F-actin by 17% (75 ± 4 % to 58 ± 10 % for basal and forskolin plus histamine, respectively p=0.004, n=7-9).

The effect of forskolin on the phosphorylation of actin regulating proteins, HSP20, cofilin, VASP, and paxillin

Forskolin treatment of smooth muscle increases the phosphorylation of HSP20 and induces relaxation [90]. To decipher the role of HSP20 phosphorylation in the regulation of actin polymerization during force suppression, HSP20 phosphorylation was examined by isoelectric focusing and western blot analysis. As expected, forskolin led to increases in the phosphorylation of HSP20 when compared to untreated or histamine treated
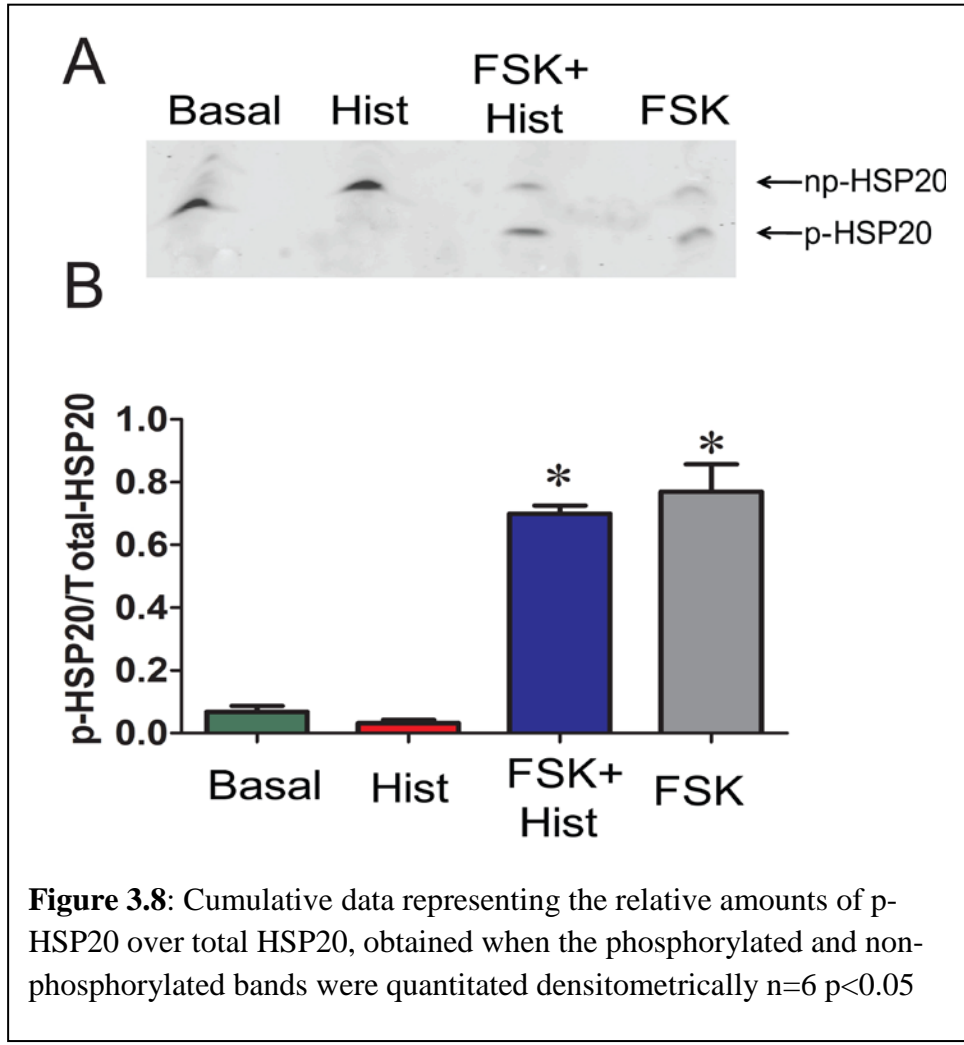
Figure 3.8: Cumulative data representing the relative amounts of p-HSP20 over total HSP20, obtained when the phosphorylated and non-phosphorylated bands were quantitated densitometrically n=6 p<0.05

tissues. (0.77 ± 0.09 p-HSP20/total HSP20 vs 0.07 ± 0.02 and 0.03 ± 0.01 for untreated and histamine, respectively, $p < 0.05$, n=4). Treatment with histamine after forskolin did not reverse HSP20 phosphorylation (0.70 ± 0.03, Figure 3.8).

Figure 3.9: Preincubation with forskolin reduces phosphorylation of cofilin in PCA. Data representing the relative amounts of p-cofilin over the total cofilin and then normalized to the basal n=4 p<0.05

Next, the effects of forskolin on cofilin and VASP phosphorylation, both of which have been demonstrated to regulate actin polymerization, were determined. Histamine increased the phosphorylation of cofilin in PCA by 2.9 ± 1.2 fold, while forskolin pretreatment prevented histamine-induced increase in the phosphorylation of cofilin in PCA (4.2 ± 0.8 and 1.5 ± 0.3 p-

cofilin/total cofilin for histamine and forskolin plus histamine, respectively ($p < 0.05$, n=4, Figure 3.9).

VASP, the vasodilator-stimulated phosphoprotein, is important in actin polymerization as well as the interface between the cytoskeleton and the extracellular matrix. VASP is affected by both cAMP and cGMP signaling, and is present in the relaxation of smooth muscle. To examine changes in VASP tissue was challenged with histamine and changes within the
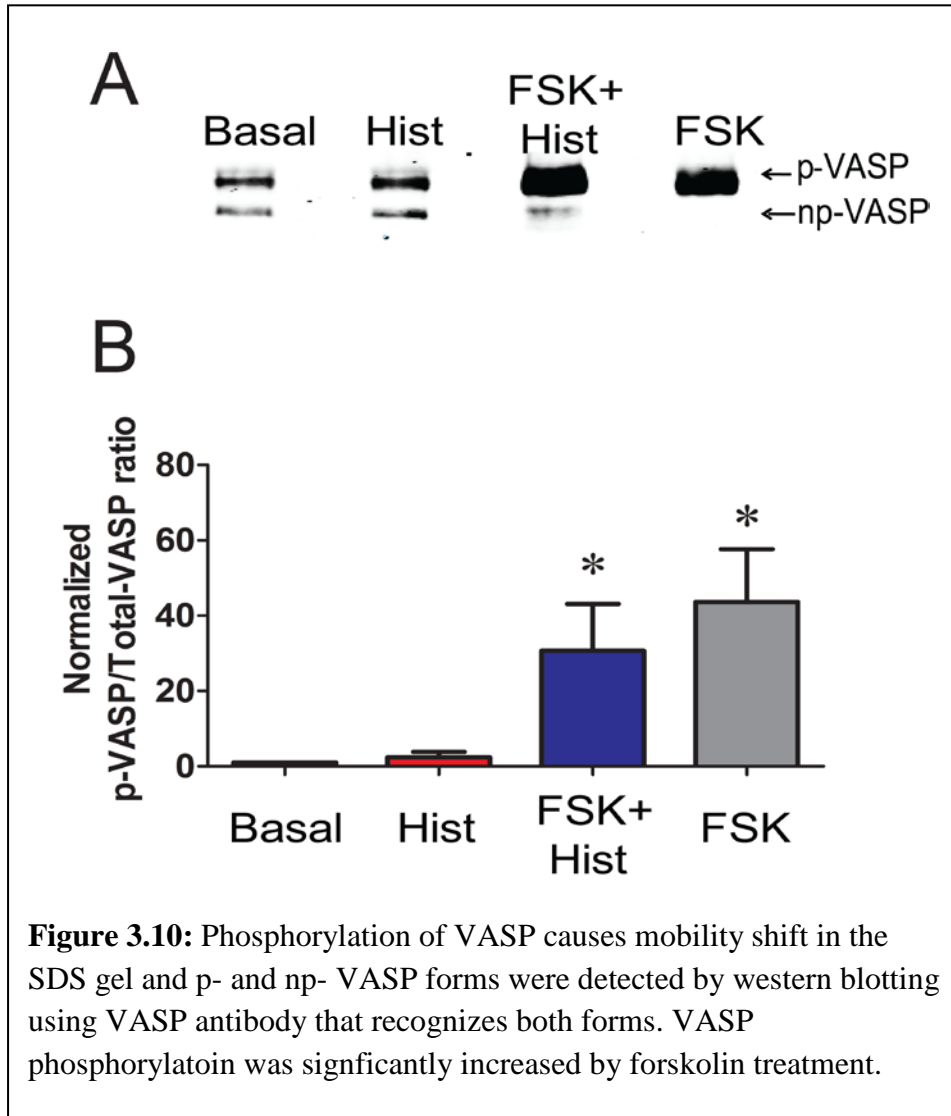
Figure 3.10: Phosphorylation of VASP causes mobility shift in the SDS gel and p- and np- VASP forms were detected by western blotting using VASP antibody that recognizes both forms. VASP phosphorylatoin was signficantly increased by forskolin treatment.

phorphorylation of VASP were examined with the treatment of forskolin. Histamine treatment did not increase the phosphorylation of VASP (2.3 ± 1.4 p-VASP/ totalVASP). VASP was phosphorylated in response to forskolin (36.5 ± 13.5 p-VASP/ totalVASP, compared to the basal value p<0.05), and the phosphorylation was not significantly changed by histamine treatment

after forskolin (25.8 ± 11.3 p-VASP/ total VASP, for forskolin plus and histamine, respectively, p<0.6 n=6, Figure 3.10).

The cytoskeletal protein, paxillin, has been shown to regulate actin polymerization during contractile activation of smooth muscle [84,91]. Hence, we studied the phosphorylation of paxillin during forskolin-induced suppression of force. Forskolin pretreatment prevented the phosphorylation of

Figure 3.11: Preincubation with forskolin abolish histamine induced paxillin phosphorylation in PCA. Panel A: Representative western blot of p-paxillin and np-paxillin. Panel B: Cumulative data representing the relative amounts of p-paxillin over total paxillin and normalized to the basal. n=4. p < 0.05. * significant compared to all other conditions.

paxillin associated with histamine stimulation (3.5 ± 0.7 and 1.1 ± 0.1, p-paxillin/ total paxillin, for histamine and forskolin plus histamine, respectively, p<0.05, n=4, Figure 3.11), suggesting that inhibition of paxillin phosphorylation interferes with the actin polymerization needed for contraction.

Discussion

In this study, a physiologic model system was developed wherein $[Ca^{2+}]_i$ was uncoupled from force, resulting in the complete suppression of force generation in the presence of a contractile agonist. Our approach is based on the premise that actin cytoskeletal regulation is an active component of cyclic nucleotide-dependent relaxation or inhibition of force. Utilizing PCA, we showed that activation of adenylyl cyclase by forskolin *prior* to histamine exposure completely suppressed half maximal force generated by histamine. This physiologic model allowed us to further define the role of actin filaments, in addition to thick filament modulation, during cyclic nucleotide-dependent force suppression. Experiments were conducted using the FluoroPlex Tissue Bath Fluorometry System, a unique muscle bath system that enables fluorescence ion recording in parallel with force measurement in intact tissues, and we measured $[Ca^{2+}]_i$ transients, MLC phosphorylation, F/G- actin levels, along with the phosphorylation of actin regulatory proteins.

While histamine-induced force generation was completely suppressed with forskolin pretreatment, a transient increase in $[Ca^{2+}]_i$ was still present (Figure1) suggesting that additional mechanisms to the reversal of activation involving decrease in $[Ca^{2+}]_i$ and crossbridge-dephosphorylation play a role in the suppression of force. However, we observed that the magnitude of the change in fluorescence ratio was significantly greater for tissue contracted with histamine when compared to tissue treated with forskolin followed by histamine (Figure 1 E). The time it took for the $[Ca^{2+}]_i$ to increase from 10% to 90% of its maximum response was significantly lower for tissue that was treated with histamine alone compared to forskolin followed by histamine treatment (data not shown), suggesting that the decoupling between $[Ca^{2+}]_i$ and force was not complete. It is possible that these changes may be due to the direct

effect of forskolin on the $[Ca^{2+}]_i$. The effect was dose-dependent as the lower forskolin concentrations (1 µM) did not abolish the transient $[Ca^{2+}]_i$ or the force, and at a higher concentration (10 µM) there was no transient increase in $[Ca^{2+}]_i$ and force was completely suppressed. These results suggest that a higher forskolin dose inhibits the agonist-induced Ca^{2+} signaling pathways, possibly due to cross activation of PKG by cAMP, as reported by several investigators [92-95]. Activation of PKG can reduce both the concentration of $[Ca^{2+}]_i$ and the force developed for a given intracellular $[Ca^{2+}]$ (i.e., the Ca^{2+} sensitivity) [96,97]. Preliminary experiments also showed that pretreatment with the nitric oxide donor, sodium nitroprusside, not only completely blocked histamine-induced increase in $[Ca^{2+}]_i$ and force but also decreased the phosphorylation of MLC (Komalavilas *et al*., unpublished results).

Pretreatment of PCA with 5 µM forskolin completely suppressed histamine-induced contraction without significantly affecting histamine-induced changes in MLC phosphorylation (Figure, 2,3). This is similar to the results obtained in swine carotid artery where forskolin-induced force suppression in histamine pre-contracted tissue occurs without a reduction in MLC phosphorylation through a mechanism that involves regional actin filament inhibition or weak inhibition of myosin binding at the thin or thick filament. [98]. However, we observed that treatment of PCA with 10 µM forskolin prior to histamine treatment significantly reduced the MLC phosphorylation suggesting activation of PKG-regulating Ca^{2+} regulatory pathways. PKG activates MLC phosphatase, thereby reducing MLC phosphorylation [96].

Actin polymerization occurs in response to contractile stimuli in many smooth muscle tissues, and force development can be significantly reduced by treatment with inhibitors of actin polymerization (reviewed in [59,83,99]). Similar to prior reports using dog trachealis [100] and swine carotid artery [98], histamine increased F-actin concentration in PCA (Figure 4). Forskolin

pretreatment prevented the histamine-induced increase in F-actin (Figure 4 A, B). This can be explained by the observation that forskolin treatment alone reduced basal F-actin concentration, suggesting cyclic-nucleotide-mediated actin depolymerization preceded any histamine-mediated cytoskeletal reorganization. We showed that reduction in F-actin was evident in the higher (5 and 10 µM) doses of forskolin tested. However, treatment of PCA with 1 µM forskolin did not completely inhibit the force or prevent the histamine induced increase in F-actin (Figure 2C). This result is in agreement to the Meeks *et al* study where no significant change in the F-actin levels was observed after forskolin (1 µM) treatment of histamine-contracted tissue [98]. It may be that forskolin induced reduced force despite increased MLC phosphorylation require only HSP20 phosphorylation while complete suppression of force with higher dose of forskolin involve HSP20 phosphorylation as well as decrease in F-actin level. It is also possible that the change in F-actin level is only detectable with the assay used when the force is completely suppressed by the use of a higher dose of forskolin, and that the subtle changes in F-actin level may not be detectable while there is only partial decrease in force using a lower dose of forskolin. Forskolin-induced suppression of force was reversible as washing the rings repeatedly allowed the PCA to contract to 5 µM histamine in a time-dependent manner (Figure 1F). Several investigators have demonstrated that latrunculin and cytochalasin, agents known to decrease actin polymerization, inhibit agonist-induced contraction [101-103]. However, these agents affect force by direct alteration of contractile filaments, while this study describes second messenger-mediated regulation of actin cytoskeletal-associated protein function.

A number of actin-associated proteins can be phosphorylated upon PKA or PKG activation. One such protein is HSP20, which can be phosphorylated on serine (Ser16) upon PKA or PKG activation leading to relaxation or force suppression independent of MLC

phosphorylation [47,55,63]. HSP20 phosphorylation mediates relaxation or suppression of force through mechanisms that involve actin cytoskeletal regulation. Forskolin at 1 µM did not significantly change the MLC phosphorylation but increased the phosphorylation of HSP20 suggesting that phosphorylation of HSP20 alone partially reduced the force generated by histamine, possibly through mechanisms other than actin depolymerization. This also suggests that complete suppression of force requires higher doses of forskolin which not only increase the phosphorylation of HSP20 but also decrease F-actin. One mechanism involves interaction of p-HSP20 with scaffolding protein 14-3-3 and the actin depolymerizing factor cofilin, which causes depolymerization of actin resulting in deactivation of actin cytoskeleton and relaxation [64]. Forskolin treatment also decreased the phosphorylation of cofilin in the model described here (Figure. 6). Cofilin in its phosphorylated form binds to the intracellular scaffolding protein, 14-3-3 [104]. When displaced from 14-3-3, cofilin becomes dephosphorylated and acts as an actin depolymerizing protein [105,106]. Phosphorylated HSP20 formed a tight complex with 14-3-3 in which dimer of 14-3-3- was bound to dimer of HSP20 [107]. Moreover, binding of 14-3-3 protein to p-HSP20 peptide prevented the association of cofilin with 14-3-3 [64]. This suggests that, forskolin treatment leads to phosphorylation of HSP20 which then binds to 14-3-3 and displaces cofilin. Consequently, the displaced cofilin is dephosphorylated leading to activation of cofilin as an actin depolymerization factor resulting in actin depolymerization [64,68]. HSP20 also has a sequence homology with troponin 1 and a peptide containing this homology bound to actin filaments, reducing actin–activated myosin ATPase activity. This mechanism leads to the relaxation of skinned smooth muscle by partial or full inhibition of local myosin binding at the thin-or thick filament level [55,98]. Phosphorylated HSP20 has been shown to promote airway smooth muscle relaxation, possibly through depolymerization of F-actin as well as inhibition of

myosin binding to actin [68,108]. In colonic smooth muscle, HSP20 is activated by PKA and modulates the association of caldesmon and tropomyosin during the maintenance of tone [109]. HSP20 may act as the functional switch for contraction and relaxation in the colonic smooth muscle [109]. HSP20-mediated force suppression may indeed involve different mechanisms in smooth muscle from various types and species.

In this study, forskolin also increased the phosphorylation of VASP, and the phosphorylation was not reversed upon histamine stimulation (Figure 7). Phosphorylation of VASP has been shown to be involved in the regulation of actin polymerization and decreases in the affinity of VASP for actin by 40 fold [110,111]. VASP knockdown experiments have demonstrated that VASP-mediated elongation of actin filaments are necessary for vascular contractility and that VASP phosphorylation is decreased during phenylephrine induced force generation [99]. VASP phosphorylation by PKA has a negative effect on actin nucleation, and may act as a negative regulator of actin dynamics [112]. Our results are consistent with this model in that forskolin-induced phosphorylation of VASP, affecting histamine-induced actin polymerization, thus preventing force generation.

This study demonstrated that histamine-induced paxillin phosphorylation was prevented by forskolin pretreatment (Figure 8). Paxillin is a focal adhesion protein that is proposed to link actin filaments to integrin rich cell adhesion sites and may be involved as a cross-linker between the thin filaments and the dense bodies [86,113]. Paxillin phosphorylation has been associated with the coordinated formation of focal adhesions and stress fibers [114]. Paxillin phosphorylation was increased during acetylcholine-induced contraction of intact trachealis smooth muscle and has been shown to play an essential role in regulating smooth muscle contraction[86]. Gunst *et al* has proposed that contractile agonists activate FAK, inducing tyrosine (118) phosphorylation of

paxillin, causing CrkII coupling and formation of the CrkII/Cdc42/N-WASp complex, leading to the activation of Cdc42, N-WASp and Arp2/3 complex and actin polymerization [115]. In swine carotid artery stimulated with high-K^+ or histamine, paxillin phosphorylation (Y118) and actin polymerization were increased only after full force development suggesting a role for paxillin phosphorylation during the sustained contraction [84,86]. Stimulus-induced tyrosine phosphorylation of paxillin is associated with increases in actin polymerization in different smooth muscle tissues (reviewed in [116]). Although paxillin is not a substrate of PKA, its phosphorylation is affected by the activation of cAMP pathway indirectly, possibly by cross talk between the tyrosine and serine/threonine kinase pathways or that an intact actin cytoskeleton is necessary for paxillin phosphorylation. Hence, inhibition of histamine-induced paxillin phosphorylation by the activation of the cAMP pathway in PCA may indeed contribute, in part, to the decreased actin polymerization observed in our model, thereby inhibiting force.

Conclusions

A physiological model was developed in which forskolin pretreatment completely suppressed histamine-induced force in PCA by regulating actin polymerization and dynamics without abolishing increases in $[Ca^{2+}]_i$ or MLC phosphorylation. Actin depolymerization creates conditions in which there is no actin filament structure on which MLC can treadmill. Thus, calcium desensitization is likely not the only mechanism of force modulation during activation of cyclic nucleotide-dependent signaling pathways. Our results further suggest that the actin cytoskeletal changes are mediated by the phosphorylation changes of actin modulatory proteins, such as HSP20, cofilin, VASP and paxillin. The force suppression model employed in this study can be used to further characterize the role of actin and its associated proteins in the regulation of vascular smooth muscle tone. Future studies may also examine later events (3-30min) of force

maintenance. In addition, cyclic nucleotide analogues can be used to decipher the different

mechanisms that contribute to these regulatory pathways.

CHAPTER 4

Calcium Dependent Force Inhibition

Aim 3 Papaverine Prevents Vasospasm by Inhibiting Force via Regulating of Myosin

Light Chain Dephosphorylation and Actin Polymerization

Text for Chapter 4 taken from:

Hocking KM, Putumbaka G, Wise E, Cheung-Flynn J, Brophy CM, Komalavilas P,

"Papaverine Prevents Vasospasm by Inhibiting Force via Regulating of Myosin Light Chain

Dephosphorylation and Actin Polymerization" in preparation

Introduction

Establishing the downstream effects of PKG activation is important for better

understanding the relationship of thick and thin filaments to contraction and relaxation. PKG

activation has been shown to decrease calcium sensitivity and reduce a rise in $[Ca^{2+}]_i$ [41,58].

Traditional vasodilators like sodium nitroprusside act through the PKG pathway by increasing

cGMP by acting as a nitric oxide donor. Papaverine is a non-selective phosphodiesterase

inhibitor found in the opium poppy. It has been shown to increase both cGMP and cAMP[117] in

smooth muscle, both of which induce vasorelaxation. Papaverine is often used as a topical

treatment in the process of autografting the human saphenous vein into arterial circulation. This

process works well in preventing local vasospasm on exposed vessels, but does not directly

transfer for treatment of cerebral vessels that are not exposed. Papaverine administered

systemically may cause hypotension due to systemic effects of the phosphodiesterase inhibitor.

Sustained contraction or impaired relaxation of vascular smooth muscle results in

vasospasm. Vasospasm contributes to "no reflow" phenomenon in coronary interventions,

55

stroke after subarachnoid hemorrhage, and early vein graft failure. The human saphenous vein

(HSV) is still the most commonly used conduit in coronary artery bypass grafting. HSV is

considered inferior to the internal mammary artery (IMA) because of 50% failure rate within 10

years compared with 5% failure for the IMA[118,119]. Damage to the endothelium, during

vasospasm, leads to a cascade of problems that result from reduced nitric oxide production.

Integrity of the endothelial layer has been shown to be an important factor in determining the

failure rate of both saphenous vein grafts and IMA grafts after implantation[120].

Saphenous vein grafts commonly develop vasospasm during harvest and this

spasm is typically treated by distension of the conduit with a hand held syringe[121] or with

pharmacologic approaches. Manual distension can result in very high intraluminal pressures (up

to 800 mmHg) that injure the fragile endothelial monolayer[122] negating the benefit of

overcoming vasospasm. Effective pharmaceutical approaches to vasospasm in HSV include:

glyceryl trinitrate, verapamil, and papaverine which have similar EC_{50} of relaxation in HSV[121].

Sodium nitroprusside and nicroandil have been shown to be less effective at treating vasospasm

in HSV[27]. For many years, papaverine has been the most commonly used agent for preventing

vasospasm of HSV.

The objective of this study is to investigate the molecular mechanism involved in

treatment of the human saphenous vein with papaverine. Norepinephrine was used to induce

vasospasm. We hypothesize that papaverine acts through both thin and thick filament

mechanisms in order to prevent vasospasm, making it a more effective treatment than sodium

nitroprusside which acts through only thick filaments. Papaverine's dual filament pathway acts

by reducing actin polymerization, intracellular calcium transients, and myosin light chain

phosphorylation as well as increase phosphorylation of actin regulatory proteins HSP20 and

VASP, both of which have been implicated in relaxation of smooth muscle tissue[123][124]. Reduction in intracellular calcium would demonstrate that PKG mediates inhibition of contraction through both changes in $[Ca^{2+}]_i$ and thin filament regulatory processes.

Methods

Materials

All chemicals were purchased from Sigma Chemical Co. (St. Louis, MO) unless specified otherwise. Pre-cast acryl amide gels, Sodium dodecyl sulfate (SDS), Tris-glycine-SDS buffer (TGS), Tris-glycine (TG) and prestained Precision Blue Protein Standards were purchased from Bio-Rad (Hercules, CA). Urea and CHAPS (write full name) were from Research Organics Inc. (Cleveland, OH). F/G Actin assay kit was from Cytoskeleton Inc., (Denver, CO). Fura 2-AM and Pluronic F-127 was purchased from Invitrogen (Carlsbad, CA).

HSV procurement and Physiological measurement of smooth muscle functional viability

Human saphenous vein samples were collected after obtaining approval of the Institutional Review Boards of the Vanderbilt University Medical Center and the VA Tennessee Valley Healthcare System, Nashville, TN. Remnants of unidentified segments of human saphenous veins left behind after the surgery were obtained from patients that underwent coronary artery bypass graft surgery. The human saphenous veins were harvested by open or minimally invasive endoscopic technique according to surgeon discretion and were stored in heparinized Plasmalyte (140 mEq sodium, 5 mEq potassium, 3 mEq magnesium, 98 mEq chloride, 27 mEq acetate, and 23 mEq gluconate, [Baxter Healthcare Corporation Deerfield, IL]) solution in the operating room. Segments of grafts that were without damage or branches were used for analysis.

Human saphenous vein segments were then dissected free of fat and connective tissue for determination of smooth muscle function in an organ bath. One-millimeter rings from the human saphenous vein segments were weighed, their lengths recorded. To focus on the smooth muscle-derived changes during inhibition of force, the endothelium was denuded by gently rolling the luminal surface of each ring at the tip of a fine forceps. Rings were suspended in a muscle bath containing a bicarbonate buffer (120 mM NaCl, 4.7 mM KCl, 1.0 mM $MgSO_4$, 1.0 mM NaH_2PO_4, 10 mM glucose, 1.5 mM $CaCl_2$, and 25 mM Na_2HCO_3, pH 7.4), equilibrated with 95% oxygen and 5% carbon dioxide at 37°C. Each ring was progressively stretched to its optimal resting tension (approximately 1 g) that would produce a maximal response to contractile agonists as determined previously, then maintained at the resting tension and equilibrated for a minimum of 2 hours [125]. Force measurements were obtained using a Radnoti Glass Technology (Monrovia, CA) force transducer (159901A) interfaced with a Powerlab data acquisition system and Chart software (ADInstruments, Colorado Springs, CO). The rings were contracted first with 110 mM KCl (with equimolar replacement of NaCl in bicarbonate buffer) to determine functional viability of the smooth muscle. Any tissue failing to contract with KCl was considered non-functional and was not used in further experiments. Viable tissues were allowed to equilibrate in the bicarbonate solution for 30 minutes and were then challenged with a physiological contractile agonist norepinephrine (10^{-7}-10^{-5} M) and relaxed with papaverine (10^{-6}-10^{-3}M). Concentration of papaverine needed to completely block norepinephrine induced contraction (10^{-5}M) was determined and used for the rest of the experiments. HSV rings were pretreated with 10^{-3}M papaverine for 10 min and then challenged with norepinephrine ($5X10^{-6}$M-10^{-5}M) and the force generated was recorded. To determine the role of phosphorylation of proteins during inhibition of force, physiologic experiments were conducted as described above

and the tissues were snap frozen under tension using forceps precooled in liquid nitrogen at 5 min and then pulverized. These pulverized tissues were stored at -80°C for later analysis using urea glycerol gel, SDS polyacrylamide gel electrophoresis (PAGE) or isoelectric focusing and western blotting. For actin assay to determine the level of F-actin compared to G-actin, the tissues were used immediately after treatment without freezing.

Contractile response was defined as stress ($[10^5$ Newtons (N)/m$^2]$ = force (g) x 0.0987 / area, where area is equal to the wet weight [(mg) / length (mm at maximal length)] divided by 1.055),[126] which was calculated using the force (g) generated by the tissue. Percent relaxation was measured as the change in stress compared to the maximal tension induced by norepinephrine as described previously [125]. We have previously demonstrated that the production of force of less than 0.025×10^5 N/m^2 in response to KCl correlates with diminished cellular viability as measured by the 3-(4,5-Dimethylthiazol-2-yl)-2,5-diphenyltetrazolium bromide (MTT) live/dead assay.[125]

Procurement of porcine coronary artery smooth muscle tissue and physiologic measurements

Fresh porcine hearts were obtained either from euthanized animals from the surgical suite at Vanderbilt University Medical Center as approved according to the Institutional Animal Care and Use Committee protocol or from the local slaughter house (C&F Meats, Triune, TN). The heart was procured and placed directly in HEPES buffer (140 mM NaCl, 4.7 mM KCl, 1.0 mM MgSO$_4$, 1.0 mM NaH$_2$PO$_4$, 1.5 mM CaCl$_2$, 10 mM glucose, and 10 mM HEPES, pH 7.4), and the coronary arteries were dissected and tested immediately or after overnight storage at 4°C. Subcutaneous fat and adventitial tissues were removed and the vessel was cut into transverse rings of 3.0 mm in width. The endothelium was denuded by gently rolling the luminal surface of

each ring at the tip of a fine forceps to focus on smooth muscle responses. Rings were suspended

in a muscle bath containing a bicarbonate buffer and the physiological responses were

determined as described above for HSV. Rings were equilibrated for an additional 30 min after

KCL challenge and then dose response curves for histamine (contractile agonist) contraction and

the vasodilators papaverine and forskolin relaxation were determined to select the correct dose of

agents for the experiment. To determine the inhibition of contraction, rings were either treated

with buffer alone (control), histamine (5 µM) for 5 min, forskolin (5 µM) for 10 min, papaverine

(1mM) for 10 min followed by histamine (5 µM) for 5 min or forskolin (5 µM) for 10 min

followed by histamine (5 µM) for 5 min. At the end of the experiments, all rings were washed

and contracted with KCl to ensure continued viability of the tissues. To determine the role of

phosphorylation of proteins during inhibition of force, physiologic experiments were conducted

as described above and the tissues were snap frozen under tension using forceps precooled in

liquid nitrogen at 5 min and then pulverized and biochemical analysis was performed as

described for HSV.

Cytosolic Ca^{2+} measurements

Cytosolic Ca^{2+} measurements were performed as described earlier [127]. Briefly, rings of

HSV were suspended on hooks in a Fluroplex (Tissue Bath Fluorometry System, IonOptix LLC,

Milton, MA), which enables fluorescence ion recording in parallel with force measurement.

Force measurements were obtained with a Radnoti force transducer (Radnoti Glass Technology

Inc., Monrovia, CA) interfaced with Power Lab from AD Instruments (Colorado Springs, CO).

Rings were loaded at room temperature with 10 µM Fura-2 AM ester and 0.01% Pluronic F-127

in the bicarbonate buffer for 4 hrs. After loading, rings were washed every 10 min with 37°C

bicarbonate buffer for 1 hr. Calcium flux was measured with optical fibers that were interfaced

with Power Lab. Fluorescence was measured at both 380 and 340 nm of wavelength, simultaneously. The ratio of the emission of the two wavelengths was used to determine intracellular changes in calcium concentration. Baseline ratio was set at 1.0 and changes in this ratio in response to stimuli were measured. Baseline calcium fluorescence was measured and the background was set to zero as an output of 1 volt. To determine the calcium response during inhibition of contraction, rings were either treated with papaverine (10^{-3}M), sodium nitroprusside (10^{-6}M) or (forskolin (5×10^{-6}M) for 10 min, followed by norepinephrine (5 µM) or norepinephrine alone. Force and calcium fluorescence were measured continuously for 15 min after the addition of norepinephrine.

Immunoblotting

Proteins from frozen muscle rings were extracted in UDC buffer (8 M urea, 10 mM dithiothreitol (DTT), 4% CHAPS containing protease inhibitor, Phosphatase I and II inhibitor cocktail (Sigma, St. Louis, MO). The mixtures were vortexed at room temperature overnight, and then centrifuged at 14,000 rpm for 15 min at 4°C. Soluble protein concentrations were determined using the Bradford assay (Pierce Chemical, Rockfort, IL). Equal amounts (20-50 µg) of proteins were placed in a Laemmli sample buffer (Bio-Rad laboratories, Inc. Hercules, CA), heated for 5 min at 100°C and separated on SDS polyacrylamide gels. Proteins from the gels were transferred onto nitrocellulose membranes (Li-COR Biosciences, Lincoln, NE) and blocked prior to incubation overnight at 4°C with the following primary antibodies: anti-HSP20 (1:3,000 dilution, Advanced Immunochemical Inc., Long Beach, CA); anti-VASP (1:2000, ECM Biosciences, Versailles, KY); anti MLC20 (1: 7000, gift from Dr. James Stull, University of Texas, Galveston TX). Membranes were washed three times with TBS containing Tween 20 (0.1%) (TBST), and incubated with appropriate infrared-labeled secondary antibodies (Li-Cor,

Lincoln, NE) for 1h at room temperature. The membranes were subsequently washed with TBST, and protein-antibody complexes were visualized and quantified using the Odyssey direct infrared fluorescence imaging system (Li-Cor). Phosphorylation was calculated as a ratio of the phosphorylated protein to total protein and was then normalized to the unstimulated control with the control value set as 1.0.

Determination of myosin light chain phosphorylation

Rings of HSV were equilibrated in the muscle bath as described above and treated with norepinephrine (5×10^{-6}M) for 5 min or pretreated with papaverine (10^{-3}M), Sodium nitroprusside (10^{-6}M), or forskolin (5×10^{-6}M) for 10 min, followed by norepinephrine for 5 min and snap frozen as described above. Myosin light chain phosphorylation was determined using a modification of an established method described earlier [88,89]. The frozen tissue was pulverized, placed in a frozen slurry of precipitating solution consisting of 90% acetone, 10% trichloroacetic acid, and 10 mM DTT, and then allowed to melt to room temperature. The precipitating solution was removed, and the tissues were washed three times with 90% acetone and 10 mM DTT. The samples were dried, and the pellets were suspended in UDC buffer as described above and vortexed to solubilize the proteins. Ten micrograms of protein were diluted with 10 μl of urea sample buffer (6.7 M urea, 18 mM Tris, 20 mM glycine, 9 mM DTT, 4.6% saturated sucrose, and .004% bromophenol blue) and separated on glycerol-urea mini gels (40% glycerol, 10% acrylamide, 0.5% bisacrylamide, 20 mM Tris, and 22 mM glycine). Proteins were transferred onto nitrocellulose membranes in a buffer containing 10 mM Na_2HPO_4 pH 7.6 at 25 V for 1 hr at 20°C. The blot was probed with anti MLC antibodies and processed as described above. The phosphorylated and non-phosphorylated MLC bands were quantitated by densitometric analysis.

62

The relative amount of the phosphorylated forms of MLC over the total amount of MLC was calculated.

Actin Assay

The amount of F-actin versus G-actin was measured using the G-actin/F-actin *In Vivo* Assay kit (Cytoskeleton, Denver, CO), per manufacturer's protocol. Briefly, treated HSV and PCA samples were homogenized in 0.25 ml of lysis buffer (50 mM PIPES pH 6.9, 50 mM NaCl, 5 mM $MgCl_2$ 5 mM EGTA, 5% (v/v) Glycerol, 0.1 % Nonidet P40, 0.1% Triton X-100, 0.1% Tween 20, 0.1% 2-mercapto-ethanol, 0.001% Antifoam C, 4 µM Tosyl arginine methyl ester, 15 µM Leupeptin, 10 µM Pepstatin A, 10 mM Benzamidine, 1 mM ATP warmed to 37°C) for 1 min with a mortar and pestle that fit into the 1.5 ml microfuge tube. The lysate (100µL) was centrifuged at 2000 rpm for 5 min at 37°C to pellet unbroken cells. The supernatants were centrifuged at 100,000 x g for 1 hr at 37°C. Supernatants (contains the G-actin) were transferred to pre-cooled tubes and placed on ice. The pellets (contain F-actin) were resuspended in 100µL of ice-cold 10 µM cytochalasin D in deionized water, and F- actin was depolymerized by incubating for 1 hr on ice with mixing every 15 min. Equal volume of supernatants and pellets along with actin standards (50-100ng) were separated on 12% SDS-polyacrylamide gels and transferred to nitrocellulose membrane in 1 X TG buffer at 100 volts for 1 hr. The membrane was probed with anti actin antibody(1:1000 dilution cytoskeleton) and the amount of actin in each fraction was quantified comparing to actin standards loaded on the same gel.

Isoelectric focusing

Phosphorylation of HSP20 in response to vasodilators was examined by isoelectric focusing, which separates the phospho- and non-phospho forms of HSP20 and detected by western blotting. 30 µg of extracted proteins from the treated HSV samples were separated on

one-dimensional isoelectric focusing gel (8.3X7.3 cm) with 5% ampholines (4 parts pI 4-7 and 1 part pI 3-10, GE Healthcare Bio-Sciences) using 20 mM sodium hydroxide as a cathode buffer and 10 mM phosphoric acid as an anode buffer. Proteins were focused for 100 V for 1 hr, 250 V for 1 hr and 500 V for 30 min and transferred to nitrocellulose membrane at 25 V in 0.7% acetic acid with the direction of the gel sandwich reversed (acetic acid give proteins a positive charge) for 1 hr at room temperature. The blot was probed with anti HSP20 antibodies as above and the phosphorylated and non-phosphorylated forms of HSP20 were quantitated by densitometry and the ratio of phospho HSP20 over total HSP20 was calculated and normalized to the control untreated tissue.

Duration of Action of Papaverine

To determine the duration of action of the effect of papaverine on human tissue, discarded samples of human saphenous vein were obtained from patients after coronary artery bypass grafting (CABG), after informed consent was obtained, as approved by the Institutional Review Board of Vanderbilt University (Nashville, TN). The veins (n=5) were obtained post-operatively, dissected free or fat and connective tissue and stored no longer than 24 hours in University of Wisconsin preservation solution prior to use. Eight rings ~1-2mm in width were cut from each vein and suspended in a muscle bath containing a bicarbonate buffer (120 mM NaCl, 4.7 mM KCl, 1.0 mM MgSO$_4$, 1.0 mM NaH$_2$PO$_4$, 10 mM glucose, 1.5 mM CaCl$_2$, and 25 mM Na$_2$HCO$_3$, pH 7.4), gassed with 95% O$_2$ / 5% CO$_2$ at 37°C. The rings were equilibrated for ~1 hr, manually stretched to 4 g of tension, and maintained at a resting tension of 1 g. for an additional 1 hr. Force measurements were obtained using a Radnoti Glass Technology (Monrovia, CA) force transducer (159901A) interfaced with a Powerlab data acquisition system and Chart software (AD Instruments, Colorado Springs, CO). The rings were contracted with

110 mM KCl (with equimolar replacement of NaCl in bicarbonate buffer) to prime the tissue.

After re-equilibration, the rings were contracted with 5µM norepinephrine (control contraction).

After maximum norepinephrine-induced contraction was reached, the rings were copiously

washed for ~1 hour. Rings were treated, in duplicate, for ten minutes with 1 mM, 10 µM and 100

µM papaverine, and two rings were left as untreated control. After ten minutes, the rings were

again challenged with 5µM norepinephrine (time zero contraction). After maximum contraction

was reached, the rings were washed for thirty minutes, via buffer exchange every five minutes.

The rings were subsequently treated with 5µM norepinephrine at one, two and four hours after

the initial treatment. All contractions are expressed as percent of maximal (control)
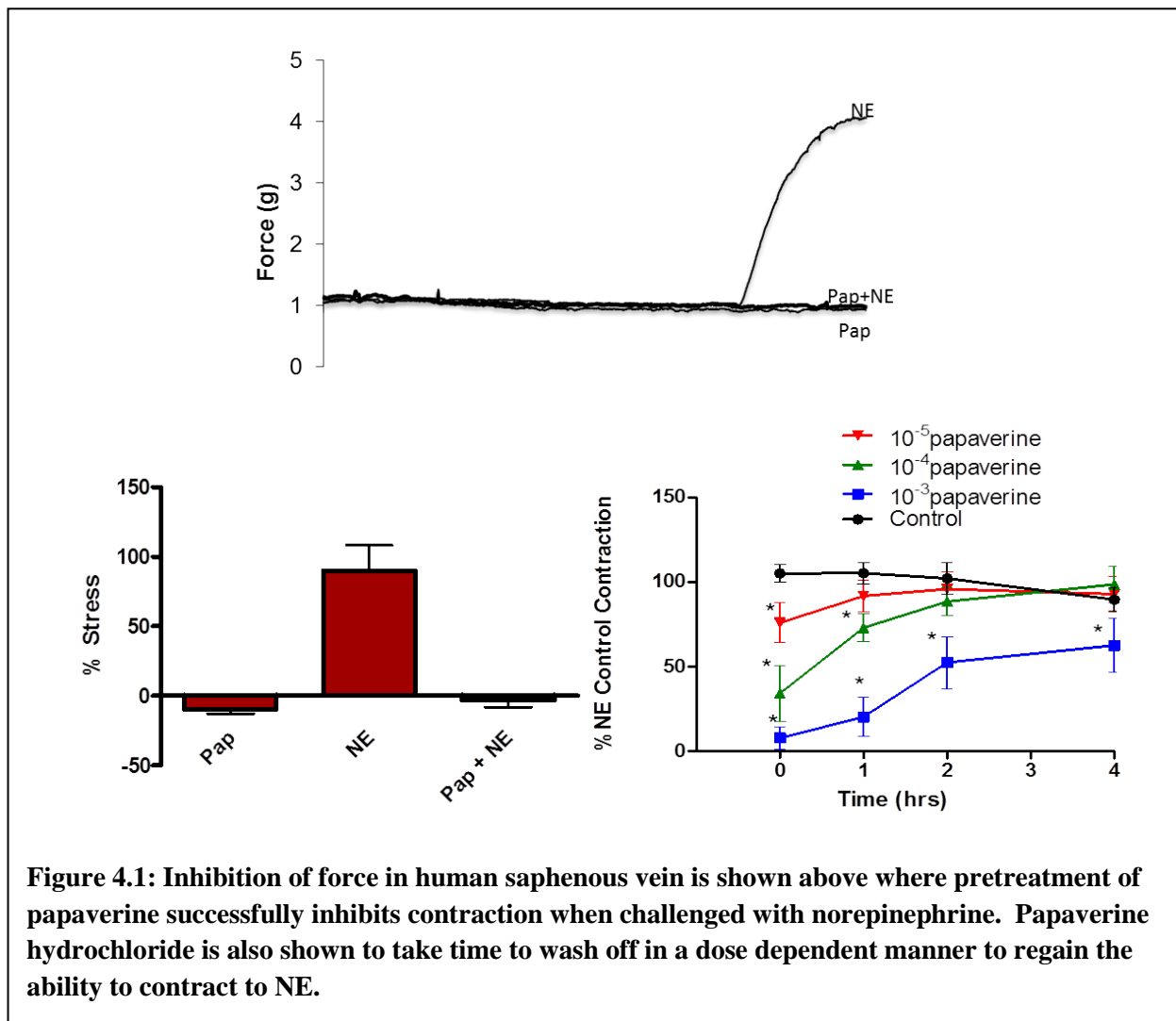
norepinephrine-induced contraction.

Statistical analysis

Values are reported as mean $\pm$ standard error of the mean (SEM). Statistical analysis

was performed by unpaired Student's *t* test or one-way *ANOVA,* followed by Tukey's post test

(GraphPad Software, Inc. San Diego, CA). The criterion for significance was *P* < 0.05.

Results

The effect of papaverine on inhibition of contraction

Initial experiments were conducted using various doses of norepinephrine (0.1 to 10 µM) to contract HSV. The dose of norepinephrine (5-10 µM) which produced greater than 60% of maximal potassium-induced contraction was selected for further experiments. Various doses of papaverine (0.1-1mM) were used to block norepinephrine induced contraction and a dose of 1 mM that completely blocked norepinephrine induced contraction was chosen for further study.
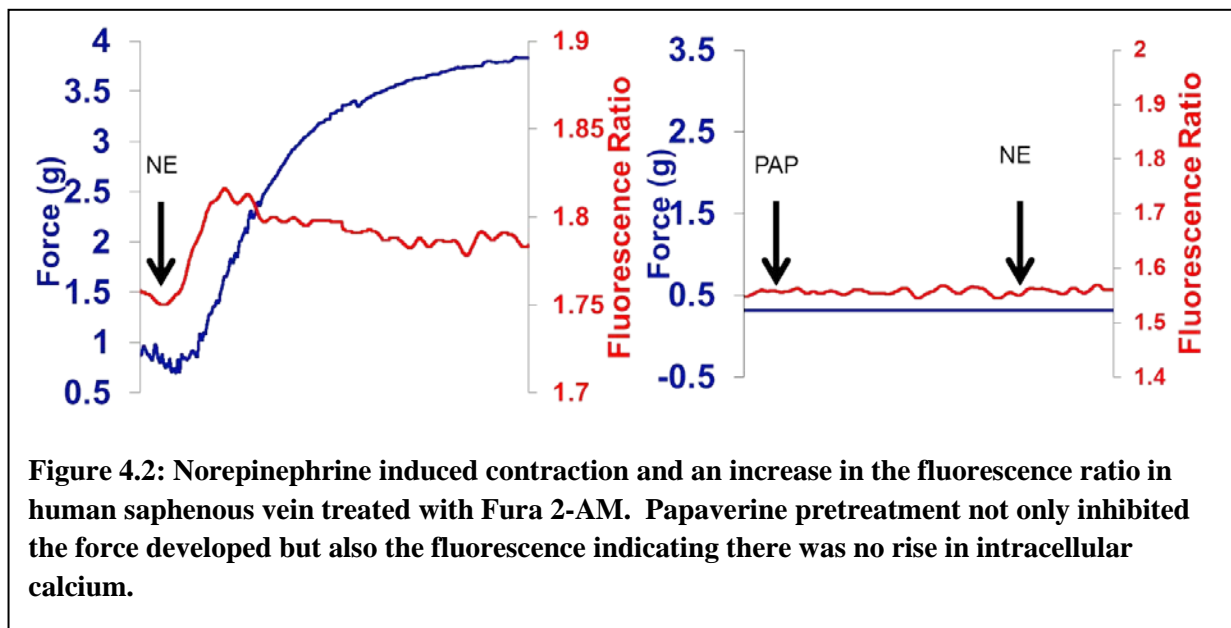

Figure 4.1: Inhibition of force in human saphenous vein is shown above where pretreatment of papaverine successfully inhibits contraction when challenged with norepinephrine. Papaverine hydrochloride is also shown to take time to wash off in a dose dependent manner to regain the ability to contract to NE.

Treatment of HSV with norepinephrine alone induced force (62 % of KCl stress Fig 4.1).

Pretreatment of HSV with 1 mM papaverine blocked norepinephrine induced force (Figure 4.1).

Papaverine-induced inhibition of force was reversible as washing the rings repeatedly allowed

the HSV to contract to 5 µM norepinephrine in a time-dependent manner (Fig.4.1), and

demonstrated that the doses of norepinephrine and papaverine used in this study did not affect

the viability of the tissue.

The effect of papaverine on Ca^{2+} transients

Figure 4.2: Norepinephrine induced contraction and an increase in the fluorescence ratio in human saphenous vein treated with Fura 2-AM. Papaverine pretreatment not only inhibited the force developed but also the fluorescence indicating there was no rise in intracellular calcium.
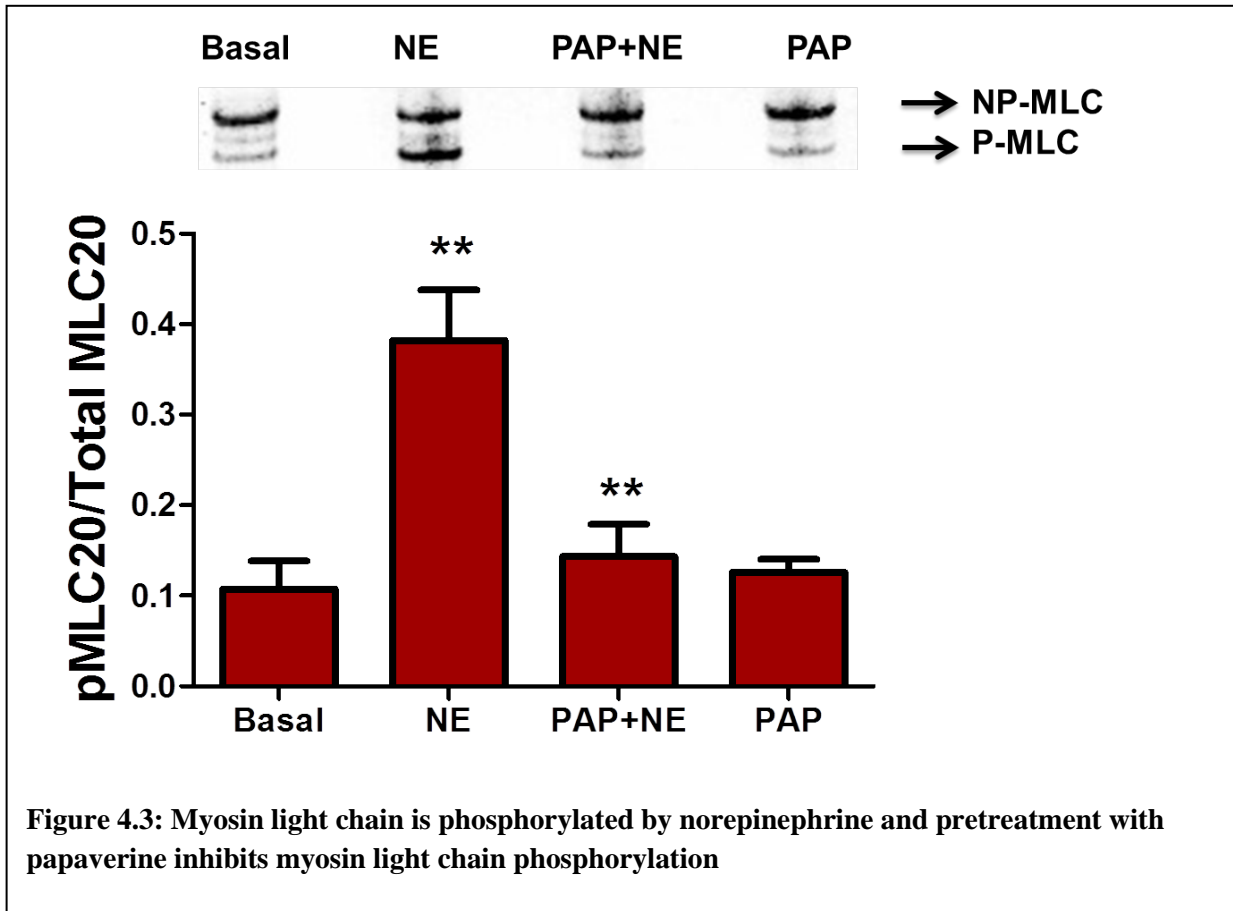
Norepinephrine induced contraction in human saphenous veins and gave rise to the

calcium fluorescence increase shown in (figure 4.2). Treatment with papaverine completely

inhibited both the force generated and the calcium fluorescence induced by norepinephrine in

human saphenous vein tissue.

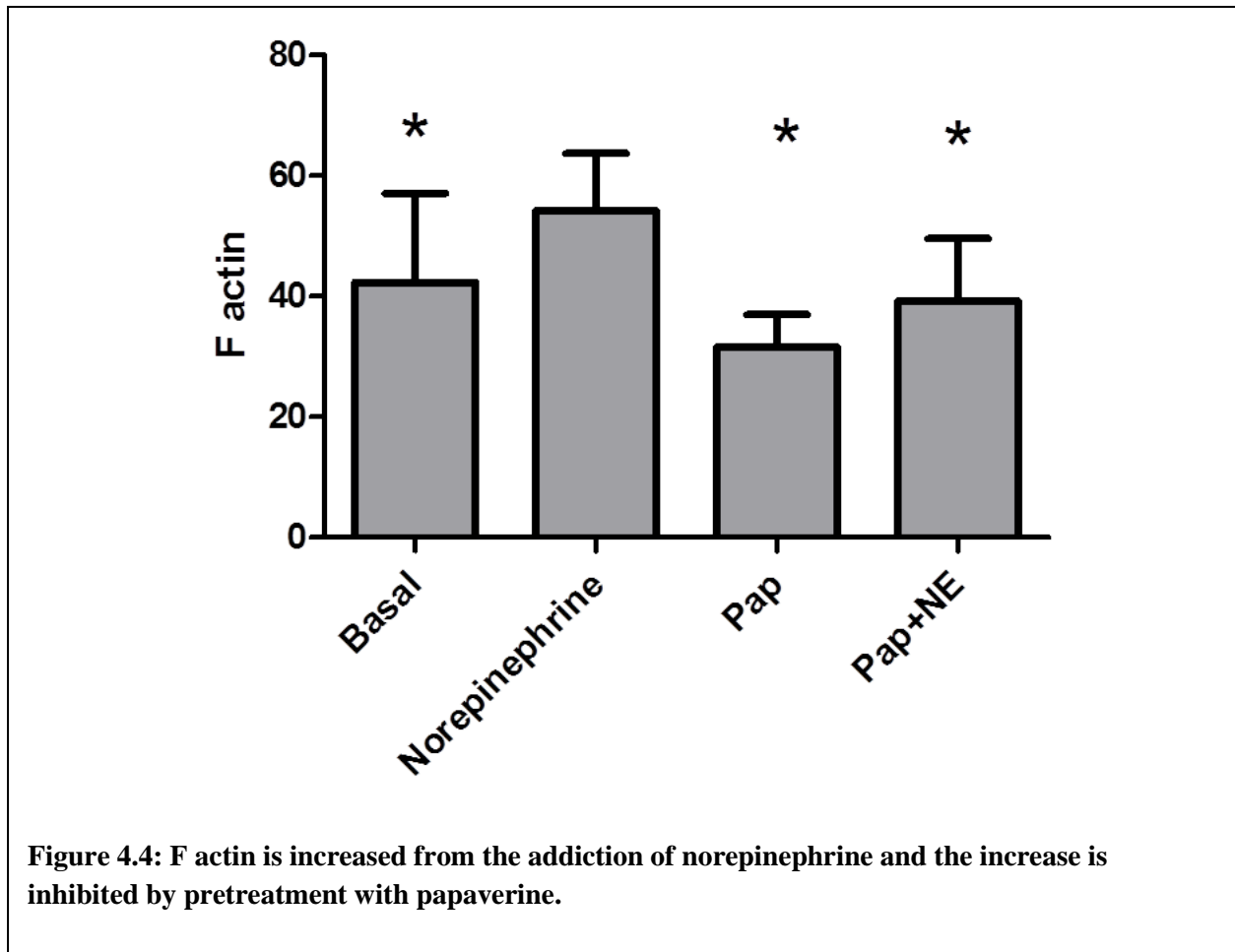The effect of papaverine on MLC phosphorylation

Norepinephrine treatment significantly increased (0.41 ± 0.04 Mol Pi/Mol MLC) the

phosphorylation of MLC when compared to untreated basal (0.09 ± 0.04 Mol Pi/MolMLC) (n=4,

Figure 4.3: Myosin light chain is phosphorylated by norepinephrine and pretreatment with papaverine inhibits myosin light chain phosphorylation

p=0.01). Papaverine + norepinephrine treatment significantly decreased (Mol Pi/Mol MLC) the

phosphorylation of MLC when compared to norepinephrine (Mol Pi/MolMLC, n=3, p=0.02)

which suggests that papaverine treatment result in significant dephosphorylation of MLC.

Papaverine treatment decreases filamentous actin levels

Several investigators have demonstrated that actin is polymerized during contraction of

smooth muscle, and agents that inhibit actin polymerization result in inhibition of contraction

Figure 4.4: F actin is increased from the addiction of norepinephrine and the increase is inhibited by pretreatment with papaverine.

(review [59]).   To examine the effect of activation of cyclic nucleotide-dependent pathways by

papaverine on actin polymerization, HSV was treated with either buffer alone (basal),

norepinephrine (5 μM, 3 min), papaverine (1 mM, 10 min) followed by norepinephrine (5 μM, 3

min), or papaverine (1 mM, 10 min). Actin polymerization was then measured. Treatment with

norepinephrine led to increases in F- actin by 15 % (75 $\pm$ 4 % to 89 $\pm$ 1% for basal and

norepinephrine, respectively), while treatment with papaverine reduced F actin by 10% (75 $\pm$ 4

% to 65 $\pm$ 6 % for basal and papaverine, respectively).   Pretreatment with papaverine for 10 min

before norepinephrine stimulation reduced the F- actin by 17% (75 $\pm$ 4 % to 58 $\pm$ 10 % for basal

and papaverine + norepinephrine, respectively p=0.004, n=7-9, Fig. 4.4), which is consistent with depolymerization of actin.

The effect of papaverine on the phosphorylation of actin regulating proteins, HSP20, and VASP

Figure 4.5: HSP20 was phosphorylated from addition of the phosphodiesterase inhibitor papaverine
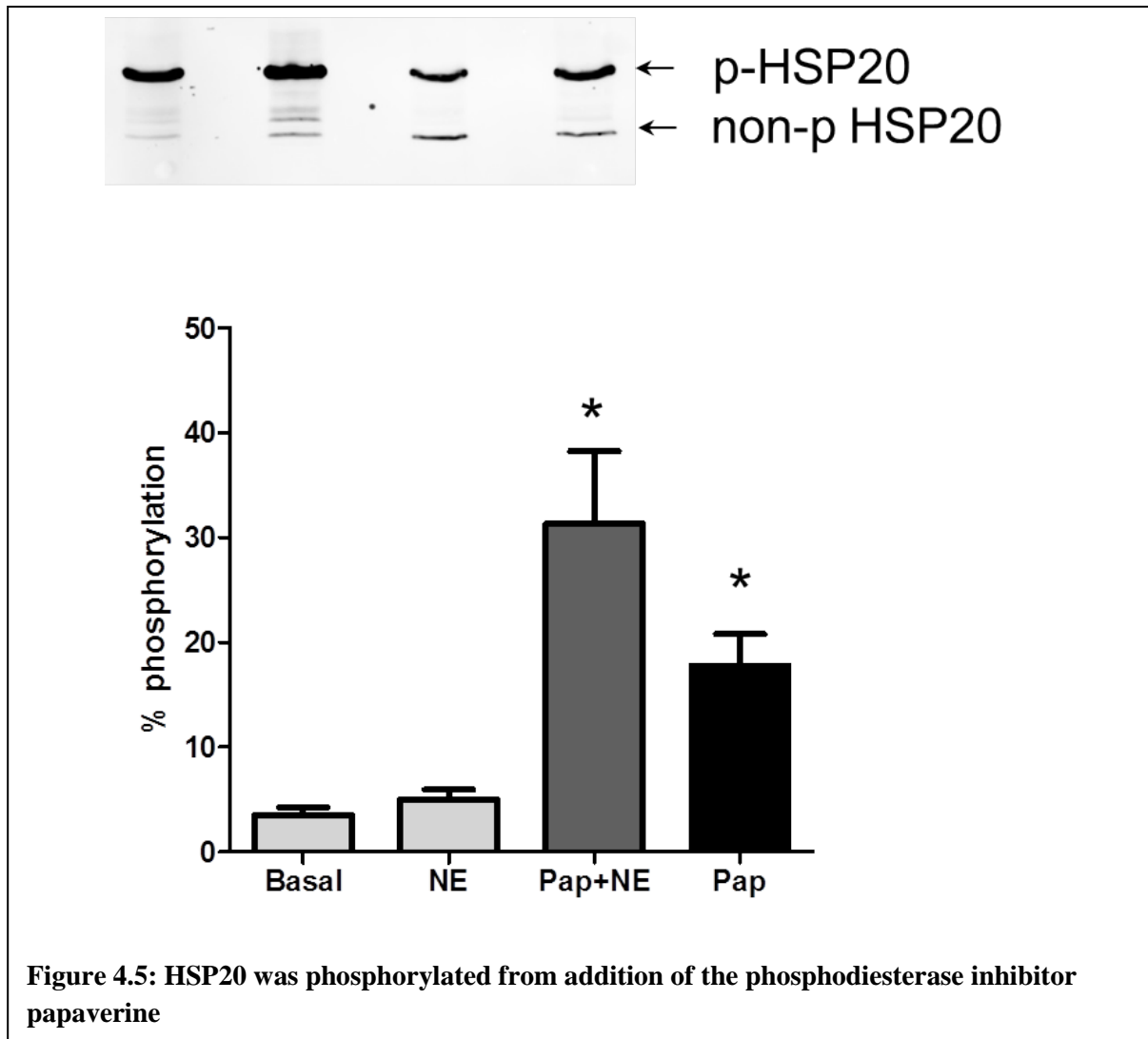
Treatment of smooth muscle with vasodilators increases the phosphorylation of HSP20 and induces relaxation [90]. To decipher the role of HSP20 phosphorylation in the regulation of actin polymerization during force inhibition, HSV was treated with basal conditions, norepinephrine, papaverine followed by norepinephrine, or papaverine, as described above.

HSP20 phosphorylation was examined by isoelectric focusing and western blot analysis.

Papaverine led to increases in the phosphorylation of HSP20 [5.03 ± 0.91 and 31.30 ± 6.96

phospho-HSP20/total HSP20 for norepinephrine and papaverine + norepinephrine, respectively
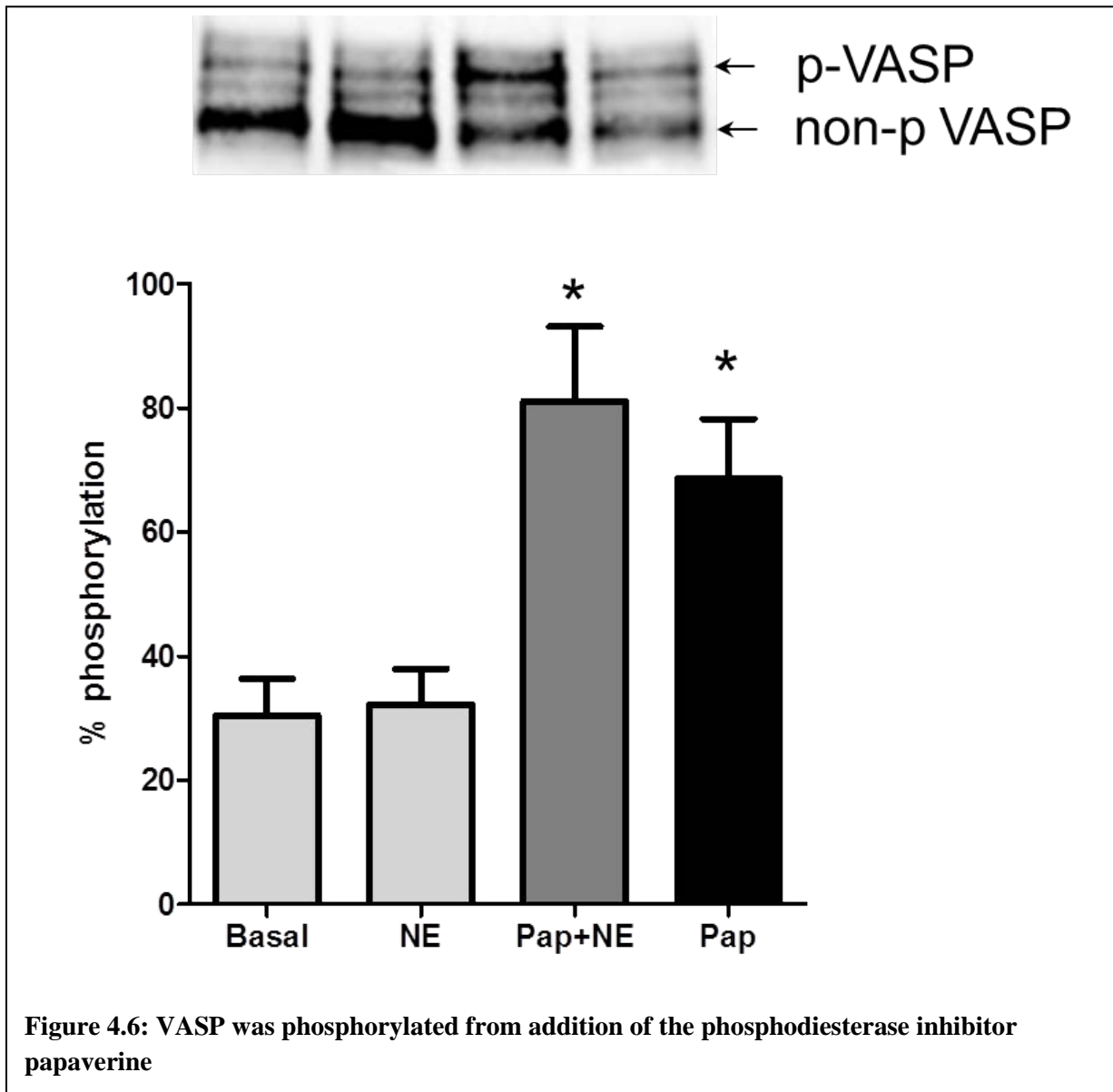
Figure 4.6: VASP was phosphorylated from addition of the phosphodiesterase inhibitor papaverine

($p < 0.05$, n=4)] in HSV, and HSP20 remained phosphorylated even after norepinephrine was

added to induce contraction (Fig 4.5).

Next, the effects of papaverine on VASP phosphorylation, which have been demonstrated to regulate actin polymerization was determined. VASP was phosphorylated in response to papaverine, but not norepinephrine treatment, and the phosphorylation was not changed by norepinephrine treatment after papaverine $(32.21 \pm 5.74$ and 81.03 ± 12.12 p-VASP/VASP for norepinephrine and papaverine + norepinephrine, respectively $p < 0.05$, n=4, Fig. 4.6).

The effect of sodium nitroprusside on inhibition of force, intracellular calcium, and MLCp

Norepinephrine treatment significantly increased $(0.38 \pm 0.05$ Mol Pi/Mol MLC) the phosphorylation of MLC.   Sodium nitroprusside and norepinephrine treatment significantly
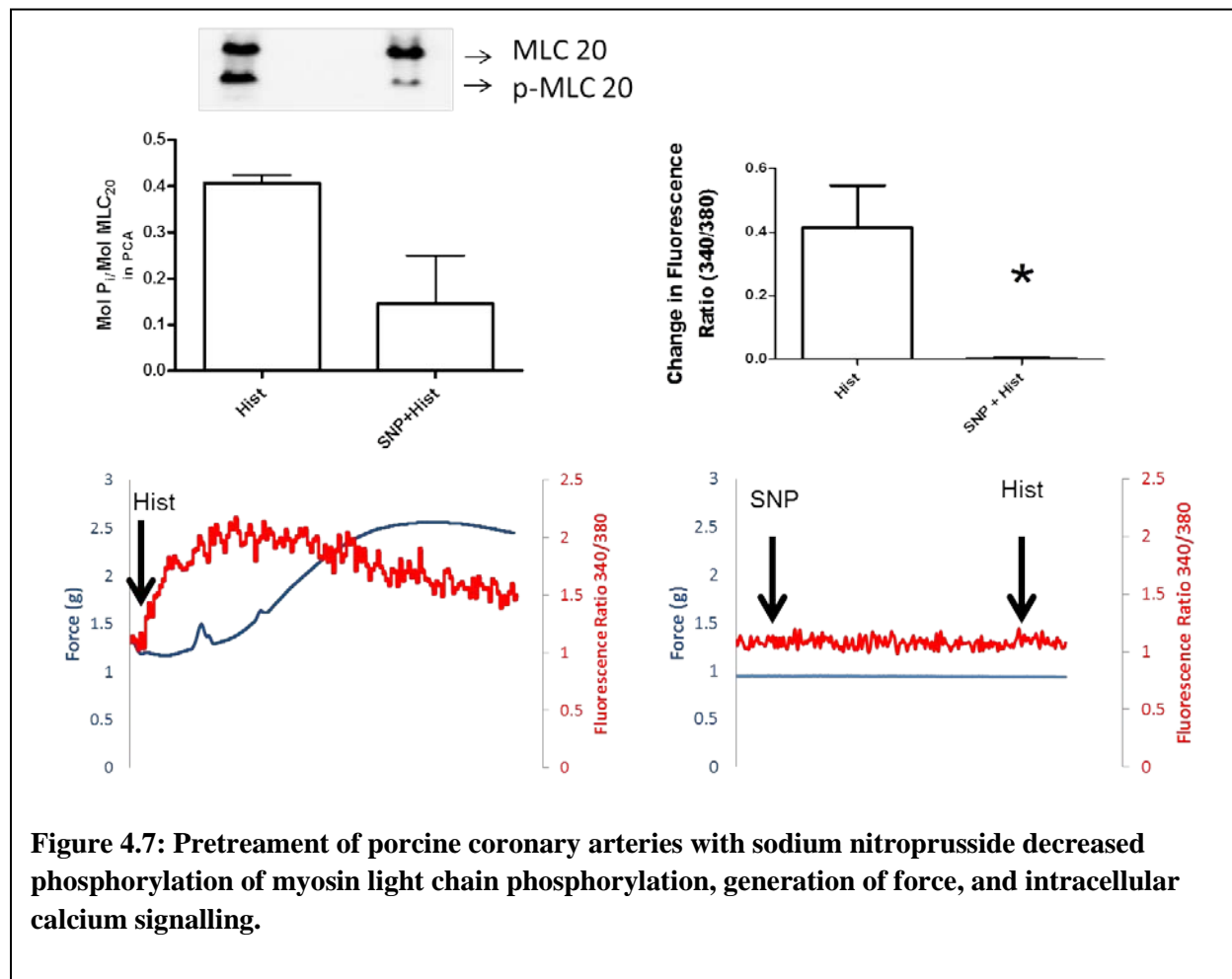
Figure 4.7: Pretreament of porcine coronary arteries with sodium nitroprusside decreased phosphorylation of myosin light chain phosphorylation, generation of force, and intracellular calcium signalling.

decreased (0.16 ± 0.10 Mol Pi/Mol MLC) the phosphorylation of MLC when compared to norepinephrine(n=3, p=0.02) which suggests that SNP treatment result in significant dephosphorylation of MLC. This observation is also seen in conjunction with the reduction of calcium transients when tissue is pretreated with sodium nitroprusside.

Initial experiments were conducted using various doses of norepinephrine (0.1 to 10 µM) to contract HSV, and a dose of norepinephrine (5-10 µM) which produced greater than 60% of maximal potassium-induced contraction was selected for our experiment. Various doses of sodium nitroprusside (0.1-10 µM) were used to block norepinephrine induced contraction and a dose of 10µM that completely blocked norepinephrine induced contraction was chosen for this study. Treatment of HSV with norepinephrine alone induced force. Pretreatment of HSV with 10 µM sodium nitroprusside blocked norepinephrine induced force (Data not shwon).

Norepinephrine induced contraction in human saphenous veins and gave rise to the calcium fluorescence increase shown in (figure 4.7). Treatment with SNP completely inhibited the force generated and calcium fluorescence induced by norepinephrine in human saphenous vein tissue.

Discussion

In this study, a physiologic system was developed wherein vasospastic properties of tissue were induced through norepinephrine. To test methods that combat the induced vasospasm papaverine and sodium nitroprusside were used. The use of these two vasodilators resulted in the complete suppression of force generation in the presence of a contractile agonist. This physiologic model allowed us to further define the role of actin filaments, in addition to thick filament modulation, during cGMP-dependent force suppression. Experiments were conducted using the FluoroPlex Tissue Bath Fluorometry System, a muscle bath system that enables

73

fluorescence ion recording in parallel with force measurement in intact tissues, and $[Ca^{2+}]_i$ transients, MLC phosphorylation, and F/G- actin levels were measured. Previous studies have demonstrated that activation of adenyl cyclase through forskolin treatment results in depolymerization of F-actin without a reduction in MLC phosphorylation or calcium transients[128].

Potency of papaverine may be due to inhibition of both thick and thin filaments in vascular smooth muscle. It has been shown that papaverine increases both cAMP and cGMP in rat aorta with a dose dependent manner, while forskolin increases cAMP in a dose dependent manner and sodium nitroprusside increases cGMP in a dose dependent manner[117]. This dual increase in cGMP and cAMP leads to not only to a reduction in intracellular calcium transients and dephosphorylation of the myosin light chain, but also reduction in F – actin filaments furthering the vasodilation in smooth muscle.

Thick filament regulation is demonstrated in the use of sodium nitroprusside as an inhibitor of contraction acting as a nitric oxide donor[129]. Nitric oxide acts through the effects of guanylyl cyclase, leading to cyclic GMP and the activation of PKG. This activation of PKG and increased intracellular cGMP inhibits calcium entry to the vascular smooth muscle cells and leads to a decrease in intracellular calcium[129,130]. The inhibition of calcium entry into the smooth muscle cells occurs by the effects on the IP3 receptor, phospholamban, and the ryanodine receptor[131]. A reduction in this intracellular calcium leads to a reduction in the phosphorylation of the myosin light chain in vascular smooth muscle, also that increases in cyclic nucleotides have been shown to increase the requirement of calcium for phosphorylation of the MLC, either through the inhibition of MLCK or by activating MLC phosphatase[131].

Thin filament regulation has been studied previously showing a calcium and myosin light chain independent relaxation in vascular smooth muscle at low doses of forskolin in porcine coronary arteries[128]. Although there was not a reduction in intracellular calcium transients and myosin light chain phosphorylation there were significant decreases in the amount of f actin in tissue treated with forskolin[128]. This relationship does not hold up at higher doses of forskolin potentially due to cross talk between cAMP and PKG that may occur[132]. At greater amounts of forskolin was used to pretreat tissue, intracellular calcium was inhibited in smooth muscle. Taken together that papaverine mediates smooth muscle relaxation through both cAMP and cGMP it is able to reduce spasm via multiple pathways.

An issue that may occur with the use of papaverine hydrochloride is the acidity of papaverine solution. Previous studies have shown that spasm and endothelial injury may be prevented by using Plasmalyte A with papaverine hydrochloride (60 mg/500 mL)[133]. Using a balanced buffered solution like Plasmalyte A is important in maintaining a normal pH of the solution. Preservation of the endothelial lining is also important because the endothelium inhibits platelet adhesion and prevents fibrin deposition on the smooth muscle[133].

Papaverine is a preferred method to dilate vessels in the operating room to manual distension. One reason papaverine would be preferred is because of the detrimental effects high pressure distension causes physiologic dysfunction and intimal hyperplasia in saphenous veins[122]. Both endothelial dependent and independent relaxation of saphenous veins were decreased by manual distension to the tissue. In an organ culture model, 14 day intimal thickness was significantly increased in tissue that was manually distended compared with the control tissue[122]. Additionally to the benefit of avoiding manual distension, PDE inhibitors may also enhance vein graft patency[134,135].

Conclusions

The activation of cGMP leads to both decreases in intracellular calcium levels and the phosphorylation of myosin light chain. The major difference in increasing cAMP from cGMP is that increasing cAMP in tissue results in calcium independent force inhibition. Increases in cGMP result in calcium desensitization as a major modulator of force making one unable to uncouple force and calcium. PKG activation inhibits force without uncoupling intracellular calcium as shown with both a nitric oxide donor and a phosphodiesterase inhibitor. This was seen by a decrease in intracellular calcium and a reduction in the phosphorylation of the myosin light chain.

CHAPTER 5

Modulation of HSP20

Aim 4 *Modulate HSP20 to uncouple force and calcium*

Text for Chapter 5 taken from:

      Hocking KM, Evans BC, Komalavilas P, Duvall CL, Brophy CM "Heat shock proteins

role in developing novel therapeutics for vasospastic vessels" in preparation

Introduction

      Subarachnoid hemorrhages affect 30,000 people each year and accounts for

between 1-7% of all strokes [75]. After the subarachnoid hemorrhage, 30 to 60% of the patients

will experience cerebral vasospasm[71]. Neurological deficit as a result of ischemia, caused by

delayed vasospasm of cerebral arteries, is the most common cause for morbidity and mortality in

patients who had subarachnoid hemorrhage [2]. Cerebral vasospasm after subarachnoid

hemorrhage is well documented and has been researched but much of the mechanism of

pathogenesis is not well understood[26]. Current treatments have not been highly successful for

patients with SAH, and a large part of this is due to these patients having normal systemic blood

pressure while cerebral vessels are spastic thus traditional vasodilators have proven

ineffective[2,27,133].

      The small heat shock proteins HSP20 and HSP27 are involved in the regulation of

smooth muscle tone[19]. HSP20 is associated with relaxation of vascular smooth muscle and this

may be relevant to the treatment of hypertension, vasospasm, asthma, preterm labor, and bladder

problems[136]. It is the phosphorylated form of HSP20 that is associated with the relaxation of

smooth muscle and is one of the most important phosphoproteins of the relaxation process.

HSP27 is involved in smooth muscle contraction and the migration of smooth muscle cells[137]. Non-phosphorylated HSP27 caps the plus end of the actin filaments, preventing new actin[137] monomers from attaching, and is a pro cellular survival mechanism[136]. HSP20 phosphorylation is correlated with an enhanced vasorelaxation response, while HSP27 phosphorylation has been associated with impairment in smooth muscle relaxation[18,39,71], this occurs by HSP27 promoting actin remodeling by enhancing actin polymerization[138]. Unphosphorylated HSP27 can cap f-actin preventing polymerization from occurring[14].

The decrease in HSP20 phosphorylation and the increase in HSP27 phosphorylation have been shown in a subarachnoid hemorrhage model[19], this change exists concurrently with a decrease in cerebral perfusion[38,39]. We hypothesize that the vasospasm occurring after subarachnoid hemorrhage is due to impaired relaxation of the artery, and that this impaired relaxation is associated with changes in the phosphorylation and expression levels of HSP20 and HSP27. With the rise in intracranial pressure and reduction in cerebral perfusion pressure the cerebral blood flow to patients is reduced. This reduction in blood flow is accompanied by cerebral vasospasm. Restoration of perfusion to these areas is necessary to prevent ischemic damage from occurring. The purpose of this study is to better understand physiologic changes that occur as a result of HSP20 downregulation and HSP27 phosphorylation changes after subarachnoid hemorrhage.

Methods

Procurement of rat aorta smooth muscle and physiologic measurements

Fresh cadaveric aortas were isolated immediately from euthanized, discarded animals from Vanderbilt University Medical Center. All procedures for collection of cadaveric tissue were reviewed and approved by the Vanderbilt University Animal Care and Use Committee. Subcutaneous fat and adventitial tissues were removed and the vessel was cut into transverse rings of 2.0 mm in width. Rings were suspended in a muscle bath containing a bicarbonate buffer (120 mM NaCl, 4.7 mM KCl, 1.0 mM MgSO$_4$, 1.0 mM NaH$_2$PO$_4$, 10 mM glucose, 1.5 mM CaCl$_2$, and 25 mM Na$_2$HCO$_3$, pH 7.4), equilibrated with 95% O$_2$ / 5% CO$_2$, at 37°C. Force measurements were obtained with either a Kent Scientific (Litchfield, CT) force transducer (TRN001) or a Radnoti force transducer (Radnoti Glass Technology Inc., Monrovia, CA) interfaced with Power Lab from AD Instruments (Colorado Springs, CO). Data were recorded with Chart software, version 5.1.1 (AD Instruments). Rings were washed every 15 min with 37°C bicarbonate buffer for 1 hr, and each ring was progressively stretched to its optimal resting tension (approximately 1 g) that would produce a maximal response to contractile agonists as determined previously, then maintained at the resting tension and equilibrated for another hour. Rings were then contracted multiple times with high extracellular potassium (110 mM KCl, with equimolar replacement of NaCl in bicarbonate buffer) and the force generated was measured. Measured force was normalized for ring weight and length and converted to Stress using the formula: Stress [10^5Newtons (N)/m^2] = force (g) x 0.0987 / area, where area is equal to the wet weight [mg / length (mm at maximal length)] divided by 1.055. The maximal tension obtained was taken as 100%. Rings were equilibrated for an additional 30 min and dose response curves for phenylephrine contraction and sodium nitroprusside relaxations were determined to select the

correct dose of agents for the experiment. To determine the inhibition of contraction, rings were either treated with buffer alone (control) or HSP20 phospho peptidomimetic for 30 min. After this the tissue was contracted again with phenylephrine, and inhibition of contraction was measured as % difference in contraction.

Preparation of HSP20 siRNA micelle

Dicer substrate siRNA were obtained from Invitrogen and screened for effectiveness against rat aortic smooth muscle cells with PCR. Once two siRNAs had been selected they were combined with a diblock copolymer composed of N,N-Dimethylaminoethyl methacrylate (DMAEMA), polypropyl acrylic acid (PAA), and butyl methacrylate synthesized using a reversible addition fragmentation chain transfer polymerization as described previously[139]. Nanoparticles were created by combing 1 mg of the polymeric diblock copolymer with 0.08 mg of siRNA as described previously[139].

Knockdown of HSP20

The siRNA nanoplexes were added to a HEPES buffered DMEM at a concentration of 50 nM. Tissue was placed into either control, scrambled siRNA nanoplexes, or HSP20 siRNA nanoplexes. After 24 hours of treatment at 37 C tissue samples were taken out of the DMEM HEPES buffer and placed on the muscle bath apparatus to determine physiologic function as described above where phenylephrine (0.1 µM) was used to contract the tissue with doses of sodium nitroprusside (10 pM to 1nM) to relax the tissue. At the end of the experiment tissue samples were frozen for quantification of HSP20 in the tissue.

Construction of cell-permeant HSP27 fusion protein

The cDNA encoding human HSP27 was polymerase chain reaction amplified from an I.M.A.G.E (Integrated Analysis of Gene Expression). Clone (clone ID 6083486; Clontech, Palo

Alto, Calif) using a forward primer (5'- ATCGAGCTCATGACCGAGCGCCGCGTC- 3') and a

reverse mutagenic primer (5'-gatcggtaccttacttggcggcagtctcatcgg- 3') then cloned into pCDNA3.1

(Invitrogen, Carlsbad, Calif), yielding pCDNA3.1-HSP27. Complementary oligonucleotides (5'-

ATGGGTGGTTATGCTAGAGCTGCTGCTAGACAAGCTAGAGCTGGTACCGAGCTCCTC

GAGG- 3' and 5'-

ATCCCTCGAGGAGCTCGGTACCAGCTCTAGCTTGTCTAGCAGCAGCTCTAGCATAAC

CACCCA- 3') encoding a PTD were annealed, phosphorylated, and ligated into *Nde*I-*BamH*I-

digested pET14b[140] yielding pET14-bPTD-HSP27. Base sequences for all DNAs were confirmed

by nucleotide seuquence analysis, and protein was expressed in Escherichia coli. Briefly, single

colonies of BL21 (DE3; Novagen) containing recombinant pET14b-PTD-HSP27 were used to

inoculate 3 liters of Luria Broth (LB) containing 50 mg/L of ampicillin. Cultures were induced

with 2 mMisopropyl-1-thio-_-D-galactopyranoside when the opticaldensity at 600-nm

wavelength reached 0.6-1. After 5 hours, cells were harvested by centrifugation (6,000 g, 10

minutes), resuspended in 1_ TNE buffer (50 mM NaCl, 1mM ethylenediaminetetraacetic acid

[EDTA], and 500mM Tris, pH 8.0), and onicated on ice. After sonication, the inclusion bodies

were harvested by centrifugation (19,000 g, 10 minutes) and resuspended in binding buffer (20

mM Na2HPO4, 0.5 M NaCl, 50 mM imidazole, pH 7.4, and 8 M urea). The sample was then

added to Ni^{2+}- charged Chelating Sepharose Fast Flow (Pharmacia Biotech, Peapack, NJ) and

incubated overnight at 4°C. The resin was then loaded into a Poly-Prep column (Bio-Rad,

Richmond, Calif), and protein was eluted with 2 mL of 500mM Imidazole and dialyzed with

phosphate buffer (20mM Na$_2$HPO$_4$, 0.5 NaCl).. Rat aortic tissue was treated for 30 min with 15

µM rPTD-HSP27 before being placed on the muscle bath.

Immunoblotting

Proteins from frozen muscle rings were extracted in UDC buffer (8 M urea, 10 mM dithiothreitol (DTT), 4% CHAPS containing protease inhibitor, phosphatase I and II inhibitor cocktail (Sigma, St. Louis, MO). The mixtures were vortexed at room temperature overnight, and then centrifuged at 14,000 rpm for 15 min at 4°C. Soluble protein concentrations were determined using the Bradford assay (Pierce Chemical, Rockfort, IL). Equal amounts (20-50 μg) of proteins were placed in a Laemmli sample buffer (Bio-Rad laboratories, Inc. Hercules, CA), heated for 5 min at 100°C and separated on SDS polyacrylamide gels. Proteins from the gels were transferred onto nitrocellulose membranes (Li-COR Biosciences, Lincoln, NE) and blocked prior to incubation overnight at 4°C with the following primary antibodies: anti-HSP20 (1:3,000 dilution, Advanced Immunochemical Inc., Long Beach, CA); and anti-GAPDH (1:250, BD Transduction Laboratories). Membranes were washed three times with TBS containing Tween 20 (0.1%) (TBST), and incubated with appropriate infrared-labeled secondary antibodies (Li-Cor, Lincoln, NE) for 1hr at room temperature. The membranes were subsequently washed with TBST, and protein-antibody complexes were visualized and quantified using the Odyssey direct infrared fluorescence imaging system (Li-Cor Biosciences NE). Ratios were calculated as the ratio of the HSP20 protein to total GAPDH protein.

Monomyer and polymer synthesis

All reagents were purchased from Sigma and were of analytical grade unless otherwise stated. 2-propylacrylic acid was synthesized according to the procedure outlined by Ferrito et al.[141] utilizing diethyl propylmalonate (Alfa Aesar) as a precursor. The 4-cyano-4-(ethylsulfanylthiocarbonyl) sulfanylvpentanoic acid (ECT) chain transfer agent (CTA) was synthesized as previously described[142]. RAFT polymerization of the PPAA homopolymer was

carried out in bulk under a nitrogen atmosphere at 70°C for 48 hours using 2,2'-azo-bis-

isobutyrylnitrile (AIBN) as the free radical initiator. The reaction mix was put through three

freeze-vacuum-thaw cycles and purged with nitrogen for thirty minutes prior to polymerization.

The molar ratio of CTA to AIBN was 1 to 1, and the monomer to CTA ratio was set so that a

degree of polymerization of 190 would be achieved at 100% conversion. Following

polymerization, the resultant polymer was dissolved in DMF and precipitated into ether 5 times

before drying overnight *in vacuo*. Gel permeation chromatography (GPC, Agilent) was used to

determine molecular weight and polydispersity (M_w/M_n, PDI) of the PPAA homopolymer using

HPLC-grade DMF containing 0.1% LiBr at 60°C as the mobile phase. Molecular weight

calculations were performed with ASTRA V software (Wyatt Technology) and were based on

experimentally-determined dn/dc values determined through offline injections of the polymer

through a refractive index detector (calculated PPAA dn/dc = 0.087 mL/g).

Polyplex

The HSP20 phosphopeptide was synthesized using solid phase synthesis and purified by

HPLC as verified through Electrospray-ionization mass spectrometry (ESI-MS) (supplementary

fig. 1). NPs were formed by simple mixing of the PPAA homopolymer with the HSP20 phospho

peptide in PBS at pH 8.0, which is between the pKa values of the primary amines present on the

HSP20 phospho peptide and the carboxylic acid moieties ensures optimal solubility and net

charge on both molecules. The PPAA polymer was chosen because of its well defined pH-

dependent membrane disruptive activity that has been shown to facilitate endosomal escape[143-145]

and successful use in animal models[146,147].

To determine optimal nanoparticle formulation conditions, a library of pHSP20 nano-

polyplexes (pHSP20-NPs) was prepared at various charge ratios (i.e. CR = ([NH$_3$$^+$]$_{MK2i}$/[COO$^-$

]$_{PPAA}$) from 10:1 to 1:10 and the size distribution and particle surface charge were characterized through dynamic light scattering (DLS) and ζ-potential analysis, respectively. As expected, pHSP20-NP ζ-potential was directly proportional to the CR, with an apparent isoelectric CR ~ 3:1 (fig.1 C). Charge ratio was found to significantly affect pHSP20-NP size and charge, with a CR=3:1 yielding a unimodal size distribution (supplementary table 1). A CR of 1:3 was chosen as the optimal formulation as this ratio consistently yielded a unimodal size distribution with minimal particle size and polydispersity (d_h=240.9 ± 15.51 nm, ζ = -0.91 ± 2.56 mV). It is hypothesized that at the lower pH, the PPAA polymer becomes protonated/deionized, and the net positive charge on the peptide causes electrostatic repulsion and disassembly of the pHSP20-NPs. This effect releases the therapeutic payload and ensures that peptide bioactivity is not sterically hindered by NP encapsulation.

Cytosolic Ca^{2+}measurements

Rings of rat aorta were suspended on hooks in a FluoroPlex Tissue Bath Fluorometry System Tissue Bath Fluorometry System (IonOptix LLC, Milton, MA and Radnoti Glass Technology Inc., Monrovia, CA), which enables fluorescence ion recording in parallel with force measurement. Force measurements were obtained with a Radnoti force transducer (Radnoti Glass Technology Inc., Monrovia, CA) interfaced with Power Lab from AD Instruments (Colorado Springs, CO). Rings were loaded at room temperature with 10 µM Fura-2 AM ester and 0.01% Pluronic F-127 in the bicarbonate buffer for 4 hrs. After loading, rings were washed every 10 min with 37°C bicarbonate buffer for 1 hr. Calcium flux was measured with optical fibers that were interfaced with Power Lab. Fluorescence was measured at both 380 and 340 nm of wavelength, simultaneously. The ratio of the emission of the two wavelengths was used to determine intracellular changes in calcium concentration. Baseline ratio was set at 1.0 and

changes in this ratio in response to stimuli were measured. Baseline calcium fluorescence was measured and the background was set to zero as an output of 1 volt. To determine the inhibition of contraction, rings were either treated with control or HSP20 phospho peptidomimetic(ppHSP20). The tissue was then challenged with phenylephrine and the % inhibition of contraction and calcium concentrations were measured. To add phenylephrine while continuously measuring intracellular calcium concentrations, an infusion line filled with bicarbonate buffer was used to keep the system in a closed light impenetrable state. The amount of buffer in the infusion line was adjusted to achieve the final concentration of the agonist in the bath. Force and calcium fluorescence were measured continuously for 15 min after the addition of phenylephrine.

Actin Assay

The amount of F-actin versus total actin (F-actin /(F-actin + G-actin)) was measured using the G-actin/F-actin *In Vivo* Assay kit (Cytoskeleton, Denver, CO), per manufacturer's protocol. Briefly, treated rat aortic samples were homogenized in 1 ml of lysis buffer (50 mM PIPES pH 6.9, 50 mM NaCl, 5 mM $MgCl_2$ 5 mM EGTA, 5% (v/v) Glycerol, 0.1 % Nonidet P40, 0.1% Triton X-100, 0.1% Tween 20, 0.1% 2-mercapto-ethanol, 0.001% Antifoam C, 4 µM Tosyl arginine methyl ester, 15 µM Leupeptin, 10 µM Pepstatin A, 10 mM Benzamidine, 1 mM ATP warmed to 37°C) for 1 min with a mortar and pestle that fit into the 1.5 ml microfuge tube. The lysate was centrifuged at 2000 rpm for 5 min at 37°C to pellet unbroken cells. The supernatants were centrifuged at 100,000 x g for 1 hour at 37°C. Supernatants (contains the G-actin) were transferred to pre-cooled tubes and placed on ice. The pellets (contain F-actin) were resuspended in 1 ml of ice-cold 10 µM cytochalasin D in deionized water, and F- actin was depolymerized by incubating for 1 hour on ice with mixing every 15 min. Equal volume of supernatants and pellets
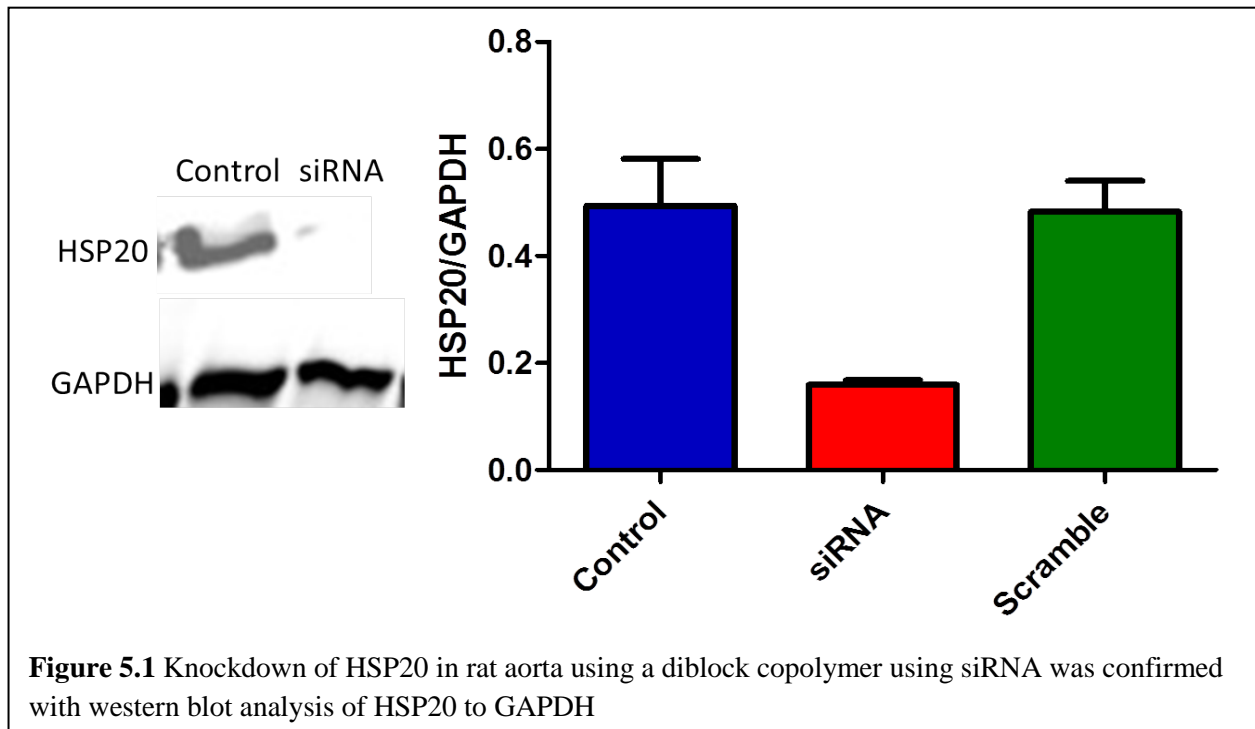
along with actin standards (2-20 µg) were separated on 12% SDS-polyacrylamide gels and transferred to nitrocellulose membrane in 1X TG buffer at 100 volts for 1 hr. The membrane was probed with anti actin antibody and the amount of actin in each fraction was quantified comparing to actin standards loaded on the same gel.
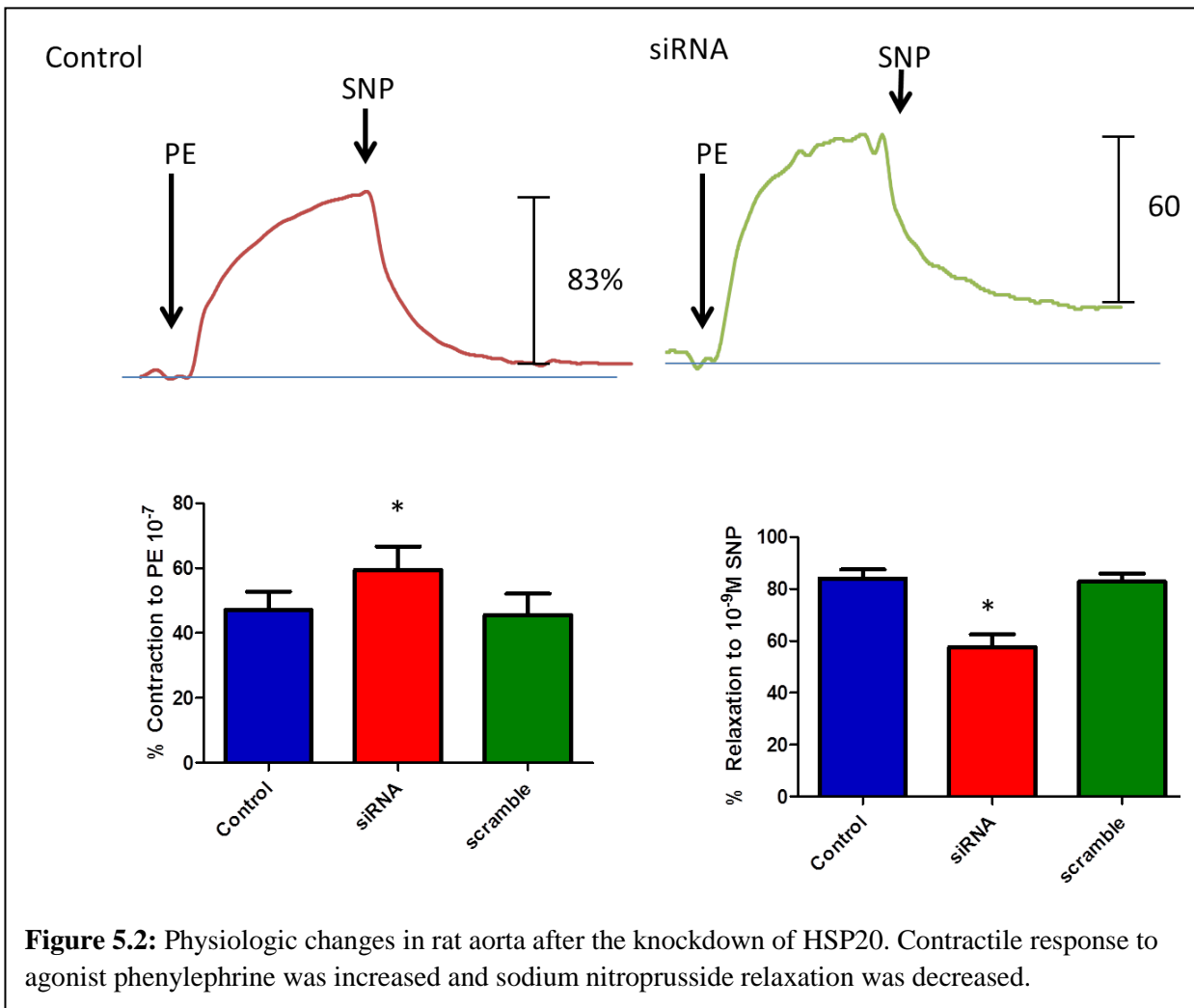
Data analysis

Data were reported as mean responses ± standard error of the mean. Paired t-tests or one-way ANOVA analyses were conducted in order to determine the significance (p value) of each experiment. A p value <0.05 was considered statistically significant.

Results

HSP20 knockdown and smooth muscle physiology

Figure 5.1 Knockdown of HSP20 in rat aorta using a diblock copolymer using siRNA was confirmed with western blot analysis of HSP20 to GAPDH

Rat aorta was incubated in either a self-assembling micelle containing HSP20 siRNA (50 nM), micelle with scramble siRNA (50 nM), or untreated (control) for 24 hours in HEPES buffered DMEM. After the 24 hour incubation the rat aorta was frozen. Knockdown of the protein was confirmed using western blot techniques to quantify HSP20 levels and was normalized to tissue GAPDH levels. Tissue treated with HSP20 siRNA (0.16 ± 0.02 A.U.) had a significantly lower amount of HSP20/GAPDH than control (0.50 ± 0.21 A.U.) or scramble groups (0.46 ± 0.16 A.U.) ($p<0.05$, n=6, Figure 5.1), suggesting that the siRNA in a self-

Figure 5.2: Physiologic changes in rat aorta after the knockdown of HSP20. Contractile response to agonist phenylephrine was increased and sodium nitroprusside relaxation was decreased.

assembling micelle successfully down modulates HSP20 expression ex vivo.

With the downregulation of HSP20 confirmed, the effect of HSP20 knockdown on the physiologic response of the rat aorta was determined on a muscle bath apparatus. Control ($47 \pm 5.7\%$) and scramble ($46 \pm 6.6\%$) treated aorta had a significantly ($p<0.01$, n=5) lower contraction to 10^{-7} M phenylephrine as a percent of max depolarization contraction from 110mM KCl compared with rat aorta that had HSP20 knocked down ($59 \pm 7.3\%$) (n=6, $p<0.05$, Figure5.2). In addition to this, relaxation of smooth muscle with knocked down HSP20 ($58 \pm 4.9\%$) had significantly ($p<0.01$, n=5, Figure 5.2) lower relaxation to 10^{-9} M SNP compared with control ($84 \pm 3.5\%$) and scramble ($83 \pm 3.0\%$) treated tissue. Tissue treated with HSP20 siRNA generated a greater contractile force when physiologically challenged with phenylephrine and did not generate as much relaxation to sodium nitroprusside. This result suggests that vascular smooth muscle containing lower amounts of HSP20 had a more contractile phenotype similar to that of spastic vessels.

PTD-HSP27 and its effect on smooth muscle

HSP27 has been shown to be upregulated in cerebral vasospasm following subarachnoid hemorrhage. To show the effect of elevated levels of HSP27 in arterial tissue, PTD-HSP27 was added to rat aorta and physiologic conditions were tested. To ensure HSP27 was increased western blot techniques were used to compare HSP27 levels with beta actin. Tissue treated with PTD-HSP27 had a significantly greater ratio of HSP27/B-actin than control. Rat aortic tissue treated with PTD-HSP27 was also suspended on a muscle bath to determine if there was a change in sodium nitroprusside induced relaxation. Rat aorta treated with PTD-HSP27 (60 ± 7 %) yielded a significantly lower relaxation to 10^{-9} M SNP than control tissue $82 \pm 11\%$) ($p<0.05$, n=4, Figure 5.3). Decreased relaxation of rat aorta from increasing the amount of HSP27 in the smooth muscle is also consistent with the physiologic actions of a spastic vessel.
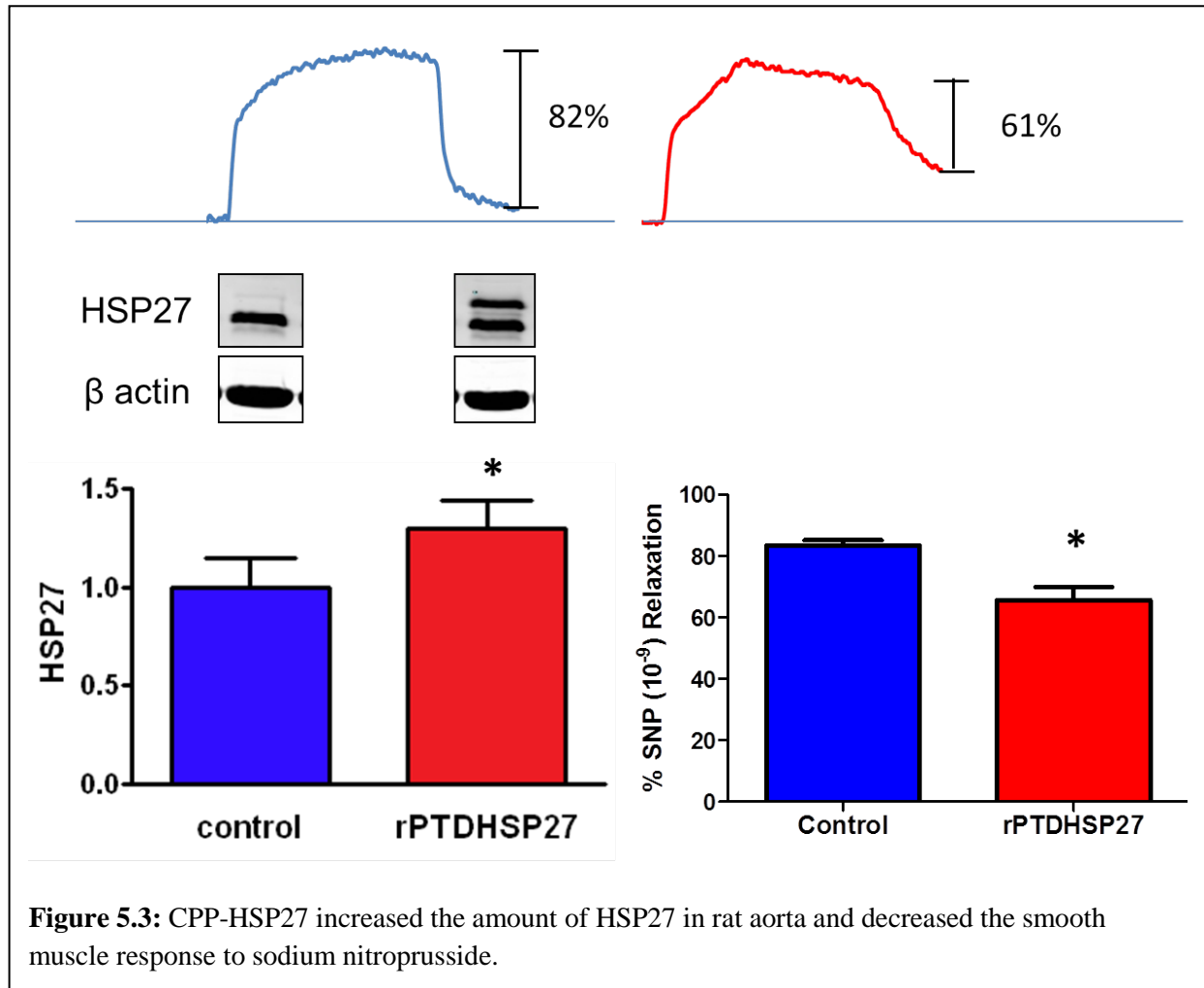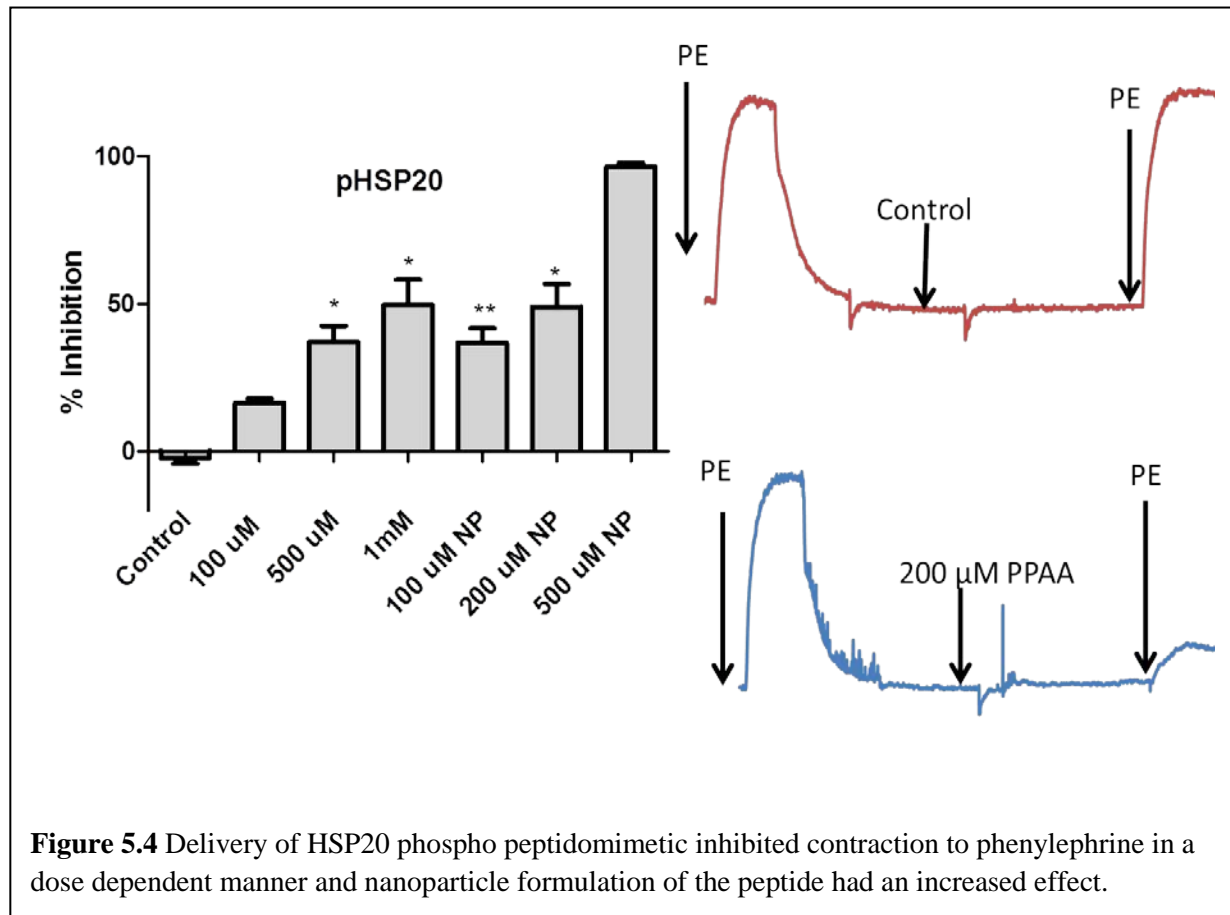
Figure 5.3: CPP-HSP27 increased the amount of HSP27 in rat aorta and decreased the smooth muscle response to sodium nitroprusside.

HSP20 phospho peptidomimetic's inhibition of contraction

HSP20 phospho peptidomimetic was delivered to rat aortic smooth muscle before it was challenged with phenylephrine to assess the vasoactive effects of the peptidomimetic. To assess the enhancement of delivery the peptide was delivered with and without the incorporation of an endosomolytic nanoplex delivery system doses (i.e. 100, 500, 1000 μM of the peptide alone and 100, 200, 500 μM of the polyplex). Percent inhibition was the readout used to determine the effect the peptide had on the tissue. Control segments (-2.4 ± 1.8 %) displayed significantly less % inhibition than all other groups (p<0.0001, n=4-6). Peptide treatment of 100 μM (16.5 ± 1.3 %) displayed significantly less % inhibition than 100 μM polyplex (36.8 ± 4.9 %), 500 μM

peptide (37.1 ± 5.3 %), 1mM peptide (49.7 ± 8.4 %), 200 μM polyplex (49.0 ± 7.7 %), and 500

μM polyplex (95.7± 1.6 %)(Figure 5.4). Both the peptide and polyplex treatments showed a dose

dependent increase in inhibition of contraction of the rat aorta. These data further suggest that

phosphorylation of HSP20 on Ser[16] causes relaxation of smooth muscle and that delivery of the

peptide can be enhanced using the endosomolytic polyplex particles. The increased

bioavailability of the peptide when the polyplex was used is attributed to enhanced endosomal

escape. This endosomal escape occurs when the polyplex is exposed to a lower pH (<6.8) in the

endosome where the peptide is released from the electrostatic complexation. Inhibition of

Figure 5.4 Delivery of HSP20 phospho peptidomimetic inhibited contraction to phenylephrine in a dose dependent manner and nanoparticle formulation of the peptide had an increased effect.

contraction also represents a physiologic state that could mimic prevention of cerebral vasospasm.

Intraceulluar calcium changes during inhibition of contraction
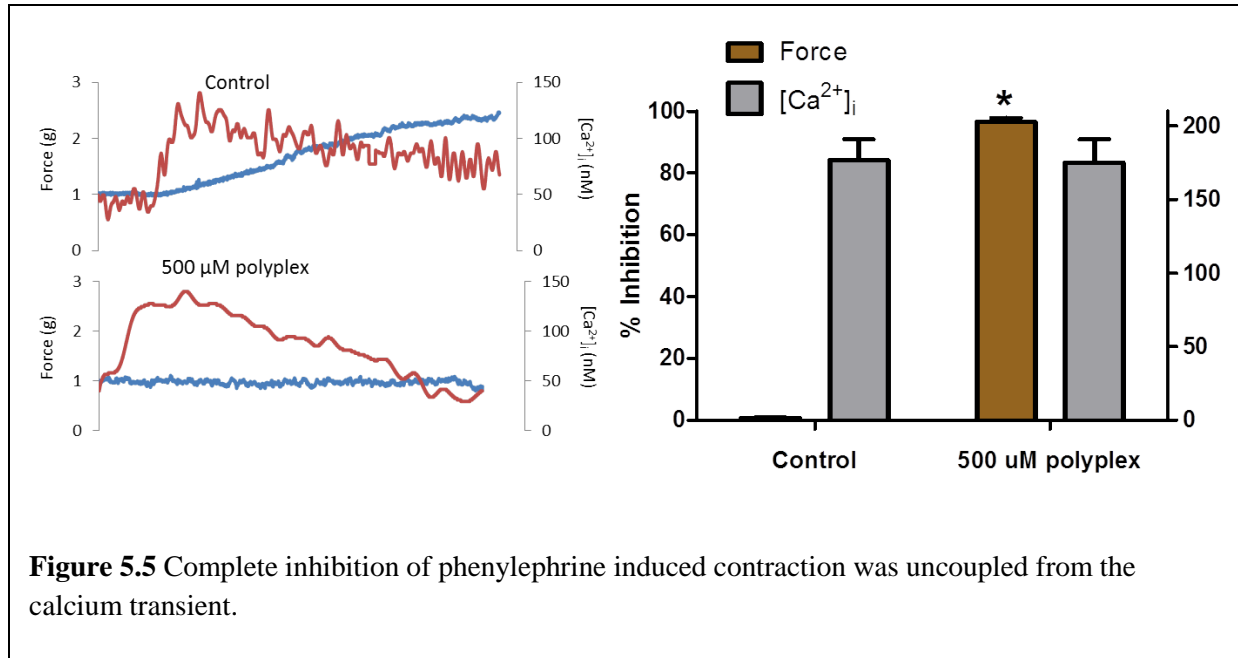

Figure 5.5 Complete inhibition of phenylephrine induced contraction was uncoupled from the calcium transient.

      Calcium modulation is involved in the regulation of smooth muscle tone [148]. To determine the role of calcium in the inhibition of contraction by ppHSP20, rat aorta was suspended on the Fluoroplex apparatus. Control segments displayed a significantly (n=4, $p < 0.05$, Figure 5.5) lower inhibition of contraction (-2.4 ± 1.8 %) compared with tissue pretreated with 500 µM polyplex (95.7± 1.6 %), but there was no difference in the intracellular calcium concentration observed once the tissue was challenged with phenylephrine (0.1 µM). This indicates that inhibition of contraction through phospho peptidomimetic HSP20 is calcium independent and verifies that the pH-responsive poly(propylacrylic acid) polymer does not inhibit contraction by acting as a calcium chelator. The greater impact for a result like this is that mean arterial blood pressure would not be impacted as greatly if intracellular calcium signaling is unchanged.

Heat Shock Protein's effect on filamentous actin levels
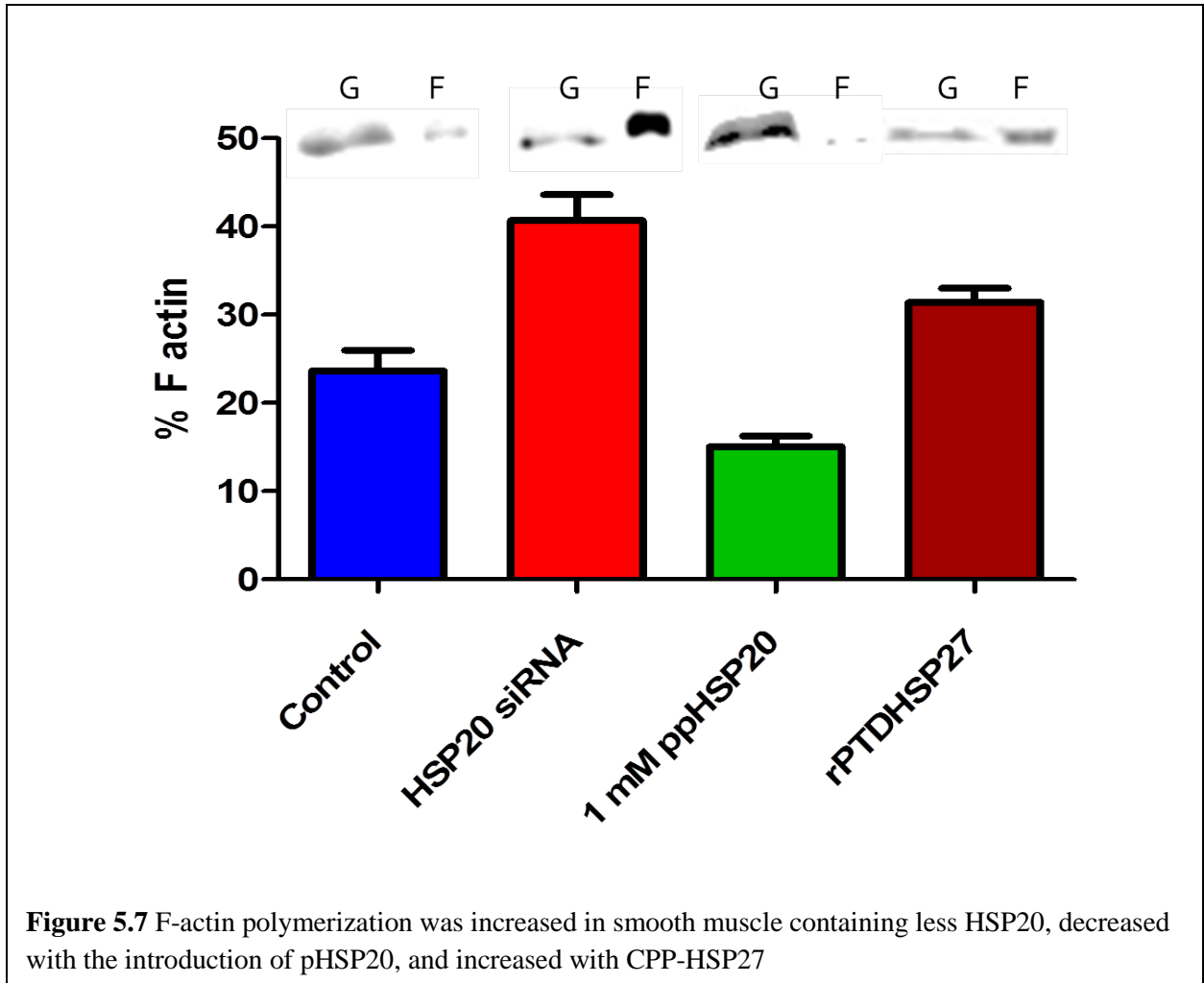
Figure 5.7 F-actin polymerization was increased in smooth muscle containing less HSP20, decreased with the introduction of pHSP20, and increased with CPP-HSP27

Actin polymerization was also analyzed for both the knockdown of HSP20 through siRNA transfection and the treatment of the HSP20 phospho peptidomimetic (1 mM). Knocking down HSP20 in rat aorta significantly increased F-actin polymerization ($p < 0.05$, n=4, Figure 5.6) (41%) compared with control (24%), and treatment with 1 mM peptide significantly reduced the amount of F-actin (17%). Treatment with rPTDHSP27 led to a significant increase in F-actin (31 %) compared to control tissue. The increase in F-actin shown by treatment with siRNA suggests that the more contractile phenotype present may be due to increased actin polymerization, and

peptide treatment shows that phospho peptidomimetic of HSP20 are causing relaxation through actin pathways and not traditional myosin light chain dephosphorylation.

Discussion

During the onset of SAH there is a rise in intracranial pressure and an initial drop in the cerebral perfusion pressure. This rise in intracranial pressure reduces the blood flow to the brain and the initial drop in CPP causes vasoconstriction in the arteries. Established vasospasm is refractory to traditional vasodilators, especially calcium channel inhibitors[17]. It has been shown that nitric oxide donors and broad scale phosphodiesterase inhibitors may block calcium signalling leading to hypotension if administered systemically. In these spastic vessels HSP20 phosphorylation is decreased and HSP27 phosphorylation is increased[149]. The purpose of this study is to develop model systems of biochemical events that occur in SAH, including the decrease in phosphorylation of HSP20 and the increase in phosphorylation of HSP27 in normal vessels to show physiologic changes that also occur in SAH.

This study used physiologic and biochemical approaches to understand the role of the heat shock protein HSP20. HSP20 was manipulated with either the use of a phospho peptidomimetic or through siRNA knockdown of the protein. Although several investigations have suggested the regulation of actin and actin-associated proteins in smooth muscle contraction (reviewed in [59]), very few reports have addressed the role of second messenger regulation of thin filament proteins during inhibition of force. By using rat aorta, a tissue that has a relatively large amount of HSP20 compared to many other tissues, we were able to knockdown the protein effectively. Rat aorta also does not have a relatively large amount of HSP27 so it was possible to upregulate HSP27 to mimic the disease state.

Downregulation of HSP20 has been associated with SAH that in a rat model [71]. This observed downregulation could be related to the constriction of the cerebral vessels. To determine if decreases in HSP20 has a direct effect on vasorelaxation, HSP20 was knocked down in rat aortic tissue and physiologic function was assessed by agonist induced contraction and relaxation to the nitric oxide donor SNP. Knockdown of HSP20 increased the maximal phenylephrine induced contraction and decreased the relaxation to SNP in rat aorta. Additionally the percentage of basal F-actin compared to total actin was significantly increased with the downregulation of HSP20. It has been shown in a rat subarachnoid hemorrhage model when HSP20 is downregulated that relaxation to nitric oxide donors is decreased[71].

SAH also increases the phosphorylation of HSP27 and is believed to be linked to the spastic nature of the cerebral vessels[149]. Human umbilical arteries also exhibit an increased amount of HSP27 compared with normal vessels and also tend to be prone to vasospasm. In this study, upregulation of HSP27 by introducing a transducible recombinant HSP27 protein in rat aortic smooth muscle led to reduced relaxation to SNP. Upregulation of HSP27 also showed an increase in the percentage of F-actin in smooth muscle tissue. HSP27 is known to stabilize the actin cytoskeleton allowing F actin to stay polymerized[138].

Peptide therapy is a new and exciting field that holds promise to have higher specificity resulting in less side effects and a lower dose. Because of the advantages peptides have over traditional drugs, the market for peptide therapy is expected to reach $25 billion by 2018 (PEG SUMMIT). In this study a phospho mimetic peptide and polypropyl acrylic acid electrostatically complexed to a phospho mimetic peptide of HSP20 were used to demonstrate the inhibition of contraction when challenged with phenylephrine in rat aortic smooth muscle tissue. There was a dose dependent inhibition of contraction with the phospho mimetic peptide, and almost a 5 fold

increase in inhibition of contraction when the peptide was combined with polypropyl acrylic acid creating a polyplex. Most importantly ppHSP20 was able to inhibit force generation without inhibiting the intracellular calcium concentration, exhibiting a full uncoupling of force generation from calcium signalling as demonstrated previously[128].

Peptide based biomacromolecular therapeutics have significant potential for use in a variety of clinical applications ranging from cancer treatment to cardiovascular disease. In comparison to small-molecule drugs, peptide based therapies are advantageous in terms of specificity, potency, and biocompatibility. The significance of using a polyplex as a carrier lies in its biocompatibility as a drug delivery platform to enhance intracellular delivery of therapeutic peptides by enhancing cellular uptake.

Conclusions

The ability to modulate tone of arteries without changing calcium signaling would prove to be useful in situations where systemic blood pressure of a patient is normal. Subarachnoid hemorrhages are one instance where only perfusion is lowered in one region resulting in instances where normal blood pressure medication cannot be used. Preventing SAH induced vasospasm would prevent costly and devastating neurologic compromise in young patients. This represents a large unmet need in that there are no current treatment modalities that are proven to be effective at preventing or reversing cerebral vasospasm after SAH.

Summary

SAH often leads to cerebral vasospasm, which in turn can lead to neurologic sequelae and a higher mortality rate for patients. Current treatment for vasospastic arteries involves the use of therapeutics that decrease intracellular calcium and cause smooth muscle relaxation. In the setting of SAH, this course of treatment is not appropriate as it can lead to systemic hypotension and decreased cerebral perfusion.

In Aim 1, a model system was developed in a porcine coronary artery tissue and tested on a Fluoroplex device. Using Fura 2-AM, a calcium binding fluorescent dye, and force transducers, calcium signaling and force were concurrently measured. More importantly, conditions were created where force was inhibited without completely inhibiting intracellular calcium signaling. In this model system, tissue was either contracted with histamine or it was pretreated with forskolin and then subsequently challenged with histamine. However, there was a decrease in the fluorescence between histamine contracted alone and forskolin pretreated tissue.

In Aim 2, the biochemistry of the determined model condition was investigated to better understand inhibition of contraction through cAMP-mediated mechanisms. With force and calcium transients already determined for the model condition, myosin light chain phosphorylation was detected to confirm the intracellular calcium increase seen in the previous aim. To understand thin filament dynamics the phosphorylation of VASP, HSP20, cofilin, actin, and paxillin was detected. Importantly, myosin light chain phosphorylation validated the intracellular calcium results, while actin depolymerization allowed a better understanding of thin filament relaxation.

Once the cAMP/PKA, actin-mediated, pathway of relaxation through actin was understood Aim 3 investigated PKG's inhibition of contraction. Using a nitric oxide donor

(SNP) that activated the PKG pathway and a phosphodiesterase inhibitor papaverine that activated both PKA and PKG pathways, the mechanism behind PKG activation was elucidated. PKG mediated inhibition of contraction did not allow intracellular calcium release or MLC phosphorylation.

Aim 4 used the information gathered in the previous aims about vascular smooth muscle physiology in order to fully uncouple force transduction from intracellular calcium signaling. Knockdown of HSP20 by siRNA was used to mimic a subarachnoid hemorrhage model in rats and demonstrated enhanced agonist-induced contractility to phenylephrine and a decrease in response to nitric oxide donors. To understand the role of HSP27 in smooth muscle relaxation, a PTD-HSP27 was used to reduce the relaxation response to nitric oxide donors. To determine whether an increase in HSP20 phosphorylation would enhance relaxation, a HSP20 phospho peptidomimetic was used to treat rat aorta. The peptidomimetic significantly inhibited force transduction in rat aorta without inhibiting release of intracellular calcium following agonist-induced contraction.

The purpose of this thesis is to better understand thin and thick filaments that govern smooth muscle function in order to develop effective therapeutics for spastic arteries by uncoupling calcium signaling and myosin light chain phosphorylation with force generation. This novel ability to uncouple the two processes suggests that there are indeed calcium-independent mechanisms of relaxation. On the other hand, activation of PKG signaling systems cannot be uncoupled, and generation of force is proportional to intracellular calcium concentrations and the MLC phosphorylation.

At least one of the mechanisms by which calcium independent signaling modulates vasomotor tone is through the small heat shock proteins A HSP20 phospho peptidomimetic or

reduction in HSP27 phosphorylation promotes enhanced relaxation of vascular smooth muscle tissue. This approach is direct and specific for the treatment of SAH-induced vasospasm in that in the setting of experimental SAH-induced vasospasm there are decreases in phosphorylated HSP20 and increases in phosphorylated HSP27 in vasospastic tissue. Hence targeting phosphorylated HSP20 and HSP27 should specifically modulate SAH-induced vasospastic vessels without causing ensuing hypotension. Taken together, this work provides insight into novel mechanisms that regulate smooth muscle tone and may provide therapeutic angles to treat SAH-induced vasospasm.

Appendix

Additional Manuscript 1

Brilliant Blue FCF Dye during vein graft preparation abrogates response to injury and inhibits intimal hyperplasia

Kyle M. Hocking, ME[1]; Michael J. Osgood, MD[2]; *Igor V. Voskresensky, MD[2]; Kevin W. Sexton, MD[2]; Jun Song, BA[2]; Padmini Komalavilas, PhD[3,2]; Colleen Brophy, MD [3,2]; Joyce Cheung-Flynn, PhD[2]

INTRODUCTION

Approximately 1,000,000 aortocoronary and peripheral vascular bypass procedures are performed annually using human saphenous vein (HSV). However, outcomes from these procedures remain limited by high rates of vein graft failure, approximating 39% and 45% at one year in the recent PREVENT III trial of infrainguinal bypass[150] and the PREVENT IV trial of aortocoronary bypass,[151] respectively. The leading cause of vein graft failure is intimal hyperplasia,[152] a process characterized by pathologic narrowing of the lumen, graft stenosis, and ultimately graft failure.[153] Intimal hyperplasia remains a significant limitation of vascular bypass and results in substantial morbidity, reintervention, limb loss, myocardial infarction, and death. Despite significant efforts to prevent intimal hyperplasia, no therapeutics, techniques, or devices, have been demonstrated to prevent this process in humans.

HSV undergoes a series of surgical manipulation during the time of explantation to prepare for implantation into the arterial circulation. Commonly employed intraoperative vein graft preparation techniques are injurious to the conduits. Paired comparison between freshly isolated, unmanipulated vein graft segments to intraoperatively prepared segments demonstrated that current means of vein graft preparation lead to cellular dysfunction, increased oxidative

stress, and promotes enhanced development of intimal hyperplasia of HSV.[20] Variable warm ischemia times in non-buffered non-physiologic storage solutions (e.g. normal saline) reduces physiologic function (unpublished data). Mechanical injury, such as stretching and pressure distention, reduces vein graft contractility and increases neointima formation. [154,155] Moreover, the off-label use of surgical skin markers to prevent twisting and kinking on implantation also injures the conduit, impairing smooth muscle and endothelial function in HSV.[156] Collectively, less injurious means of preparing HSV prior to autologous transplantation may improve outcomes of the procedures.

Brilliant Blue FCF (FCF) is a non-toxic food dye that is structurally related to Brilliant Blue G (BBG) that has been shown to ameliorate stretch induced injury in the spinal cord.[157] The hypothesis of this investigation was that FCF is a nontoxic alternative to mark SVG during harvest and preparation. During the conduct of these studies it was determined that FCF has pharmacologic properties that may be due to purinergic receptor inhibition. In this study, we evaluated the influence of topically-applied FCF on physiologic function and on the development of intimal hyperplasia in vein grafts. These studies suggest that FCF may be not only nontoxic but also a beneficial component of the vein graft preparation.

METHODS

Materials

All chemicals were purchased from Sigma Chemical Co. (St. Louis, MO) unless specified otherwise.

Human saphenous vein (HSV) procurement

HSV were obtained after approval from the Institutional Review Boards of Vanderbilt University Medical Center and the Tennessee Valley Veterans Affairs Medical Center from patients undergoing coronary artery bypass grafting. Method of vein harvest (open or endoscopic) and graft preparation, including hydrostatic distention with a hand-held syringe, dotted or continuous marking with a surgical skin marker, and placement in heparinized Plasmalyte (HP; 10 units heparin/mL Plasmalyte) at room temperature for storage until implantation, was at the discretion of the surgical team. HSV segments were collected just prior to arterial implantation and transported to laboratory for experimentation within 30 minutes of collection.

Animal procedures

Animal procedures followed study protocols approved by the Vanderbilt Institutional Animal Care and Use Committee and adhered to National Institute of Health guidelines for care and use of laboratory animals.

Porcine saphenous vein (PSV) procurement

Immediately after euthanasia, greater saphenous veins (n=6) were procured from adult Yorkshire pigs (Oak Hill Genetics, Ewing, IL) using an open harvest method and stored in heparinized Plasmalyte (HP) at room temperature prior to experimentation. Veins were used for experimentation within 30 minutes of collection.

Rat aorta procurement

Immediately after euthanasia, aortae were gently dissected from adult male Sprague-Dawley rats (n=8). The vessel was stored in HP at room temperature and used for experimentation within 30 minutes of collection.

Mechanical stretch injury of PSV

PSV segments were dissected free of fat and connective tissue and divided into segments. Unmanipulated PSV segments were reserved as control vessels and additional segments were stretched to 200% the resting length as previously described.[155] This amount of stretch is equivalent to the extent of passive stretch that PSV segments would tolerate. PSV segments were then either left untreated or painted with a solution of FCF (2.6 mM) and sectioned into 1-mm rings and incubated in incubated in HP solution for 30 min. Endothelium was denuded in order to assess smooth muscle function.

Measurement of physiologic responses

Rings from PSV segments were suspended in a muscle bath containing a bicarbonate buffer (120 mM sodium chloride, 4.7 mM potassium chloride, 1.0 mM magnesium sulfate, 1.0 mM monosodium phosphate, 10 mM glucose, 1.5 mM calcium chloride, and 25 mM sodium bicarbonate, pH 7.4) equilibrated with 95% O2 / 5% CO_2 at 37ºC, equilibrated for 1 hr at a resting tension of 1g, manually stretched to 3-4 times the resting tension, and maintained at resting tension for an additional 1 hr. This produced the maximal force tension relationship as previously determined (Voskresensky *et al*, JAMA Surgery, In Press). Force measurements were obtained using the Radnoti force transducer (model 159901A) interfaced with a PowerLab data acquisition system and Chart software (AD Instruments). After equilibration, the rings were

contracted with 110 mM potassium chloride (with equimolar replacement of sodium chloride in bicarbonate buffer) to determine smooth muscle functional viability. Tissues produced <0.025 $x10^5$ N/m^2 were considered non-viable and were not used in further studies.[155]

To determine contraction in response to the P2X$_7$R agonist, 2′(3′)-O-(4-Benzoylbenzoyl)adenosine 5′-triphosphate triethylammonium salt (BzATP), rings from HSV segments were suspended in the muscle bath and equilibrated and contracted with 110 mM KCl as described above for PSV. Next, rings were either left untreated or treated with 50 µM FCF for 30 min prior to contraction with 100 µM BzATP. BzATP-induced contraction was expressed as the percentage of maximum KCl-induced contraction.

Immunohistochemistry of HSV

Antigen retrieval of formalin fixed tissue sections were performed using citrate buffer (pH 6) at 95°C for 12 min (HSV). After pre-incubation with 5% goat serum to block non-specific sites, sections were incubated with primary antibodies against P2X$_7$R (Alomone, Israel) overnight at 4ºC. The sections were then incubated with Alexa 568-tagged anti-rabbit antibodies (Invitrogen, CA) for 1hr. Controls were performed by pre-absorbing the primary antibody with the immunogen peptide. Immunostaining was analyzed under a fluorescence microscope.

Measurement of cytosolic calcium ion flux

Rat aorta was dissected free of fat and connective tissue. The aorta was then sectioned into 1-mm rings and suspended in a FluoroPlex Tissue Bath Fluorometry System (IonOptix LLC, Milton, MA and Radnoti Glass Technology Inc., Monrovia, CA), which enables fluorescence ion recording in parallel with force measurement. Rings were loaded with 10 µM Fura-2 AM ester (Invitrogen, Carlsbad, CA) and 0.01% Pluronic F-127 (Invitrogen) in the bicarbonate buffer for 4

hrs at room temperature. The rings were subsequently washed every 10 min with bicarbonate

buffer for 1hr at 37°C. Next, the rings were either left untreated or treated with FCF (50 µM), or

P2X$_7$R antagonists periodate oxidized sodium salt (oATP; 50 µM), KN-62 (10 µM), or brilliant

blue-G (BBG, 50 µM) for 30 min prior to contraction with BzATP (100 µM). Force and calcium

fluorescence were measured continuously for 15 min after the addition of BzATP.

Fluorescence was simultaneously measured at 380 and 340 nanometer (nm) wavelengths.

The ratio of the emission of the two wavelengths was used to determine changes in intracellular

calcium concentrations ($[Ca^{2+}]_i$) as previously described. [158]

Measurement of vascular smooth muscle cell migration

Migration of rat aortic smooth muscle cell (A7r5; American Type Culture Collection,

Manassas, VA) was determined by using a scratch assay. Cells were cultured in 6-well dishes,

allowed to grow to 80% confluence in DMEM medium supplemented with 10% fetal bovine

serum and serum starved for 24 hrs. A sterile pipet tip was used to scrape a straight line down

the well and cells were then either left untreated or pretreated with FCF (50 µM) for 2 hrs in the

serum-deprived medium. Cells were then treated with platelet-derived growth factor (PDGF,

20ng/mL; Life Technologies, Grand Island, NY) in serum-free medium for 48 hrs. Three

pictures taken per well at 0, 24, and 48 hrs on a Zeiss Axiovert 200M epifluorescence

microscope at a magnification of 40x and the number of cells that invaded the scratch was

determined.

Measurement of vascular smooth muscle cell proliferation

A7r5 cells were cultured in 96-well plates and allowed to grow to 60% confluence. After

a 24-hr serum starvation, cells were then either left untreated or pretreated with FCF for 1 hour

prior to PDGF treatment (10 ng/ml) for 24 hrs. Each treatment was performed in at least 6 wells. Proliferation was measured by the MTT assay.

HSV organ culture

Rings (1-2 mm in width) were cut from HSV segments. Two rings were placed in 10% neutral buffered formalin to measure basal (pre-culture) intimal thickness. Additional rings were either left untreated or treated with FCF (50 µM) in organ culture medium (RPMI 1640 medium supplemented with 30% FBS, 1% L-glutamine and 1% penicillin/streptomycin) for 2 hrs. The rings were maintained in organ culture medium in the absence of FCF for 14 days at 37˚C in an atmosphere of 5% CO_2 in air. After 14 days, rings were fixed in 10% formalin, paraffin-embedded, sectioned and stained using Verhoeff-Van Gieson (VVG) to allow the visualization of the internal elastic lamina. Measurements of intimal and medial thickness were made on transverse sections of each vessel using a Zeiss Axiovert 200M microscope (Carl Zeiss) with a computerized image analysis system (Zeiss software and Adobe Photoshop) as described previously.[154]

In vivo rabbit carotid interposition model

Vein bypass grafts were constructed and interposed into the common carotid arteries with an anastomotic cuff technique as previously described.[159] Briefly, external jugular veins (EVJ) were harvested (3.0-4.0 cm in length) from male New Zealand White rabbits (3.0–3.5 kg) for creation of a reversed interposition graft into the common carotid artery. EVJ ends were passed through polymer cuffs (Terumo Medical, Elkton, MD), everted, and fixed with 6-0 silk. An IV heparin bolus (250 U/kg) was administered immediately prior to carotid cross clamp and arteriotomy. Vein graft was inserted and secured with 3-0 silk around the cuff. After 28 days, vein grafts were systemically perfusion fixed *in situ* with 10% neutral buffered formalin, excised,

divided into four segments, paraffin-embedded, sectioned and stained using the VVG stain for morphometric analysis as described above.

Statistical analysis

Contractile responses were defined by stress, calculated using force generated by tissues as follows: Stress ($\times 10^5$ N/m^2) = Force (g) x 0.0987 / area, where area = wet weight (mg)/ at maximal length (mm)]/1.055. Data were reported as mean responses ± standard error of the mean. Paired t-tests were conducted to determine the significance (*p* value) of each experiment. A *p* value <0.05 was considered statistically significant.

Results

FCF restored functional responses in PSV impaired by mechanical stretch injury

A model of stretch injury of PSV was used to determine if the effect of stretch and FCF on smooth muscle contractile responses. Compared with control PSV segments, PSV subjected to stretch injury generated significantly less contractile force in response to depolarizing KCl stimulus (0.61±0.048 x10^{5}N/m^2 vs 0.48±0.049 x10^{5}N/m^2, p=0.0085, Figure 1). Pre-treatment with a topical application of FCF had no effect on smooth muscle physiologic responses in PSV not subjected to stretch injury, (0.66±0.082 x10^{5}N/m^2, p=0.59, Figure 1) suggesting that FCF was not toxic to the smooth muscle. Pre-treatment with a topical application of FCF restored the contractile response of stretch-injured PSV (0.71±0.111x10^{5}N/m^2 vs 0.48±0.049x10^{5}N/m^2, *p*=0.0342; Figure 1).

FCF blocked P2X$_7$ purinergic receptor-induced contraction and cytosolic Ca^{2+} fluxes

Since spinal cord stretch injury has been shown to be ameliorated by treatment with an analogue of FCF and the mechanism is thought to be via P2X$_7$R antagonism,[157] we used theP2X$_7$R agonist BzATP to elicit a contraction in HSV.[23] Preincubation with FCF significantly

reduced contraction to BzATP when compared to the control rings (11.9 ± 1.4% vs 7.7 ± 0.6% of maximum KCl-induced contraction, Figure 2A and B) suggesting that FCF inhibits $P2X_7R$ activation. Expression of $P2X_7R$ in HSV was confirmed by immunohistochemistry (Figure 2C and D).

$P2X_7R$ activation leads to increases in intracellular calcium concentrations $[Ca^{2+}]_i$,[160] we used a FluoroPlex apparatus to measure force generation and $[Ca^{2+}]_i$ concurrently. Rat aortic rings were used as a model system because of the availability of tissue, the thin nature of the arterial wall allowing penetration of the fluorochrome and the reproducibility of the results. Similar to HSV, pretreatment with FCF blocked BzATP-induced contraction in rat aorta (0.019 ±0.014 10^5 N/m^2 vs 0.005±0.002 10^5N/m^2; Figure 3A). Additionally, FCF blocked BzATP-induced calcium ion flux (0.139 ±0.008 A.U. vs 0.050±0.012 A.U.; Figure 3B). FCF inhibition of BzATP-induced contraction and Ca^{2+} fluxes was comparable to those mediated by known $P2X_7R$ antagonists oATP, KN-62 and BBG (Figure 3A and B), implicating that FCF is an antagonist of the $P2X_7R$ in vascular tissues.

FCF inhibited rat vascular smooth muscle cell migration and proliferation

Migration and proliferation are hallmark cellular events associated with intimal hyperplasia. To determine the mechanism of action of FCF, the effects of FCF on A7r5 cell migration and proliferation were examined. In a scratch assay, FCF significantly reduced PDGF-induced migration by 36±11% and 28±8% at 25 µM and 50µM, respectively, compared to untreated cells (Figure 4A; $p<0.05$). FCF pretreatment also significantly reduced PDGF-induced proliferation of A7r5 cells in a dose-dependent fashion by 35±21% and 28±14% at 50µM and 100µM, respectively, as measured using MTT assay (Figure 4B; $p<0.05$).

FCF reduced intimal thickening in cultured HSV

Since injury leads to the development of intimal hyperplasia, the effect of a single pre-treatment with FCF on the development of intimal hyperplasia was determined in an organ culture model of HSV. HSV were pretreated with FCF (50 µM, 2hr) prior to organ culture or placed in organ culture after HP (control) treatment.   After 14 days of organ culture, intimal thickening was significantly reduced in segments of FCF-pretreated HSV with compared to untreated tissues (15.8 ± 13.6 % vs 67.1 ± 24.6 %; Figure 5), suggesting that treatment with FCF at the time of vein graft explantation may have an inhibitory effect on neointimal thickening *ex vivo*.

FCF reduced development of intimal hyperplasia in a rabbit carotid interposition model

Because pretreatment with FCF reduced intimal thickness in organ culture of HSV (Figure 5), we hypothesized that treating vein grafts with FCF at the time of explantation would reduce intimal hyperplasia *in vivo*. Bilateral EJV carotid interposition grafts were constructed in a rabbit model (Figure 6). Grafts stored in FCF (50 µM)-containing HP during a 30 min explantation period developed significantly reduced intimal thickening compared with control grafts (56.66±7.05 µm vs. 119.2±30.25 µm; n=13; Figure 6B). There was no significant difference in the medial thickness between the two groups (96.6±26.4 µm vs. 131.4±60.9 µm). The intimal-to-medial ratio was significantly lower in grafts placed in FCF compared with control grafts (0.54±0.08 vs 0.79±0.14; Fig. 6C).

DISCUSSION

Intimal hyperplasia is the leading cause of vein graft failure. While the specific inciting events remain uncertain, there is general agreement that this process is a 'response to injury' initiated by vein graft harvest, surgical preparation, implantation, reperfusion, and

exposure to arterial hemodynamics.[161,162] Surgical dissection of the vein graft from the surrounding adipose tissue and ligation of the side branches invariably causes disruption of the vasa vasorum and may cause significant mechanical stretch injury. Intraoperative preparation of the vein graft, also injure the conduit. [20] After completion of the anastomoses the vein graft is subject to ischemia-reperfusion injury caused by reperfusion with arterial blood which simultaneously exposes the graft to pulsatile arterial hemodynamics with inherent differences in shear, flow, and turbulence, particularly in the perianastomotic regions of the graft.[163] Collectively, common intraoperative preparation routines are deleterious to vein grafts and optimization of these techniques may reduce intimal hyperplasia

FCF improves endothelial and smooth muscle functional responses in HSV suggesting that FCF has pharmacologic properties (Voskresensky *et al*, JAMA Surgery, In Press). In this study, FCF pretreatment restored functional viability after stretch injury in PSV (Figure 1). Additionally, FCF inhibits the selective $P2X_7R$ agonist BzATP- induced smooth muscle force generation (Figure 2A and 3A) and calcium ion flux to levels comparable to other known antagonists of the receptor, oATP, KN-62, and BBG (Figure 3B), implying that FCF is an antagonist of the $P2X_7R$ in HSV. While injury leading to release of ATP activates the $P2X_7R$, the increases in intracellular calcium resulting from activation of the $P2X_7R$ may result in further ATP release thus propagating the injury response.[160]

In this investigation, we demonstrated that FCF pretreatment prevents both PDGF-induced migration and proliferation of A7r5 cells (Figures 5A and B). This is not surprising as $P2X_7R$ activation by ATP or other cellular damage enhances migration and proliferation, which is inhibited by $P2X_7R$ antagonism in other cell types.[164,165] These data suggest that the inhibition

of smooth muscle cell migration and proliferation may in part account for the mitigation of intimal hyperplasia by FCF. FCF blocked $P2X_7R$-induced contraction and cytosolic Ca^{2+} fluxes.

A single short-term FCF pretreatment, analogous to the *ex vivo* treatment conditions in the operating room, inhibits intimal hyperplasia of vein grafts (Figures 5 and 6). The observation that FCF treatment during explantation prevents neointimal thickening suggests that there is a therapeutic window of opportunity at the time of explant. Moreover, vein graft treatment during explantation maximizes exposure of the therapeutic to the conduit and limits systemic exposure.

Chamberlain *et. al* showed that $P2X_7R$-deficient mice developed intimal hyperplasia similar to wild-type animals in a carotid ligation model.[166] In contrast, our results indicated that therapeutic targeting of the $P2X_7R$ impedes the development of intimal hyperplasia. It is conceivable that overexpression of other purinergic receptors, such as $P2X_1$, may compensate for the absence of $P2X_7R$ and their activation may cause other deleterious events that promote intimal thickening in the $P2X_7R$-deficient mice. Alternatively, FCF treatment may lead to a partial blockade of $P2X_7R$ while allowing a subset of $P2X_7R$ function that normally exert preventive effects on intimal thickening. FCF treatment may also activate pannexin 1 functions (*Voskrensensky et al*, JAMA Surgery, In Press), a hemichannel that is part of the P2X7R death complex, [167] in HSV that may otherwise contribute to neointima formation such as platelet activation.[168]

We have previously demonstrated that vein graft injury is a sufficient stimulus for the development of intimal hyperplasia in HSV *ex vivo,* suggesting a role of early injury in the cellular processes that contribute to the development of intimal hyperplasia.[20] The findings of the current study offer evidence that effects of harvest induced injury can be ameliorated by treatment with FCF. The mechanism for the pharmacologic properties of FCF may be due to

inhibition of the P2X$_7$ purinergic receptor (Figure 7). These data also suggest that pharmacologic intervention at the time of explantation is a clinically relevant approach to preventing intimal hyperplasia and vein graft failure.

POTENTIAL LIMITATIONS

While our stretch injury model of PSV recapitulated the potential injury incur to the vein grafts, these tissues came from healthy animals. The model system used for these experiments has the advantage of more homogeneity and greater reproducibility compared to HSV. The rabbit interposition graft model did not include distension which is a technique commonly performed to HSV. Moreover, the mechanistic links between P2X$_7$R blockade and restoration of smooth muscle injury or reduction in intimal thickening requires further evaluation. Aside from changes in Ca^{2+} flux, it remains to be determined whether treatment with FCF affects downstream events elicited by P2X$_7$R activation that have been characterized in other cell types.

CONCLUSIONS

We have demonstrated that transient P2X$_7$R blockade during vein graft preparation inhibits the injury response in vascular tissues, prevents smooth muscle migration and proliferation, and inhibits intimal hyperplasia *in vitro* and *in vivo*. To our knowledge, this is the first report of the role of P2X$_7$R in early vein graft injury. Further work is needed to better characterize the mechanism of action of FCF and to elucidate the potential role of this agent in vein graft preparation in human subjects. Treatment with FCF represents a nontoxic and possibly therapeutic clinical alternative to marking with surgical skin markers during preparation of vein graft conduits.

CLINICAL RELEVANCE

Saphenous veins remain the most commonly used conduits for bypass procedures. Current surgical harvest and vein graft preparation induces injury to the conduits and promotes development of intimal hyperplasia, arguing for less injurious means to preserve vein graft function during explanation period. FCF presents a potential therapeutic to be included as part of the vein graft preparation.

Figure A.1. FCF restores functional viability after stretch injury in porcine saphenous

vein. Pig saphenous veins were left untreated (non-stretch; n=6), stretched to twice their resting

length (stretched; n=6). A solution of FCF (2.6 mM, in 5% propylene glycol and water) or

vehicle was then applied with a cotton swab in a longitudinal line to the untreated or the

stretched vein segments (FCF). The segments were incubated at room temperature for 15 min in

Plasmalyte and then cut into rings, suspended in a muscle bath and treated with KCl (110 mM).

Force generated was converted to stress. Results are presented as mean±SEM. *$p < 0.05$
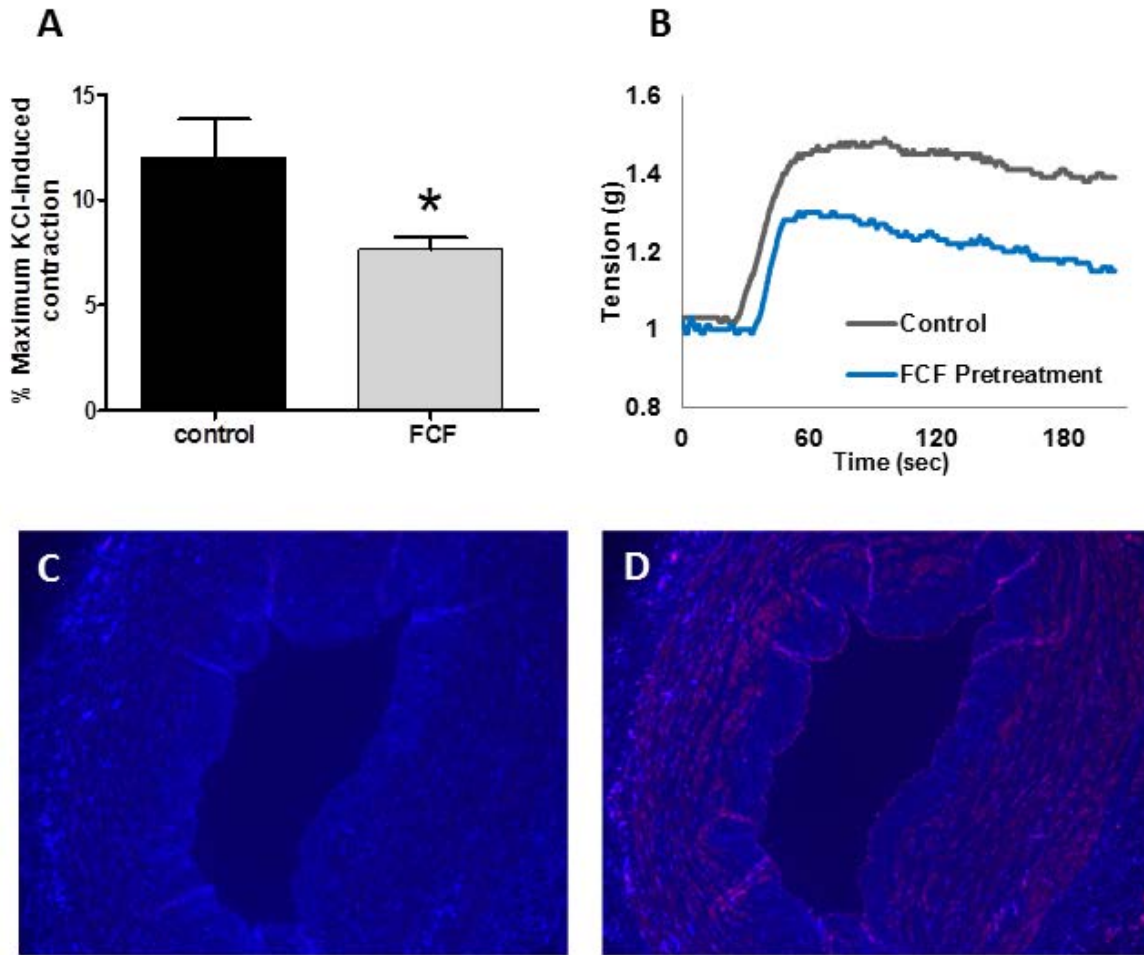
Figure A.2. FCF inhibits $P2X_7R$-mediated contraction in human saphenous vein. A. Rings of HSV (n=4) were suspended in the muscle bath, either left untreated (control) or treated with 50μM FCF for 30min prior to contraction with BzATP. B. Representative muscle bath force tracings of BzATP-induced contraction in HSV. Results are presented as mean±SEM. *p=0.04. Expression of P2X7R in HSV as detected by immunohistochemistry using pre-absorbed (C) or normal P2X7R-specific antibody (D). $P2X_7R$ were stained red.

Figure A.3. FCF inhibits P2X$_7$R-mediated cytosolic Ca^{2+} fluxes in rat aorta. Rat aortic rings (n=3-8) were suspended in the FluoroPlex muscle bath, either left untreated (control) or treated with FCF or other P2X$_7$R antagonists oATP, KN62 or BBG prior to contraction with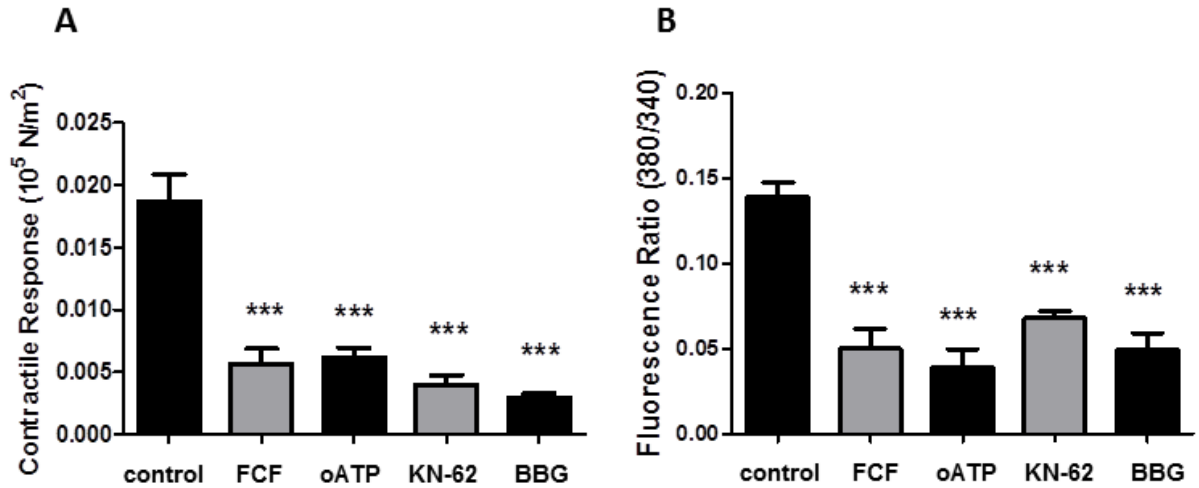 BzATP. Concurrent force generation (A) and cytosolic Ca^{2+} flux (B) were measured. Results are presented as mean±SEM. ***$p<0.0001$.
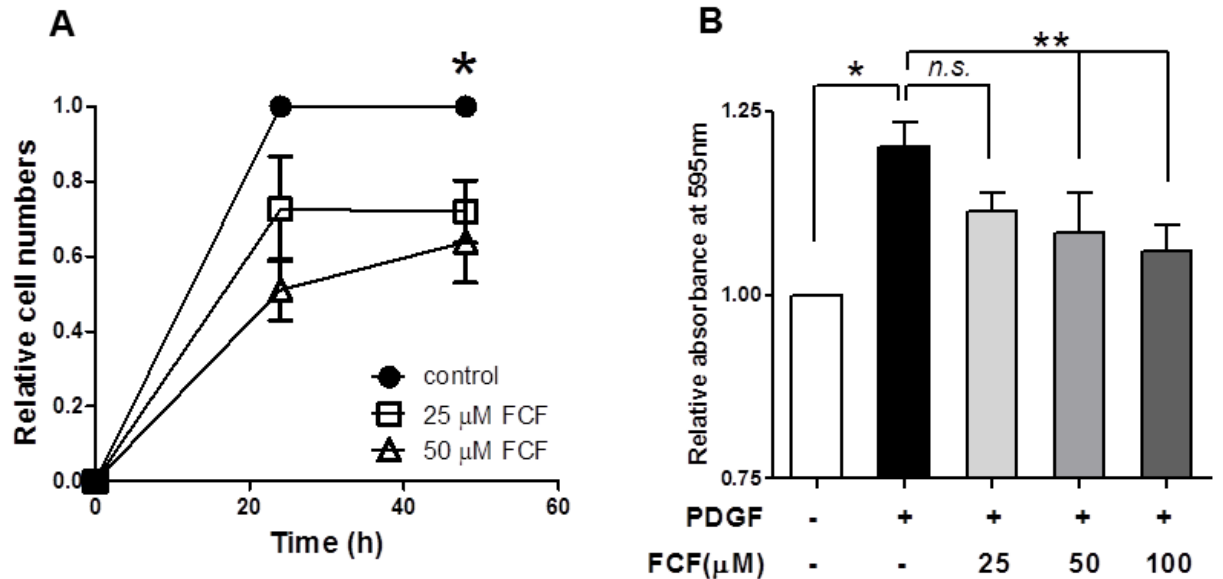
Figure A.4. FCF inhibit PDGF-mediated migration and proliferation in vascular smooth muscle cells. A7r5 cells pretreated without (control) or with different concentration of FCF prior to stimulation with PDGF. A. Migration of A7r5 cells were measured in a scratch assay in 6-well plates. Cell invading the scratch were counted after 24 and 48hours. Results are reported as relative increase in cell number compared to the control wells as mean±SEM. *p<0.05, n≥4. B. Proliferation of A7r5 cells were measured using MTT assay in 96-well plates. Each treatment was performed in at least 6 wells and averaged for each assay. Results are reported as mean±SEM. *p<0.05, **p<0.005, *n.s.*, statistically nonsignifcant, n=6.
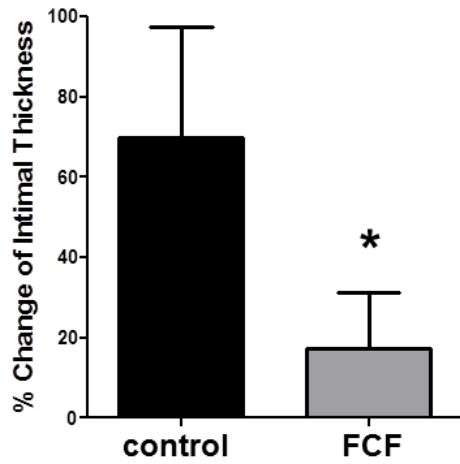
Figure A.5. FCF pretreatment reduced intimal thickness of HSV in organ culture. HSV

rings (n=8) were left untreated (control) or pretreated with FCF (50μM) for 2hr prior to culture

in RPMI medium supplemented with 30% FBS for 14 days. Veins were stained using Verhoff

Van Gieson stain and intimal layer thickening was measured. Results are presented as

mean±SEM. *p=0.016
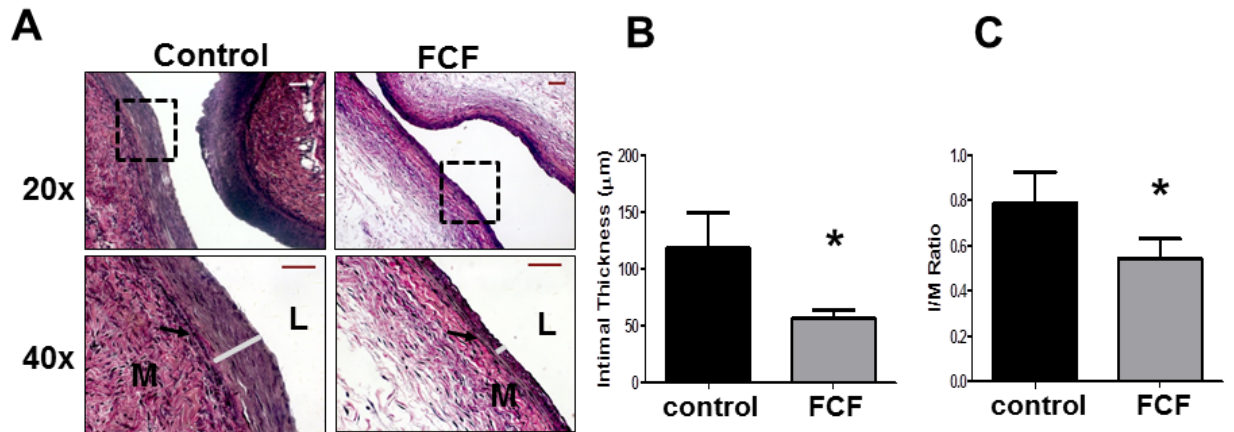
Figure A.6. FCF treatment during graft explantation reduced intimal hyperplasia in the rabbit carotid interposition graft model. The external jugular veins from rabbits (n=13) were either stored in heparinzed PlasmaLyte without (control) or supplemented with 50µM FCF (FCF) during a 30-min explantation period prior to implantation into the carotid artery. Grafts were harvested after 28 days and stained to visualized the elastic lamina. Intimal and medial thickness were measured. A, Representative Verhoff Van Gieson stained grafts in control or FCF treated animals. Boxed areas in the 20x magnification indicated areas in the 40x images. Scale bar = 50 µm. Intimal thickness are indicated by bars (gray). L= lumen, M=medial, arrows indicate internal elastic laminar. B, Intimal thickness and C, intimal-to-medial thickness ratio were determined. Results are presented as mean±SEM. *$p < 0.05$.
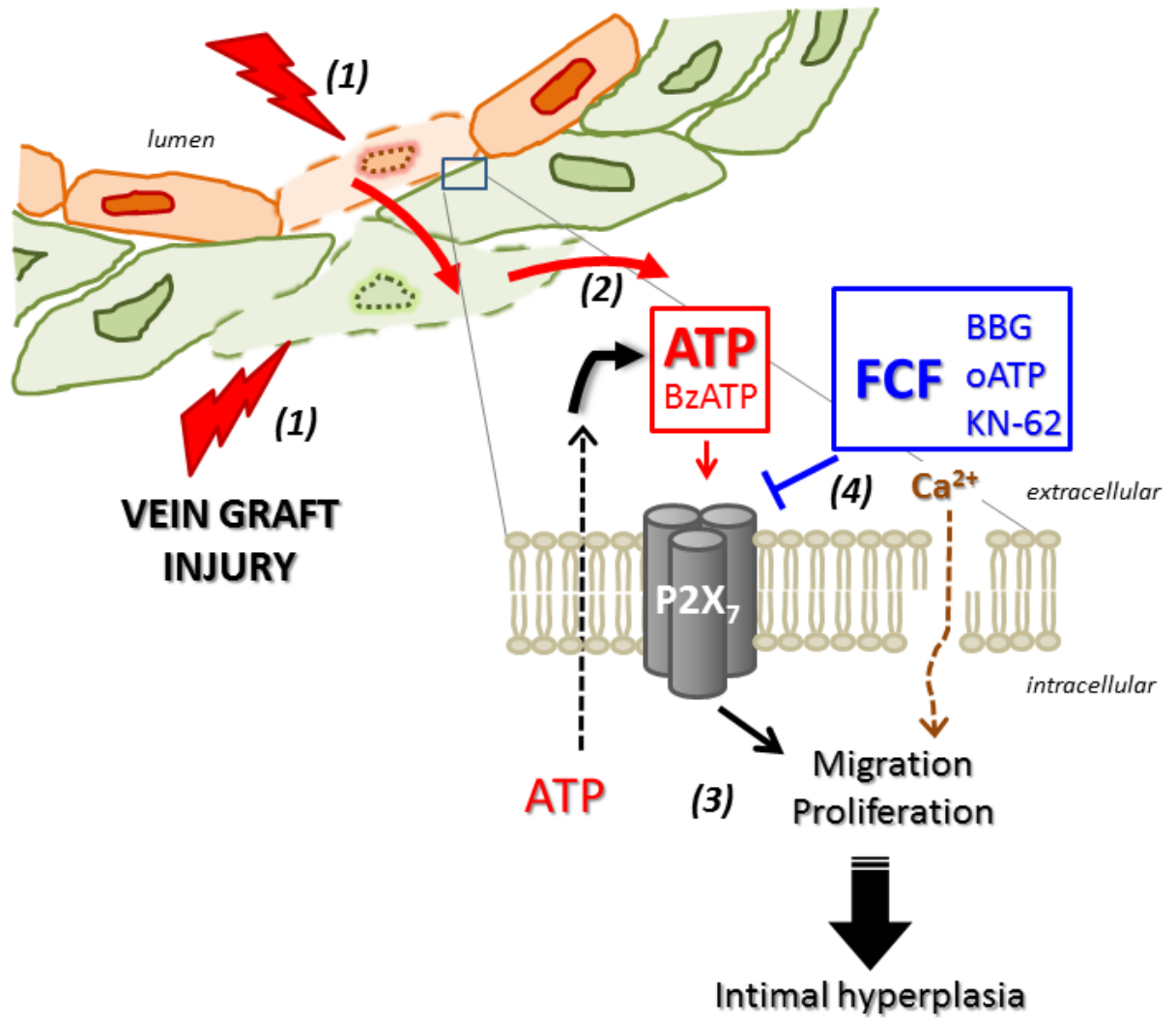
Figure A.7. Model of $P2X_7R$ activation during vein graft preparation injury. Surgical harvest and preparation induced vein graft injury (1) leading to release of ATP (2). ATP activates the $P2X_7$ receptor on neighboring cells, propagating the response to injury (3). FCF may mitigate the effect of $P2X_7R$ activation (4) by inhibiting membrane pore formation, $[Ca^{2+}]_I$ flux, and additional release of extracellular ATP. (Agonists, red; inhibitors, blue)

Additional Manuscript 2

Surgical vein graft preparation promotes cellular dysfunction, oxidative stress, and intimal hyperplasia in human saphenous vein

Michael J. Osgood, MD[2]; Kyle M. Hocking, ME[1]; Igor V. Voskresensky, MD[2]; FanDong Li; Padmini Komalavilas, PhD[3,2]; Joyce Cheung-Flynn, PhD[2]; Colleen Brophy, MD [3,2]

INTRODUCTION

Approximately 1,000,000 aortocoronary and peripheral vascular reconstructions are performed annually using human saphenous vein (HSV). The leading cause of vein graft failure is intimal hyperplasia (IH).[169] This process leads to pathologic narrowing of the vessel lumen, graft stenosis, and ultimately graft failure.[170] IH remains the primary factor limiting the durability of vein bypass grafts and contributes to significant morbidity, reintervention, limb loss, myocardial infarction, and death. While technical errors, poor outflow, thrombosis, and vasospasm are the principle etiologies of vein graft failure in the immediate postoperative period (<30 days), IH and atherosclerosis are the leading causes of vein graft failure in the short-term (30 days-2 years) and long-term (>2 years) time frames, respectively.[163] Two recent large phase III multicenter, randomized, double-blinded, placebo-controlled clinical trials have examined outcomes in coronary artery bypass grafting (CABG) and peripheral vascular bypass grafting (PVBG). The Project of Ex-vivo Vein Graft Engineering via Transfection (PREVENT) III trial demonstrated a 61% primary patency rate at one year following PVBG.[171] The per patient vein graft failure rate after CABG was 45% in the PREVENT IV trial at 12 to 18 months.[172] These trials set a modern standard for benchmark outcomes from these procedures.

Successive and additive levels of vein graft injury occur during vein conduit harvest and preparation. These include mechanical stretch,[125] conduit distension using a hand-held syringe

for identification of leaks and side branches,[173] marking of the conduit using surgical skin

markers for purposes of orientation,[174] and vein conduit storage in acidic solutions.[175] The

surgical literature has focused primarily on the histologic and morphologic changes occurring to

the vein graft following surgical harvest and preparation, including disruption of the vasa

vasorum,[176] surgical trauma to the endothelium,[177] and tunica media.[153] However, the degree to

which these morphologic changes impact the cellular viability and physiology of the HSV graft

has not been well investigated. Moreover, the standard process of vein graft preparation

including distension, marking, and warm ischemia in solution has never been validated or

demonstrated to adequately preserve tissue viability.

Oxidative stress is a well-known mechanism mediating vascular injury in multiple

cardiovascular diseases.[178] The production of reactive oxygen species becomes magnified and

dysregulated in pathophysiologic states and serves as a secondary mediator of injury. Oxidative

stress has been postulated to contribute to vein graft dysfunction,[179] but evidence of this is

lacking in human tissue. Therefore, we investigated the influence of surgical vein graft

preparation on cellular viability and HSV physiology, the role of surgical vein graft preparation

in the development of IH *in vitro*, and the role of oxidative stress as a mechanistic contributor to

vein graft dysfunction in human saphenous vein.

METHODS

HSV procurement

HSV samples were obtained after approval from the Institutional Review Boards of

Vanderbilt University Medical Center and the Tennessee Valley Veterans Affairs Medical

Center, Nashville, TN. HSV segments were collected after obtaining informed consent from patients undergoing CABG. Method of vein harvest (open or endoscopic) and graft preparation was at the discretion of the surgical team. Vein segments were collected immediately following surgical harvest ("unmanipulated" vein samples, UM) and were used immediately following collection for experiments described below. Additional vein segments were collected again later after a series of manipulations, including hydrostatic distention with a hand-held syringe, dotted or continuous marking with a surgical skin marker, and placement in heparinized plasmalyte (HP, 10 units heparin/mL plasmalyte) at room temperature for storage until implantation ("after manipulation" vein samples, AM, see Figure 1), and were used immediately prior to implantation for the experiments described below. Veins were used for experimentation within 15 minutes of collection. When open harvest was employed, the vein was divided distally, cannulated, and crystalloid was intermittently infused to aid in side branch ligation. For all HSV used in this study, we obtained paired UM/AM samples, except where specified. All HSV used for the experiments described below was stored in HP at room temperature until experimentation. All AM-HSV segments procured for this study were small pieces removed from either end of the conduits used for revascularization and were collected at the time of arterial implantation. Areas of HSV subjected to clamp or crush injury were discarded. Therefore, all segments of AM-HSV we obtained were intended for use as part of bypass conduits and were obtained at the time of arterial implantation. The particular anatomic portion of HSV which was procured (i.e. proximal versus distal) was, again, at the discretion of the surgical team and was not recorded for this study.

Collection of clinical demographic variables

Along with prospective collection of HSV tissue, demographic variables of the source patients were prospectively collected, including age, gender, race, body mass index (BMI), medical comorbidities, preoperative laboratory values, preoperative medication regimen, and method of HSV harvest.

Physiological measurement of HSV smooth muscle functional viability

HSV samples were sectioned into 1-mm rings. These were weighed and their diameter was measured. HSV rings were suspended in a muscle bath containing a bicarbonate buffer as previously described.[180] Smooth muscle viability was determined by contracting HSV with potassium chloride (KCl), which causes membrane depolarization and contraction of functionally viable smooth muscle.[181] Rings were then washed to remove KCl and equilibrated in bicarbonate buffer for 30 minutes.[125] The concentration of the physiologic agonist phenylephrine (PE) that induces submaximal contractile responses was determined by treating the tissue with increasing doses (0.01, 0.1, and 1 μM) of PE. Contractile response was defined as stress ([10^5 Newtons (N)/m^2] = force (g) x 0.0987 / area, where area is equal to the wet weight [(mg) / length (mm at maximal length)] divided by 1.055),[126] which was calculated using the force (g) generated by the tissue. We have previously demonstrated that the production of force of less than 0.025×10^5 N/m^2 in response to KCl correlates with diminished cellular viability as measured by the 3-(4,5-Dimethylthiazol-2-yl)-2,5-diphenyltetrazolium bromide (MTT) live/dead assay.[125]

Physiological measurement of HSV smooth muscle-dependent vasorelaxation

HSV was prepared as described above except that the endothelium was gently mechanically denuded. Viable HSV was pre-contracted with PE and treated with escalating

doses of sodium nitroprusside (SNP) necessary to achieve measurable vasorelaxation (10^{-8} to 10^{-6} M).

Physiological measurement of HSV endothelial-dependent vasorelaxation

HSV was prepared and tested as described above except that the endothelium was preserved. Viable HSV was pre-contracted with PE and then exposed to carbachol (CCH, 5×10^{-7} M), an acetylcholine analog, and the maximal relaxation response was determined.[182]

HSV immunohistochemical staining for CD31 and eNOS

HSV segments were fixed in 10% formalin and sent to the Vanderbilt Translational Pathology Shared Resource for processing. Tissues were dehydrated with ethanol, embedded in paraffin, and immunostained using a Leica Bond Max IHC stainer. Heat induced antigen retrieval was performed using their Epitope Retrieval 2 solution for 20 minutes. Slides were incubated with CD31 (NCL-CD31-1A10, Leica Microsystems, Buffalo Grove, IL) at 1:100 dilution or eNOS (ab91205, Abcam, Inc., Cambridge, MA) at 1:600 dilution for one hour. The Bond Polymer Refine detection system was used for visualization. Slides were then dehydrated, cleared and coverslipped. The degree of endothelial staining for eNOS and CD31 was assessed using an Axiovert (Zeiss) at 20x-100x magnification. The intensity of staining was assessed by a blinded observer using a qualitative score from (1+) to (4+) based on the proportion of vein circumference with visible staining: (1+), <25% vein circumference; (2+), 25-49%; (3+), 50-74%; and (4+), 75-100%.

HSV physiologic measurements as a function of storage time

In order to investigate whether storage time had any influence on the physiology of UM versus AM-HSV, we measured physiology as a function of storage time. UM-HSV was procured as described above, sectioned into rings, and placed in HP at room temperature for 30 minutes, 1 hour, 2 hours, and 3 hours. At the end of incubation, HSV rings were suspended in a muscle bath in duplicate for measurement of contractile force, smooth muscle-dependent relaxation, and endothelial-dependent relaxation.

HSV organ culture

Additional UM-HSV and AM-HSV rings (3 mm in length) were cut, placed in eight-well chamber slides in duplicate, and maintained in RPMI 1640 medium with 30% FBS, 1% L-glutamine, and 1% penicillin/streptomycin for 14 days at 37°C/5% CO_2 as previously described.[183] After 14 days, tissue was fixed in formalin, imbedded in paraffin, and histologic sections were prepared and stained with Verhoeff-Van Gieson (VVG). Four-quadrant measurements were made of intimal and medial thickness of pre-culture and post-culture rings by a blinded observer and intimal-to-medial ratio was calculated.

Measurement of reactive oxygen species in HSV

UM-HSV and AM-HSV were divided into 1-mm rings and immediately processed by the Vanderbilt Free Radical in Medicine Core for measurement of reactive oxygen species. Tissues were incubated for 30 minutes at 37°C in 1 mL of Krebs/HEPES buffer containing 50 µmol/L of dihydroethidium (DHE). Superoxide ($O_2^{\cdot-}$) was measured using DHE and a high-performance liquid chromatography (HPLC)-based assay.[184] The reaction of DHE with $O_2^{\cdot-}$ generates 2-

hydroxyethidium. The 2-hydroxyethidium peak on HPLC reflects the amount of $O_2^{\cdot-}$ formed in the tissue during the incubation and is expressed per milligram of protein.

Experimental induction of oxidative stress in HSV

UM-HSV was cut into 1-mm rings and placed in HP containing hydrogen peroxide (H_2O_2) concentrations of 100 µM, 1 mM, and 10 mM for one hour at room temperature. HSV physiological measurements were then performed in the muscle bath as described above.

Data analysis

Data is reported as mean ± standard error of the mean unless indicated otherwise. Paired two-tailed t-tests were conducted to assess the statistical significance of each experiment using GraphPad Prism software (LaJolla, CA). P value of ≤0.05 was considered statistically significant. Statistical significance was indicated on figures with the following annotations: (*), $p<0.05$; (**), $p<0.01$; (***), $p<0.001$.

RESULTS

HSV collection and patient demographic variables

The demographic variables for the patients included in this analysis are listed in Table 1. The demographics are typical for patients undergoing coronary revascularization. Unless stated otherwise, all experiments were performed with paired UM/AM samples from the same patients. Over half of the paired UM/AM-HSV samples were harvested endoscopically, and the remainder of the paired UM/AM-HSV samples were harvested utilizing conventional open harvest

126

technique. Open versus endoscopic vein graft harvest did not produce any significant differences in the physiologic parameters we examined (data not shown). Angioscopy or valvulotomy were not utilized on any of the HSV collected for this study. Papaverine was not used during vein graft preparation.

HSV smooth muscle functional viability

UM-HSV generated significantly greater contractile force (0.13 ± 0.009x10^5 N/m^2) compared with AM-HSV (0.05 ± 0.006x10^5, n=47, p<.0001, Figure 2A). All UM-HSV generated force of 0.025x10^5 N/m^2 or greater, and therefore, all UM-HSV was functionally viable by our pre-established criteria.[125] Of AM-HSV, 35 of 47 samples (74%) were viable. UM-HSV generated significantly greater contractile force in response to PE (0.08 ± 0.008x10^5 N/m^2) compared with AM-HSV (0.04 ± 0.005x10^5, n=41, p<.0001, Figure 2B). These data suggest that surgical vein graft preparation causes injury which compromises smooth muscle viability.

HSV smooth muscle-dependent vasorelaxation

UM-HSV generated significantly greater smooth muscle-dependent relaxation ($62\pm4\%$) compared with AM-HSV ($31\pm4\%$, n=34, p<.0001, Figure 2C). These data further suggest that surgical vein graft preparation causes injury which compromises smooth muscle viability.

HSV endothelial-dependent vasorelaxation

UM-HSV generated significantly greater endothelial-dependent relaxation ($21\pm3\%$) compared with AM-HSV ($1\pm2\%$, n=36, p<.0001, Figure 2D). These data suggest that

surgical vein graft preparation causes injury which compromises endothelial viability. Given that that endothelium is the most fragile tissue component in HSV, these findings are not unexpected, and argue for less injurious means of surgical vein graft preparation in order to preserve this fragile monolayer.

Immunohistochemical staining for eNOS and CD31

We observed 3+ or 4+ CD31 staining in UM-HSV (Table 2). Surgical vein graft preparation was associated with diminished CD31 staining in 8 of 11 samples of AM-HSV; endothelial coverage remained unchanged in the remaining 3 of 11 samples after surgical vein graft preparation. We observed more variability in UM-HSV eNOS staining. Among UM-HSV samples, 9 of 11 had 3+ or 4+ eNOS staining, and 2 of 11 had 1+ or 2+ eNOS staining. Surgical vein graft preparation was associated with diminished eNOS staining in 9 of 11 samples and this was more pronounced than loss of CD31 staining: 2 of 11 AM-HSV samples had 3+ staining; 3 of 11 samples had 2+ staining, and the remaining 6 of 11 had 1+ staining. Representative photomicrographs are illustrated in Figure 3. These data suggest that the diminished endothelial viability observed following surgical vein graft preparation results in part from endothelial denudation, and furthermore from loss of eNOS.

HSV physiologic measurements as a function of storage time

We measured physiologic parameters in UM-HSV samples obtained from 6 patients. Duration of vein graft storage for up to three hours at room temperature in HP did not significantly impair or improve the physiologic variables tested (Figure 4). There was no significant change in contractile response to KCl (n=6, p=ns, Figure 4A), contractile response to

128

PE (n=6, p=ns, Figure 4B), SNP-induced smooth muscle-dependent relaxation (n=6, p=ns, Figure 4C), or CCH-induced endothelial-dependent relaxation (n=6, p=ns, Figure 4D). These data suggest that the duration of time in a physiologic storage solution does not cause HSV dysfunction. Therefore, it must be the other components of surgical vein graft preparation – distension and marking – that contribute to vein graft dysfunction. These data suggest that the vein graft dysfunction we observed in AM-HSV was not due to the additional storage time in HP.

HSV organ culture

After two weeks in organ culture, we observed an increase in intimal thickness of 22.81 ± 18.77 µm in UM-HSV, and intimal/medial ratio increased by $22\pm27\%$. We observed an increase in intimal thickness by 38.53 ± 26.48 µm in AM-HSV, and intimal/medial ratio increased by $50\pm37\%$. Compared with UM-HSV, AM-HSV developed a 69% increase in intimal thickness (n=11, p=.043, Figure 5A), and a 122% increase in intimal/medial ratio (n=11, p=.015, Figure 5B). These observations demonstrate that surgical vein graft preparation causes injury beyond that induced by harvest alone and which is sufficient to promote neointimal growth.

Measurement of reactive oxygen species in HSV

Levels of 2-hydroxyethidium in UM-HSV were 227.6 ± 40.44 pmol/mg protein versus 382.5 ± 43.07 in AM-HSV (n=4, p=.03, Figure 6), indicating increased generation of ROS after surgical vein graft preparation. These observations demonstrate that surgical vein graft preparation causes additional ROS generation beyond that induced by harvest alone.

Experimental induction of oxidative stress in HSV

We performed these experiments in UM-HSV samples obtained from 6 patients. One-hour treatment of UM-HSV with H_2O_2 resulted in significant blunting of endothelial-dependent relaxation at concentrations of 1 mM and 10 mM, but not at 100 μM (Figure 7). Endothelial-dependent relaxation in UM-HSV was 27±9% in comparison with 9±5% in UM-HSV treated with 1 mM H_2O_2 (n=6, p=.04) and 10±4% in UM-HSV treated with 10 mM H_2O_2 (n=5, p=.03). These data demonstrate that ROS can cause endothelial dysfunction in HSV. Therefore, the presence of increased ROS, such as that generated secondary to surgical vein graft preparation, serves as a secondary mediator of vein graft dysfunction.

DISCUSSION

Human saphenous vein (HSV) is harvested, prepared, stored, and then reimplanted as a conduit to bypass arterial stenoses and occlusions. Therefore, HSV is an autotransplanted organ, but is not widely considered or treated as such. Surgical vein graft preparation causes successive injury at multiple levels prior to arterial implantation (Figure 1). Vein graft harvest is injurious secondary to hypoxia, stretch and traction injury.[125] After harvest, *ex vivo* vein graft preparation is performed on the "back table." While methods of vein graft preparation remain surgeon-dependent, most distend the conduit with a hand-held syringe in order to identify leaks and overcome spasm. We have measured intraluminal pressures generated during gentle distension and these uniformly exceed 750 mmHg (data not shown), regardless of syringe size or perceived force placed on the syringe plunger. Conduit distension causes significant morphologic changes, including endothelial denudation and smooth muscle damage.[173,185] Additionally, most surgeons

mark the vein graft for orientation using a sterile surgical marking pen intended for use on the skin. We have recently demonstrated that this common practice causes smooth muscle and endothelial dysfunction secondary to toxic components in the ink, including isopropyl alcohol (a solvent).[174] Isopropyl alcohol is converted to acetone *in vivo*,[186] which increases oxidative stress by causing generation of reactive oxygen species.[187] Finally, the conduit is placed in a storage solution for a variable duration. Normal saline is a commonly utilized storage solution and is an acidic, non-buffered solution with pH <6.0. Despite the non-physiologic properties of this storage solution, normal saline was utilized by 40% of centers (JH Alexander, MD, unpublished data, 2013) in the PREVENT IV trial.[172] Vein preparation techniques have yet to be scientifically validated despite their widespread application.

Our results indicate that surgical vein graft preparation causes significant cellular dysfunction of the two principle HSV cell types: smooth muscle and endothelium (Figure 2A-D). We have previously demonstrated that the production of force of less than 0.025×10^5 N/m^2 in response to KCl correlates with diminished cellular viability as measured by the 3-(4,5-Dimethylthiazol-2-yl)-2,5-diphenyltetrazolium bromide (MTT) live/dead assay.[125] AM-HSV produced significantly diminished contractile force in response to KCl (Figure 2A), and PE (Figure 2B). Smooth muscle-dependent vasorelaxation in response to SNP (Figure 2C) was also diminished. Therefore, surgical vein graft preparation causes additional vascular smooth muscle injury beyond that incurred during surgical vein graft harvest alone. To our knowledge, smooth muscle dysfunction has not been demonstrated to occur in HSV grafts this early *ex vivo*. These findings implicate surgical vein graft preparation as an important mediator of vein graft dysfunction.

The injury of potentially greatest consequence to the long-term success of the bypass conduit is the loss of endothelial function following surgical vein graft preparation (Figure 2D). We observed a contractile response to CCH rather than relaxation in many of the AM-HSV samples. Acetylcholine (and its analog, CCH) act on vascular smooth muscle to cause vasoconstriction in tissue with endothelial injury or loss.[188] These measurements of diminished to absent endothelial function correlated with loss of endothelial coverage on immunohistochemical staining for CD31, with superimposed and more pronounced loss of eNOS staining (Table 2 and Figure 3). These results suggest that, while harvest leads to mild endothelial denudation and loss of eNOS, these insults are magnified following *ex vivo* surgical vein graft preparation. A viable and intact endothelium serves multiple protective roles. Nitric oxide released by the endothelium promotes vasodilation and prevents platelet adhesion and thrombosis. In contrast, dysfunctional endothelium exerts prothrombotic properties[189] and allows attachment of circulating platelets and leukocytes which secrete growth factors, a critical step in the development of the hyperplastic lesion.[190] Endothelial denudation therefore increases the risk of thrombosis in the immediate postoperative period (<30 days), and may initiate further cascades of vascular injury and damage, leading to the development of IH in the short- and long-term lifespan of the conduit.

Surgically harvested HSV (UM-HSV) that does not undergo *ex vivo* surgical vein graft preparation exhibits preservation of physiologic function for up to three hours of storage in heparinized plasmalyte at room temperature (HP, 10 U/mL) (Figure 4). We have identified HP as a buffered physiologic storage solution which is superior to most other commonly utilized storage solutions for preservation of vein graft physiology (data not shown) and this solution has been universally adopted at our institution. These data demonstrate that the additional storage

time in HP to which the AM-HSV segments were subjected in the course of our experimental design did not contribute to physiologic dysfunction. This suggests that the other manipulations occurring during this period, such as hydrostatic distention and marking, are the primary factors leading to smooth muscle and endothelial dysfunction (Figure 2A-D).

Injury incurred during surgical vein graft preparation is a sufficient stimulus for the promotion of IH in organ culture, a well-validated *in vitro* model that replicates the smooth muscle proliferation, migration, and extracellular matrix deposition occurring in IH.[183,191] We observed a significant increase in both intimal thickness and intimal/medial ratio in HSV subjected to surgical vein graft preparation (Figure 5). These data support the hypothesis that early vein graft injury is an important stimulus leading to IH. Importantly, this injury response can occur in the absence of the turbulent and pulsatile hemodynamic alterations associated with placement of a venous graft in arterial circulation and in the absence of growth factors released from circulating leukocytes and platelets, further implicating preexisting tissue injury as an inciting agent in this process.

Our data indicate that cellular vein graft dysfunction is mediated in part by oxidative stress. Levels of reactive oxygen species nearly doubled in response to surgical vein graft preparation (Figure 6). Moreover, experimentally induced oxidative stress is a secondary mediator of endothelial dysfunction in UM-HSV (Figure 7). Therefore, ROS are generated during vascular injury and serve as secondary mediators of tissue injury, particularly involving the endothelium.[178] Even brief exposure to ROS has been demonstrated to stimulate vascular smooth muscle cell proliferation in cultured cell lines persisting well beyond the time of exposure.[192] The NADPH oxidases are the most important source for superoxide production and they are activated by vascular injury and hypoxia.[193,194] Oxidative stress enhances endothelial

permeability and promotes leukocyte attachment.[178] Binding and activation of neutrophils causes superoxide generation as part of the respiratory burst.[195] Superoxide production can initiate a cascade of other ROS (H_2O_2, hydroxyl radicals, and peroxynitrite), which indiscriminately react with and oxidize lipids, proteins, and DNA in the vicinity and cause cellular damage and death.[178,194] ROS further react with and deplete NO, forming peroxynitrite.[194] Therefore, oxidative stress is a plausible mechanistic contributor to the near-complete loss of measurable endothelial function (Figure 2D) in HSV subjected to surgical vein graft preparation.

While oxidative stress has been implicated in the pathogenesis of multiple cardiovascular diseases, it remains to be demonstrated whether this contributes to vein graft dysfunction in human tissue. Our data demonstrate increased levels of reactive oxygen species induced very early following surgical vein graft preparation; these ROS cause secondary injury to the vein graft. ROS have been demonstrated to initiate cellular responses with long-lasting effects persisting beyond the time of exposure. For example, it has been shown that very brief exposure to reactive oxygen species lasting only 10 minutes is a sufficient stimulus for vascular smooth muscle proliferation in cultured cell lines.[192] It is not known yet whether avoiding vein graft injury alone is sufficient to prevent ROS generation, or whether antioxidant agents have therapeutic efficacy. We have demonstrated that University of Wisconsin organ preservation solution (which contains the antioxidant glutathione) preserves vascular smooth muscle function significantly better than plasmalyte alone (data not shown). Furthermore, preliminary proteomics data point to a possible role of vascular smooth muscle apoptosis in vein graft failure. Whether this process is related to ROS production is an area of future investigation.

Based on these data, the following recommendations should be considered. Conduit distention must be gentle and pressures must be limited to physiologic levels when possible. A

simple but effective method for achieving this is to perform the proximal arterial anastomosis first, and then to revascularize and distend the conduit using arterial blood inflow. This method has the advantages of limiting conduit pressures to systemic arterial blood pressures, and shortening the period of "warm ischemia" during which the vein is otherwise stored at room temperature in hypoxic conditions. Marking the vein graft with surgical skin marking pens should be avoided. The toxic components in these pens cause significant vein graft dysfunction. When it is mandatory to mark the conduit, i.e. during tunneling so as to avoid twisting, we urge clinicians to consider interrupted rather than continuous marking. A buffered physiologic storage solution such as plasmalyte, University of Wisconsin solution, or heparinized blood should be used to store the conduit. Saline should be avoided as a storage solution given its acidic and non-buffered properties.

This study has several limitations. First, collection of human tissue from different surgical teams introduced variability in the way the tissue was handled prior to experimentation. However, the advantage of this approach is that the AM-HSV segments obtained were sections from the actual vein grafts used to revascularize patients and we obtained the tissue for experimentation immediately prior to arterial implantation. In addition, our data regarding IH was derived from an organ culture model possessing limitations, including the absence of hemodynamic alterations occurring in arterial circulation and the absence of circulating leukocytes and other circulating blood components that may modulate the development of IH. Future areas of investigation include further mechanistic work into the means by which ROS induce vein graft failure, and also to investigate whether ROS generation can be avoided using antioxidants or inhibitors of the NADPH oxidases.

In summary, surgical vein graft preparation causes endothelial and smooth muscle dysfunction, diminished smooth muscle viability, production of ROS, and IH. These results collectively argue for less injurious means of surgical vein graft preparation. The *ex vivo* component of vein graft preparation provides a unique therapeutic window for delivery of compounds, antioxidants, or drugs directly to the vein graft to prevent cellular dysfunction and injury. Preservation of cellular viability in transplanted organs is achieved in physiologic buffered storage solutions with antioxidants. Since vein grafts are autotransplanted organs, improved HSV preservation should be the focus of future practices of surgical vein graft preparation in order to enhance vein graft function and patency.

Figures

Steps in vein graft preparation   **HSV tissue acquired**

Surgical vein graft harvest
(Open or endoscopic)

"Unmanipulated"
(UM)-HSV samples

Ex vivo vein graft preparation
- Hydrostatic distention
- Marking with skin marker
- Leak repair / side branch ligation

Warm ischemia time
in storage solution

Arterial vein graft implantation
and revascularization

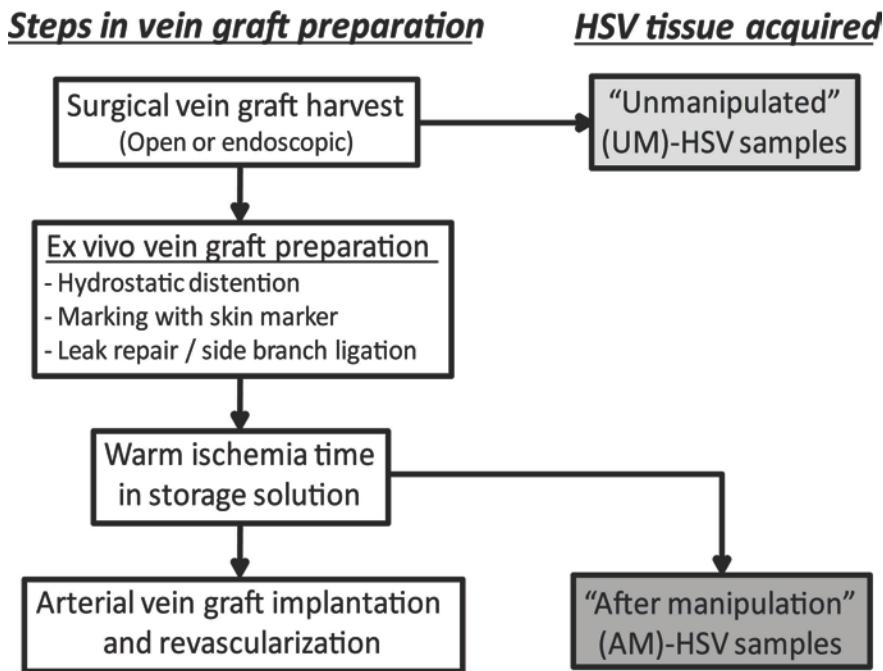"After manipulation"
(AM)-HSV samples

Figure 1. Steps in surgical vein graft preparation and sources of tissue used in this investigation. Following human saphenous vein (HSV) harvest, vein graft preparation is performed. *Ex vivo* manipulations include hydrostatic distention to identify leaks and overcome

spasm, marking with a surgical skin marker for orientation purposes, and repair of leaks. The
conduit is then placed in a storage solution at room temperature where it undergoes a variable
period of warm ischemia. These steps all precede eventual surgical implantation in the arterial
circulation. For this investigation, HSV obtained immediately following harvest
("unmanipulated," UM-HSV) was compared with HSV obtained following surgical vein graft
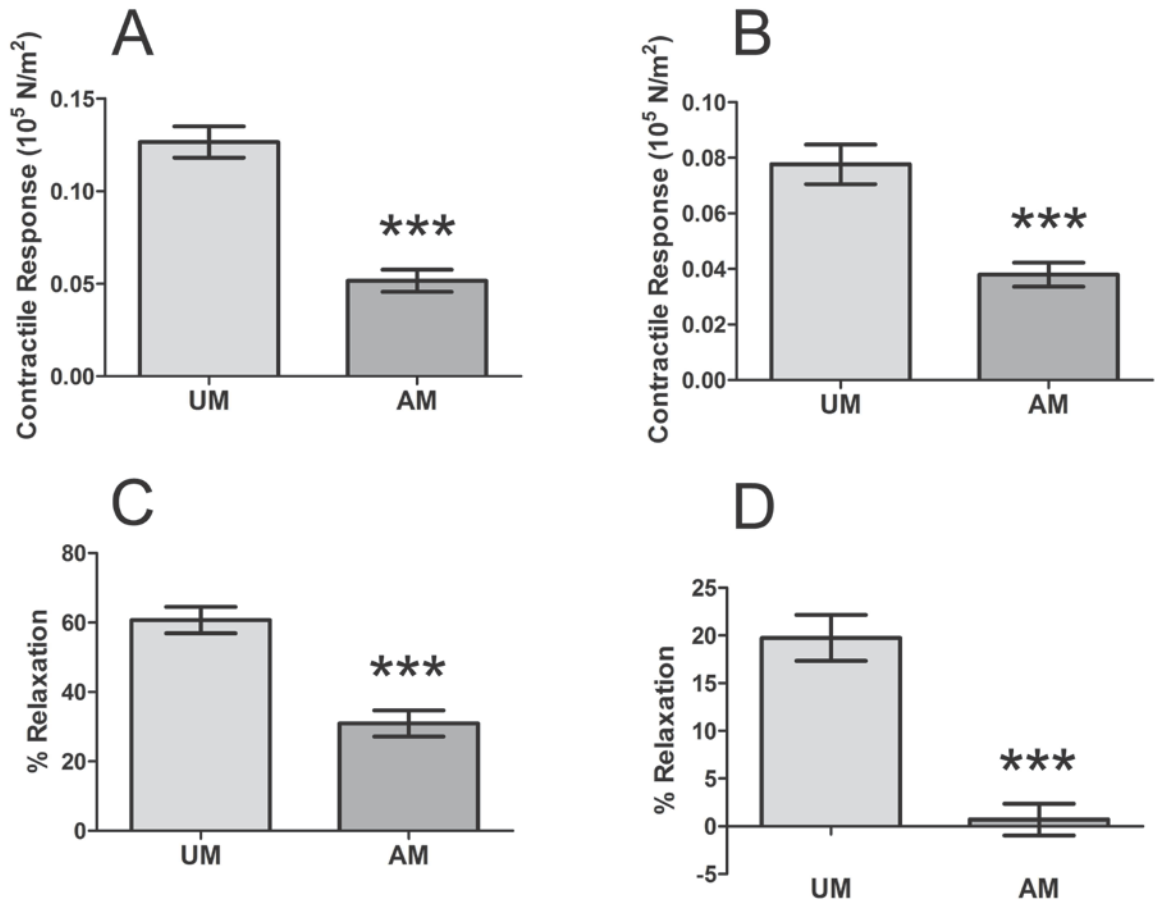preparation ("after manipulation," AM-HSV).

Figure 2. Physiologic measurements of human saphenous vein (HSV) smooth muscle and
endothelial function before and after surgical vein graft preparation. Physiologic responses are
significantly impaired in HSV obtained after manipulation (AM) compared with paired samples
of unmanipulated (UM)-HSV; these include contractile response to potassium chloride (KCl,

n=47, p<.0001, Panel A), contractile response to phenylephrine (PE, n=41, p<.0001, Panel B), smooth muscle-dependent relaxation in response to sodium nitroprusside (SNP, n=34, p<.0001, Panel C), and HSV endothelial function in response to carbachol (CCH, n=36, p<.0001, Panel D).
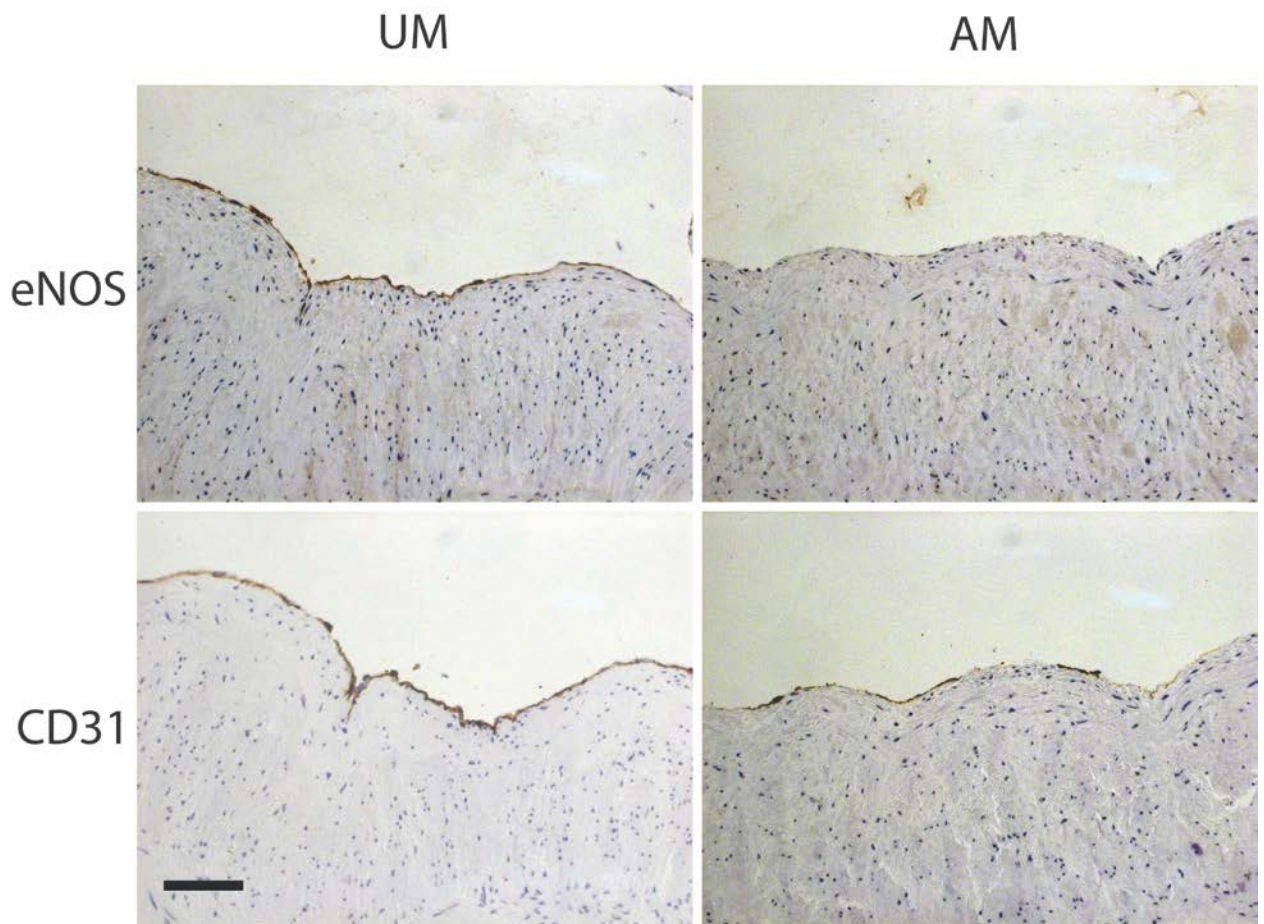
Figure 3. Immunohistochemical staining of human saphenous vein (HSV) for eNOS and CD31. Unmanipulated HSV (UM-HSV) exhibits continuous (4+) eNOS and CD31 staining. HSV obtained after surgical manipulation (AM-HSV) exhibits near absence of eNOS staining (1+) and patchy loss of endothelial coverage by CD31 staining (2+). Photomicrographs are representative of 11 HSV samples. The scale bar represents 100 µm.
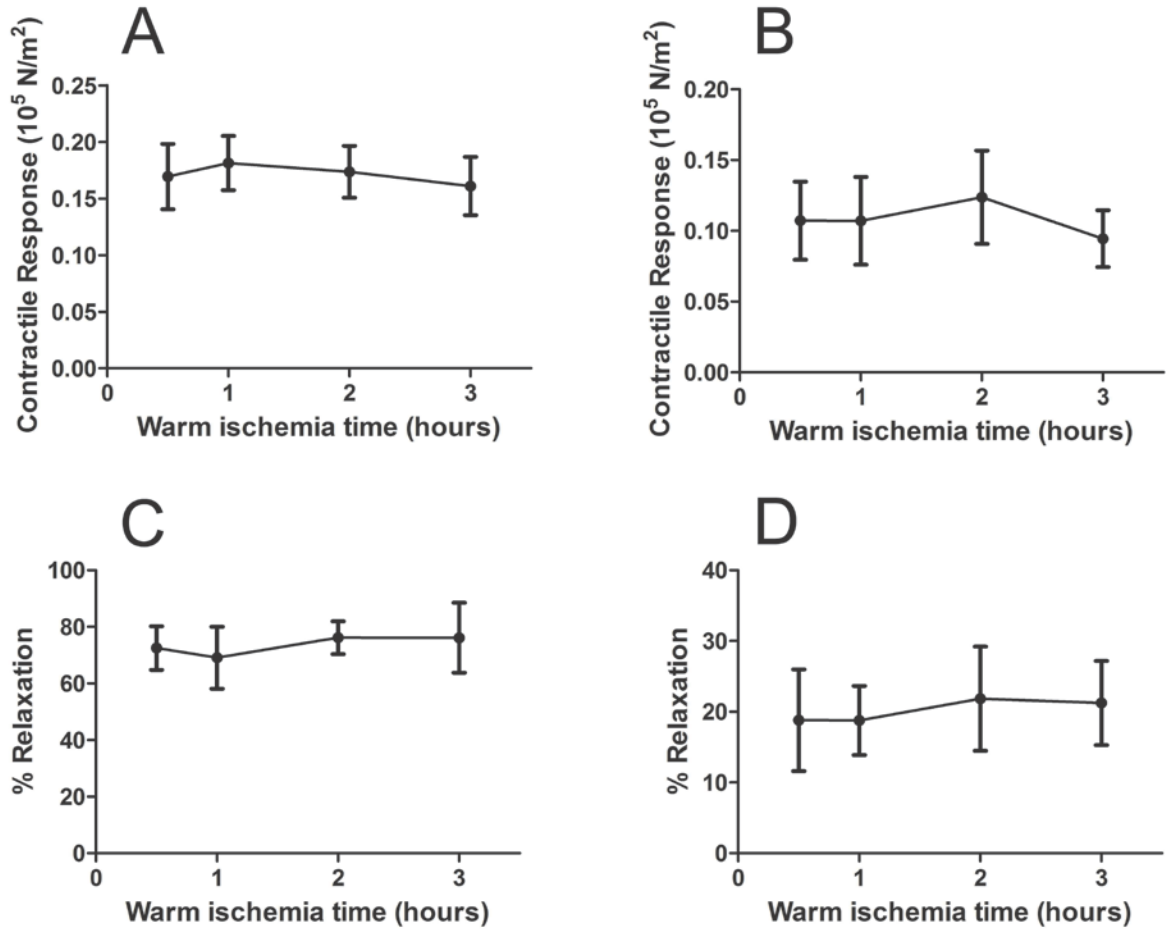
Figure 4. Human saphenous vein (HSV) physiological measurements as a function of warm ischemia time in heparinized plasmalyte. Duration of warm ischemia for up to 3 h does not influence smooth muscle contractile response to potassium chloride (KCl, n=6, p=ns, Panel A), smooth muscle contractile response to phenylephrine (PE, n=6, p=ns, Panel B), smooth muscle-dependent relaxation in response to sodium nitroprusside (SNP, n=6, p=ns, Panel C), or endothelial-dependent relaxation in response to carbachol (CCH, n=6, p=ns, Panel D).
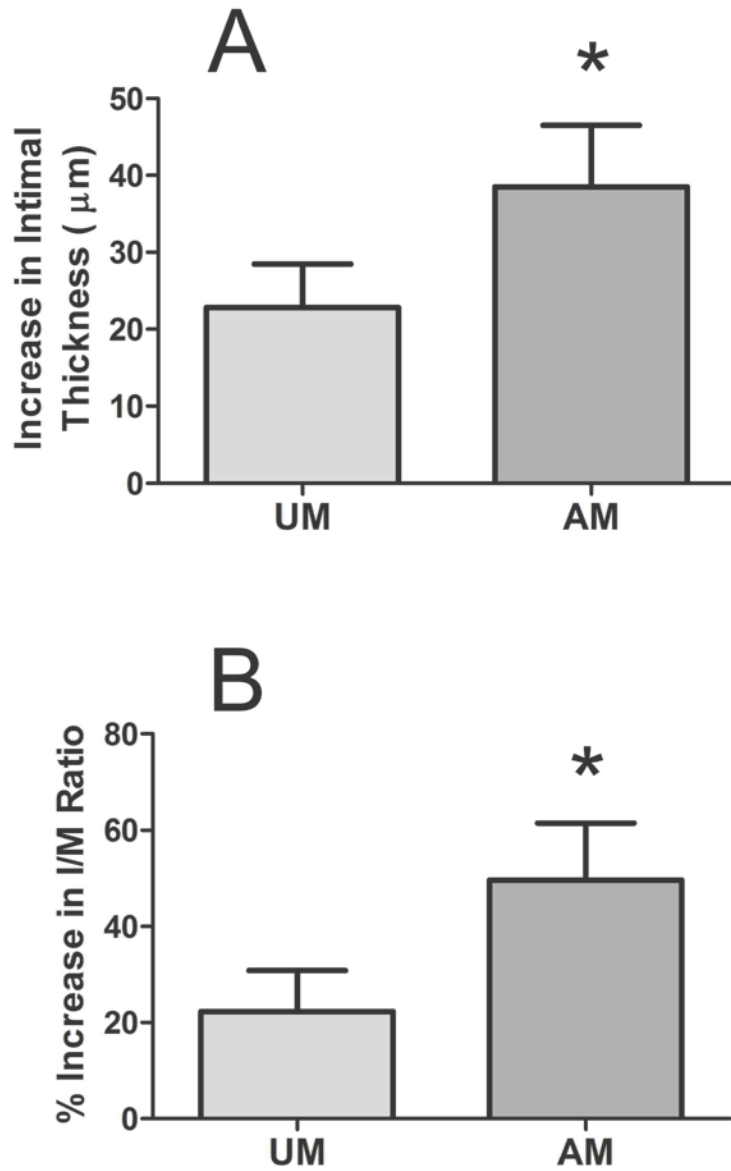
Figure 5. Surgical vein graft preparation promotes development of intimal hyperplasia in organ culture. Panel A. The increase in intimal thickness (μm) is significantly greater in human saphenous vein (HSV) obtained after surgical manipulation (AM) compared with HSV obtained unmanipulated (UM) after two weeks in organ culture (n=11, p=.043). Panel B. The percent

increase in intimal to medial ratio (I/M ratio) is significantly greater in AM-HSV compared with

UM-HSV (n=11, p=.015).
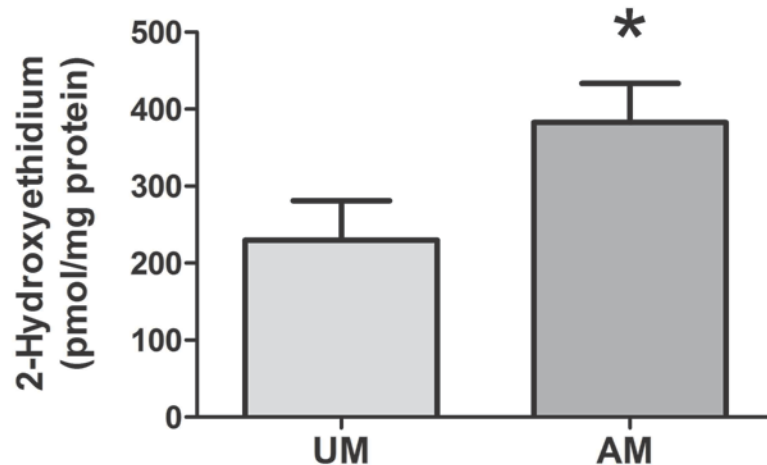
Figure 6. The generation of reactive oxygen species (ROS) in human saphenous vein

(HSV) is increased after undergoing surgical vein graft preparation. Levels of ROS were

assessed by measuring by the conversion of dihydroxyethidium (DHE) to 2-hydroxyethidium.

Levels of 2-hydroxyethidium were significantly greater in HSV obtained after *ex vivo* surgical

vein graft preparation injury compared with HSV immediately following surgical vein graft

harvest (n=4, p=.03).
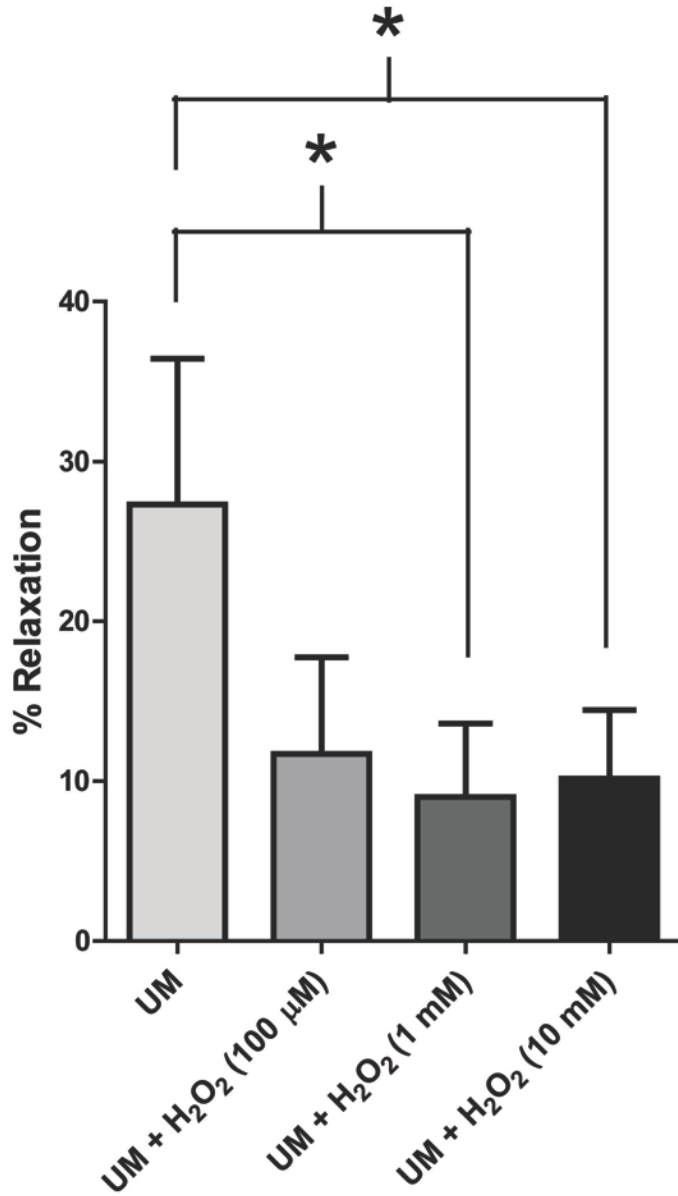
Figure 7. Experimental induction of oxidative stress causes endothelial dysfunction in human saphenous vein (HSV). Compared with unmanipulated (UM)-HSV, one-hour treatment of UM-HSV with hydrogen peroxide (H_2O_2) caused a significant decline in endothelial-dependent relaxation when exposed to 1 mM H_2O_2 (n=6, p=.04) and 10 mM H_2O_2 (n=5, p=.03).

Additional Manuscript 3

Introduction

Over one million coronary artery bypass (CABG) and peripheral revascularization procedures are performed each year. Despite the higher patency rate of the internal mammary artery when compared with the human saphenous vein (HSV) and increased interest in other arterial conduits, HSV remains the most widely used conduit for CABG procedures. Vein graft failure rate remains high, however, approaching 40% at 18 months postoperatively.[196]

The predominant histological finding in failed vein grafts is intimal hyperplasia, which is thought to be the manifestation of cellular responses to injury.[190] Vein graft injury during intraoperative graft preparation leads to intimal hyperplasia, accelerated atherosclerosis, and subsequent graft failure.[190,197] Injurious mechanisms during graft preparation include endovascular harvesting techniques, radial distension, and choice of storage solution.[196,198,199] Optimal vein graft preparation prior to surgical anastomosis is hence important for long-term graft patency.[200]

Vein graft marking is a practice frequently used to properly orient the graft prior to implantation. Originally intended for use in marking the skin area around surgical sites, surgical skin markers are sterile, inexpensive, and readily available to surgeons for vein graft marking. The chemical constituents of these markers consist of alcohol-based solvents and the dyes methylene blue or gentian violet. Vein marking with methylene blue impairs both endothelium-dependent and endothelium-independent graft function.[201] Similarly, gentian violet leads to a decrease in endothelium-independent relaxation to sodium nitroprusside.[202] While the deleterious effects of gentian violet and methylene blue are well established, the practice of using skin markers still remain widely accepted for CABG and peripheral vascular procedures. Although

143

surgical skin markers are non-toxic in dermatology applications, little is known about the effects

of applying the marker directly to the vein grafts. This study examined the effects of surgical

skin markers on functional viability of HSV used for autologous bypass procedures.

Methods

Human saphenous vein procurement

All human saphenous vein graft remnants (HSV) were obtained after the approval of the

Institutional Review Boards of the Vanderbilt University Medical Center and the VA Tennessee

Valley Healthcare System, Nashville, TN. De-identified remnant segments of HSV (n=38) were

collected from patients undergoing coronary artery bypass (CABG) and peripheral vascular

bypass procedures. The veins were procured according to the surgeon's discretion in terms of

surgical and medical interventions, intraoperative graft handling such as distention and the use

of surgical skin markers. The veins were stored in heparinized saline solution until the end of the

surgical procedure at which time they were placed in cold University of Wisconsin transplant

harvest buffer at 4°C [100 mM potassium lactobionate, 25 mM KH_2PO_4, 5 mM $MgSO_4$, 30 mM

raffinose, 5 mM adenosine, 3 mM glutathione, 1 mM allopurinol, 50g/L hydroxyethyl starch, pH

7.4]. The vessels were tested within 24 hours of harvest.

For endothelial-dependent relaxation experiments, HSV (n=8) were collected

immediately after surgical harvest without any further intraoperative manipulations such as the

use of skin markers or distention and tested within 2 hrs of surgical procurement.

Physiological measurements of functional viability

The HSV and dissected free of adipose and connective tissue and 1 mm rings were cut.

The rings were weighed and their lengths were measured. In order to focus on smooth muscle

responses, the endothelium was mechanically denuded by gently rolling the luminal surface of

each ring at the tip of fine vascular forceps before suspension in a muscle bath containing a

bicarbonate buffer (120 mM NaCl, 4.7 mM KCl, 1.0 mM $MgSO_4$, 1.0 mM NaH_2PO_4, 10 mM

glucose, 1.5 mM $CaCl_2$, and 25 mM Na_2HCO_3, pH 7.4), equilibrated with 95% O_2 and 5% CO_2

at 37°C. The rings were progressively stretched to the optimal resting tension (approximately 1

gm) that would produce a maximal response to contractile agonists as described previously, and

then maintained at the resting tension and equilibrated for a minimum of 2 hrs. [203,204] Force

measurements were obtained using a Radnoti Glass Technology (Monrovia, CA) force

transducer (159901A) interfaced with a Powerlab data acquisition system and Chart software

(AD Instruments, Colorado Springs, CO). Smooth muscle functional viability was determined

by contracting the HSV rings repeatedly with 110 mM KCl (with equimolar replacement of NaCl

in bicarbonate buffer) until the maximal response was generated. Potassium challenge (110mM)

causes depolarization of the membrane leading to contraction of functionally viable smooth

muscle.[181] Tissues that failed to respond to KCl (generated a contractile force equivalent to

stress $<0.025 \times 10^5$ N/m^2) were not tested further. Rings that generated stress of $\geq 0.025 \times 10^5$ N/m^2

were washed to remove the KCl and equilibrated in bicarbonate buffer for 30 minutes.[205]

Concentration of physiologic agonists that would induce submaximal contractile responses, was

pre-determined by treating the tissue with increasing doses (0.01, 0.1, and 1 μM) of

norepinephrine (NE) or phenylephrine (PE). Tissues were then washed with bicarbonate buffer

to remove the agonists and treated with 10^{-6} M NE or 10^{-6}M PE (submaximal doses) to determine

contractile responses.

Physiological measurements of endothelial-derived vasorelaxation

Rings from HSV that were not manipulated intraoperatively were prepared and tested essentially as described above except that the endothelium was preserved. Viable tissues were pre-contracted with 10^{-6} M PE and then treated with 5×10^{-7} M carbachol, and the maximal relaxation response was determined.[182]

Effect of surgical skin markers on vascular reactivity

To study the effect of surgical skin markers and their chemical constituents, three commercially-available surgical skin markers were obtained (SSM1, Devon Skin Marker and Ruler, Covidien, Mansfield, MA; SSM2, Cardinal Health Corp., Dublin, OH; SSM3, MediChoice, Sunrise, FL).. These marking pens were used at the institutions where HSV were collected for this study and all contained 50% isopropyl alcohol and the dye gentian violet. Rings from unmarked HSV remnant segments were painted on the surface with either SSMs, or a cotton swab saturated with 1% methylene blue (Akorn, Inc., Lake Forest IL), or submerged in 50% isopropyl alcohol at room temperature for 15 min. Contraction to 110mM KCl and contractile agonists was measured in the muscle bath as described above.

To assess the effect of surgical skin markers on endothelial-dependent vasorelaxation responses, rings from minimally manipulated HSV were painted with surgical skin marking pens and incubated in 0.5 ml PlasmaLyte A (Baxter, Deerfield, IL), a pH balanced physiological solution used for storing HSV during graft preparation, at room temperature for 15 min.

Vascular responses to 110mM KCl and contractile agonists were measured in the muscle bath as described above.

Data analysis

Contractile response was defined by stress ($[10^5$Newtons (N)/m^2] = force (g) x 0.0987 / area, where area is equal to the wet weight [(mg) / length (mm at maximal length)] divided by 1.055) , which was calculated using the force generated by the tissues.[126] Any tissue that generated stress of 0.025×10^5 N/m^2 or greater was considered functionally viable, which correlates to 0.5 g of force for a 10 mg, 1mm thick, 4mm diameter ring. Data was reported as mean responses ± standard error of the mean. Unpaired t-tests were conducted in order to determine the significance (p value) of each experiment using GraphPad Prism software (LaJolla, CA). A p value ≤0.05 was considered statistically significant.

Results

Contractile response of human saphenous vein grafts

Thirty-eight HSV surgical remnant segments were obtained and 22 (58%) had visible blue marking from surgical skin marker at the time of collection from the operating room. HSV segments that had no visible blue marking generated significantly ($p<0.0001$) greater contractile responses to 110 mM KCl (0.174 ± 0.023 10^5 N/m^2, n=16) than those that were marked (0.047 ± 0.014 10^5 N/m^2, n=22) (Figure 1A). Viable HSV rings (≥0.025 N/m^2, n=30) were then treated with a submaximal dose of the contractile agonist, norepinephrine (NE; 10^{-6}M). HSV without blue marking generated significantly ($p=0.0004$) greater contractile responses to NE (0.1244 ± 0.02765 N/m^2, n=13) than those that had visible blue marking (0.02288 ± 0.006272 N/m^2, n=17) (Figure 1B).

Surgical skin marker chemical constituents decreased HSV smooth muscle contractile

response

We next determined whether isopropyl alcohol, a solvent used in surgical skin markers, impairs contractile responses of HSV. Rings were cut from HSV segments that were void of blue marking. These rings were either left untreated, marked with surgical skin marker SSM1, treated with 50% isopropyl alcohol, or treated with 1% methylene blue, and exposed to 110mM KCl. HSV rings that were left untreated produced significantly greater contractile response $(0.110 \pm 0.014 \ 10^5 \ N/m^2$, n=12) than the rings that were marked with SSM1 $(0.003 \pm 0.001 \ 10^5$ N/m^2, n=5, p=0.0002), 50% isopropyl alcohol $(0.005 \pm 0.003 \ 10^5 \ N/m^2$, n=5, p=0.002), or methylene blue $(0.014 \pm 0.010 \ 10^5 \ N/m^2$, n=10, p<0.0001) (Figure 2).

Surgical skin markers impaired HSV endothelial-dependent relaxation

The effect of marking with surgical skin marker on the endothelium-dependent vasorelaxation ability of the vein grafts was determined. Pressure distension during surgical harvest can lead to loss of endothelial-dependent functions; therefore, HSV segments were collected immediately after harvest and prior to being subjected to any intraoperative manipulation.[206] Rings from the HSV were either left unmarked or marked with surgical skin markers SSM2 or SSM3. Contractile response to high potassium chloride was significantly reduced by 20-30% (Figure 3A; n=4, p<0.03) in segments marked with SSM2 (0.06681 ± 0.02713) and SSM3 (0.07455 ± 0.02901) when compared to the untreated segments (0.09638 ± 0.02261). A similar effect was seen in the agonist-induced contractile response to phenylephrine. Marking with SSM2 $(0.04277 \pm 0.01956 \ N/m^2)$ or SSM3 $(0.04773 \pm 0.01935$ $N/m^2)$ significantly reduced contractile force generation by 40-50% (p<0.03) when compared to

148

the unmarked segments (0.07760 ± 0.01586N/m^2) following exposure to PE (Figure 3B). When the segments were pre-contracted with PE, endothelium-dependent vasorelaxation to carbachol was significantly reduced in HSV (Figure 4; n=3, p<0.02) marked with either SSM2 ($3.560 \pm 1.672\%$) or SSM3 ($7.334 \pm 2.192\%$) when compared to the unmarked segments ($19.94 \pm 1.529\%$).

Discussion

Vein graft failure following coronary artery bypass procedures has been attributed to injury to the endothelial and/or medial layers of the saphenous vein and remains an enigmatic, morbid, and expensive problem. Vein graft failure leads to myocardial infarction, heart failure, repeat hospitalizations, and repeat surgical or percutaneous interventions. Injury to veins by mechanical damage, including distension and endovascular harvesting techniques, lead to thrombosis, intimal hyperplasia, and ultimately vein graft failure.[162] We have previously reported that vein grafts used in revascularization procedures display variable contractile function and viability[205]. A (3-(4,5-Dimethylthiazol-2-yl)-2,5-diphenyltetrazolium bromide, or MTT, live/dead assay illustrated that the loss of the contractility of smooth muscle directly correlates to the loss of cellular viability in HSV suggesting surgical preparation and manipulation lead to cell death and hence significant loss of conduit function. Prior to implantation, HSV is prepared on a "back table" where marking vein grafts is routinely employed for graft orientation and prevention of graft kinking. While mechanical damage to HSV grafts has been described in detail, there remains a paucity of literature outlining the effects of surgical marking pens on vein graft function. Consequently, the widely accepted technique of vascular marking with a sterile surgical skin marker persists, despite unknown effects on vein grafts. The current study offers

evidence that exposure of HSV to surgical skin markers contribute to impaired graft function and viability.

Vein grafts fail in 5 to 10% of patients as early as the first postoperative week and is associated with adverse outcomes.[207-209] A common theme for early vein graft failure (occurs within one month) is vascular endothelial injury.[210-212] Manchio *et al* showed that, at five days post coronary artery bypass surgery, thrombosed veins had only 10% of the endothelial layer remained intact, compared to 50% intact endothelium in patent vein grafts, implicating endothelial damage as a cause of early vein graft failure.[212] Additionally, reendothelialization attenuates intimal hyperplasia following distension injury.[213] Intact endothelium expresses nitric oxide synthase, eNOS, which is responsible for the conversion of L-arginine to nitric oxide. Nitric oxide inhibits platelet aggregation and vascular smooth muscle proliferation in addition to modulating vascular tone. During graft procurement and preparation, disruption of vascular endothelium exposes collagen, a substrate for thrombosis independent of platelet activation or presence of a hypercoagulable state.[212,214]

By 12 to 18 months post-CABG, vein graft failure is observed in approximately 40% of patients.[196] While loss of endothelium integrity correlates with early vein graft failure, the primary histologic finding in late vein graft failure (> 1 month post-bypass) is intimal hyperplasia (IH).[197] Evidence of IH may be seen as early as 3 weeks to 3 months following coronary artery bypass surgery.[215,216] Characterized by vascular smooth muscle cell proliferation, IH is a response to injury and the inciting substrate for accelerated atherogenesis associated with late graft failure.[197] Phenotypic changes in vascular smooth muscle cells include conversion of a contractile, filament-rich structure to a metabolically active, organelle rich phenotype. Synthesis

of extracellular matrix proteins, an important component of vein graft failure, is also increased.[217]

Numerous attempts to ameliorate IH, including E2F decoys, chemotherapeutic, and anti-platelet agents have failed.[172,190,218]However, preservation of vein graft integrity does prevent morphologic changes associated with IH. A 'no-touch' method of vein graft harvesting appears to preserve vein structure and function and slows the rate of atherosclerosis formation following coronary artery bypass grafting.[219] Long-term evaluation of vein grafts (> 8 years) following non-injurious harvesting methods have significantly fewer and smaller atherosclerotic plaques and significantly less IH compared to conventional harvesting.[219] In addition to mechanical injury, chemical damage from storage solutions, such as normal saline, also leads to IH.[175] Grohs *et al* demonstrated a marked decrease in receptor-independent depolarization and agonist-mediated contractility with prolonged storage in various storage media.[199] Taken together, a protective role of intact endothelium and a functional, viable medial layer in vein graft patency is critical.

Given the crucial association between IH and vein graft failure, we examined the effects of surgical marking on function and viability vein graft. In the remnant human saphenous vein grafts examined in this study, almost 60% had been marked intraoperatively. The marked veins demonstrated a 73% reduction in vascular smooth muscle contractility compared to HSV with no visible blue marking. HSV that were not manipulated after harvesting had a ~ 50% decrease in smooth muscle contractile function following exposure to SSM. The difference in functional loss seen in those that were marked by the surgeons intraoperatively compared to those marked experimentally implicates that marking with surgical skin marker alone did not explain the

decrease in smooth muscle function. Other graft preparation techniques may also account for more severe functional impairment observed in veins marked intraoperatively.

Since cellular viability correlates with functional viability of HSV[205], our results infer that vein marking with surgical skin markers is deleterious to the conduit and that the loss of HSV contractile response to both receptor-dependent contraction and depolarization can be attributed in part by the use of SSM and its chemical composition, particularly ~ 50% isopropyl alcohol. While short-term dermal application is non-toxic, isopropyl alcohol intoxication via chronic dermal exposure has been reported.[220] In addition, isopropyl alcohol is converted by alcohol dehydrogenase (ADH) to acetone, a solvent used to fix tissues.[186] ADH is present in human vessels with majority of the activity found in the medial layer.[221] Treating the vein with isopropyl alcohol or direct contact of the vein with a surgical skin marker essentially converts the tissue to a decellularized vein, analogous to cryopreserved veins. When used for peripheral vascular reconstructions, cryopreserved veins have dismal 30% and 18% patency rates at 1 and 2 years, respectively.[222]

Because endothelial function is often abolished due surgical harvest and intraoperative handling [211], we obtained HSV specimens that were collected immediately after surgical harvest and prior to "back table" preparation and subsequently marked with SSM in the laboratory. Our results indicated that marking with surgical skin markers profoundly impaired endothelial-dependent vasorelaxation to carbachol in minimally manipulated HSV. Shoemaker *et al*. previously showed that gentian violet did not affect endothelium-dependent response to $<10^{-6}$M acetycholine.[202] The reason for the different findings may lie in the presence of isopropyl alcohol in the SSM or the surgical procurement and manipulation of the HSV specimens used in

the separate studies. Notwithstanding, our data demonstrated that the endothelium is rendered non-functional when exposed to these two surgical skin markers.

It is logical that cellular death and graft organ injury may result from exposure to SSM in a time and dose-dependent manner. Saphenous veins are typically marked on the conduit surface after initial harvesting and are often stored at room temperature for up to 3 hrs before implantation. How much isopropyl alcohol is absorbed into the vein and the time frame during which conversion to acetone peaks within the tissue is not known. However, the fact that endothelial and medial damage was observed after a 15 min exposure to the SSM in this study suggests that contents of the SSM is readily absorbed through the full thickness of the vein. Further, the extent of vein marking varies among surgeons. We observed that non-contiguous marking along the length of HSV resulted in greater smooth muscle functional viability of vein graft compared to heavily marked veins (data not shown). At the conclusion of the procedure, the chest is often thoroughly irrigated with normal saline; leeching of alcohol in and around the graft may result in untoward effects on HSV viability.

The current study is limited by the use of de-identified tissues and the lack of intraoperative data regarding procurement techniques and graft preparation method. Additionally, patient demographics were not available which may contribute to the variability of vascular responses to injury and experimental conditions. It is also limited by the lack of long-term follow-up to infer how marking with surgical skin markers affects HSV graft patency.

In conclusion, our findings suggest that marking human saphenous veins with a surgical skin marker prior to implantation causes a profound decrease in contraction and relaxation function of these grafts and interfere with the activation of cellular signaling pathways involved in normal physiological responses in endothelial and vascular smooth muscle. Nevertheless,

153

implications of these findings on development of IH graft patency remain to be determined. Until alternatives become available, restricted use of surgical skin markers for vein graft marking is advised.

Figure Captions
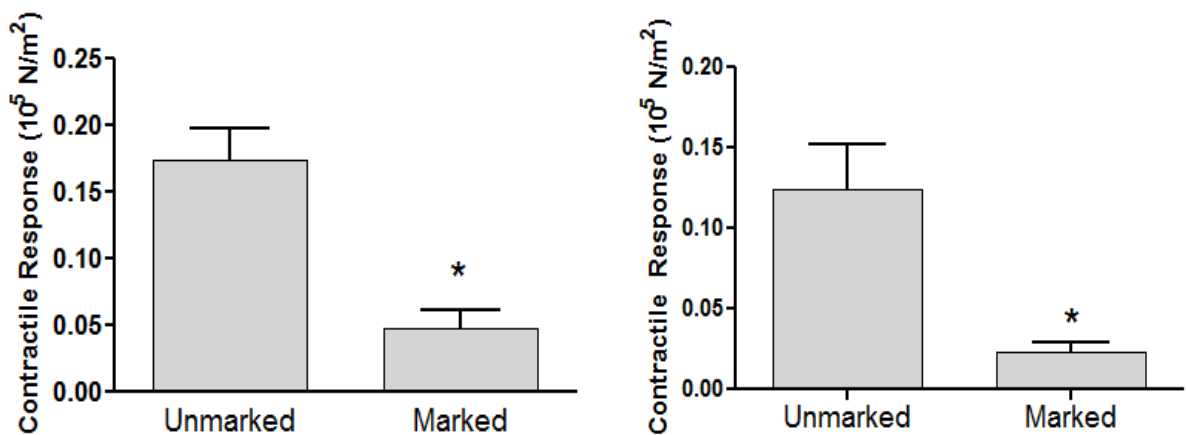
Figure 1. Human saphenous vein grafts with blue markings displayed impaired contractile responses. Remnant saphenous vein from patients undergoing coronary artery bypass or peripheral vascular revascularization surgery were collected (n=38). Rings from each vein were suspended in a muscle bath, contracted with 110mM KCl (A), 10^{-6}M norepinephrine (B), force was measured and converted to stress (10^5 N/m^2). Unmarked (n=16) – no visible sign of markers when collected; marked (n=22) – had visible sign of marking. The error bars show the standard error of the mean. * p<0.0001.
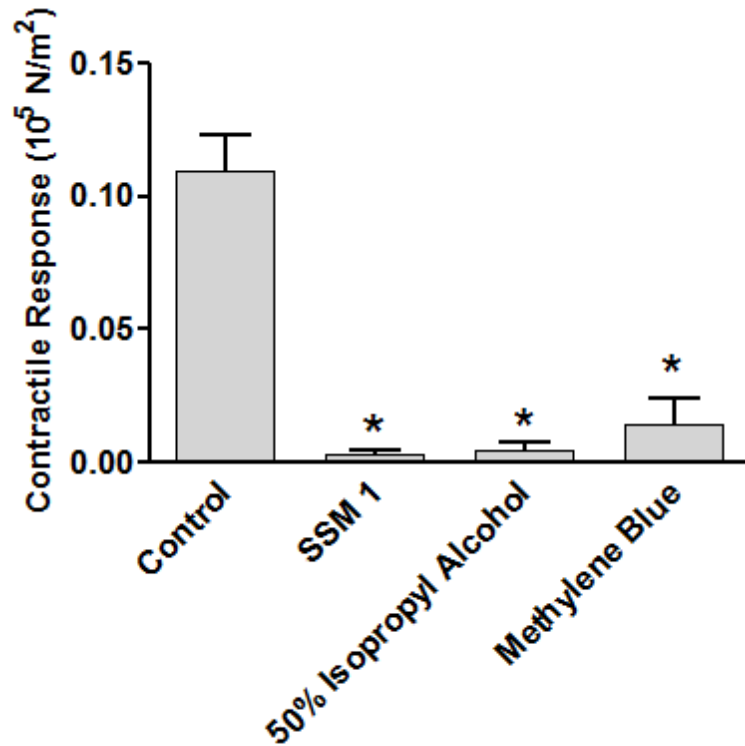
Figure 2. Surgical skin markers and its chemical constituents reduced contractility of remnant human saphenous vein grafts. Rings cut from remnant human saphenous vein grafts were left unmarked (control; n=12), marked with a surgical skin marker (SSM1; n=5), treated with 50% isopropyl alcohol, or with 1% methylene blue (n=10). The rings were then suspended in a muscle bath and exposed to 110mM KCl. Force was measured and converted to stress (10^5 N/m^2). The error bars show standard error of the mean. * $p<0.0002$.
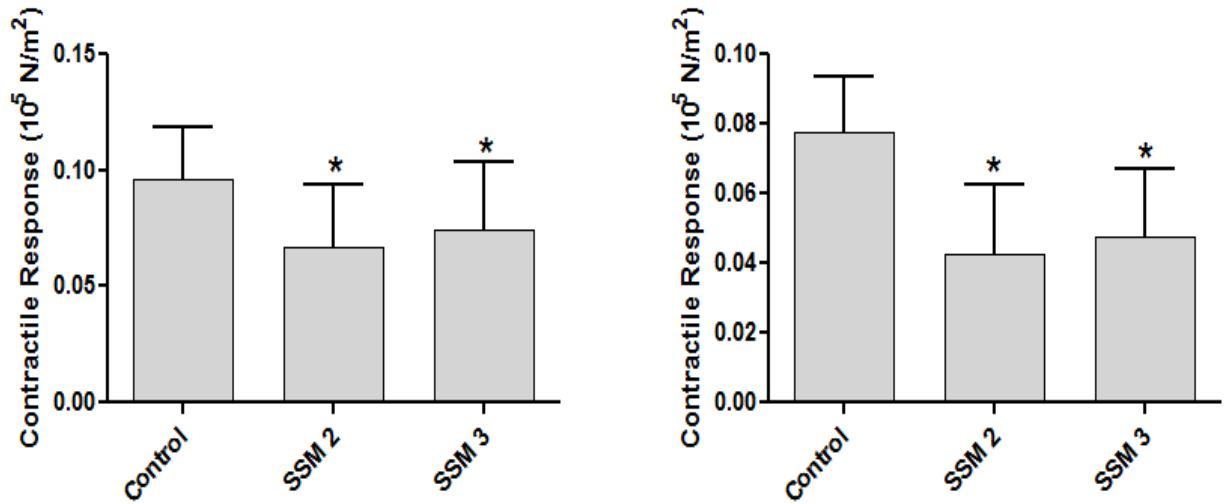
Figure 3. Surgical skin markers impaired contractile response in minimally manipulated human saphenous vein grafts. Saphenous vein from patients undergoing coronary artery bypass or peripheral vascular revascularization surgery were collected prior to any intro-operative preparation (n=4). Rings from each vein were either left untreated (control), or treated with one of two different surgical skins markers (SSM2 or SSM3), and suspended in a muscle bath. Rings were contracted with 110mM KCl (A), or 10^{-6}M phenylephrine (B), force was measured and converted to stress (10^5 N/m^2). The error bars show standard error of the mean. *p<0.003.
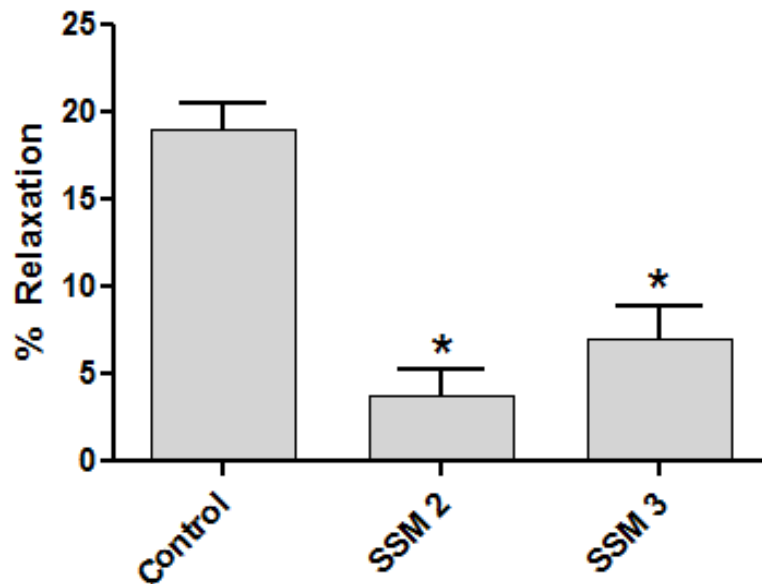
Figure 4. Surgical skin markers impaired endothelial-dependent relaxation in minimally manipulated human saphenous vein grafts. Saphenous vein from patients undergoing coronary artery bypass or peripheral vascular revascularization surgery were collected prior to any intra-operative preparation (n=3). Rings from each vein were either left untreated (control), or treated with one of two different surgical skin markers (SSM2 or SSM3), and suspended in a muscle bath. Rings were pre-contracted with 10^{-6}M phenylephrine and then exposed to 5×10^{-7}M carbachol. Force was measured and converted to stress (10^5 N/m^2). The error bars show standard error of the mean. * p<0.002.

Additional Manuscript 4

PRESSURE CONTROL DURING PREPARATION OF SAPHENOUS VEINS

PREVENTS ENDOTHELIAL INJURY AND REDUCES NEOINTIMA FORMATION

Fan Dong Li, PhD[1]; Susan Eagle, MD[2]; Colleen Brophy, MD[3]; Kyle M Hocking, MEng[3];

Michael Osgood, MD[3]; Padmini Komalavilas, PhD[3], and Joyce Cheung-Flynn, PhD[3¶]

Abstract

Background - The human saphenous veins (HSV) remains the most commonly used autologous conduits for coronary artery bypass grafting (CABG) procedures. Despite advances in surgical techniques and therapeutic interventions, long-term patency of the conduits remains limited due to vein graft failure (VGF). VGF has been reported to be as high as 45% at 12-18 months after surgery and leads to redo surgery, myocardial infarction, recurrent angina, and death. Preparation of HSV prior to implantation leads to endothelial injury which may promote VGF.

Objective – To demonstrate that pressure distention during vein graft preparation leads to endothelial injury and intimal thickening. We hypothesized that limiting intraluminal pressure during pressure distention by using a pressure release valve preserves endothelial function and prevents neointima thickening.

Methods – HSV were collected from CABG patients immediately after harvest (UM), after pressure distention (AD), and after typical intraoperative surgical graft preparation (AM). Porcine saphenous veins (PSV) were subjected to manual pressure distention with or without an in-line pressure release valve that prevents pressures of ≥ 140 mmHg. Endothelial function of the HSV and PSV was determined in a muscle bath, and endothelial integrity was assessed by

immunohistological examination of CD31 and eNOS. Intimal thickening in PSV was evaluated

histomorphometrically after 14 days in organ culture.

Results - Pressure distention of HSV led to decreased endothelial-dependent relaxation

and denudation. Additional intraoperative manipulation further decreased the function of the

conduits. Distention of PSV with the pressure release valve preserved endothelial-dependent

relaxation, prevented denudation and reduced intimal thickening.

Conclusion - Use of a pressure release valve during graft preparation limits intraluminal

pressure generated by manual distension, preserves endothelial integrity and reduces intimal

hyperplasia. Integration of this simple device may contribute to improved long term vein graft

patency.

INTRODUCTION

Human saphenous vein (HSV) is an autologous transplanted organ most commonly used for aortocoronary bypass (CABG) and peripheral vascular (PV) revascularization procedures. Despite advances in surgical techniques and therapeutic interventions, long-term patency of the conduits remains limited due to vein graft failure (VGF). The per patient VGF rate has recently been reported to be 45% and 39% at 12-18 month post-procedure in CABG and PV patients, respectively [171,172]. Common causes of vein graft failure include loss of endothelial coverage, intimal hyperplasia, and thrombosis [223]. Graft patency rates are influenced by patient characteristics, intrinsic quality of the conduit, and surgical technique [162]. Despite concerns about graft preparation techniques, beginning with the seminal work by LoGoerfo *et al* in the early 1980s, preservation of endothelial and medial integrity of the conduits during graft preparation remains suboptimal and as such, VGF is attributable at least in part to tissue handling [170,224]. Common trauma incurred to the vein during 'back-table' graft preparation includes conduit storage in acidic solutions, conduit marking using toxic surgical skin markers, and pressure distension by hand-held syringes to identify branches and overcome vasospasm [125,156,225,226].

Flushing the vessel with uncontrolled pressure results in high intraluminal pressure, which often exceeds 600 mmHg, leading to denudation of the endothelium that potentiates inflammatory responses [227-229]. Distention also induces damage to the medial smooth muscle layer that results in apoptosis and dedifferentiation of smooth muscle cells [230-232]. Given that the primary cause of graft failure is intimal hyperplasia, which represents a "response to injury" [233], limiting this "response" may influence the progression of cellular processes that lead to neointima formation and facilitate maximum re-adaptation of the conduit after arterialization.

The objective of this study was to demonstrate that pressure distention during vein graft preparation leads to endothelial injury and intimal thickening. We hypothesized that limiting pressure during distention reduces neointima thickening and preserves vascular functions of the grafts. We identified a pressure-limiting device that can be readily integrated into current distention technique and reduces intraluminal pressure.

METHODS

Material and reagents

All chemicals were purchased from Sigma (St. Louis, MO) unless otherwise specified.

Procurement of HSV

HSV grafts were obtained following approval of the Institutional Review Board of the Vanderbilt University Medical Center, Nashville, TN, from patients undergoing coronary artery bypass (CABG) bypass procedures. Segments were collected immediately after surgical harvest (unmanipulated, UM) and after manual distention (after distention, AD). An additional segment was collected immediately after further intraoperative manipulation according to the surgeon's discretion - such as use of skin markers and storage in a solution – prior to implantation (after manipulation, AM) from the same patients. Veins were collected in heparinized (10 units/ml) Plasmalyte solution and transported to the laboratory for immediate testing.

Collection of clinical demographic variables

Demographic variables were retrospectively collected, including age, gender, race, body mass index (BMI), medical comorbidities, preoperative laboratory values, preoperative medication regimen, and method of HSV harvest.

Procurement of porcine saphenous veins (PSV)

PSV were collected from euthanized animals from the animal surgical laboratory at Vanderbilt University Medical Center.   Animal procedures followed study protocols approved by Vanderbilt Institutional Animal Care and Use Committee (IACUC) and were in compliance with NIH guidelines for care and use of laboratory animals. PSV were dissected using an open harvest technique immediately after euthanasia, side branches ligated with 3-0 silk sutures, placed in heparinized Plasmalyte, and transported to laboratory for testing immediately.

Physiological measurements of vasocontractility and vasorelaxaiton

Force measurements were obtained using a Radnoti Glass Technology (Monrovia, CA) force transducer (159901A) interfaced with a Powerlab data acquisition system and Chart software (AD Instruments, Colorado Springs, CO) as described previously [234].   Briefly, 1-mm rings were cut from segments of saphenous veins, dissected free of fat and connective tissue, and then suspended in a muscle bath containing bicarbonate buffer (120 mM NaCl, 4.7 mM KCl, 1.0 mM $MgSO_4$, 1.0 mM NaH_2PO_4, 10 mM glucose, 1.5 mM $CaCl_2$, and 25 mM Na_2HCO_3, pH 7.4) equilibrated with 95% O_2 and 5% CO_2 at 37^oC for 2 hr.   Rings were contracted first with 110 mM KCl to determine smooth muscle functional viability. Tissues generating $\geq 0.02510^5 Newtons(N)/m^2$ of stress were considered viable and were further evaluated [125]. Viable tissues were then contracted with increasing doses (10^{-8}-10^{-6} M) of phenylephrine (PE), a

physiologic agonist. Optimal PE dose was determined as the concentration generating 70-80% of maximal 110 mM KCl-induced contraction. PE pre-contracted tissues were then treated with 5×10^{-7} M carbachol or increasing doses of sodium nitroprusside (SNP; 10^{-8}-10^{-5} M) to determine maximal endothelial-dependent and –independent relaxation response, respectively [182].

Measurement of intraluminal distension pressure in saphenous veins

Additional segments of HSV obtained after typical surgical manipulation (AM) were cannulated proximally and distally with an olive tip needle (Medtronic, Minneapolis, MN) and secured with 3-0 silk sutures on each end. A 30-ml hand-held syringe was connected to the distal end and the proximal end was connected to a manometer to record actual pressure attained during distension. For distension with limited pressure, a pressure release valve (Vasoprep Surgical, LLC, Morristown, NJ) was placed in-line between the distal olive tipped needle and the hand held syringe. Heparinized (10U/ml) Plasmalyte in the syringe was then injected to distend the segments and pressure was held for 2 min. For treatment of PSV, veins were divided into segments and randomly assigned to one of the three groups: non-distended (control), distended with unlimited pressure using a hand held syringe (distended), or distended with pressure release valve (PRV) as described for HSV.

Histomorphometric Analysis of PSV in an Organ Culture Model

Rings (1-2 mm in width) were cut from PSV segments before and after distension. Two rings were placed in 10% neutral buffered formalin to measure basal (pre-culture) intimal thickness. Two rings were placed in organ culture as described previously[235]. This method of vein culture has been validated as an *ex vivo* model system of the changes occurring *in vivo* and

has been used previously in our laboratory [235]. After 14 days, rings were fixed in 10% formalin and sent for histological preparation and Verhoeff-Van Gieson (VVG) at the Pathology Histochemistry Core at Vanderbilt University. Measurements of intimal and medial thickness were made on transverse sections of each vessel using a Zeiss Axiovert 200M microscope (Carl Zeiss, Thornwood, N.Y., USA) with a computerized image analysis system (Zeiss software and Adobe Photoshop) as described previously [234].

Immunohistochemistry

Tissue sections were stained using the avidin-biotinylated peroxidase complex (ABC) method (Vector lab, Burlingame, CA). Antigen was retrieved using citrate buffer (pH 6) at 95°C for 5 min (PSV) or 12 min (HSV). Endogenous peroxidase was blocked by immersing slides in 3% hydrogen peroxide for 15 min. Non-specific sites were blocked by incubating sections in 5% goat serum prior to incubation with primary antibodies against eNOS (Abcam, Cambridge, MA) or CD31 (DAKO, Carpinteria, CA) for 1hr at room temperature. Biotinylated IgG (Vector lab) was used as secondary antibody at 10 ng/ml. Immunostaining negative controls were performed by omitting the primary antibody.

Data analysis

Contractile response was defined by stress, calculated using force generated by tissues. Stress [10^5 Newtons (N)/m^2] = force (g) x0.0987/area, where area is equal to wet weight [(mg)/length (mm at maximal length)] divided by 1.055. Any tissue that generated stress of 0.025x10^5 N/m^2 or greater was considered functionally viable [125]. Data were reported as mean responses ± standard error of the mean. Paired t-tests or one-way ANOVA analyses were

conducted in order to determine the significance (*p* value) of each experiment. A *p* value <0.05 was considered statistically significant.

RESULTS

Patient demographics

The demographics variables for the patients from which saphenous veins were collected and are typical for patients undergoing CAGB procedures. See eTable 1.

Manual distension and physiologic function of HSV

Segments of HSV were collected either as unmanipulated (UM) or post-distension (AD) segments from the same patients (n=13). Intraoperative distension of vein grafts significantly reduced contraction to PE (1-5 x 10^{-6} M) in the AD segments (0.035±0.008 N/m^2) as compared with cognate UM segments (0.081±0.017 N/m^2, respectively) (Figure 1A). Vascular relaxation was similarly impaired by intraoperative distension. UM segments produced significantly greater endothelial-dependent (Figure 1B; 13.7±2.5%, vs. 5.3±2.3%) and -independent relaxation (Figure 1C; 61.6±7.5% vs. 41.9±8.3%) than the AD segments.

Functional integrity of both endothelium and smooth muscle was further reduced in segments after additional "back-table" manipulation which included marking with a surgical skin marker and storage prior to implantation (AM; n=6). PE-induced contraction was reduced to 0.011±0.006 N/m^2 (Figure 1A) and endothelial-dependent and –independent relaxation further decreased to -3.2±3.2% and 12.8±6.3%, respectively, (Figures 1B and 1C). There is a statistically significant difference as determined by one-way ANOVA for PE contraction ($F_{(2,28)}$=5.372, *p*=0.01), endothelial-dependent ($F_{(2,29)}$=8.448, *p*=0.0013) and independent

relaxation (F(2,25)=7.773, p=0.0024) among UM, AD and AM segments from the same patients (n=6).

Manual distension and endothelial integrity of HSV

   Immunohistochemical examination of the UM HSV segments revealed normal venous morphology and intact endothelium (Figure 2A & C). In contrast, intraoperative manual distension increased luminal area and damaged the endothelium of AD segments (Figure 2B & D). Strong CD31 staining was seen along the endothelium of the UM segments (Figure 2C), whereas distension resulted in patchy staining (Figure 2D), suggesting loss of endothelial integrity after manual distension.

Intraluminal pressure in HSV distended using a pressure release valve

   Intraluminal pressure, as measured by a manometer at the proximal end of remnant HSV (n=3), was 883.7±37.1 mmHg when vessels were "gently" distended without the pressure release valve using a 30ml syringe. When a pressure release valve (Figure 3 inset) calibrated to release at pressures greater than 2.5 psi (or 130 mmHg ± 10% crack tolerance) was used, intraluminal pressure was limited to 135.5±1.9 mmHg (Figure 3).

Physiologic functions of PSV distended with limited intraluminal pressure

Because the length of UM HSV segments obtained for this study were insufficient for distension, porcine saphenous vein (PSV), a conduit of similar caliber to HSV, was used (n=7). Manual distension reduced tissue response to PE when compared to the control segment (0.155±0.034 N/m^2 vs.0.235±0.039 N/m^2 Figure 4A). Contractile responses to PE did not

decrease when distension pressure was limited using the pressure release valve (PRV, 0.193 ± 0.024 N/m^2; Figure 4A). Manual distension reduced endothelial-dependent ($7.6\pm4.4\%$ vs.$61.9\pm10.2\%$ in Control; Figure 4B) and -independent relaxation in PSV ($42.1 \pm 3.4\%$ vs. $78.0\pm7.8\%$ in Control; Figure 4C). Limiting intraluminal pressure to 140mmHg with the pressure release valve preserved endothelial-dependent (PRV, $50.3 \pm 9.6\%$; Figure 4B) and – independent relaxation ($87.3\pm5.8\%$; Figure 4C).

Endothelial integrity of PSV distended with limited intraluminal pressure

Undistended PSV segments exhibited continuous intraluminal immunohistological staining for endothelial markers eNOS and CD31 (Figure 5A). PSV segments that were distended in the absence of the pressure release valve revealed patchy endothelial disruption (arrows; Figure 5A), whereas the endothelium remained intact in segments distended in the presence of the pressure release valve (Figure 5A).

Intimal thickening of PSV distended with limited intraluminal pressure

Basal intimal thickness of PSV was 31.3 ± 6.2 µm (n=8; Figure 5B). After 14 days of organ culture, intimal thickness was significantly greater in distended compared with control segments (Figure 5B). The intima thickness increased by 2.2 ± 0.8 µm and 15.0 ± 1.4 µm in control and distended groups, respectively. The use of the pressure release valve prevented significant increases in neointima formation (3.4 ± 0.8µm; Figure 5B).

Comments

Vein graft failure (VGF) following aortocoronary bypass procedures remains a significant problem. While it has been suggested that certain pre-operative characteristics, such as endothelial coverage, wall thickness and vein lumen diameter may predict long-term graft patency, conduit damage in the operative arena has been widely implicated in vein graft failure [236]. Minimizing vein graft manipulation and preserving vascular integrity using a "no-touch" technique have reportedly resulted in improved outcomes [224,237].

In the current study, HSV segments were collected from CABG patients prior to and after intraoperative manual distension and impact on vascular functions were examined. Distension under typical operating room conditions reduced contractile responses and impaired endothelial-dependent and -independent relaxation of the conduits (Figure 1), suggesting that the functional integrity of both the endothelium and medial layer is impacted. Because cellular viability correlates with functional viability of veins in a muscle bath [125], our results further implicate that the number of viable cells within the AD and AM segments were diminished by graft manipulation. Intraoperative manual distension resulted in structural damage, yielding a flaccid and distended appearance of the lumen (Figure 2B) and denudation of the endothelium of HSV grafts (Figure 2D).

Intra-luminal pressures > 600 mmHg have been recorded with hand held syringe distension [238,239] and we routinely detected $\geq$ 850 mmHg when uncontrolled manual distension was performed by different surgeons (Figure 3). Thus, the pressure generated by manual distension, while varied broadly and considered "gentle" by most surgeons, would most likely exceed pressures that have been reported to cause conduit damages [173,206,238,240,241]. There was a further reduction in contractile response and virtually abolished endothelial-dependent and –

168

independent relaxation of HSV collected after completion of graft preparation, suggesting that manipulation after manual distension caused additional damage to the vein graft (Figures 1). Observations from our previous study suggest that this reduction was not attributable to ischemia during storage of the graft in Plasmalyte [225]. Graft preparation techniques such as graft handling, storage in heparinized saline solution and marking with toxic surgical skin markers may contribute to this increased damage [156,175,211]. Collectively, preparation of the vein graft after harvest and prior to implantation significantly injures conduits that are implanted into the CABG patients.

Distension under uncontrolled pressure also reduced both endothelial-dependent and -independent functions (Figure 4) in the PSV. Moreover, distention damaged the endothelial layer (Figure 5) and led to increased neointima formation in cultured PSV (Figure 5), demonstrating a causal relationship between pressure distention, endothelial injury and neointima formation. Distension pressure of 300 mmHg has been shown to result in 50% and 200% growth of the intima in HSV in organ culture [242] and in the porcine carotid artery-jugular vein interposition bypass graft model [231], respectively.

Distension not only results in functional and morphological changes in the vessel wall, but also elicits a myriad of signaling cascades that promote neointima formation. Mechanical force induces phosphorylation of p38MAPK.[232] The acute loss of endothelial-independent function in the saphenous veins may be due to the p38MAPK-mediated degradation of the α-actin filament in the venous smooth muscle,[243] The loss of endothelial integrity also exposes the underlying medial layer to platelet aggregation and circulating growth modulators[244]. Venous smooth muscle cells dedifferentiate, leading to increases matrix metelloproteases activity and expression of cytoskeleton associated proteins which enable migration and proliferation of the

smooth muscle cells[230]. In additional, up-regulation of adhesion molecules, increased neutrophil adhesion by damaged endothelium, and the secretion of smooth muscle mitogens by inflammatory cells further extends the distention-induced damage to the medial layer[227,228,231,232].

While the 'no touch' harvest techniques have shown promise in reducing VGF [237], the adoption of this method is limited to a few centers; hence, the conventional harvest techniques dominate and manual distention remain common for CABG procedures likely due to , familiarity, reliability, and limited alternatives. Currently, there are two FDA-approved pressure-controlling devices: The Saphenous Vein Distension System (DMC Medical, County Clare, Ireland; www.dmcmedical.net) which comprises a pressure-limiting balloon connected to a syringe which relies on proper balloon inflation, vessel priming, and stopcock manipulation to deliver flushing fluid with designated pressure; and the Vasoshield Pressure Controlling Syringe (Maquet, Wayne, NJ; www.maquet.com) which delivers irrigation fluid at a selectable pressure that must be secured by a dial on a specialty syringe. These devices have not been widely incorporated into routine graft preparation possibly due to high cost and difficulty of use and the effect of these devices on vascular function and intimal hyperplasia prevention has not been reported.

Here, we identified a simple pressure release valve that limits distension pressure to ≤140 mmHg (Figure 3, inset). This valve can be placed in line with a standard syringe and vein cannula, requiring no special manipulation or change to current distention routines. When distended using the pressure release valve, PSV endothelium remained intact (Figure 5) and both endothelial-dependent and –independent function was preserved (Figure 4). More importantly, the use of this pressure release valve significantly reduced intimal thickening of PSV in organ culture compared to PSV distended manually (Figure 5). It is plausible that by protecting the

endothelial and smooth muscle cells from injury, the initial cell-mediated inciting factors leading to intimal hyperplasia, such as the release of mitogenic factors, recruitment of inflammatory factors by the endothelium, and the signaling cascades that ensues, were minimized. This is the first demonstration that limiting intraluminal pressure using a pressure release valve prevents intimal thickening, a crucial step in the progression of graft occlusion.

Limitations of this study include the lack of feasibility to test the pressure release valve in HSV, since only small segments of human tissue were available. PSV represents a reasonable model system to test vein graft preparation techniques. The organ culture model lacks in vivo elements (pressure, flow and exposure to blood components) that may influence the development of IH. Further work is needed to determine the effect of limiting intraluminal pressure on development of intimal hyperplasia in vivo.

Taken together, our findings demonstrate a causal association among manual pressure distension, endothelial and medial injury, and intimal hyperplasia. Prevention of endothelial denudation - hence dysfunction - and intimal hyperplasia can be achieved in a cost- and time-efficient manner using a simple pressure release valve that limits maximum sustained pressure during manual distension. This approach offers an effective mean to mitigate the damaging effects of manual distension during bypass procedures while preserving procedural efficiency and ability to use techniques that are familiar to surgeons. Results from this study warrant future clinical studies to determine whether this improved vein graft preparation will result in better graft patency.

Figure legends

Figure 1. Intraoperative manual distention and graft preparation impaired contractility and vasorelaxation of human saphenous vein grafts.

HSV were collected as unmanipulated segment (UM), post intraoperative manual distention (AD), or after surgical manipulation (AM). Phenylephrine-induced contraction (A), endothelial-dependent (B) and –independent relaxation (C) was determined in the muscle bath. *$p<0.05$ *vs* UM; # $p<0.05$ *vs* AM.

Figure 2. Intraoperative manual distention distorted luminal area and disrupt endothelial integrity of human saphenous veins.

Unmanipulated (UM) and post-distention (AD) segments were immunostained for CD31. Images were obtained at 50X (A, B) and 200X (C, D) magnifications. M=media, L= lumen.

Figure 3. A pressure release valve (PRV) reduced intraluminal pressure during manual distention of human saphenous veins.

Intraluminal pressure was measured by connecting the distal end of the conduits to a manometer during manual distention in the absence (Manual) or absence of the PRV.   * $p<0.05$. Inset: pressure release valve.

Figure 4. Use of the PRV during manual distention preserved contractility and vasorelaxation of porcine saphenous veins. PSV were left undistended (control), subjected to pressure distention in the absence (Distended) or presence of the PRV. Phenylephrine-induced

contraction (A), endothelial-dependent (B) and –independent relaxation (C) was determined in the muscle bath. *$p<0.05$ vs. Control; # $p<0.05$ vs. PRV; n.s., statistically non-significant.

Figure 5. Use of the PRV during manual distention preserved endothelial integrity and prevented intimal hyperplasia *in vitro* in porcine saphenous veins. Immediately after distention, PSV were fixed for eNOS and CD31 immunostaining (A). Organ cultured PSV were fixed for the Verhoeff Van Gieson's stain (VVG) to measure intimal thickness (B). Arrows indicate areas of disruption. *$p<0.05$ vs. Control; # $p<0.05$ vs. PRV. n.s., statistically non-significant. Bar = 100µm.

Figure 1

174
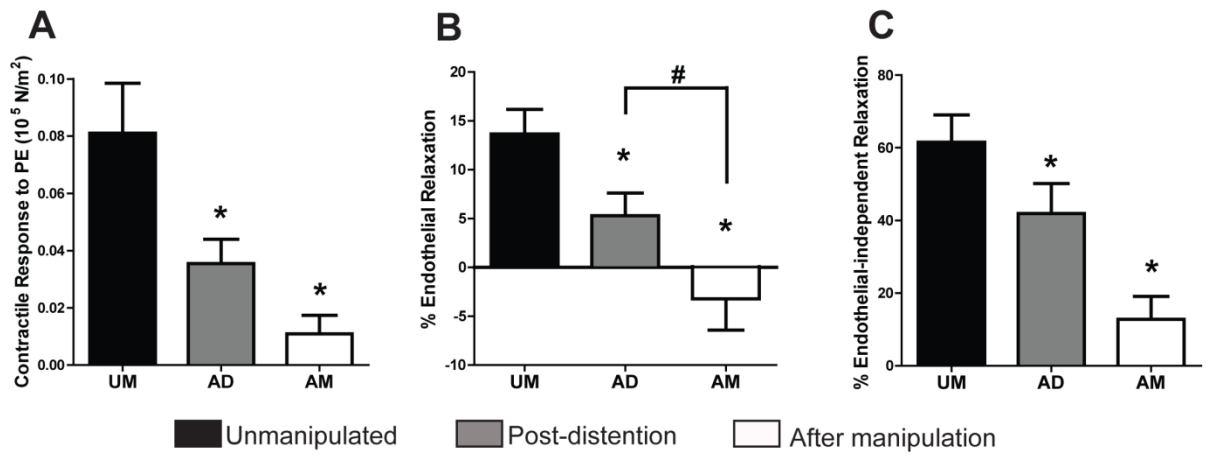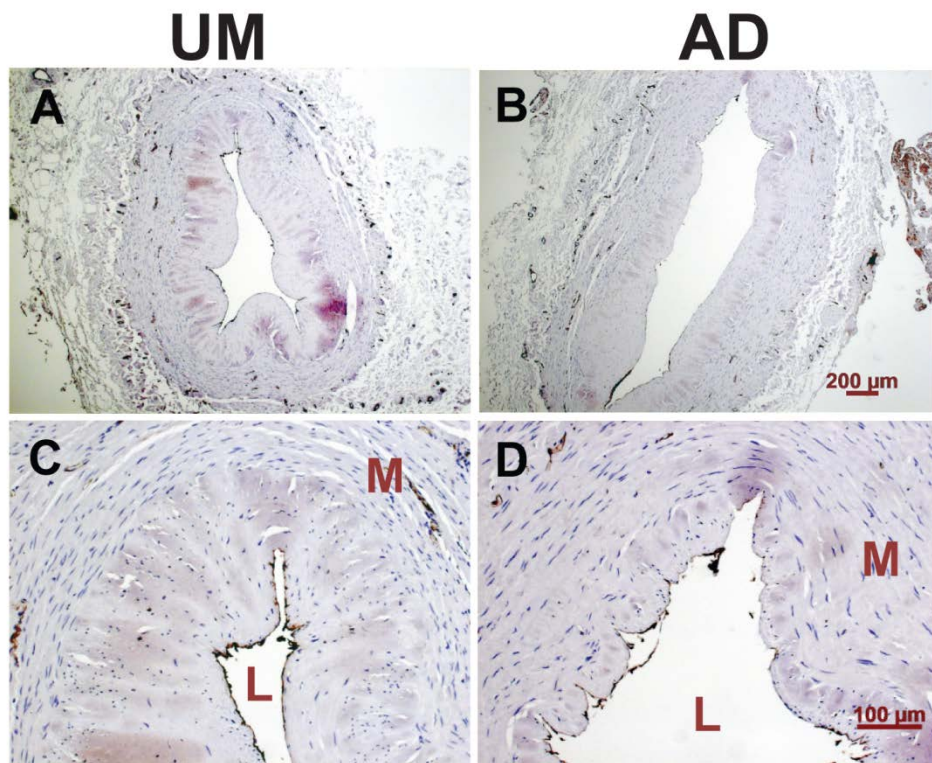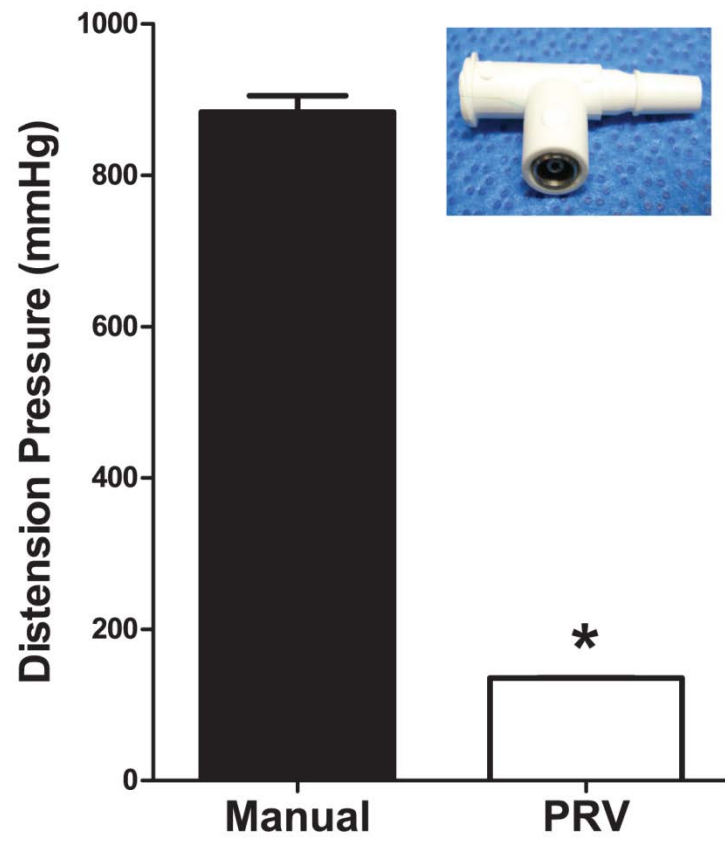
Figure 2

Figure 3

Figure 4
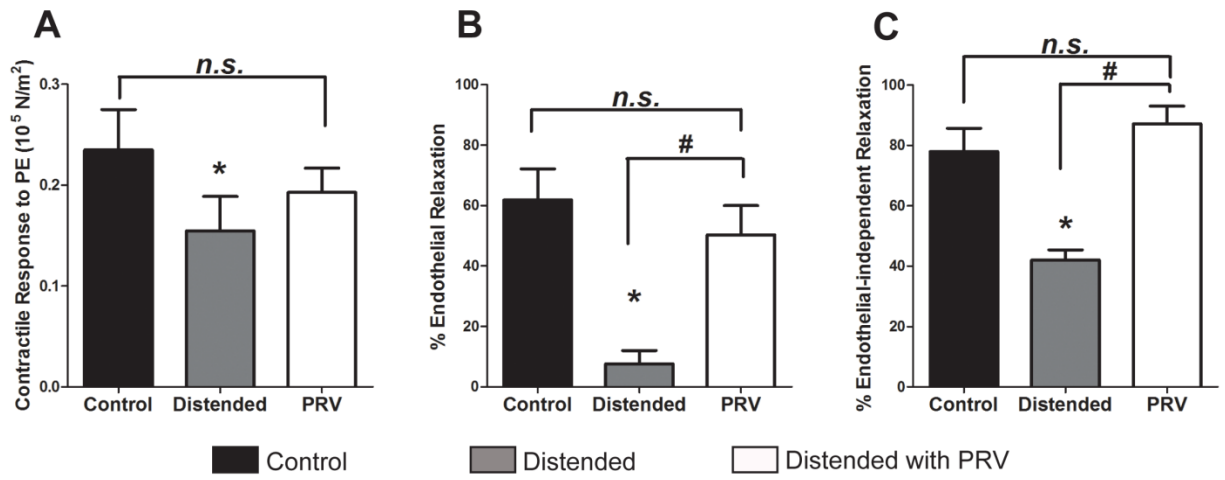
Figure 5
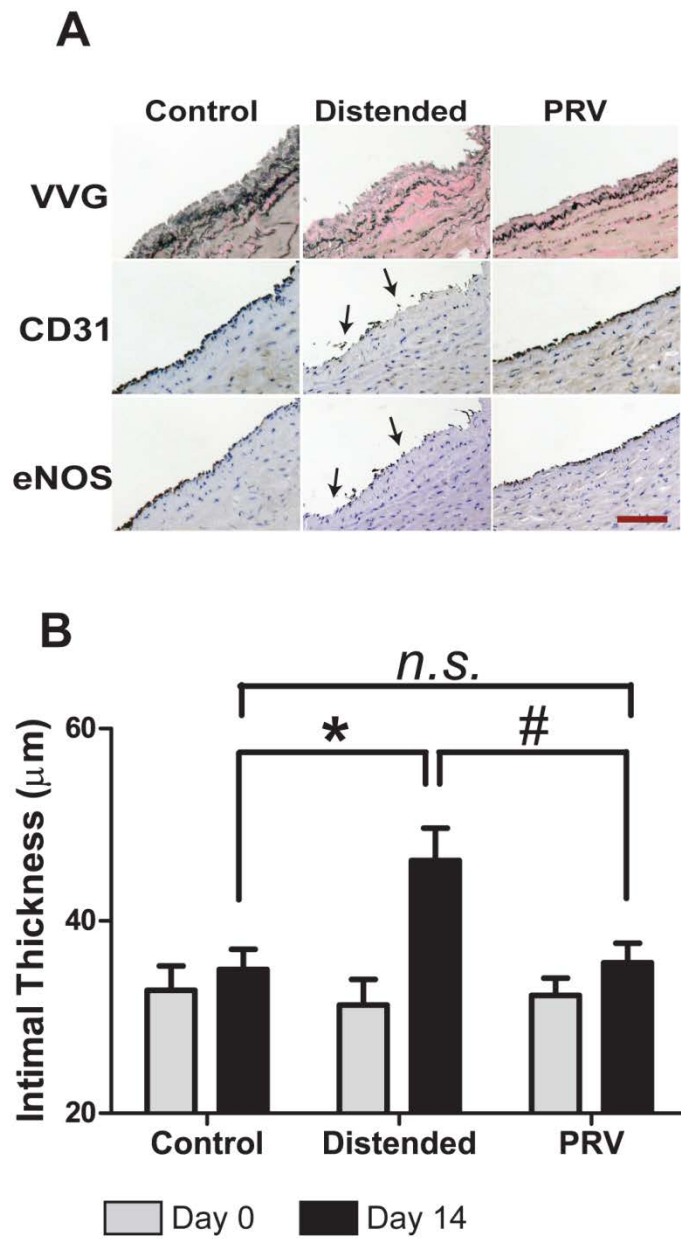
eTable 1. Patient demographic variables.

Age (years, mean±SD)	66.09±8.83
Gender (% male)	77%
Body Mass Index (mean±SD)	26.7±6.6
Race: Caucasian (%) / African American (%)	92% / 8%
History of smoking (%)	62%
Hypertension (%)	92%
Number of Antihypertensives (mean±SD)	1.62±0.76
ACE Inhibitor Use (%)	54%
Beta Blocker Use (%)	62%
Diabetes Mellitus (%)	69%
Preoperative Hemoglobin A1c (Mean±SD)	7.5±2.5
Hyperlipidemia (%)	77%
Statin Use (%)	69%
Left Ventricular Ejection Fraction (Mean)	51%±16
End Stage Renal Disease, Dialysis Dependent (%)	8%
Peripheral Vascular Disease (%)	8%

Additional Manuscript 5

Intimal Thickness Associates with Endothelial Dysfunction in Human Vein Grafts

Fan Dong Li, PhD[*,§]; Kevin W. Sexton, MD[*]; Kyle M. Hocking, BE[*]; Michael J. Osgood, MD [*], Susan Eagle, MD[*]; Joyce Cheung-Flynn, PhD[*]; Colleen M. Brophy, MD[¶,*], and Padmini Komalavilas, PhD[¶,*,]

INTRODUCTION

Human saphenous vein continues to be the most commonly used conduit for coronary artery bypass grafting and peripheral revascularization surgery [245]. Veins implanted into the arterial circulation undergo several changes and many develop neointimal hyperplasia within 4 to 6 weeks, leading to stenosis, thrombosis, and ultimately graft occlusion and graft failure [120,246,247]. The vein graft failure rate per patient in 1920 patients at 12 to 18 months in the Project of Ex-vivo Vein Graft Engineering via Transfection (PREVENT) IV trial was 45% [172].

Intimal hyperplasia remains the leading cause of vein graft failure [120,246]. Intimal hyperplasia is a complex process involving migration, proliferation, and phenotypic modulation of the vascular smooth muscle cells from a contractile to a synthetic phenotype, and extracellular matrix production [248,249]. Intimal hyperplasia in vein grafts occurs due to a combination of factors such as the vessel wall adapting to the higher intraluminal pressure of the arterial circulation, and the endothelial dysfunction associated with the harvest and surgical preparation of the vein for grafting.

Vein biopsy, angioscopy, and duplex ultrasonography have been proposed for quality assessment of human saphenous vein before implantation [250]. Histological and ultrastructural evaluation of the vein graft prior to implantation have demonstrated that morphological changes of the graft wall correlate significantly with early postoperative complications [223]. Preexisting

conditions such as low endothelial cell coverage, stenotic lesions of the lumen and thickness of the intima and media of the graft walls have been considered responsible for the early occlusion of grafts [223]. In fact, approximately 20% of human saphenous vein conduits used as vascular grafts are angioscopically normal, yet contain histological lesions such as atheromatous plaques, fibrous strands, and thickened valve cusps [250,251].

The endothelium is the primary regulator of vessel wall homeostasis, controlling vascular tone, the coagulation cascade, leukocyte recruitment, and angiogenesis. The term endothelial dysfunction has now become synonymous with reduced nitric oxide production [252,253]. Loss of endothelial nitric oxide production by denudation predisposes to vasospasm, vascular smooth muscle cell proliferation, platelet aggregation, leukocyte migration, and adhesion [254,255]. Endothelial cells play an important role in regulating intimal growth through a number of tonic growth-inhibitory mechanisms and the loss of endothelial layer markedly attenuates these growth-modulating effects [248,256]. Impaired brachial artery endothelial function has been demonstrated to predict long term cardiovascular events in patients with peripheral arterial disease [257]. Thus preservation of the endothelial layer during vein harvesting and preparation is of primary importance to reduce intimal hyperplasia.

To date, few studies have simultaneously evaluated basal thickness of the intima histologically and endothelial functional viability of human saphenous vein physiologically. In this study we explored the relationships between pre-existing basal intimal thickness, endothelial function, and intimal thickening in organ culture, an *in vitro* model system of vein graft intimal hyperplasia. We hypothesized that the basal intimal thickness could be used to predict endothelial dysfunction of human saphenous vein and the subsequent development of intimal hyperplasia.

181

MATERIALS AND METHODS

Chemicals and reagents

All chemicals were purchased from Sigma Aldrich (St. Louis, Mo) unless specified otherwise.

Procurement of human saphenous veins

Human saphenous vein samples were collected after obtaining approval of the Institutional Review Boards of the Vanderbilt University Medical Center and the VA Tennessee Valley Healthcare System, Nashville, TN. Forty-one unidentified segments of human saphenous veins and 5 Left Internal Mammary Arteries were obtained from patients that underwent coronary artery bypass graft surgery. For endothelial-dependent relaxation experiments, human saphenous vein segments (n=20) were collected immediately after surgical harvest without any further intraoperative manipulation ('back table' preparation, such as marking and manual distention) and tested within 2 hrs of surgical procurement. The human saphenous veins were harvested by open or minimally invasive endoscopic technique according to surgeon discretion and were stored in heparinized Plasmalyte (140 mEq sodium, 5 mEq potassium, 3 mEq magnesium, 98 mEq chloride, 27 mEq acetate, and 23 mEq gluconate, [Baxter Healthcare Corporation Deerfield, IL]) solution in the operating room. Upon gross inspection of the segments, regions of the grafts that were damaged intraoperatively by forceps or clamps were discarded. Only regions that were without damage or branches were used for physiological analysis since complete rings without branches gives consistent responses to contractile agonists and relaxants. All human saphenous vein segments were cut into sequential rings that were fixed in 10% buffered formalin immediately for basal intimal thickness. Additional rings were cut and placed into organ culture for 14 days prior to fixation in formalin. Human saphenous vein

182

segments were then dissected free of fat and connective tissue for determination of endothelial function in an organ bath.

Physiologic measurements of human saphenous veins

One-millimeter rings from the human saphenous vein segments were weighed and their lengths recorded. Rings were suspended in a muscle bath containing a bicarbonate buffer (120 mM NaCl, 4.7 mM KCl, 1.0 mM $MgSO_4$, 1.0 mM NaH_2PO_4, 10 mM glucose, 1.5 mM $CaCl_2$, and 25 mM Na_2HCO_3, pH 7.4), equilibrated with 95% oxygen and 5% carbon dioxide at 37°C. Each ring was progressively stretched to its optimal resting tension (approximately 1 g) that would produce a maximal response to contractile agonists as determined previously, then maintained at the resting tension and equilibrated for a minimum of 2 hours [125]. Force measurements were obtained using a Radnoti Glass Technology (Monrovia, CA) force transducer (159901A) interfaced with a Powerlab data acquisition system and Chart software (ADInstruments, Colorado Springs, CO). The rings were contracted first with 110 mM KCl (with equimolar replacement of NaCl in bicarbonate buffer) to determine functional viability of the smooth muscle. Any tissue failing to contract with KCl was considered non-functional and was not used in further experiments. Viable tissues were allowed to equilibrate in the bicarbonate solution for 30 minutes and were then exposed to the contractile agonist phenylephrine (10^{-6} M). Endothelial-dependent relaxation was determined by treating the pre-contracted veins with 5×10^{-7} M carbachol. In the absence of a functional endothelial layer carbachol will induce contraction instead of relaxation of human saphenous vein. Force was converted to stress using the equation [10^5 Newtons (N)/m^2] = force (g) x 0.0987 / area, where area is equal to the wet weight [(mg) / length (mm at maximal length] divided by 1.055. Percent

relaxation was measured as the change in stress compared to the maximal tension induced by phenylephrine as described previously [125].

Human saphenous vein organ culture and morphometric analyses

Two rings of human saphenous vein from each patient were placed in 10% neutral buffered formalin to measure the basal intimal thickness. To measure intima development *in vitro*, two rings were placed in 8-well chamber slides, and maintained in RPMI 1640 medium supplemented with 30% FBS (Gibco, Carlsbad, CA), 1% L-glutamine, and 1% penicillin/streptomycin for 14 days at 37˚C in an atmosphere of 5% CO_2 in air. The culture medium was replaced every 2-3 days. After 14 days rings were fixed in 10% formalin, and sent to the Pathology Histochemistry Core at Vanderbilt University or Wax-it Histology Services Inc. (Vancouver, BC, Canada) for histological preparation. The rings were embedded in paraffin, sectioned (5 µm) and multiple sections were stained using Verhoeff-Van Gieson to allow the visualization of the internal elastic lamina. Measurements of intimal and medial thickness were made on transverse sections of each vessel using a Zeiss Axiovert 200M microscope (Carl Zeiss, Thornwood, N.Y., USA) with a computerized image analysis system (Zeiss software and Adobe Photoshop). Intima was defined as tissue on the luminal side of the internal elastic lamina and the medial layer was contained within the intimal layer and the external elastic lamina. Four measurements were made in each image, one from each quadrant, for 3 vein sections for a total of 12 measurements made on each vein section. The mean intimal thickness was the average of 24 measurements on 6 histological sections from 2 vein rings from a single human saphenous vein sample.

Statistical Analysis

Data are reported as mean responses ± standard deviation. Unpaired *t* tests and correlation of intimal thickness to endothelial-dependent relaxation or post 14 day culture intimal thickening analysis were conducted using Graph Pad Prism software and the *P* values are reported (LaJolla, CA).

RESULTS

Variability in the pre-existing intimal thickness of human saphenous vein

Forty-one vein segments were collected in heparinized plasmalyte and were fixed in formalin stained using Verhoeff-Van Gieson stain and the pre-existing basal intimal thickness was measured. The basal intimal thickness of veins was highly variable with an average thickness of 85.96±53.00 µm and a range of 18.80 to 241.3 µm (n=41, Figure 1 and 2). When compared to human saphenous vein, left internal mammary artery had significantly lower basal intimal thickness (average 23.010±14.37 ☐m and a range 2).

Endothelial–dependent relaxation of human saphenous vein is highly variable

We next examined whether the intimal thickness had an effect on the functional viability of the human saphenous vein, particularly the endothelial function. One of the most reliable methods to assess endothelial function is endothelial-dependent relaxation which can be determined in a muscle bath; hence, endothelial-dependent relaxation was measured in each segment. Human saphenous vein segments were pre-contracted with phenylephrine (10^{-6} M) then treated with carbachol ($5x10^{-7}$ M) and maximal relaxation was determined (Figure 3A). The majority of the human saphenous vein segments collected as surgical remnants after 'back table' preparation (surgical preparation of the vein segment after harvest involving marking with a surgical marker to orient the vein and distention to locate the branches to prepare for grafting)

demonstrated very little to no endothelial-dependent relaxation (-2.12±1.886 % data not shown).

Thus, 20 human saphenous vein segments were collected immediately after harvest without any marking, distention, or other surgical preparation on the 'back table' to preserve the endothelial function. These human saphenous vein segments demonstrated various endothelial-dependent relaxation to carbachol with an average relaxation of 16.28±8.11 % and a range from 0 to 27.59 % relaxation, (n=20, Figure 3B). Endothelial-dependent relaxation of human saphenous vein was significantly lower than the left internal mammary artery, with a mean relaxation of 63.89±12.73% (n=5, Figure 3B).

Basal intimal thickness inversely correlates with endothelial-dependent relaxation

Linear regression analysis of basal intimal thickness versus endothelial-dependent relaxation had a significantly non-zero slope of -0.07264±0.028 (P=0.02 R^2=0.2634, Figure 4A), indicating a linear relationship between basal intimal thickness and endothelial-dependent relaxation. There was a sharp decline in endothelial function when basal intimal thickness exceeded 120 µm (Figure 4B). Human saphenous vein with intimal thickness greater than 120 µm had significantly less endothelial-dependent relaxation (8.90±6.32 % relaxation, n=6) than those with intimal thickness less than 120 µm (21.97±10.64 % relaxation n=14, P=0.0119, Figure 4B).

Basal intimal thickness correlates with intimal hyperplasia in organ culture

Since intimal hyperplasia is a leading cause of vein graft failure, we investigated whether the basal intimal thickness of the human saphenous vein segments had an effect on the development of intimal hyperplasia *in vitro* in an organ culture model. Human saphenous vein segments had an average basal intimal thickness of 73.82 µm and this thickness increased to 111.6 µm after 14 days in culture. There was a positive correlation with basal intimal thickness

and the intimal thickening developed during organ culture (Figure 5A). A linear regression between basal intimal thickness and intimal thickness after organ culture demonstrated a significant non-zero slope of 1.127 ± 0.1375 ($p<0.0001$, n=21 $R^2=0.7794$, Figure 5A). Greater basal I/M ratio also correlated with greater I/M ratio after organ culture, non-zero slope of 1.109 ± 0.1435 with $P<0.0001$ (n=21 $R^2=0.7587$, Figure 5B).

DISCUSSION

Failure of human saphenous vein bypass conduits due to intimal hyperplasia remains a major limitation of aortocoronary and peripheral vascular bypass procedures [172]. Studies have demonstrated that 20% of venous grafts occlude during the first year after bypass and 50% of venous grafts occlude 10 years later, while the remaining 50% had significant atheromatous lesions [258,259]. Several factors are considered responsible for the early occlusion of grafts and preoperative quality assessment of human saphenous vein for pre-existing wall changes has been proposed to predict later graft failure [251,260]. In this study we examined basal intimal thickness, endothelial function, and the effect of basal intimal thickness on intimal thickening *in vitro* on conduits used for coronary artery bypass grafting. We demonstrated that the pre-existing intimal thickness of the conduits used for revascularization was highly variable with a range from 18 ▢m to 241▢m (Figure 2) for the 41 vein segments analyzed. Using histologic assessment, Kanellaki-Kyparissi *et al*, reported that prior to implantation, 91% of vein grafts have varying degrees of histological lesions such as local thickening of the vessel wall especially the intima, which was accompanied by a decrease of endothelial coverage only in the stenotic part of the vessel [250]. By histological and ultrastructural evaluation of saphenous vein grafts before implantation Kokkona *et al* reported that patients with early postoperative complications had a mean intimal thickness of 206.56 ± 32.29 ▢m, while patient

complications had a mean intimal thickness of 67.44 ± 10.17 µmTo evaluate the viability

and quality of human saphenous vein used in coronary artery bypass operation, a functional

method was used since the presence of an intact structure of the vessel wall, as obtained by

morphological studies, does not necessarily imply normal function of the tissue [261].

Intimal hyperplasia in vein grafts is thought to be a response to injury. Several factors

have been shown to cause injury to the vein segments. Harvest and intraoperative handling of

vein grafts have been shown to decrease the expression of endothelial nitric oxide synthase and

nitric oxide production when compared to 'no-touch' method of vein harvest [[262]. We have

recently demonstrated that mechanical stretch and the use of surgical skin markers for labeling

markedly reduce the functional viability of human saphenous vein [125,156]. In this study, we found

that the majority of the vein segments that were collected after the 'back table' preparation had

little to no detectable endothelial-dependent relaxation. In contrast, those collected immediately

after harvest and prior to any further graft preparation displayed a significantly higher

endothelial-dependent relaxation suggesting that the endothelial dysfunction is further

exacerbated by the current, commonly employed surgical graft preparation methods. When the

histological morphology was compared to the endothelial-dependent relaxation we observed a

negative correlation, implying that preexisting thickness of the intima can influence the

functional state of the vein graft. Human saphenous vein with intimal thickness greater than 120

µm correlated with impaired endothelial–dependent relaxation (Figure 4). A link between

increased basal intimal thickness and postoperative complications has been reported earlier [223].

Our study demonstrates that increased basal intimal thickness also decreases endothelial-

dependent relaxation suggesting that endothelial dysfunction associated with increased thickness

may partly be responsible for the postoperative complications affecting their graft patency.

However, this needs to be confirmed with long term studies. Evaluation of vein grafts for basal intimal thickness may be useful to identify candidate conduits for coronary artery bypass surgery and may reduce postoperative complications.

Since intimal hyperplasia is associated with vein graft stenosis, we also examined the growth of intimal layer in a 14-day organ culture model. This *in vitro* model of intimal hyperplasia has been reported as a representative model of the changes that occur *in vivo* after vein graft transplantation [263], and had been used previously in our laboratory. We compared the basal intimal thickness to the subsequent increase in intimal thickening to determine the effect of basal intimal thickness on intimal hyperplasia formation. We observed a direct correlation between high basal intimal thickness and increased rate of intimal thickening *in vitro* when the vein segments were grown in culture with high serum (Figure 5). Our results demonstrated that higher basal intimal thickness of the vein potentiate the increase of intimal thickness in culture, suggesting that higher basal intimal thickness may predispose the graft to develop intimal hyperplasia more rapidly compared to vein grafts with lower basal intimal thickness. These results suggest that basal wall thickening of human saphenous vein could be a precursor for the formation of intimal hyperplasia in the arterialized graft.

Preservation of endothelium-dependent relaxation plays an important role in inhibiting the development of intimal hyperplasia of vein graft. There is a direct link between the degree of preservation of nitric oxide function in vein grafts and the magnitude of intimal hyperplasia formation [264]. Analysis of retrieved vein grafts (ranged from 5-17 years) from patients undergoing repeat coronary artery bypass grafting demonstrated that grafts with the most pronounced intimal hyperplasia exhibited the least amount of endothelium-dependent relaxation. Taken together, it is plausible that the loss of endothelial nitric oxide synthase expression in the

189

grafts is the central contributor to the loss of endothelial-dependent relaxation along with increased intimal thickness.

The limitations of this study are that tissues were de-identified and the demographic information of the patients was not available, hence we were not able to determine the effect of basal intimal thickness on graft patency in these patients. Also, intimal thickness could not be correlated to drug use in these patients. We did not measure endothelial function along the entire length of the conduit; therefore we did not determine whether the correlation of intimal thickness to endothelial-dependent relaxation was uniform along the conduit or unique to the region that we tested. Since the majority of the veins were harvested by endoscopy we have not directly compared the endothelial dependent relaxation and intimal thickness of veins harvested conventionally versus endoscopically in this investigation. Vein grafts harvested endoscopically undergo more injury and have inferior patency compared to veins harvested by open method [26]. Besides intimal thickening other factors such as harvesting techniques, intrinsic vasospasm, degree of heart failure, peripheral vessel disease and patient demographics may also account for the variability in endothelial-dependent relaxation. Even though evaluation of the vein grafts may help identify ideal conduits for coronary artery bypass grafting and for lower extremity arterial grafts, this study does not provide a "real-time" method of assessing conduits.

In summary these data suggest that basal intimal thickness greater than 120 µm is a predictor of human saphenous vein endothelial dysfunction. Greater basal intimal thickness also leads to increased intimal hyperplasia formation in organ culture suggesting that higher basal intimal thickness may predispose the vein graft to develop intimal hyperplasia more rapidly compared to vein grafts with lower basal intimal thickness. Further studies are needed to

determine optimal methods of preoperative vein assessment. The mechanism of the reduction of

endothelial-dependent relaxation due to increased intimal thickening is not known. Future

studies are also needed to determine if any correlation exists between basal intimal thickness and

clinical demographics or clinical outcomes.

Figure legends:
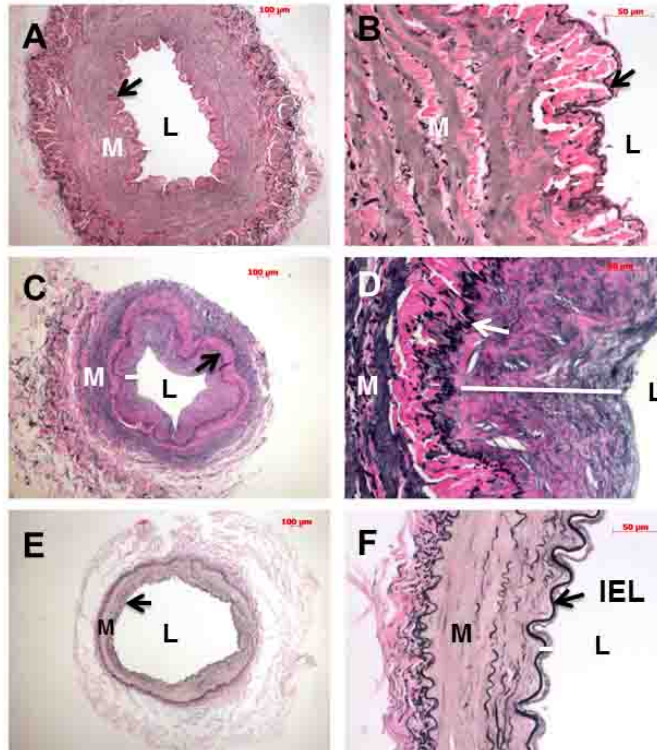
FIGURE 1. Basal intimal thickening in human saphenous veins and left internal mammary artery. Human saphenous vein and left internal mammary artery rings were fixed in formalin, sectioned and stained with Verhoeff-Van Gieson stain and examined by microscopy. Representative images of two saphenous vein segments with thin (A, 5x image and B, 40x image) and thick (C, 5x image and D, 40x image) intima and a left internal mammary artery (E, 5X image and F, 40X image) stained with Verhoeff-Van Gieson. In the image: L=lumen, IEL=internal elastic lamina (arrow), M=media, white line=thickness of intima. Scale bar=100 µm for 5x images and 50 µm for 40X images.
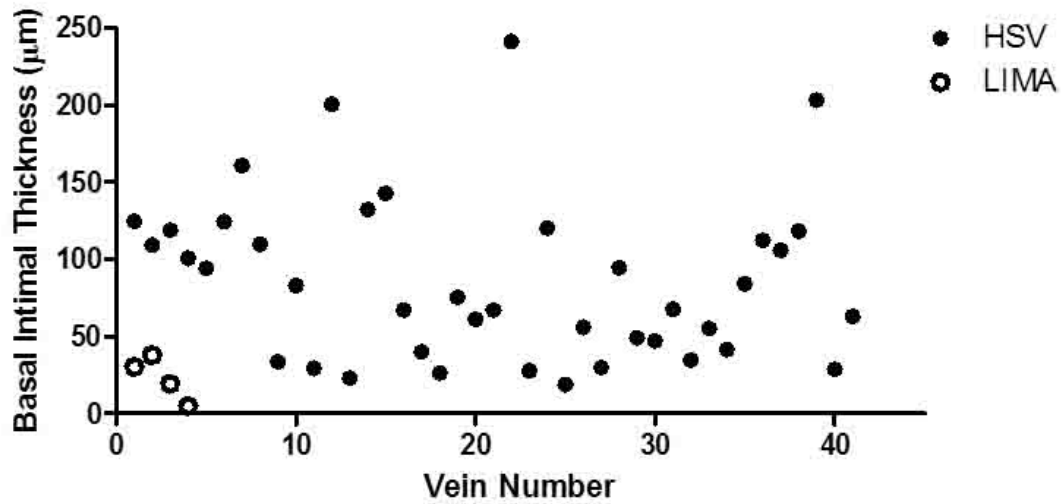
FIGURE 2. Variability of intimal thickening in Human saphenous veins and left internal mammary artery: Human saphenous vein (HSV, n=41) and left internal mammary artery (LIMA, n=4) rings were fixed in formalin, sectioned and stained with Verhoeff-Van Gieson stain and examined by microscopy. Scatter plot demonstrating the variability of basal intimal thickness measured as an average from two vein segments from each patient as described in the methods section.
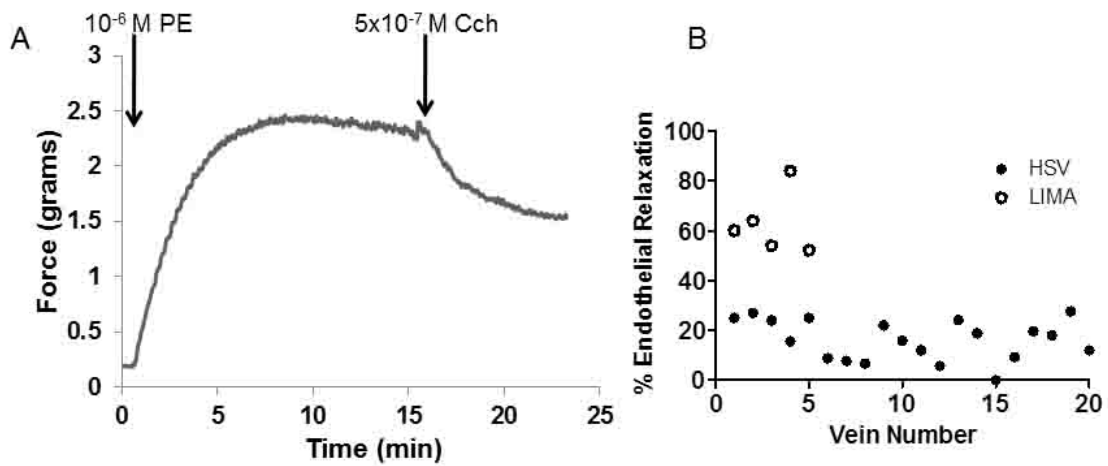
FIGURE 3. Variability of endothelial-dependent relaxation in human saphenous veins.

Human saphenous vein and left internal mammary artery segments were collected immediately

after harvest and subjected to physiologic measurement in a muscle bath. Endothelial-dependent

relaxation was measured by contracting with 10^{-6} M phenylephrine (PE) and relaxing with 5×10^{-7}

M carbachol (Cch). A) Representative tracing of pre-contracted HSV relaxed with carbachol to

24.22%. B) Endothelial-dependent relaxation variability for saphenous veins (HSV) and left

internal mammary artery (LIMA).
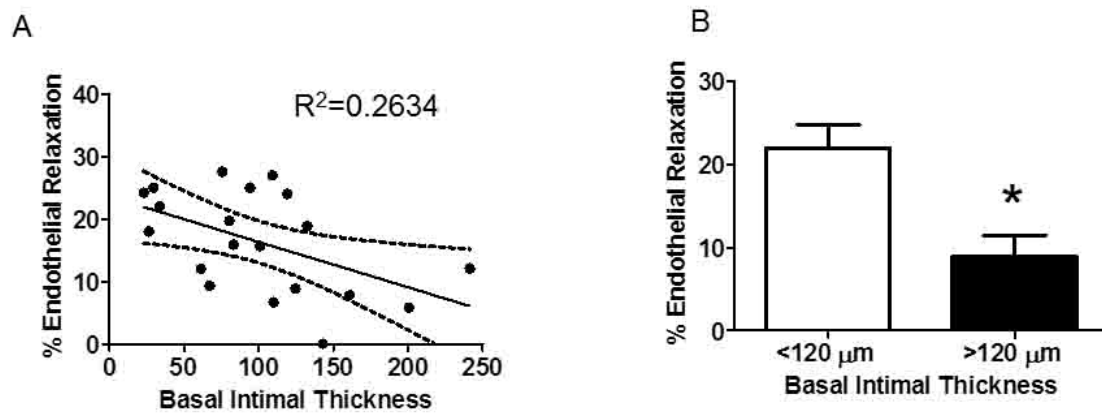
FIGURE 4. Endothelial-dependent relaxation of human saphenous vein correlates

negatively with increase in basal intimal thickness. Human saphenous vein segments obtained

from coronary artery bypass surgery were subjected to physiologic measurement of endothelial-

dependent relaxation to carbachol in a muscle bath. Histological examination using the Verhoeff-

Van Gieson stain was used for the visualization of the internal elastic lamina and the basal

intimal thickening was measured. A) A linear regression of the percent endothelial-dependent

relaxation as a function of basal intimal thickness was run yielding R^2=0.2634, (P=0.02, n=20).

B) Vein segments with basal intimal thickening greater than 120 µm had impaired endothelial

dependent relaxation (P=0.0119, n = 20).
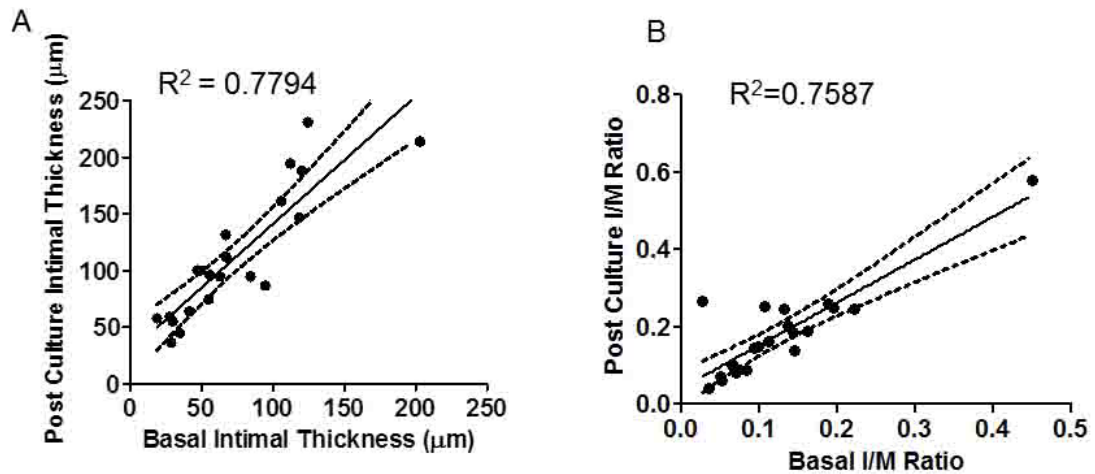
FIGURE 5. Intimal thickening in the basal state predicts degree of thickening in organ culture. Human saphenous vein segments were obtained from coronary artery bypass surgery and were cultured in RPMI medium with 30% serum for 14 days (post culture). Rings were fixed, sectioned, stained with Verhoeff-Van Gieson and analyzed by microscopy and intimal thickness was measured and compared to the intimal thickness before culture. A) Linear Regression of the change in intimal thickness from basal to post 14 day culture $R^2 = 0.7794$ (*P*<0.0001, n=21) shows a positive correlation where a higher basal intimal thickening leads to a higher intimal thickening in culture. B) Linear Regression of the change in intimal to medial ratio from basal to post 14 day culture $R^2=0.7587$ (*P*<0.0001, n=21) also showing a positive correlation between basal intimal thickening and intimal thickening in culture.

REFERENCES

1.   Optix I. FluoroPlex. 2010.

2.   Lee KH, Lukovits T, Friedman JA. "Triple-H" therapy for cerebral vasospasm following subarachnoid hemorrhage. Neurocrit Care 2006;4:68-76.

3.   Teunissen LL, Rinkel GJ, Algra A, van Gijn J. Risk factors for subarachnoid hemorrhage: a systematic review. Stroke 1996;27:544-9.

4.   Powell J, Kitchen N, Heslin J, Greenwood R. Psychosocial outcomes at three and nine months after good neurological recovery from aneurysmal subarachnoid haemorrhage: predictors and prognosis. J Neurol Neurosurg Psychiatry 2002;72:772-81.

5.   Hellinger FR, Bloor BM, Mc CJ. Total cerebral blood flow and oxygen consumption using the dye-dilution method. A study of occulusive arterial disease and cerebral infarction. Journal of neurosurgery 1962;19:964-70.

6.   Morawetz RB, DeGirolami U, Ojemann RG, Marcoux FW, Crowell RM. Cerebral blood flow determined by hydrogen clearance during middle cerebral artery occlusion in unanesthetized monkeys. Stroke; a journal of cerebral circulation 1978;9:143-9.

7.   Morawetz RB, Jones TH, Ojemann RG, Marcoux FW, DeGirolami U, Crowell RM. Regional cerebral blood flow during temporary middle cerebral artery occlusion in waking monkeys. Acta Neurol Scand Suppl 1977;64:114-5.

8.   Bederson JB, Germano IM, Guarino L. Cortical blood flow and cerebral perfusion pressure in a new noncraniotomy model of subarachnoid hemorrhage in the rat. Stroke 1995;26:1086-91; discussion 91-2.

9.   Rosner MJ. Introduction to cerebral perfusion pressure management. Neurosurg Clin N Am 1995;6:761-73.

10.   Lee KH, Lukovits T, Friedman JA. "Triple-H" therapy for cerebral vasospasm following subarachnoid hemorrhage. Neurocritical care 2006;4:68-76.

11.   Murphy RA, Rembold CM. The latch-bridge hypothesis of smooth muscle contraction. Can J Physiol Pharmacol 2005;83:857-64.

12.   Karaki H, Ozaki H, Hori M, et al. Calcium movements, distribution, and functions in smooth muscle. Pharmacol Rev 1997;49:157-230.

13.   Kamm KE, Stull JT. The function of myosin and myosin light chain kinase phosphorylation in smooth muscle. Annu Rev Pharmacol Toxicol 1985;25:593-620.

14.   Wettstein G, Bellaye PS, Micheau O, Bonniaud P. Small heat shock proteins and the cytoskeleton: an essential interplay for cell integrity? Int J Biochem Cell Biol 2012;44:1680-6.

15.   Kai Y, Maeda Y, Sasaki T, Kanaide H, Hirano K. Basic and translational research on proteinase-activated receptors: the role of thrombin receptor in cerebral vasospasm in subarachnoid hemorrhage. Journal of pharmacological sciences 2008;108:426-32.

16.   Carr KR, Zuckerman SL, Mocco J. Inflammation, Cerebral Vasospasm, and Evolving Theories of Delayed Cerebral Ischemia. Neurol Res Int 2013;2013:506584.

17.   Ciurea AV, Palade C, Voinescu D, Nica DA. Subarachnoid hemorrhage and cerebral vasospasm - literature review. J Med Life 2013;6:120-5.

18.   Macdonald RL, Weir BK. A review of hemoglobin and the pathogenesis of cerebral vasospasm. Stroke; a journal of cerebral circulation 1991;22:971-82.

19.   Choudhri TF, Hoh BL, Solomon RA, Connolly ES, Jr., Pinsky DJ. Use of a spectrophotometric hemoglobin assay to objectively quantify intracerebral hemorrhage in mice. Stroke; a journal of cerebral circulation 1997;28:2296-302.

20.   Osgood MJ, Hocking KM, Voskresensky IV, et al. Surgical vein graft preparation promotes cellular dysfunction, oxidative stress, and intimal hyperplasia in human saphenous vein. J Vasc Surg 2013.

21.   Miao FJ, Lee TJ. Effects of bilirubin on cerebral arterial tone in vitro. J Cereb Blood Flow Metab 1989;9:666-74.

22.   Fujiwara S, Kassell NF, Sasaki T, Nakagomi T, Lehman RM. Selective hemoglobin inhibition of endothelium-dependent vasodilation of rabbit basilar artery. Journal of neurosurgery 1986;64:445-52.

23.   Ross R. Platelet-derived growth factor. Lancet 1989;1:1179-82.

24.   Shimokawa H, Ito A, Fukumoto Y, et al. Chronic treatment with interleukin-1 beta induces coronary intimal lesions and vasospastic responses in pigs in vivo. The role of platelet-derived growth factor. J Clin Invest 1996;97:769-76.

25.   Onda H, Kasuya H, Takakura K, et al. Identification of genes differentially expressed in canine vasospastic cerebral arteries after subarachnoid hemorrhage. J Cereb Blood Flow Metab 1999;19:1279-88.

26.   Dumont AS, Dumont RJ, Chow MM, et al. Cerebral vasospasm after subarachnoid hemorrhage: putative role of inflammation. Neurosurgery 2003;53:123-33; discussion 33-5.

27.   Rowland MJ, Hadjipavlou G, Kelly M, Westbrook J, Pattinson KT. Delayed cerebral ischaemia after subarachnoid haemorrhage: looking beyond vasospasm. Br J Anaesth 2012;109:315-29.

28.   Zhou C, Yamaguchi M, Colohan AR, Zhang JH. Role of p53 and apoptosis in cerebral vasospasm after experimental subarachnoid hemorrhage. J Cereb Blood Flow Metab 2005;25:572-82.

29.   Sun Y, Jin K, Xie L, et al. VEGF-induced neuroprotection, neurogenesis, and angiogenesis after focal cerebral ischemia. J Clin Invest 2003;111:1843-51.

30.   Ostrowski RP, Colohan AR, Zhang JH. Mechanisms of hyperbaric oxygen-induced neuroprotection in a rat model of subarachnoid hemorrhage. J Cereb Blood Flow Metab 2005;25:554-71.

31.   Bederson JB, Levy AL, Ding WH, et al. Acute vasoconstriction after subarachnoid hemorrhage. Neurosurgery 1998;42:352-60; discussion 60-2.

32.   Kerz T, Boor S, Beyer C, Welschehold S, Schuessler A, Oertel J. Effect of intraarterial papaverine or nimodipine on vessel diameter in patients with cerebral vasospasm after subarachnoid hemorrhage. Br J Neurosurg 2012;26:517-24.

33.   Kaku Y, Yonekawa Y, Tsukahara T, Kazekawa K. Superselective intra-arterial infusion of papaverine for the treatment of cerebral vasospasm after subarachnoid hemorrhage. J Neurosurg 1992;77:842-7.

34.   Numaguchi Y, Zoarski GH, Clouston JE, et al. Repeat intra-arterial papaverine for recurrent cerebral vasospasm after subarachnoid haemorrhage. Neuroradiology 1997;39:751-9.

35.   Grimes CM. Cerebral balloon angioplasty for treatment of vasospasm after subarachnoid hemorrhage. Heart Lung 1991;20:431-5.

36.   Bulters DO, Birch AA, Hickey E, et al. A randomized controlled trial of prophylactic intra-aortic balloon counterpulsation in high-risk aneurysmal subarachnoid hemorrhage. Stroke 2013;44:224-6.

37.   Fujii Y, Takahashi A, Yoshimoto T. Effect of balloon angioplasty on high grade symptomatic vasospasm after subarachnoid hemorrhage. Neurosurg Rev 1995;18:7-13.

38.   Gules I, Satoh M, Clower BR, Nanda A, Zhang JH. Comparison of three rat models of cerebral vasospasm. Am J Physiol Heart Circ Physiol 2002;283:H2551-9.

39.   Furnish EJ, Brophy CM, Harris VA, et al. Treatment with transducible phosphopeptide analogues of the small heat shock-related protein, HSP20, after experimental subarachnoid hemorrhage: prevention and reversal of delayed decreases in cerebral perfusion. J Neurosurg 2010;112:631-9.

40.   Suzuki H, Hasegawa Y, Kanamaru K, Zhang JH. Mitogen-activated protein kinases in cerebral vasospasm after subarachnoid hemorrhage: a review. Acta Neurochir Suppl 2011;110:133-9.

41.   Somlyo AP, Somlyo AV. Ca2+ sensitivity of smooth muscle and nonmuscle myosin II: modulated by G proteins, kinases, and myosin phosphatase. Physiol Rev 2003;83:1325-58.

42.   Horowitz A, Menice CB, Laporte R, Morgan KG. Mechanisms of smooth muscle contraction. Physiol Rev 1996;76:967-1003.

43. Kamm KE, Stull JT. The function of myosin and myosin light chain kinase phosphorylation in smooth muscle. Annu Rev Pharmacol Toxicol 1985;25:593-620.

44. McDaniel NL, Chen XL, Singer HA, Murphy RA, Rembold CM. Nitrovasodilators relax arterial smooth muscle by decreasing [Ca2+]i and uncoupling stress from myosin phosphorylation. Am J Physiol 1992;263:C461-7.

45. Dillon PF, Aksoy MO, Driska SP, Murphy RA. Myosin phosphorylation and the cross-bridge cycle in arterial smooth muscle. Science 1981;211:495-7.

46. Morgan JP, Morgan KG. Vascular smooth muscle: the first recorded Ca2+ transients. Pflugers Arch 1982;395:75-7.

47. Woodrum DA, Brophy CM, Wingard CJ, Beall A, Rasmussen H. Phosphorylation events associated with cyclic nucleotide-dependent inhibition of smooth muscle contraction. Am J Physiol 1999;277:H931-9.

48. Gerthoffer WT, Murphy RA. Myosin phosphorylation and regulation of cross-bridge cycle in tracheal smooth muscle. Am J Physiol 1983;244:C182-7.

49. Gunst SJ. Effects of muscle length and load on intracellular Ca2+ in tracheal smooth muscle. Am J Physiol 1989;256:C807-12.

50. Gunst SJ, Bandyopadhyay S. Contractile force and intracellular Ca2+ during relaxation of canine tracheal smooth muscle. Am J Physiol 1989;257:C355-64.

51. Singer HA, Kamm KE, Murphy RA. Estimates of activation in arterial smooth muscle. Am J Physiol 1986;251:C465-73.

52. Driska SP, Aksoy MO, Murphy RA. Myosin light chain phosphorylation associated with contraction in arterial smooth muscle. Am J Physiol 1981;240:C222-33.

53. Rembold CM, Murphy RA. Histamine concentration and Ca2+ mobilization in arterial smooth muscle. Am J Physiol 1989;257:C122-8.

54. Ratz PH, Murphy RA. Contributions of intracellular and extracellular Ca2+ pools to activation of myosin phosphorylation and stress in swine carotid media. Circ Res 1987;60:410-21.

55. Rembold CM, Foster DB, Strauss JD, Wingard CJ, Eyk JE. cGMP-mediated phosphorylation of heat shock protein 20 may cause smooth muscle relaxation without myosin light chain dephosphorylation in swine carotid artery. J Physiol 2000;524 Pt 3:865-78.

56. Lincoln TM, Dey N, Sellak H. Invited review: cGMP-dependent protein kinase signaling mechanisms in smooth muscle: from the regulation of tone to gene expression. J Appl Physiol 2001;91:1421-30.

57. Morgado M, Cairrao E, Santos-Silva AJ, Verde I. Cyclic nucleotide-dependent relaxation pathways in vascular smooth muscle. Cell Mol Life Sci 2012;69:247-66.

58.   Karaki H. The intracellular calcium-force relationship in vascular smooth muscle. Time- and stimulus-dependent dissociation. Am J Hypertens 1990;3:253S-6S.

59.   Gunst SJ, Zhang W. Actin cytoskeletal dynamics in smooth muscle: a new paradigm for the regulation of smooth muscle contraction. Am J Physiol Cell Physiol 2008;295:C576-87.

60.   Reinhard M, Halbrugge M, Scheer U, Wiegand C, Jockusch BM, Walter U. The 46/50 kDa phosphoprotein VASP purified from human platelets is a novel protein associated with actin filaments and focal contacts. EMBO J 1992;11:2063-70.

61.   Salinthone S, Tyagi M, Gerthoffer WT. Small heat shock proteins in smooth muscle. Pharmacol Ther 2008;119:44-54.

62.   Salinthone S, Tyagi M, Gerthoffer WT. Small heat shock proteins in smooth muscle. Pharmacol Ther 2008;119:44-54.

63.   Beall A, Bagwell D, Woodrum D, et al. The small heat shock-related protein, HSP20, is phosphorylated on serine 16 during cyclic nucleotide-dependent relaxation. J Biol Chem 1999;274:11344-51.

64.   Dreiza CM, Brophy CM, Komalavilas P, et al. Transducible heat shock protein 20 (HSP20) phosphopeptide alters cytoskeletal dynamics. Faseb J 2005;19:261-3. .

65.   Rembold CM, Foster DB, Strauss JD, Wingard CJ, Eyk JE. cGMP-mediated phosphorylation of heat shock protein 20 may cause smooth muscle relaxation without myosin light chain dephosphorylation in swine carotid artery. The Journal of physiology 2000;524 Pt 3:865-78.

66.   Yoshino Y, Sakurai W, Morimoto S, Watanabe M. Synthetic peptides of actin-tropomyosin binding region of troponin I and heat shock protein 20 modulate the relaxation process of skinned preparations of taenia caeci from guinea pig. Jpn J Physiol 2005;55:373-8.

67.   Fuchs LC, Giulumian AD, Knoepp L, et al. Stress causes decrease in vascular relaxation linked with altered phosphorylation of heat shock proteins. Am J Physiol Regul Integr Comp Physiol 2000;279:R492-8.

68.   Komalavilas P, Penn RB, Flynn CR, et al. The small heat shock-related protein, HSP20, is a cAMP-dependent protein kinase substrate that is involved in airway smooth muscle relaxation. Am J Physiol Lung Cell Mol Physiol 2008;294:L69-78.

69.   Bamburg JR. Proteins of the ADF/cofilin family: essential regulators of actin dynamics. Annu Rev Cell Dev Biol 1999;15:185-230.

70.   Chitaley K, Chen L, Galler A, Walter U, Daum G, Clowes AW. Vasodilator-stimulated phosphoprotein is a substrate for protein kinase C. FEBS Lett 2004;556:211-5.

71.   Kim HR, Graceffa P, Ferron F, et al. Actin polymerization in differentiated vascular smooth muscle cells requires vasodilator-stimulated phosphoprotein. American journal of physiology Cell physiology 2010;298:C559-71.

72. Brindle NP, Holt MR, Davies JE, Price CJ, Critchley DR. The focal-adhesion vasodilator-stimulated phosphoprotein (VASP) binds to the proline-rich domain in vinculin. The Biochemical journal 1996;318 (Pt 3):753-7.

73. Harbeck B, Huttelmaier S, Schluter K, Jockusch BM, Illenberger S. Phosphorylation of the vasodilator-stimulated phosphoprotein regulates its interaction with actin. The Journal of biological chemistry 2000;275:30817-25.

74. Huang Y, Day RN, Gunst SJ. Vinculin phosphorylation at Tyr1065 regulates vinculin conformation and tension development in airway smooth muscle tissues. The Journal of biological chemistry 2014;289:3677-88.

75. Sun Z, Huang S, Li Z, Meininger GA. Zyxin is involved in regulation of mechanotransduction in arteriole smooth muscle cells. Front Physiol 2012;3:472.

76. Convertine AJ, Benoit DS, Duvall CL, Hoffman AS, Stayton PS. Development of a novel endosomolytic diblock copolymer for siRNA delivery. J Control Release 2009;133:221-9.

77. McGregor DP. Discovering and improving novel peptide therapeutics. Curr Opin Pharmacol 2008;8:616-9.

78. Kaspar AA, Reichert JM. Future directions for peptide therapeutics development. Drug Discov Today 2013;18:807-17.

79. Kaplan IM, Wadia JS, Dowdy SF. Cationic TAT peptide transduction domain enters cells by macropinocytosis. J Control Release 2005;102:247-53.

80. Ho A, Schwarze SR, Mermelstein SJ, Waksman G, Dowdy SF. Synthetic protein transduction domains: enhanced transduction potential in vitro and in vivo. Cancer Res 2001;61:474-7.

81. Rembold CM, Murphy RA. Muscle length, shortening, myoplasmic [Ca2+], and activation of arterial smooth muscle. Circ Res 1990;66:1354-61.

82. Lu Z, Swartz DR, Metzger JM, Moss RL, Walker JW. Regulation of force development studied by photolysis of caged ADP in rabbit skinned psoas fibers. Biophysical journal 2001;81:334-44.

83. Gerthoffer WT, Gunst SJ. Invited review: focal adhesion and small heat shock proteins in the regulation of actin remodeling and contractility in smooth muscle. J Appl Physiol 2001;91:963-72.

84. Rembold CM, Tejani AD, Ripley ML, Han S. Paxillin phosphorylation, actin polymerization, noise temperature, and the sustained phase of swine carotid artery contraction. Am J Physiol Cell Physiol 2007;293:C993-1002.

85. Turner CE. Paxillin and focal adhesion signalling. Nat Cell Biol 2000;2:E231-6.

86. Pavalko FM, Adam LP, Wu MF, Walker TL, Gunst SJ. Phosphorylation of dense-plaque proteins talin and paxillin during tracheal smooth muscle contraction. Am J Physiol 1995;268:C563-71.

87. Butt E, Abel K, Krieger M, et al. cAMP- and cGMP-dependent protein kinase phosphorylation sites of the focal adhesion vasodilator-stimulated phosphoprotein (VASP) in vitro and in intact human platelets. J Biol Chem 1994;269:14509-17.

88. Persechini A, Kamm KE, Stull JT. Different phosphorylated forms of myosin in contracting tracheal smooth muscle. J Biol Chem 1986;261:6293-9.

89. Komalavilas P, Mehta S, Wingard CJ, et al. PI3-kinase/Akt modulates vascular smooth muscle tone via cAMP signaling pathways. J Appl Physiol 2001;91:1819-27.

90. Beall AC, Kato K, Goldenring JR, Rasmussen H, Brophy CM. Cyclic nucleotide-dependent vasorelaxation is associated with the phosphorylation of a small heat shock-related protein. J Biol Chem 1997;272:11283-7.

91. Mehta D, Tang DD, Wu MF, Atkinson S, Gunst SJ. Role of Rho in Ca(2+)-insensitive contraction and paxillin tyrosine phosphorylation in smooth muscle. Am J Physiol Cell Physiol 2000;279:C308-18.

92. Francis SH, Noblett BD, Todd BW, Wells JN, Corbin JD. Relaxation of vascular and tracheal smooth muscle by cyclic nucleotide analogs that preferentially activate purified cGMP-dependent protein kinase. Mol Pharmacol 1988;34:506-17.

93. Komalavilas P, Lincoln TM. Phosphorylation of the inositol 1,4,5-trisphosphate receptor. Cyclic GMP-dependent protein kinase mediates cAMP and cGMP dependent phosphorylation in the intact rat aorta. J Biol Chem 1996;271:21933-8.

94. White RE, Kryman JP, El-Mowafy AM, Han G, Carrier GO. cAMP-dependent vasodilators cross-activate the cGMP-dependent protein kinase to stimulate BK(Ca) channel activity in coronary artery smooth muscle cells. Circ Res 2000;86:897-905.

95. Barman SA, Zhu S, Han G, White RE. cAMP activates BKCa channels in pulmonary arterial smooth muscle via cGMP-dependent protein kinase. Am J Physiol Lung Cell Mol Physiol 2003;284:L1004-11.

96. Surks HK, Mochizuki N, Kasai Y, et al. Regulation of myosin phosphatase by a specific interaction with cGMP- dependent protein kinase Ialpha. Science 1999;286:1583-7.

97. Schlossmann J, Ammendola A, Ashman K, et al. Regulation of intracellular calcium by a signalling complex of IRAG, IP3 receptor and cGMP kinase Ibeta. Nature 2000;404:197-201.

98. Meeks MK, Ripley ML, Jin Z, Rembold CM. Heat shock protein 20-mediated force suppression in forskolin-relaxed swine carotid artery. Am J Physiol Cell Physiol 2005;288:C633-9.

99. Kim HR, Gallant C, Leavis PC, Gunst SJ, Morgan KG. Cytoskeletal remodeling in differentiated vascular smooth muscle is actin isoform dependent and stimulus dependent. Am J Physiol Cell Physiol 2008;295:C768-78.

100. Mehta D, Gunst SJ. Actin polymerization stimulated by contractile activation regulates force development in canine tracheal smooth muscle. J Physiol 1999;519 Pt 3:829-40.

101. Adler KB, Krill J, Alberghini TV, Evans JN. Effect of cytochalasin D on smooth muscle contraction. Cell Motil 1983;3:545-51.

102. Saito SY, Hori M, Ozaki H, Karaki H. Cytochalasin D inhibits smooth muscle contraction by directly inhibiting contractile apparatus. J Smooth Muscle Res 1996;32:51-60.

103. Shaw L, Ahmed S, Austin C, Taggart MJ. Inhibitors of actin filament polymerisation attenuate force but not global intracellular calcium in isolated pressurised resistance arteries. J Vasc Res 2003;40:1-10; discussion

104. Birkenfeld J, Betz H, Roth D. Identification of cofilin and LIM-domain-containing protein kinase 1 as novel interaction partners of 14-3-3 zeta. Biochem J 2003;369:45-54.

105. Niwa R, Nagata-Ohashi K, Takeichi M, Mizuno K, Uemura T. Control of actin reorganization by Slingshot, a family of phosphatases that dephosphorylate ADF/cofilin. Cell 2002;108:233-46.

106. Gohla A, Birkenfeld J, Bokoch GM. Chronophin, a novel HAD-type serine protein phosphatase, regulates cofilin-dependent actin dynamics. Nat Cell Biol 2005;7:21-9.

107. Chernik IS, Seit-Nebi AS, Marston SB, Gusev NB. Small heat shock protein Hsp20 (HspB6) as a partner of 14-3-3gamma. Mol Cell Biochem 2007;295:9-17.

108. Ba M, Singer CA, Tyagi M, et al. HSP20 phosphorylation and airway smooth muscle relaxation. Cell health and cytoskeleton 2009;2009:27-42.

109. Somara S, Gilmont RR, Varadarajan S, Bitar KN. Phosphorylated HSP20 modulates the association of thin-filament binding proteins: caldesmon with tropomyosin in colonic smooth muscle. Am J Physiol Gastrointest Liver Physiol 2010;299:G1164-76.

110. Reinhard M, Giehl K, Abel K, et al. The proline-rich focal adhesion and microfilament protein VASP is a ligand for profilins. EMBO J 1995;14:1583-9.

111. Laurent V, Loisel TP, Harbeck B, et al. Role of proteins of the Ena/VASP family in actin-based motility of Listeria monocytogenes. J Cell Biol 1999;144:1245-58.

112. Harbeck B, Huttelmaier S, Schluter K, Jockusch BM, Illenberger S. Phosphorylation of the vasodilator-stimulated phosphoprotein regulates its interaction with actin. J Biol Chem 2000;275:30817-25.

113. Brown MC, Turner CE. Paxillin: adapting to change. Physiol Rev 2004;84:1315-39.

114. Burridge K, Turner CE, Romer LH. Tyrosine phosphorylation of paxillin and pp125FAK accompanies cell adhesion to extracellular matrix: a role in cytoskeletal assembly. The Journal of cell biology 1992;119:893-903.

115.   Tang DD, Zhang W, Gunst SJ. The adapter protein CrkII regulates neuronal Wiskott-Aldrich syndrome protein, actin polymerization, and tension development during contractile stimulation of smooth muscle. J Biol Chem 2005;280:23380-9.

116.   Gerthoffer WT. Actin cytoskeletal dynamics in smooth muscle contraction. Can J Physiol Pharmacol 2005;83:851-6.

117.   Kaneda T, Shimizu K, Nakajyo S, Urakawa N. The difference in the inhibitory mechanisms of papaverine on vascular and intestinal smooth muscles. Eur J Pharmacol 1998;355:149-57.

118.   Sogo N, Campanella C, Webb DJ, Megson IL. S-nitrosothiols cause prolonged, nitric oxide-mediated relaxation in human saphenous vein and internal mammary artery: therapeutic potential in bypass surgery. Br J Pharmacol 2000;131:1236-44.

119.   Grondin CM, Campeau L, Thornton JC, Engle JC, Cross FS, Schreiber H. Coronary artery bypass grafting with saphenous vein. Circulation 1989;79:I24-9.

120.   Motwani JG, Topol EJ. Aortocoronary saphenous vein graft disease: pathogenesis, predisposition, and prevention. Circulation 1998;97:916-31.

121.   Rosenfeldt FL, He GW, Buxton BF, Angus JA. Pharmacology of coronary artery bypass grafts. Ann Thorac Surg 1999;67:878-88.

122.   Li FD, Eagle S, Brophy C, et al. Pressure Control During Preparation of Saphenous Veins. JAMA Surg 2014.

123.   Defawe OD, Kim S, Chen L, et al. VASP phosphorylation at serine239 regulates the effects of NO on smooth muscle cell invasion and contraction of collagen. J Cell Physiol 2010;222:230-7.

124.   Komalavilas P, Penn RB, Flynn CR, et al. The small heat shock-related protein, HSP20, is a cAMP-dependent protein kinase substrate that is involved in airway smooth muscle relaxation. Am J Physiol Lung Cell Mol Physiol 2008;294:L69-78.

125.   Hocking KM, Brophy C, Rizvi SZ, et al. Detrimental effects of mechanical stretch on smooth muscle function in saphenous veins. J Vasc Surg 2011;53:454-60.

126.   Khalil RA, Crews JK, Novak J, Kassab S, Granger JP. Enhanced vascular reactivity during inhibition of nitric oxide synthesis in pregnant rats. Hypertension 1998;31:1065-9.

127.   Hocking K.M. BFJ, Putumbaka G, Venkatraman S, Cheung-Flynn J, Brophy C.M., and Komalavilas K. Role of Cyclic Nucleotide-Dependent Actin Cytoskeletal Dynamics: [Ca2+] and Force Suppression in Forskolin-Pretreated Porcine Coronary Arteries. . PLoS One 2013.

128.   Hocking KM, Baudenbacher FJ, Putumbaka G, et al. Role of cyclic nucleotide-dependent actin cytoskeletal dynamics:Ca(2+)](i) and force suppression in forskolin-pretreated porcine coronary arteries. PloS one 2013;8:e60986.

129.   Ignarro LJ, Kadowitz PJ. The pharmacological and physiological role of cyclic GMP in vascular smooth muscle relaxation. Annu Rev Pharmacol Toxicol 1985;25:171-91.

130.   Schultz K, Schultz G. Sodium nitroprusside and other smooth muscle-relaxants increase cyclic GMP levels in rat ductus deferens. Nature 1977;265:750-1.

131.   Karaki H, Ozaki H, Hori M, et al. Calcium movements, distribution, and functions in smooth muscle. Pharmacol Rev 1997;49:157-230.

132.   Zaccolo M, Movsesian MA. cAMP and cGMP signaling cross-talk: role of phosphodiesterases and implications for cardiac pathophysiology. Circ Res 2007;100:1569-78.

133.   LoGerfo FW, Haudenschild CC, Quist WC. A clinical technique for prevention of spasm and preservation of endothelium in saphenous vein grafts. Arch Surg 1984;119:1212-4.

134.   Kudo FA, Kondo Y, Muto A, et al. Cilostazol suppresses neointimal hyperplasia in canine vein grafts. Surg Today 2009;39:128-32.

135.   Sakaguchi T, Asai T, Belov D, et al. Influence of ischemic injury on vein graft remodeling: Role of cyclic adenosine monophosphate second messenger pathway in enhanced vein graft preservation. J Thorac Cardiovasc Surg 2005;129:129-37.

136.   Dubinska-Magiera M, Jablonska J, Saczko J, Kulbacka J, Jagla T, Daczewska M. Contribution of small heat shock proteins to muscle development and function. FEBS Lett 2014;588:517-30.

137.   Garrido C, Paul C, Seigneuric R, Kampinga HH. The small heat shock proteins family: the long forgotten chaperones. Int J Biochem Cell Biol 2012;44:1588-92.

138.   Gerthoffer WT, Gunst SJ. Invited review: Focal adhesion and small heat shock proteins in the regulation of actin remodeling and contractility in smooth muscle. Journal of Applied Physiology 2001;91:963-72.

139.   Nelson CE, Kim AJ, Adolph EJ, et al. Tunable delivery of siRNA from a biodegradable scaffold to promote angiogenesis in vivo. Adv Mater 2014;26:607-14, 506.

140.   Lopes LB, Brophy CM, Flynn CR, et al. A novel cell permeant peptide inhibitor of MAPKAP kinase II inhibits intimal hyperplasia in a human saphenous vein organ culture model. J Vasc Surg 2010;52:1596-607.

141.   Ferrito MaT, D. A. Poly(2-ethylacrylic acid). Macromolecular Syntheses 1992;11:59-62.

142.   Convertine AJ, Benoit DS, Duvall CL, Hoffman AS, Stayton PS. Development of a novel endosomolytic diblock copolymer for siRNA delivery. J Control Release 2009;133:221-9.

143.   Jones RA, Cheung CY, Black FE, et al. Poly(2-alkylacrylic acid) polymers deliver molecules to the cytosol by pH-sensitive disruption of endosomal vesicles. Biochem J 2003;372:65-75.

144. Lackey CA, Press OW, Hoffman AS, Stayton PS. A biomimetic pH-responsive polymer directs endosomal release and intracellular delivery of an endocytosed antibody complex. Bioconjugate Chemistry 2002;13:996-1001.

145. Murthy N, Robichaud JR, Tirrell DA, Stayton PS, Hoffman AS. The design and synthesis of polymers for eukaryotic membrane disruption. J Control Release 1999;61:137-43.

146. Foster S, Duvall CL, Crownover EF, Hoffman AS, Stayton PS. Intracellular delivery of a protein antigen with an endosomal-releasing polymer enhances CD8 T-cell production and prophylactic vaccine efficacy. Bioconjug Chem 2010;21:2205-12.

147. Murthy N, Campbell J, Fausto N, Hoffman AS, Stayton PS. Bioinspired pH-responsive polymers for the intracellular delivery of biomolecular drugs. Bioconjug Chem 2003;14:412-9.

148. Al-Hassani MH, Garcia JGN, Gunst SJ. Differences in Ca 2+ mobilization by muscarinic agonists in tracheal smooth muscle. American Journal of Physiology - Lung Cellular and Molecular Physiology 1993;264:L53-L9.

149. Macomson SD, Brophy CM, Miller W, Harris VA, Shaver EG. Heat shock protein expression in cerebral vessels after subarachnoid hemorrhage. Neurosurgery 2002;51:204-10; discussion 10-1.

150. Conte MS, Bandyk DF, Clowes AW, et al. Results of PREVENT III: a multicenter, randomized trial of edifoligide for the prevention of vein graft failure in lower extremity bypass surgery. Journal of vascular surgery 2006;43:742-51; discussion 51.

151. Alexander JH, Hafley G, Harrington RA, et al. Efficacy and safety of edifoligide, an E2F transcription factor decoy, for prevention of vein graft failure following coronary artery bypass graft surgery: PREVENT IV: a randomized controlled trial. JAMA : the journal of the American Medical Association 2005;294:2446-54.

152. Clowes AW, Reidy MA. Prevention of stenosis after vascular reconstruction: pharmacologic control of intimal hyperplasia--a review. J Vasc Surg 1991;13:885-91.

153. LoGerfo FW, Quist WC, Cantelmo NL, Haudenschild CC. Integrity of vein grafts as a function of initial intimal and medial preservation. Circulation 1983;68:II117-24.

154. Li FD, Eagle, S.E., Brophy, C.M., Hocking, K.M., Osgood, M.J., Komalavilas, P., and Cheung-Flynn, J. Pressure control during preparation of saphenous veins. JAMA Surgery 2013;In press.

155. Hocking KM, Brophy C, Rizvi SZ, et al. Detrimental effects of mechanical stretch on smooth muscle function in saphenous veins. Journal of Vascular Surgery 2011;53:454-60.

156. Eagle S, Brophy CM, Komalavilas P, et al. Surgical skin markers impair human saphenous vein graft smooth muscle and endothelial function. Am Surg 2011;77:922-8.

157. Peng W, Cotrina ML, Han X, et al. Systemic administration of an antagonist of the ATP-sensitive receptor P2X7 improves recovery after spinal cord injury. Proc Natl Acad Sci U S A 2009;106:12489-93.

158. Hocking KM BF, Putumbaka G, Venkatraman S, Cheung-Flynn J, Borphy CM, Komalavilas P. Role of cyclic nucleotide-dependent actin cytoskeletal dynamics: Ca2+ and force supression in forskolin-pretreated porcine coronary arteries. PLoS One 2013.

159. Jiang Z, Wu L, Miller BL, et al. A novel vein graft model: adaptation to differential flow environments. Am J Physiol Heart Circ Physiol 2004;286:H240-5.

160. Ballerini P, Rathbone MP, Di Iorio P, et al. Rat astroglial P2Z (P2X7) receptors regulate intracellular calcium and purine release. Neuroreport 1996;7:2533-7.

161. Newby AC, Zaltsman AB. Molecular mechanisms in intimal hyperplasia. J Pathol 2000;190:300-9.

162. Conte MS. Technical factors in lower-extremity vein bypass surgery: how can we improve outcomes? Semin Vasc Surg 2009;22:227-33.

163. Davies MG, Hagen PO. Pathophysiology of vein graft failure: a review. Eur J Vasc Endovasc Surg 1995;9:7-18.

164. Gao L, Cao L, Qiu Y, et al. Blocking P2X receptors can inhibit the injury-induced proliferation of olfactory epithelium progenitor cells in adult mouse. Int J Pediatr Otorhinolaryngol 2010;74:747-51.

165. Murphy N, Lynch MA. Activation of the P2X(7) receptor induces migration of glial cells by inducing cathepsin B degradation of tissue inhibitor of metalloproteinase 1. Journal of neurochemistry 2012;123:761-70.

166. Chamberlain J, Evans D, King A, et al. Interleukin-1beta and signaling of interleukin-1 in vascular wall and circulating cells modulates the extent of neointima formation in mice. Am J Pathol 2006;168:1396-403.

167. Locovei S, Scemes E, Qiu F, Spray DC, Dahl G. Pannexin1 is part of the pore forming unit of the P2X(7) receptor death complex. FEBS letters 2007;581:483-8.

168. Shoji KF, Saez PJ, Harcha P, Aguila HL, Saez JC. Pannexin1 channels act downstream of P2X receptors in ATP-induced murine T-cell death. Channels (Austin) 2014;8.

169. Clowes AW, Reidy MA. Prevention of stenosis after vascular reconstruction: pharmacologic control of intimal hyperplasia--a review. J Vasc Surg 1991;13:885-91.

170. LoGerfo FW, Quist WC, Cantelmo NL, Haudenschild CC. Integrity of vein grafts as a function of initial intimal and medial preservation. Circulation 1983;68:II117-24.

171. Conte MS, Bandyk DF, Clowes AW, et al. Results of PREVENT III: a multicenter, randomized trial of edifoligide for the prevention of vein graft failure in lower extremity bypass surgery. J Vasc Surg 2006;43:742-51; discussion 51.

172.   Alexander JH, Hafley G, Harrington RA, et al. Efficacy and safety of edifoligide, an E2F transcription factor decoy, for prevention of vein graft failure following coronary artery bypass graft surgery: PREVENT IV: a randomized controlled trial. Jama 2005;294:2446-54.

173.   Angelini GD, Passani SL, Breckenridge IM, Newby AC. Nature and pressure dependence of damage induced by distension of human saphenous vein coronary artery bypass grafts. Cardiovasc Res 1987;21:902-7.

174.   Eagle S, Brophy CM, Komalavilas P, et al. Surgical skin markers impair human saphenous vein graft smooth muscle and endothelial function. Am Surg 2011;77:922-8.

175.   Davies MG, Hagen PO. Influence of perioperative storage solutions on long-term vein graft function and morphology. Ann Vasc Surg 1994;8:150-7.

176.   Karayannacos PE, Hostetler JR, Bond MG, et al. Late failure in vein grafts: mediating factors in subendothelial fibromuscular hyperplasia. Ann Surg 1978;187:183-8.

177.   Svendsen E, Dalen H, Moland J, Engedal H. A quantitative study of endothelial cell injury in aorto-coronary vein grafts. J Cardiovasc Surg (Torino) 1986;27:65-71.

178.   Lum H, Roebuck KA. Oxidant stress and endothelial cell dysfunction. Am J Physiol Cell Physiol 2001;280:C719-41.

179.   Weaver H, Shukla N, Ellinsworth D, Jeremy JY. Oxidative stress and vein graft failure: a focus on NADH oxidase, nitric oxide and eicosanoids. Curr Opin Pharmacol 2012;12:160-5.

180.   Wingard CJ, Browne AK, Murphy RA. Dependence of force on length at constant cross-bridge phosphorylation in the swine carotid media. J Physiol 1995;488 (Pt 3):729-39.

181.   Herlihy JT, Murphy RA. Length-tension relationship of smooth muscle of the hog carotid artery. Circ Res 1973;33:275-83.

182.   Furchgott RF, Zawadzki JV. The obligatory role of endothelial cells in the relaxation of arterial smooth muscle by acetylcholine. Nature 1980;288:373-6.

183.   Tessier DJ, Komalavilas P, Liu B, et al. Transduction of peptide analogs of the small heat shock-related protein HSP20 inhibits intimal hyperplasia. J Vasc Surg 2004;40:106-14.

184.   Dikalov S, Griendling KK, Harrison DG. Measurement of reactive oxygen species in cardiovascular studies. Hypertension 2007;49:717-27.

185.   Kennedy JH, Lever MJ, Addis BJ, Paneth M. Changes in vein interstitium following distension for aortocoronary bypass. J Cardiovasc Surg (Torino) 1989;30:992-5.

186.   Kapp RW, Jr., Bevan C, Gardiner TH, Banton MI, Tyler TR, Wright GA. Isopropanol: summary of TSCA test rule studies and relevance to hazard identification. Regul Toxicol Pharmacol 1996;23:183-92.

187. Dhar A, Desai K, Kazachmov M, Yu P, Wu L. Methylglyoxal production in vascular smooth muscle cells from different metabolic precursors. Metabolism 2008;57:1211-20.

188. Collier J, Vallance P. Biphasic response to acetylcholine in human veins in vivo: the role of the endothelium. Clin Sci (Lond) 1990;78:101-4.

189. Stern DM, Nawroth PP, Kisiel W, Handley D, Drillings M, Bartos J. A coagulation pathway on bovine aortic segments leading to generation of Factor Xa and thrombin. J Clin Invest 1984;74:1910-21.

190. Wallitt EJ, Jevon M, Hornick PI. Therapeutics of vein graft intimal hyperplasia: 100 years on. Ann Thorac Surg 2007;84:317-23.

191. Porter KE, Varty K, Jones L, Bell PR, London NJ. Human saphenous vein organ culture: a useful model of intimal hyperplasia? Eur J Vasc Endovasc Surg 1996;11:48-58.

192. Liao DF, Jin ZG, Baas AS, et al. Purification and identification of secreted oxidative stress-induced factors from vascular smooth muscle cells. J Biol Chem 2000;275:189-96.

193. Brunssen C, Arsov A, Eickholt C, et al. Hypoxia upregulates NADPH oxidase 4 by a HIF-independent mechanism in endothelial cells. Circulation 2012;126:A15323.

194. Selemidis S, Sobey CG, Wingler K, Schmidt HH, Drummond GR. NADPH oxidases in the vasculature: molecular features, roles in disease and pharmacological inhibition. Pharmacol Ther 2008;120:254-91.

195. Jeremy JY, Yim AP, Wan S, Angelini GD. Oxidative stress, nitric oxide, and vascular disease. J Card Surg 2002;17:324-7.

196. Lopes RD, Hafley GE, Allen KB, et al. Endoscopic versus open vein-graft harvesting in coronary-artery bypass surgery. N Engl J Med 2009;361:235-44.

197. Wu J, Zhang C. Neointimal hyperplasia, vein graft remodeling, and long-term patency. Am J Physiol Heart Circ Physiol 2009;297:H1194-5.

198. Rousou LJ, Taylor KB, Lu XG, et al. Saphenous vein conduits harvested by endoscopic technique exhibit structural and functional damage. Ann Thorac Surg 2009;87:62-70.

199. Grohs JG, Kadletz M, Wodratzka M, Wolner E, Raberger G. Contractile function of human veins after long-term storage in different media. J Cardiovasc Pharmacol 1996;28:89-93.

200. Raja SG, Haider Z, Ahmad M, Zaman H. Saphenous vein grafts: to use or not to use? Heart Lung Circ 2004;13:403-9.

201. Barber DA, Rubin JW, Zumbro GL, Tackett RL. The use of methylene blue as an extravascular surgical marker impairs vascular responses of human saphenous veins. J Thorac Cardiovasc Surg 1995;109:21-9.

202.   Shoemaker K, Rubin J, Zumbro GL, Tackett R. Evans blue and gentian violet: alternatives to methylene blue as a surgical marker dye. J Thorac Cardiovasc Surg 1996;112:542-4.

203.   Wingard CJ, Browne AK, Murphy RA. Dependence of force on length at constant cross-bridge phosphorylation in the swine carotid media. J Physiol (Lond) 1995;488 (Pt 3):729-39.

204.   Bai TR, Bates JH, Brusasco V, et al. On the terminology for describing the length-force relationship and its changes in airway smooth muscle. J Appl Physiol 2004;97:2029-34.

205.   Hocking KM, Brophy C.M., Rizvi, S. Z. , Komalavilas, P. , Eagle, S. , Leacche M. , Balaguer, J. M. , and Cheung-Flynn, J. **Detrimental Effects Of Mechanical Stretch On Smooth Muscle Function In Saphenous Veins**

Journal of Vascular Surgery In Press

206.   Viaro F, Capellini VK, Celotto AC, et al. Immunohistochemical evaluation of three nitric oxide synthase isoforms in human saphenous vein exposed to different degrees of distension pressures. Cardiovasc Pathol 2010.

207.   Halabi AR, Alexander JH, Shaw LK, et al. Relation of early saphenous vein graft failure to outcomes following coronary artery bypass surgery. Am J Cardiol 2005;96:1254-9.

208.   Fabricius AM, Gerber W, Hanke M, Garbade J, Autschbach R, Mohr FW. Early angiographic control of perioperative ischemia after coronary artery bypass grafting. Eur J Cardiothorac Surg 2001;19:853-8.

209.   Fitzgibbon GM, Kafka HP, Leach AJ, Keon WJ, Hooper GD, Burton JR. Coronary bypass graft fate and patient outcome: angiographic follow-up of 5,065 grafts related to survival and reoperation in 1,388 patients during 25 years. J Am Coll Cardiol 1996;28:616-26.

210.   Tsui JC, Souza DS, Filbey D, Karlsson MG, Dashwood MR. Localization of nitric oxide synthase in saphenous vein grafts harvested with a novel "no-touch" technique: potential role of nitric oxide contribution to improved early graft patency rates. J Vasc Surg 2002;35:356-62.

211.   Dashwood MR, Savage K, Dooley A, Shi-Wen X, Abraham DJ, Souza DS. Effect of vein graft harvesting on endothelial nitric oxide synthase and nitric oxide production. Ann Thorac Surg 2005;80:939-44.

212.   Manchio JV, Gu J, Romar L, et al. Disruption of graft endothelium correlates with early failure after off-pump coronary artery bypass surgery. Ann Thorac Surg 2005;79:1991-8.

213.   Asahara T, Bauters C, Pastore C, et al. Local delivery of vascular endothelial growth factor accelerates reendothelialization and attenuates intimal hyperplasia in balloon-injured rat carotid artery. Circulation 1995;91:2793-801.

214.   Poston R, Gu J, Brown J, et al. Hypercoagulability affecting early vein graft patency does not exist after off-pump coronary artery bypass. J Cardiothorac Vasc Anesth 2005;19:11-8.

215. Kobayashi T, Makuuchi H, Naruse Y, et al. [Assessment of saphenous vein graft wall characteristics with intravascular ultrasound imaging]. Jpn J Thorac Cardiovasc Surg 1998;46:701-6.

216. Yamada T, Itoh T, Nakano S, Tokunaga O. Time-dependent thickening of the intima in aortocoronary saphenous vein grafts: clinicopathological analysis of 24 patients. Heart Vessels 1995;10:41-5.

217. Sharony R, Pintucci G, Saunders PC, et al. Matrix metalloproteinase expression in vein grafts: role of inflammatory mediators and extracellular signal-regulated kinases-1 and -2. Am J Physiol Heart Circ Physiol 2006;290:H1651-9.

218. Chu WW, Rha SW, Kuchulakanti PK, et al. Efficacy of sirolimus-eluting stents compared with bare metal stents for saphenous vein graft intervention. Am J Cardiol 2006;97:34-7.

219. Johansson BL, Souza DS, Bodin L, et al. Slower progression of atherosclerosis in vein grafts harvested with 'no touch' technique compared with conventional harvesting technique in coronary artery bypass grafting: an angiographic and intravascular ultrasound study. Eur J Cardiothorac Surg 2010.

220. Martinez TT, Jaeger RW, deCastro FJ, Thompson MW, Hamilton MF. A comparison of the absorption and metabolism of isopropyl alcohol by oral, dermal and inhalation routes. Vet Hum Toxicol 1986;28:233-6.

221. Allali-Hassani A, Martinez SE, Peralba JM, et al. Alcohol dehydrogenase of human and rat blood vessels. Role in ethanol metabolism. FEBS Lett 1997;405:26-30.

222. Farber A, Major K, Wagner WH, et al. Cryopreserved saphenous vein allografts in infrainguinal revascularization: analysis of 240 grafts. J Vasc Surg 2003;38:15-21.

223. Kouzi-Koliakos K, Kanellaki-Kyparissi M, Marinov G, et al. Prebypass histological and ultrastructural evaluation of the long saphenous vein as a predictor of early graft failure. Cardiovasc Pathol 2006;15:336-46.

224. LoGerfo FW, Haudenschild CC, Quist WC. A clinical technique for prevention of spasm and preservation of endothelium in saphenous vein grafts. Arch Surg 1984;119:1212-4.

225. Osgood MJH, K.M.; Voskresensky, I.V; Li, F.D.;Komalavilas, P.; Cheung-Flynn, J. ; Brophy,C.M. Surgical Vein Graft Preparation Promotes Cellular Dysfunciton, Oxidative Stess, and Intimal Hyperplasia in Human Saphenous Vein. J Vasc Surg 2013

226. Chester AH, Buttery LD, Borland JA, et al. Structural, biochemical and functional effects of distending pressure in the human saphenous vein: implications for bypass grafting. Coron Artery Dis 1998;9:143-51.

227. Chello M, Mastroroberto P, Frati G, et al. Pressure distension stimulates the expression of endothelial adhesion molecules in the human saphenous vein graft. Ann Thorac Surg 2003;76:453-8; discussion 8.

228. Khaleel MS, Dorheim TA, Duryee MJ, et al. High-pressure distention of the saphenous vein during preparation results in increased markers of inflammation: a potential mechanism for graft failure. The Annals of thoracic surgery 2012;93:552-8.

229. Hinokiyama K, Valen G, Tokuno S, Vedin JB, Vaage J. Vein graft harvesting induces inflammation and impairs vessel reactivity. Ann Thorac Surg 2006;82:1458-64.

230. Johnson JL, van Eys GJ, Angelini GD, George SJ. Injury induces dedifferentiation of smooth muscle cells and increased matrix-degrading metalloproteinase activity in human saphenous vein. Arterioscler Thromb Vasc Biol 2001;21:1146-51.

231. Chung AW, Rauniyar P, Luo H, Hsiang YN, van Breemen C, Okon EB. Pressure distention compared with pharmacologic relaxation in vein grafting upregulates matrix metalloproteinase-2 and -9. J Vasc Surg 2005;42:747-56.

232. Cornelissen J, Armstrong J, Holt CM. Mechanical stretch induces phosphorylation of p38-MAPK and apoptosis in human saphenous vein. Arterioscler Thromb Vasc Biol 2004;24:451-6.

233. Clowes AW. Intimal hyperplasia and graft failure. Cardiovasc Pathol 1993;2:179S-86S.

234. Li FD, Sexton KW, Hocking KM, et al. Intimal thickness associated with endothelial dysfunction in human vein grafts. The Journal of surgical research 2012.

235. Tessier DJ, Komalavilas P, Liu B, et al. Transduction of peptide analogs of the small heat shock-related protein HSP20 inhibits intimal hyperplasia. J Vasc Surg 2004;40:106-14.

236. Souza DS, Johansson B, Bojo L, et al. Harvesting the saphenous vein with surrounding tissue for CABG provides long-term graft patency comparable to the left internal thoracic artery: results of a randomized longitudinal trial. J Thorac Cardiovasc Surg 2006;132:373-8.

237. Souza DS, Dashwood MR, Tsui JC, et al. Improved patency in vein grafts harvested with surrounding tissue: results of a randomized study using three harvesting techniques. Ann Thorac Surg 2002;73:1189-95.

238. Okon EB, Millar MJ, Crowley CM, et al. Effect of moderate pressure distention on the human saphenous vein vasomotor function. Ann Thorac Surg 2004;77:108-14; discussion 14-5.

239. Zhao J, Andreasen JJ, Yang J, Rasmussen BS, Liao D, Gregersen H. Manual pressure distension of the human saphenous vein changes its biomechanical properties-implication for coronary artery bypass grafting. J Biomech 2007;40:2268-76.

240. Chong CF, Ong PJ, Moat N, Collins P. Effects of hydrostatic distention on in vitro vasoreactivity of radial artery conduits. J Thorac Cardiovasc Surg 2004;128:609-14.

241. Wendling WW, Krasner LJ, Cooper SC, et al. Effects of stretch or distention on phenylephrine-induced constriction of human coronary artery bypass grafts. J Cardiothorac Vasc Anesth 2001;15:717-22.

242. Stigler R, Steger C, Schachner T, et al. The impact of distension pressure on acute endothelial cell loss and neointimal proliferation in saphenous vein grafts. European journal of cardio-thoracic surgery : official journal of the European Association for Cardio-thoracic Surgery 2012;42:e74-9.

243. Goldman J, Zhong L, Liu SQ. Degradation of alpha-actin filaments in venous smooth muscle cells in response to mechanical stretch. Am J Physiol Heart Circ Physiol 2003;284:H1839-47.

244. Reidy MA. Factors controlling smooth-muscle cell proliferation. Arch Pathol Lab Med 1992;116:1276-80.

245. Bonow RO, Bennett S, Casey DE, Jr., et al. ACC/AHA Clinical Performance Measures for Adults with Chronic Heart Failure: a report of the American College of Cardiology/American Heart Association Task Force on Performance Measures (Writing Committee to Develop Heart Failure Clinical Performance Measures): endorsed by the Heart Failure Society of America. Circulation 2005;112:1853-87.

246. Owens CD. Adaptive changes in autogenous vein grafts for arterial reconstruction: clinical implications. Journal of vascular surgery : official publication, the Society for Vascular Surgery [and] International Society for Cardiovascular Surgery, North American Chapter 2010;51:736-46.

247. Conte MS, Mann MJ, Simosa HF, Rhynhart KK, Mulligan RC. Genetic interventions for vein bypass graft disease: a review. J Vasc Surg 2002;36:1040-52.

248. Allaire E, Clowes AW. Endothelial cell injury in cardiovascular surgery: the intimal hyperplastic response. Ann Thorac Surg 1997;63:582-91.

249. Mosse PR, Campbell GR, Wang ZL, Campbell JH. Smooth muscle phenotypic expression in human carotid arteries. I. Comparison of cells from diffuse intimal thickenings adjacent to atheromatous plaques with those of the media. Lab Invest 1985;53:556-62.

250. Kanellaki-Kyparissi M, Kouzi-Koliakou K, Marinov G, Knyazev V. Histological study of arterial and venous grafts before their use in aortocoronary bypass surgery. Hellenic J Cardiol 2005;46:21-30.

251. Sales CM, Marin ML, Veith FJ, et al. Saphenous vein angioscopy: a valuable method to detect unsuspected venous disease. J Vasc Surg 1993;18:198-204; discussion -6.

252. Yetik-Anacak G, Catravas JD. Nitric oxide and the endothelium: history and impact on cardiovascular disease. Vascul Pharmacol 2006;45:268-76.

253. Viaro F, Capellini VK, Celotto AC, et al. Immunohistochemical evaluation of three nitric oxide synthase isoforms in human saphenous vein exposed to different degrees of distension pressures. Cardiovasc Pathol 2010;19:e211-20.

254. Walford G, Loscalzo J. Nitric oxide in vascular biology. J Thromb Haemost 2003;1:2112-8.

255. Maxwell AJ. Mechanisms of dysfunction of the nitric oxide pathway in vascular diseases. Nitric Oxide 2002;6:101-24.

256.   Verrier ED, Boyle EM, Jr. Endothelial cell injury in cardiovascular surgery. Ann Thorac Surg 1996;62:915-22.

257.   Gokce N, Keaney JF, Jr., Hunter LM, et al. Predictive value of noninvasively determined endothelial dysfunction for long-term cardiovascular events in patients with peripheral vascular disease. Journal of the American College of Cardiology 2003;41:1769-75.

258.   Bourassa MG. Fate of venous grafts: the past, the present and the future. J Am Coll Cardiol 1991;17:1081-3.

259.   Lawrie GM, Morris GC, Jr., Earle N. Long-term results of coronary bypass surgery. Analysis of 1698 patients followed 15 to 20 years. Ann Surg 1991;213:377-85; discussion 86-7.

260.   Giannoukas AD, Labropoulos N, Stavridis G, Bailey D, Glenville B, Nicolaides AN. Pre-bypass quality assessment of the long saphenous vein wall with ultrasound and histology. Eur J Vasc Endovasc Surg 1997;14:37-40.

261.   Rinia-Feenstra M, Stooker W, de Graaf R, et al. Functional properties of the saphenous vein harvested by minimally invasive techniques. Ann Thorac Surg 2000;69:1116-20.

262.   Dashwood MR, Savage K, Dooley A, Shi-Wen X, Abraham DJ, Souza DS. Effect of vein graft harvesting on endothelial nitric oxide synthase and nitric oxide production. The Annals of thoracic surgery 2005;80:939-44.

263.   Porter KE, Varty K, Jones L, Bell PR, London NJ. Human saphenous vein organ culture: a useful model of intimal hyperplasia? European journal of vascular and endovascular surgery : the official journal of the European Society for Vascular Surgery 1996;11:48-58.

264.   Komori K, Gloviczki P, Bourchier RG, Miller VM, Vanhoutte PM. Endothelium-dependent vasorelaxations in response to aggregating platelets are impaired in reversed vein grafts. Journal of vascular surgery : official publication, the Society for Vascular Surgery [and] International Society for Cardiovascular Surgery, North American Chapter 1990;12:139-47.